PhD degree in Systems Medicine (curriculum in Molecular Oncology)

European School of Molecular Medicine (SEMM),

University of Milan and University of Naples "Federico II"

Settore disciplinare: MED/O4

Identification of new MYC dependencies among RNA-binding proteins

Clarissa Spataro

European Institute of Oncology (IEO)

Supervisor: Dr. Bruno Amati

Added Supervisor: Dr. Arianna Sabò

European Institute of Oncology (IEO)

PhD Coordinator: Prof. Saverio Minucci

Anno accademico 2020-2021

Acknowledgements

This work would not have been possible without the support of many people.

First and foremost I am extremely grateful to my supervisors Dr. Bruno Amati and Dr. Arianna Sabò for their precious guidance, continuous support and mentoring during my PhD studies. Their inspiring knowledge, genuine scientific passion and experience have encouraged me in all these years and motivated my efforts on this project.

I would like to thank also all the lab members, present and past, for technical and personal support, for constant encouragement and scientific guidance: Gianni Gamarra, Eirini Moysidou, Veronica Vallelonga, Dr. Giulio Donati, Mirko Doni, Alessandro Verrecchia, Dr. Nina Tanaskovic, Dr. Giorgia Ceccotti, Dr. Francesco Severi, Dr. Andrea Bisso, Paola Nicoli, Dr. Marco Filippuzzi and in particular Dr. Mattia Dalsass, for his contribution on analyzing part of the data described, and Lucrezia Trastus, who completed her master internship focusing on a part of this study and was my first mentoring experience.

I am also grateful to all the IIT group members and leaders, my internal advisor Prof. Diego Pasini and external advisor Prof. Oskar Capetillo for their advices and scientific discussions, which gave me the opportunity to grow professionally and gain more self-confidence.

I would like to thank our collaborator Dr. Johannes Zuber for providing the tools and precious input towards the successful execution of different parts of this study.

Thanks also to the IEO specialized Units of Cell Culture, Flow cytometry and Genomics for all the technical assistance which accelerated the implementation of specific techniques.

Finally, very special thanks to Signor Giovanni Amadio who gave me the opportunity to work on this project through the AIRC funding agency for part of my PhD and the next phase of my career and with his kindness and generous contribution prompted me to do my best and tackle this work as a personal mission.

Ringraziamenti

Tante sono le persone alle quali sono estremamente grata per il grande supporto personale ricevuto durante questi quattro anni di dottorato.

A Francesco, per aver reso più dolce e felice questo percorso, per essere il mio punto di riferimento, sempre presente incondizionatamente, per sostenermi e per spronarmi a dare il meglio, mettermi in gioco e uscire dal porto sicuro.

Ai miei genitori devo tutto: le infinite possibilità che mi si sono presentate fin dall'inizio grazie alle loro scelte coraggiose e difficili; l'esempio dato dal loro spirito di sacrificio che mi spinge sempre ad impegnarmi e mi aiuta a crescere in tutti i fronti; i valori della famiglia, dell'etica del lavoro, dell'onestà, della generosità e dell'amore che mi hanno trasmesso e che sono diventati pilastri portanti della mia intera persona; l'infinito incoraggiamento e sostegno morale per tutte le scelte fatte e pianificazioni future; l'essere sempre dalla mia parte. Sarò eternamente grata per tutto questo.

Alle mie sorelle, per essere la mia sicurezza, il mio sostegno, la mia più grande fortuna e il mio scudo, grazie alle quali non mi sono mai sentita sola nell'affrontare tutte le sfide di questo percorso.

Grazie anche ai miei nonni materni, che con il loro incoraggiamento e entusiasmo infinito hanno sempre inondato il mio cuore di gioia e vitalità, trasmettendomi costante calore anche quando lontani.

Grazie al mio nonno paterno, a cui non ho potuto dire di aver raggiunto questo traguardo, difficile per lui da comprendere eppure sempre supportato.

Ai miei cognati Fabrizio, Mary e Salvatore, per il loro genuino sostegno e per aver dato vita a due magnifici nipotini, fonte di allegria, serenità e amore puro che si sono rivelati fondamentali durante questi anni.

A Milena e Rinaldo, che come genitori mi hanno accompagnato lungo questo percorso con continui incoraggiamenti, sincero sostegno ed entusiasmo.

Infine, un immenso ringraziamento va anche a tutti gli amici del Campus che ho avuto la fortuna di incontrare e conoscere, per aver alleggerito il peso di questo

viaggio, per la spensieratezza, l'allegria, il divertimento e la felicità che mi hanno regalato nei momenti di maggiore bisogno. In particolare Simona, Shirali, Ottavio, Alejandro, Gianni, Eirini, Lucrezia, Veronica, Giulio, Mirko, Ale, Nina, Olga, Giorgia e molti altri, per aver reso questo PhD un viaggio entusiasmante e più facile da affrontare.

Table of Contents

List of Abbreviations

AGO = Argonaute
AGO2 = Argonaute RISC catalytic component 2
AMPK = 5' AMP-activated protein kinase
ARF = ADP-ribosylation factor
ARK5 = AMPK-related kinase 5
ARS2 = Arsenite-resistance protein 2 (or SRRT)
ATF4 = Activating transcription factor 4
ATM = Ataxia-telangiectasia mutated kinase
ATR = Ataxia telangiectasia and Rad3-related protein
AUF1 = ARE/poly(U)-binding/degradation factor 1
AURKA = Aurora kinase A
BCL2 = B-cell lymphoma 2
BET = Bromodomain and extra-terminal domain
BFP = Blue fluorescent protein
bHLH-LZ = Basic helix-loop-helix-leucine-zipper domain
BIN1 = Bridging integrator 1
Blast = Blasticidin resistance gene
BleoR = Bleomycin resistance gene
BRD4 = Bromodomain Containing 4
BrdU = 5'-Bromo-2'-Deoxyuridine
BSA = Bovine serum albumin
C-terminal = Carboxy-terminal
Cas9 = CRISPR associated protein 9
CASC3 = Cancer susceptibility candidate 3
CB = Cajal body
CBC = Capping binding complex
CCR4-NOT = Carbon catabolite repression 4 –negative on TATA-less
CD90.1 = Cluster of differentiation 90.1 (or Thy1.1)
CDK = Cyclin dependent kinase
cDNA = Complementary DNA
CECR2 = Cat eye syndrome chromosome region candidate 2
CELF1 = CUGBP Elav-Like Family Member 1
CHK1 = Checkpoint kinase 1
CK1 = Casein kinase 1
CRISPR = Clustered regularly interspaced short palindromic repeats
CSD = Cold-shock domain
DCP = Decapping protein
DCPC = Decapping complex
DDR = DNA damage response
DHL = Double hit lymphoma
DHX34 = DEAH box pelypeptide 34
DHX9 = DExH-Box Helicase 9
DKC1 = Dyskerin pseudouridine synthase 1
DLBCL = Diffuse large B cell lymphoma
DMEM = Dulbecco's modified eagle medium
DNA = Deoxyribonucleic acid
DNMT1 = DNA methyltransferase 1
dNTP = Deoxyribonucleotide triphosphate
DR5 = Death receptor 5
DSB = Double-strand breaks
DSIF = DRB Sensitivity Inducing Factor
dsRBD = Double-stranded RBD
dsRNA = Double-stranded RNA
E-box = Enhancer box
EDTA = Ethylenediaminetetraacetic acid
EED = Embryonic ectoderm development
eIF = Eukaryotic initiation factor
EJC = Exon-junction complex
ELAVL1 = Embryonic lethal abnormal vision like protein 1 (or HuR)
elncRNA = Enhancer-associated lncRNA
ER = Estrogen receptor
eRF = Eukaryotic release factor
EZH2 = Enhancer of zeste homolog 2
Eμ-Myc = IgH enhancer-Myc
FAD24 = Factor for adipocyte differentiation 24 (or NOC3L)
FBW7 = F-Box and WD repeat domain containing 7 (or FBXW7)
FC = Fold change
FDA = Food and drug administration
FDR = False discovery rate
FSC = Forward scatter
FUBP = Far upstream element-binding protein
Fw = Forward
G4 = Guanine quadruplex

GCN5 = General Control Non-repressed 5
gDNA = Genomic DNA
GFP = Green fluorescent protein
GLS = Glutaminase
GMD = Glucocorticoid receptormediated mRNA decay
GRSF-1 = Grich RNA sequence binding factor 1
GSK3b = Glycogen synthase kinase 3b
GWAS = Genome-wide association study
HAT = Histone acetyltransferase
HAT = Histone acetyltransferases
HBD = Hormone-binding domain
HCFC1 = Host cell factor C1
HCL = Hydrochloric acid
HDAC = Histone deacetylases
HMD = Histone mRNA decay
HNRNP = Heterogeneous nuclear ribonucleoprotein
HR = Homologous recombination
hTERT = Human telomerase reverse transcriptase
HuR = Human antigen R (or ELAVL1)
IDR = Intrinsically disordered regions
IGF2BP1 = Insulin Like Growth Factor 2 mRNA Binding Protein 1
IgH = Immunoglobulin heavy chain
IL-3 = Interleukin 3
IMDM = Iscove's Modified Dulbecco's Medium
IRES = Internal ribosome entry site
JAK = Janus kinase
JQ1 = Thieno-triazolo-1,4-diazepine
kDa = kilodaltons
KH = K homology
KHSRP = KH-type splicing regulatory protein (or FUBP2)
KO = Knockout
KRAS = Kirsten rat sarcoma virus
lncRNA = Long non-coding RNA
MAGeCK = Model-based analysis of genome-wide CRISPR-Cas9 knockout
MAX = MYC Associated Factor X
MB = MYC box
MCL1 = Myeloid cell leukemia-1
MCM6 = Minichromosome Maintenance Complex Component 6
MGA = MAX Dimerization Protein
MgCl2 = Magnesium chloride
miRNA = MicroRNA
MIZ1 = MYC-interacting zinc finger protein 1
MNK2 = Mitogen-activated protein kinase interacting protein kinases 2
MOI = Multiplicity of infection
mRBP = mRNA-binding protein
mRNA = Messenger RNA
mTOR = Mechanistic target of rapamycin
mTORC1 = mTOR complex 1
MXD = MAX dimerization protein
MYC = Myelocytomatosis oncogene
N-terminal = Amino-terminal
Na2B4O7 = Sodium tetraborate decahydrate
NaOAc = Sodium acetate
NCBP2 = Nuclear cap binding subunit 2
ncRNA = Non-coding RNA
NELF = Negative elongation factor
Neo = Neomycin resistant gene (or NeoR)
NF-kB = Nuclear factor kappa-light-chain-enhancer of activated B cells
NGS = Next generation sequencing
NHEJ = Non-homologous end joining
NK = Natural killer
NLS = Nuclear Localization Signal
NMD = Nonsense-mediated decay
NOC3L = Nucleolar complex-associated protein 3-like protein (or FAD24)
NuA4 = Nucleosome acetyltransferase of H4
OHT = 4-hydroxyamoxifen
ORF = Open reading frame
OxPhos = Oxidative phosphorylation
p-TEFb = Positive transcription elongation factor b
PABP = Poly(A)-binding proteins
PAN2 = Poly(A)-nuclease subunit 2
PARN = Poly(A)-specific ribonuclease
PARP = Poly(ADP-ribose) polymerase
PBS = Phosphate-buffered saline
PCNA = Proliferating cell nuclear antigen
PCR = Polymerase chain reaction
PD-1 = Programmed cell death protein 1
PD-L1 = Programmed death-ligand 1
PES1 = Pescadillo Ribosomal Biogenesis Factor 1
PEST = Proline, glutamic acid, serine, tyrosine

PI = Propidium iodide
PI3Ks = Phosphoinositide 3-kinases
piRNA = PIWI-interacting RNA
PLK1 = Polo Like Kinase 1
PMO = Phosphorodiamidate morpholino oligomer
PNRC2 = Proline-rich nuclear receptor co-activator 2
PNUTS = Phosphatase 1 nuclear targeting subunit
Pol = Polymerase
PP2A = Protein phosphatase 2A
PRC2 = Polycomb repressive complex 2
pri-miRNA = Primary miRNA
PRMT5 = Protein arginine methyltransferase 5
PROTAC = Proteolysis-targeting chimera
PSF = Polypyrimidine tract binding protein-associated splicing factor
PSMA1 = Proteasome 20S subunit alpha 1
PTBP1 = Polypyrimidine tract binding protein 1
PTC = Premature termination codon
PTCD3 = Pentatricopeptide repeat domain 3
PuroR = Puromycin resistant gene
qPCR = Quantitative PCR
R-CHOP = Rituximab, cyclophosphamide, doxorubicin, vincristine, prednisone
RBD = RNA-binding domain
RBM39 = RNA binding motif protein 39
RBP = RNA binding proteins
RGG = Arginine-glycine-glycine
RMD = Regnase1-mediated decay
RNA = Ribonucleic acid
RNAi = RNA interfering
RNaseA = Ribonuclease A
RNP = Ribonucleoprotein
RNPS1 = RNA binding protein with serine rich domain 1
RP = Ribosomal protein
RPA = Replication protein A
RPE1 = Retinal pigment ephitilial-1
RPMI = Roswell park memorial institute
RRM = RNA-recognition motif
RRM1 = Ribonucleotide reductase catalytic subunit M1
rRNA = Ribosomal RNA
RT-PCR = Reverse transcriptase PCR
Rv = Reverse
S62 = Serine 62
S6K1 = S6 kinase 1
SAE1 = SUMO1 activating enzyme subunit 1
scaRNA = Cajal body-specific RNA
SEM = Standard error of the mean
SERBP1 = SERPINE1 mRNA binding protein 1
SF = Splicing factor
sgRNA = Single-guide RNA
shRNA = Short hairpin RNA
siRNA = Small interfering RNA
Ski7 = Superkiller protein 7
SMD = Staufen1-mediated decay
SMG1 = Suppressor with morphogenetic effect on genitalia 1
SNIP1 = Smad nuclear-interacting protein 1
snoRNA = Small nucleolar RNA
SNP = Single nucleotide polymorphisms
snRNA = Small nuclear RNA
snRNP = Small nuclear RNP
SNRPF = Small Nuclear ribonucleoprotein polypeptide F
SR = Serine and arginine-rich
SRRT = Serrate (or ARS2)
SRSF1 = Serine and arginine rich splicing factor 1
SSC = Side scatter
STAGA = SPT3-TAFII31-GCN5L acetylase
STAT = Signal transducers and activators of transcription
SUMO = Small ubiquitin-like modifier
SYNCRIP = Synaptotagmin binding cytoplasmic RNA interacting protein
T58 = Threonine 58
TAD = Transactivation domain
TBP = TATA-box binding protein
TC = Termination codon
TF = Transcription factor
TCGA = The cancer genome atlas
TGFß = Transforming growth factor ß
Thy1.1 = Thymus cell antigen 1 (or CD90.1)
TNPO1 = Transportin 1
TOP2A = Topoisomerase II alpha
TRA2B = Transformer 2 beta homolog
TRFC = Transferrin receptor protein 1
TRIM71 = Tripartite Motif Containing 71
tRNA = Transfer RNA

TRRAP = Transactivation/transformation-associated protein
TumiD = Tudor- staphylococcal/micrococcal-like nuclease-mediated microRNA decay
U2AF1 = U2 small nuclear RNA auxiliary factor 1
uORF = Upstream ORF
UPF1 = Up-frameshift protein 1
UTR = Untranslated region
WDR5 = WD repeat-containing protein 5
WT = Wild type
XRN1 = 5'-3' exoribonuclease 1
YB-1 = Y-box binding protein 1
YBX1 = Y-Box Binding Protein 1
YTHDF2 = YTH domain-containing family protein 2
ZC3H4 = Zinc finger CCCH-type containing 4
ZnF = Zinc finger

List of Figures

List of Tables and Supplementary Tables

Abstract

Increased expression and activity of the MYC protein is a widespread cancer hallmark and renders tumor cells addicted to sustained activation of a variety of other gene products. Identification of those dependencies can offer new therapeutic approaches against MYC-driven tumors. Previous studies showed that RNA processing events have a critical role in MYC-induced tumorigenesis and survival. Moreover, we and others observed that multiple genes encoding RNA-Binding Proteins (RBPs) were positively regulated upon MYC activation in various cell types. Hence, we hypothesized that the activity of specific RBPs could become rate-limiting for the growth and/or survival of MYC-overexpressing cells. Toward the identification of those RBPs, we set up high-throughput genetic dropout screens, involving both RNAi and CRISPR/Cas9 technologies. We designed lentiviral shRNA and sgRNA libraries targeting 730 RBPs, which we transduced in cell lines allowing controlled super-activation of MYC, in order to identify genes whose expression was specifically required in this condition. A series of candidates emerged from our screens, including UPF1 and XRN1, two RBPs involved in mRNA turnover and in particular in nonsense-mediated mRNA decay (NMD). Biological validation in different systems confirmed our screening results and allowed us to extend our observations to other NMD factors, thus identifying NMD as a critical pathway in MYC-overexpressing cells. Addressing the mechanisms underlying the synthetic lethality between MYC and NMD shall not only allow us to unravel this unexpected crosstalk, but shall also pave the way toward the development of new therapeutic opportunities against MYC-dependent tumors.

1. Introduction

1.1 MYC

1.1.1 The discovery of MYC

The c-*MYC* proto-oncogene, or *MYC*, was discovered ca. 40 years ago as the cellular homolog of the retroviral avian myelocytomatosis oncogene *v-myc*[1,2]. Soon thereafter, the gene was shown to be the target of chromosomal translocation events in human and murine lymphomas[3,4] and to be amplified in other malignancies events in human cancer[5]; since then, *MYC* has recurrently emerged as one of the most common drivers in human cancer[6,7]. Two other members of the MYC family were initially observed in neuroblastoma (hence called N-MYC)[8,9] and in lung cancer (L-MYC)[10] but soon found to be expressed in other cancer types[7,11]. The three MYC proteins are expressed during normal development, with MYC being prevalent in most tissues and its two paralogs showing more tissue-specific distributions[12]. In post-natal life MYC is mostly expressed in dividing cells and is modulated in response to extracellular stimuli, being generally activated by mitogens and repressed by cell-cell contact or differentiation signals[13]. Altogether, MYC acts as a central node in the integration of mitogenic signals and in the implementation of downstream cellular responses; as we shall see below, MYC establishes this connection through the regulation of a great variety of genes involved in cell cycle, apoptosis, differentiation, metabolism, ribosome biogenesis and protein synthesis[6,14–16].

1.1.2 MYC structure, function and interactors

The MYC protein product is a transcriptional factor of 439 amino acids that belongs to the basic helix-loop-helix-leucine-zipper domain (bHLH-LZ) family. The structural organization of the three MYC-family proteins is generally conserved, consisting in an amino-terminal (N-terminal) transactivation domain (TAD; residues 16-143 in MYC; Figure 1)[17], through which co-activators are recruited[18], and a carboxy-terminal (C-terminal) bHLH-LZ (residue 355-439; Figure 1) required for

dimerization with MAX and DNA binding[19–21], through which MYC regulates transcription[21,22] and a widespread range of cellular biological processes[14,15,23,24].

Figure 1. Protein structure of MYC. The MYC protein is composed of 439 amino acids, a N-terminus transactivation domain (TAD, in yellow), a central region rich in proline, glutamic acid, serine and tyrosine (PEST, in blue) and a basic region helix-loop-helix (BHLH) leucin zipper (LZ) domain (in red). The conserved elements or MYC boxes (MB0, MBI, MBII, MBIIIa, MBIIIb and MBIV are indicated in orange). The primary nuclear localization signal (NLSI, light blue) is present within the central region, with a secondary (NLSII) in the basic region. Image adapted from *Beaulieu et al., Cells, 2020* (ref. 16).

N-terminal domain. MYC-mediated regulation of gene expression is achieved by the recruitment of multiple interacting proteins which in turn modulate gene expression, remodel the active chromatin and regulate MYC stability[25]. Interactions take place mostly within the TAD and involve three elements, called "MYC boxes" (MB0, MBI and MBII; Figure 1) initially identified as highly conserved sequences among MYC proteins. This domain was demonstrated to be sufficient for transcriptional activation when fused in-frame with a heterologous DNA binding domain[17]. MB0 mediates a plethora of interactions, for example with PNUTS which regulates MYC stability and oncogenic functions[26,27] and with transcription elongation factors via direct binding to the general transcription factor TFIIF, which is required for tumor initiation and growth[28]. MBI is involved in the ubiquitylation and proteasomal-mediated degradation of MYC and N-MYC, which are characterized by a very low half-life (20 to 30 minutes in normal cells)[29]. Among the many discovered E3 ubiquitin ligases that regulate MYC stability, FBXW7 (or FBW7) is the best-studied which leads to MYC degradation in response to phosphorylation of Serine 62 followed by Threonine 58 (both sites present in MBI)[30]. Both MB0 and MBI were observed to bind to the PIN1 prolyl-isomerase[31], which takes part of the dynamic control of MYC stability by facilitating the two phosphorylation events[32], and, in MYCN, to interact with Aurora kinase A (AURKA), which stabilizes MYC by preventing its binding to FBXW7[33]. Many human B-cell lymphomas are characterized by point mutations in the MBI element, which became a hot spot owing to the loss of FBXW7 binding and the consequent increase in MYC stability[34].

MYC-mediated transformation and apoptosis are modulated by the interaction with BIN1 trough MBI[35]. This region is involved in the interaction through multiple touchpoints with TATA box-binding protein (TBP), part of the multimeric protein complex TFIID responsible for the assembly of RNA polymerase II at the transcriptional start site of gene promoters[36]. Furthermore, MBI interacts with p-TEFb (positive transcription elongation factor b) that is composed of the cyclin-dependent kinase CKD9 and its regulatory subunit cyclin T, and phosphorylates the Serine 2 of the carboxyl-terminal-domain of the larger subunit of RNA polymerase II as well as negative elongation factors NELF and DSIF, thereby enhancing elongation of transcription[37,38]. The MBII region is involved in chromatin remodelling and modification mediated by interactions with coactivators and has been prove to be required for cell transformation[28]: in particular, histone acetyltransferase (HAT)-containing complexes are recruited via TRRAP (transactivation/transformation-associated protein)[28,39], a MYC interactor that is essential for MYC transformation activity[39]. TRRAP is itself an integral subunit of two distinct HAT complexes, STAGA and NuA4, associated with the catalytic subunits GCN5/PCAG and NuA4, respectively, whose activities favour chromatin decompaction and transcriptional activity[18,40–44].

Central region. Other three MBs (MBIIIa, MBIIIb and MBIV) are present in the central region of *MYC* (residues 144-354), which also contains the main Nuclear Localization Signal (NLSI, residues 320-328 – while the second is placed in the bHLH domain and induces only a partial nuclear localization)[45] and a domain rich in proline, glutamic acid, serine and tyrosine (PEST) (Figure 1). MBIIIa, lost in *L-MYC*, has been shown to play an important role for the pro-apoptotic and transforming activities of MYC[46] and to contribute to transcriptional repression, possibly via its association with histone deacetylases[47]. WD repeat-containing protein 5 (WDR5), which is part of various chromatin remodeling complexes, has been demonstrated to interact with MYC through the MBIIIb region and this interaction is important to direct MYC association with a substantial fraction of its target loci on chromatin and for tumor maintenance[48,49]. The MBIV region was initially found important for MYC-

induced apoptosis and transformation[18] and recently also observed involved in transcriptional activation through interacting with the co-transcription factor HCFC1[50].

Altogether, the above examples highlight the complex, modular nature of functional regulatory domains in MYC and other transcription factors: to complicate things further, these domains are largely unstructured, and overlap with low-complexity or intrinsically disordered regions (IDRs), which have been involved in both multivalent interactions and biophysical phase separation, the contributions of which are still controversial[31,51–53] and will not be discussed here in further detail.

C-terminal domain. Unlike transactivation domains, the DNA-binding domains of transcription factors belong to well-defined structural families[54]. As mentioned above, MYC and MAX dimerize and bind DNA through their bHLH-LZ domain, the structure of which was resolved through X-ray crystallography[55,56]. MYC-MAX complex preferentially recognizes a consensus sequence (CACGTG), called Enhancer box (E-box), that is present in the promoter of target genes and through which MYC activates transcription[19–22,57]. In line with these early findings, recent genomic data indicate that the association with E-boxes in promoters correlates with transcriptional activation by MYC[15,58] and is required for MYC-dependent gene regulation[59].

Beyond dimerization, the MYC and MAX bHLH-LZ domains are likely to mediate interactions with other proteins, such as MIZ1, which can mediate both MYC oncogenic functions as well as tumor-suppressive responses to its oncogenic levels[60–62]. Finally, besides MYC/MAX dimers, MAX can form homodimers, as well as heterodimers with a series of other bHLH-LZ proteins (MXD1-4, MNT or MGA): these proteins interact with a variety of co-repressors and are generally viewed as MYC antagonists[25,63,64], but may in some cases have more subtle activities that support the oncogenic action of MYC[65].

1.1.3 MYC regulation

The accumulation of MYC is tightly controlled in normal cells, at all stages of the protein's life cycle, including its synthesis, sub-cellular distribution and degradation.

These regulatory processes, which I shall briefly introduce below, can be altered at multiple levels in cancer cells, contributing to aberrant MYC accumulation and to its oncogenic activity[6,15].

Transcription of MYC. *MYC* was identified as one of the so-called immediate-early genes, the expression of which is directly induced by serum mitogens in the absence of intervening proteins synthesis[66,67]. Further works showed that growth-regulatory and oncogenic signalling pathways generally activate MYC expression, as exemplified by NOTCH1[68], WNT[69], Hedgehog[70], B-cell receptor[71,72] or JAK-STAT signalling[73]. In a reciprocal manner, growth-inhibitory pathways, such as TGFß signalling in epithelial cells[74], generally repress *MYC* transcription. Altogether, the control of *MYC* transcription is a key convergence point of mitogenic signalling pathways, through which cells integrate those signals; most of the same pathways can be deregulated in cancer, leading – among other effects – to aberrant MYC expression[15]. Furthermore, a negative feedback regulation constrains MYC levels in normal cells, in case of ectopic expression of MYC which represses endogenous *Myc* expression, while in transformed cells this regulation is frequently disrupted enabling expression of elevated levels of MYC[75].

MYC mRNA stability. The export of MYC mRNA into the cytoplasm in regulated by the translation initiation factor eIF4E[76] in response to mitogenic signals. The half-life of MYC mRNA is very short as well[77] and finely controlled by a numbers of RNA binding proteins such as AUF1[78],ELAVL1 (or HuR)[79], IGF2BP1 together with 4 associated proteins (HNRNPU, SYNCRIP, YBX1 and DHX9)[80] and AGO2[81], as well as by microRNAs[82,83].

Translation of MYC. Translation of the MYC mRNA into protein is another step that can be regulated in cells. In particular, the mTORC1 downstream effector S6K1 positively modulates the efficiency of MYC translation by regulating the phosphorylation state of eukaryotic initiation factor eIF4B, necessary for the 5' UTR unwinding of MYC[84]. Indeed, this untranslated region presents a complex structure which obstructs translation initiation[85] and requires an additional level of control given by an internal ribosome entry site (IRES) that recruits the ribosomal subunits

and induces an alternative translation initiation[86]. It has been observed that ribosome recruitment is dependent upon the presence of four identified proteins, GRSF-1, YB-1, PSF and its binding partner P54NRB, that bind to the MYC family IRESs[87]. Furthermore, particular stress agents, such as UV irradiation, known to induce DNA damage and possible oncogenic mutations, can suppress MYC mRNA translation via association of the TIAR protein with the 3' UTR, which promotes the formation of translationally silent stress granules[88]. It is not surprising, given the multitude of roles of MYC and its potential capacity of cell transformation, that both transcription and translation are highly regulated through multiple ways.

MYC protein stability. A number of mechanisms and pathways have been shown to impact MYC protein stability. First, MYC turnover is stringently regulated by the ubiquitin-proteosome system (UPS). As mentioned above (see section 1.1.2), the best-studied E3 ubiquitin ligase that controls MYC stability is FBW7: as other F-box proteins, FBW7 is the substrate-targeting subunit of an SCF-type (Skp–Cullin–F box) RING-FINGER domain ubiquitin ligase complex[89] – in this case, denoted as SCF^{FBW7} complex. The FBW7-mediated turnover of MYC is controlled by two conserved phosphorylation sites within MBI, threonine 58 (T58) and serine 62 (S62), which are part of a phospho-degron sequence that is recognized by FBW7. In response to growth stimulation, S62 is phosphorylated by ERK and/or CDKs[90,91] thus stabilizing MYC protein. Following PIN1-mediated proline 63 isomerization, S62 phosphorylation augments MYC transcriptional activity at pro-proliferative target genes[92,93]. Phospho-S62 primes the subsequent T58 phosphorylation by GSK-3ß[94,95], which allows a second PIN1-mediated isomerization step to facilitate PP2A-mediated dephosphorylation of the phosphate at S62[96,97]. Finally, phosphoT58-MYC is recognized by FBW7 which promotes 26S proteasome-mediated MYC degradation[30,98].

A regulator of FBW7-mediated degradation is USP28, a ubiquitin-specific protease that cleaves ubiquitin chains to antagonize the activity of ubiquitin[99]. USP28 binds MYC via interaction with FBW7 and stabilizes MYC in tumor cells[100]. However, this does not happen in case of UV irradiation, which induced DNA damage leads to a

dissociation of USP28 from FBW7 and consequent MYC degradation[101]. Another FBW7 antagonist is the F-box protein b-TRCP, which binds to a phospho-recognition sequence of MYC and mediate direct ubiquitination of the amino terminus that stabilizes the protein for cell cycle reentry after S-phase arrest[102]. Yet another F-box protein, SKP2, has been shown to mediate MYC poly-ubiquitination and degradation of MYC, but in this case in a phosphorylation-independent manner[103]: this factor can bind to both the N- and C-termini of MYC, and also acts as a transcriptional coactivator of gene expression and oncogene[103,104]. Other ubiquitin ligases, including HECTH9, TRUSS, TRIM32, FBX29 and CHIP also contribute to MYC turnover, and will not be discussed here in detail (reviewed in ref. 30).

As ubiquitination occurs on Lysine, other modifications of the same residues may compete with it. This was proposed for acetylation, which was also shown to induce MYC protein stabilization[105–107]. Likewise, the small ubiquitin-like protein SUMO can also be conjugated to MYC proteins[108–110] and may add a further level of competition with the above processes. Indeed, the SUMO E3 ligase PIAS1 SUMOylates MYC to promote MYC phosphorylation at Serine 62 and dephosphorylation at Threonine 58 which brings to a reduced MYC turnover and subsequently an increased transcriptional activity[111].

Finally, it is noteworthy here that MYC can also be cleaved by calpains in a calcium-dependent manner in the cytoplasm[112]. The site of cleavage is in the central region of the protein structure, which produces a "MYC-nick" of 298 amino acids amino-terminal segment and the removal of all the remaining carboxyl terminus, necessary for nuclear import, DNA binding and transcriptional activity[113].

1.1.4 MYC: a general or a selective transcription factor?

Numerous studies have profiled the association of MYC with the genomic DNA in live cells, based on chromatin immunoprecipitation (ChIP) followed by qPCR[114], microarray hybridization[115–118] and most recently high-throughput sequencing (ChIP-seq)[119–121]. Altogether, two major observations have emerged from these studies: (i.) MYC shows promiscuous binding profiles, cross-linking to a large

fraction of promoters and distal elements (enhancers) across the genome; (ii.) MYC binding is strictly associated with chromatin features that mark active promoters and enhancers, such as histone H3 lysine 4 methylation (H3K4me3, H3K4me1), lysine 27 acetylation (H3K27ac), CpG islands, presence of the basal transcription machinery (in particular RNA Polymerase II) and DNaseI-hypersensitive sites[118,122,123]. Genome-wide binding profiling showed that MYC can be present at both promoters and enhancers according to its level of expression: when it is low (physiological condition) MYC is preferentially detected to high affinity sites (E-boxes), whereas in high-expressed condition it "invades" many other low affinity sites in an active chromatin state[120,121,124,125].

These observations led to the proposal that MYC does not act as a classical sequence-dependent transcription factor, but rather as a general amplifier of transcription at all expressed loci: according to this model, MYC overexpression in cancer cells would result in widespread binding to all active promoters and enhancers, which would in turn produce a global increase - termed "amplification" - of transcriptional activity and RNA levels[120,124].

Based on data produced in our laboratory[58,59,121,126–128], new data by other groups[129] and careful interpretation of the evidence presented in the aforementioned studies, our own group has confuted this amplification model, as discussed in several publications[15,59,130]: altogether, the available body of data point to one unifying model according to which MYC acts as a transcriptional activator/repressor of a discrete set of genes, leading to the activation – among others – of anabolic and biosynthetic pathways that drive the secondary increases in global RNA and protein production. Thus, the observed widespread binding is actually productive (i. e. generates new RNA molecules) for only target genes. More recently, the specificity of MYC-mediated gene activation was also confirmed by acutely degradation of MYC which lead to the downregulation of only few genes, differently from the general transcriptional shutdown upon degradation of Brd4, a general transcriptional co-factor[129,130].

1.1.5 Biological functions of MYC

As outlined above, MYC regulates genes involved in key biological processes and pathways: some of these are illustrated in Figure 2 and briefly discussed here.

Cell Growth and Proliferation. As outlined above, a key function of MYC is to promote cell growth and proliferation in response to mitogens. This is achieved through the regulation of multiple processes, that collectively contribute to cellular activation.

First, MYC can directly impact on cell cycle control, by either inducing genes involved in cell cycle entry (such as *cyclin D* and *cyclin E*) or repressing genes coding for cell cycle inhibitors (*p27*, *p21* and *p15*), as previously reviewed[131,132]. MYC also regulates genes involved in DNA replication and, beyond its transcriptional activity, has been proposed to directly impact the replication process[133–135].

Another essential link between MYC activity and cell growth/proliferation – perhaps the main one – lies in the regulation of pathways involved in biomass accumulation and energy production. In particular, MYC promotes the accumulation of ribosomal proteins and other components of the protein biosynthetic apparatus, and upregulates enzymes implicated in different metabolic processes, such as glycolysis, glutaminolysis, lipogenesis, mitochondrial biogenesis, iron metabolism and purine and pyrimidine biosynthesis[136,137]. By modulating cell metabolism and protein synthesis, MYC functions lead to the accumulation of cell mass and cell size, stimulating overall cell growth[138,139]. Most remarkably, this represents a fundamentally conserved function if MYC, from Drosophila to humans[140].

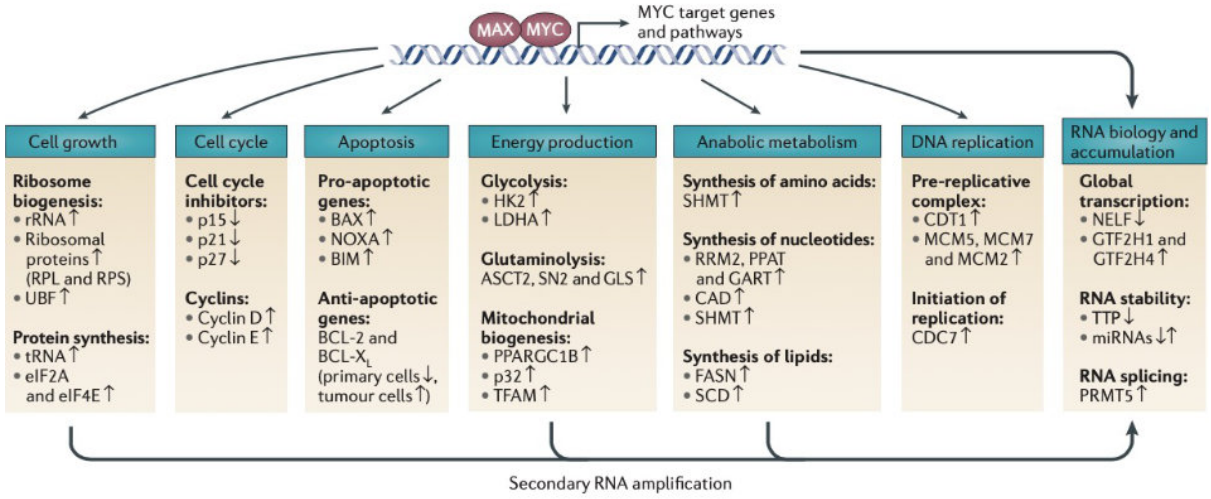

Figure 2. Main genes and pathways regulated by MYC. Schematic representation of the main processes and pathways regulated by MYC, with a list of some of the gene products involved (note that this is a selected list, and represents a small minority of MYC-regulated genes). Details of the pathways and genes illustrated here are described in the text. Image adapted from *Kress et al., Nature Review Cancer, 2015* (ref.15).

RNA biology. Following from the above, MYC regulates ribosomal biogenesis by inducing the synthesis of multiple factors: ribosomal RNA (rRNA) via RNA polymerase I; ribosomal subunits, factors for rRNA processing and for ribosomal subunit transport as well as the eukaryotic translation initiation factors (such as eIF2A and eIF4E) via RNA polymerase II; finally tRNAs mediated by RNA polymerase III[141–145]. For example, nucleolin, nucleoplasmin, *Nop56* and others are known MYC target genes which process rRNAs into 18S, 5.8S and 28S rRNAs[146]. Hence, MYC not only regulates the transcription of genes encoding components of the translation machinery, but also ensures their proper maturation.

As hinted above, MYC also regulates genes that, in turn, contribute to global RNA production: by inducing the expression of general transcription factors and co-factors, such as GTF2H1 and GTF2H4[121]. MYC also regulates expression of other transcription factors, with specific impacts on transcriptional profiles: an example is AP4, which was shown to maintain actively expressed MYC-target genes and the activation state of CD8+ T lymphocytes following immune stimulation and transient MYC expression[147]. Another mechanism by which MYC regulates RNA abundance is mediated by the indirect control of RNA stabilization. For example, Smad nuclear-interacting protein 1 (SNIP1) was first found as interacting with MYC and enhancing its transcriptional activity and protein stability[148] and then observed as

co-transcriptionally and post-transcriptionally regulator of some MYC target gene mRNAs[149]. Moreover, during lymphomagenesis MYC can repress the tristetraprolin (*Ttp*) gene, which function is to degrade AU-rich element (ARE)-containing mRNA, thus indirectly stabilizing 16% of coding gene mRNAs[150,151].

Another important function of MYC is provided by its impact on RNA splicing. Indeed, MYC modulates the transcription of RNA binding proteins involved in alternative splicing, such as the splicing factors serine/arginine-rich splicing factor 1 (SRSF1)[152], the heterogeneous nuclear ribonucleoprotein A1 and A2 (hnRNPA1/2)[153] and the core small nuclear ribonucleoprotein particle (snRNP) assembly genes, including the protein arginine N-methyltransferase 5 (PRMT5)[154]. Finally, during iPSC reprogramming, MYC and its transcriptional co-activator SAGA (i. e. the GCN5 HAT complex) regulate the transcription of splicing factors critical for pluripotency[155].

Apoptosis. Beyond its function in inducing cell division, MYC can also trigger apoptosis as a safety mechanism to defend against inappropriate proliferation. This death program is balanced by the presence of survival factors, thus prevailing apoptosis results when MYC expression is deregulated in conjunction with the absence of specific survival factors or presence of anti-proliferative signals[156–159]. In line with these findings, MYC-null mouse cells were incapable to undergo apoptosis under diverse apoptotic stimuli[160,161]. Mechanism by which MYC induces programmed cell death are diverse, and were reviewed previously[162,163]: in a nutshell, MYC can activate both the ARF-MDM2-p53 axis (in particular through the induction of ARF) and the intrinsic apoptotic pathway (through up- and down-modulation of diverse BCL2-family members), both of these mechanisms contributing to the suppression of MYC-induced tumors[160,164–174].

Altogether, MYC constitutes a key regulatory node in the control of cell proliferation and death. Among the fundamental processes regulated by MYC, the control of RNA biology (biogenesis, maturation and turnover) appears to be particularly critical for its biological and oncogenic activities. This is further highlighted by additional findings, such as the synthetic-lethal interactions between

MYC and components of the splicing machinery[154,175,176] (see below, section 1.1.8), and provides a fundamental rationale for the work described in this thesis.

1.1.6 MYC as an oncogene

Cancer is a complex disorder characterized by countless genetic events and the acquisition of the hallmarks of cancer[177], many of which can be promoted by MYC activation, such as proliferation, cell survival, self-renewal, metabolism, genomic instability, invasiveness, angiogenesis and ultimately immune evasion (Figure 3)[64,178]. Indeed, the central position of MYC in the cellular circuity (Figure 2; see above) endows MYC with potent oncogenic activity when aberrantly expressed[6,7,14,179]. As a matter of fact, deregulated MYC signalling has been suggested to be a molecular hallmark of cancer on its own[180].

In a milestone paper of 1985, Adams and colleagues[181] showed that transgenic overexpression of MYC in mice was sufficient to generate B cell lymphomas (see also paragraph 1.1.9). However, additional mutagenic events were found to be necessary for tumor formation and maintenance as evidenced by a significant delay before tumor[182,183]. As illustrated above by MYC-induced apoptosis, activation of MYC in normal cells elicits protective mechanisms that limit uncontrolled proliferation and tumor development. Depending on the tissue and circumstances, these mechanisms may also include cell cycle arrest or cellular senescence, which like apoptosis may be mediated by p53, cell-cycle checkpoint, or others: hence, inactivation of such genes (or activation of anti-apoptotic factor or cell-cycle stimulators) can cooperate with MYC signaling to drive cancer initiation and/or progression[164,165,184–190].

Differently from oncogenes like *Ras*, typically mutated in their coding sequence[191], oncogenic activation of *MYC* occurs primarily through mechanisms that cause its deregulated expression, including genomic alterations that directly alter the locus, or mutations that leave *MYC* intact, but impinge on its regulation, at multiple levels: these mechanisms will be briefly introduced below.

Genomic alterations. As shown in Figure 4, the three *MYC* genes altogether show a substantial high prevalence of genetic alteration across 16 major human cancer

types included in the TCGA (The Cancer Genome Atlas)[179], with *MYC* being more frequently altered than *MYCN* or *MYCL*. Gene amplification and chromosomal translocations constitute the main genomic alterations of *MYC* (Figure 5, left)[7,192,193], with amplification being found in solid tumors and translocations in B or T cell leukaemias and lymphomas[192,194]. For example, Burkitt's B-cell lymphomas can be characterized by a reciprocal translocation involving a portion of *MYC*-carrying chromosome 8 and chromosome 14 or, less frequently, chromosomes 2 and 22, all of which carrying immunoglobulin gene elements[3]. Other translocation events were found in other types of B-cell lymphomas, such as follicular B-cell lymphoma, diffuse large B-cell lymphoma and chronic lymphocytic leukemia, as well as multiple myeloma, all characterized by a more aggressive clinical picture and poor prognosis[180,195,196].

Transcriptional alterations. MYC can be aberrantly expressed also in an indirect manner, triggered by abnormal activity of other oncogenes acting in upstream signalling pathways (see section 1.1.3 – Transcription of MYC) such as WNT in colon cancer[69,197], NOTCH in T-cell leukemia[68,198] or STAT3[73]. On the other hands, the loss of tumor suppressors such as APC[69] can result as well in MYC overexpression and oncogenesis (Figure 5, centre).

Of particular interest, transcriptional deregulation of MYC may also be driven by different Single Nucleotide Polymorphisms (SNPs) present in distal regulatory elements: such SNPs, generally identified through GWAS studies for cancer association, may impact on MYC transcription by modifying binding sites for regulatory transcription factors[199–201].

Post-translational alterations. An additional mechanism through which MYC activity is augmented is increased protein stability (Figure 5, right). As said above, MYC protein half-life is very short and finely regulated through phosphorylation events and consequent proteasomal degradation (see paragraph 1.1.2)[90]. Tumors with high levels of the phospho-Serine 62 (pS62) and low phospho-Threonine 58 (pT58) have been found[97,98]: increased pS62, hence MYC accumulation, may follow from a series of events, including activation of mitogenic pathways (such as RAS-

MEK-ERK), decreased levels of the serine/threonine phosphatase PP2A, elevated PIN1 (which functionally regulates MYC phosphorylation trough isomerization)[97,202–204], as well mutations that affect the T58 residue of MYC[205]. Moreover, the E3 ligase FBW7 that controls MYC proteasomal degradation via ubiquitination is a tumor suppressor, frequently inactivated in human cancer[206,207]. Altogether, MYC overexpression occurs in up to 70% of human tumors[6].

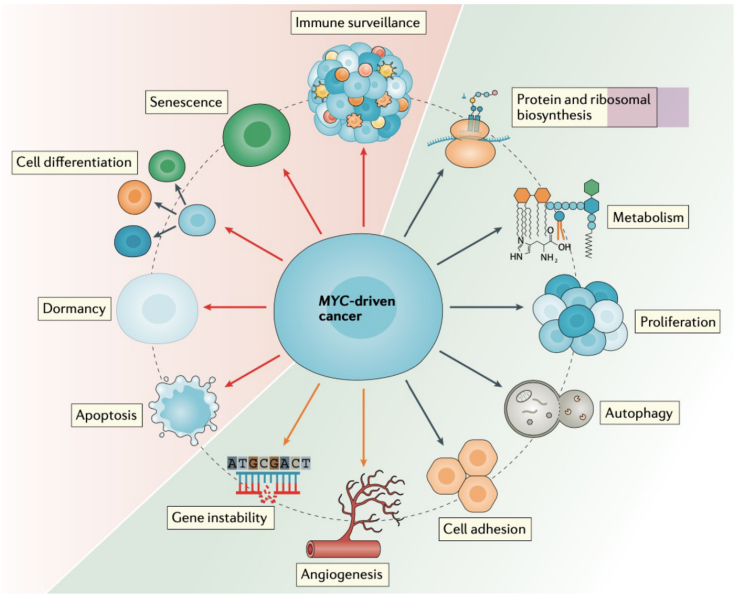

Figure 3. MYC regulates cancer cell-intrinsic and host-dependent processes. MYC oncogenic functions comprise cell growth and survival (green area) by regulating proliferation, metabolism, invasiveness, autophagy, gene instability, cell adhesion, protein and ribosomal biosynthesis, as well as inhibition of cellular protective mechanism (red areas), such as senescence, cell differentiation, dormancy and apoptosis[208]. In particular, MYC enables tumor cells to evade and inhibits immune surveillance and ultimately drives cancer progression[208]. Image adapted from *Dhanasekaran et al., Nature Reviews Clinical Oncology, 2021* (ref. 208).

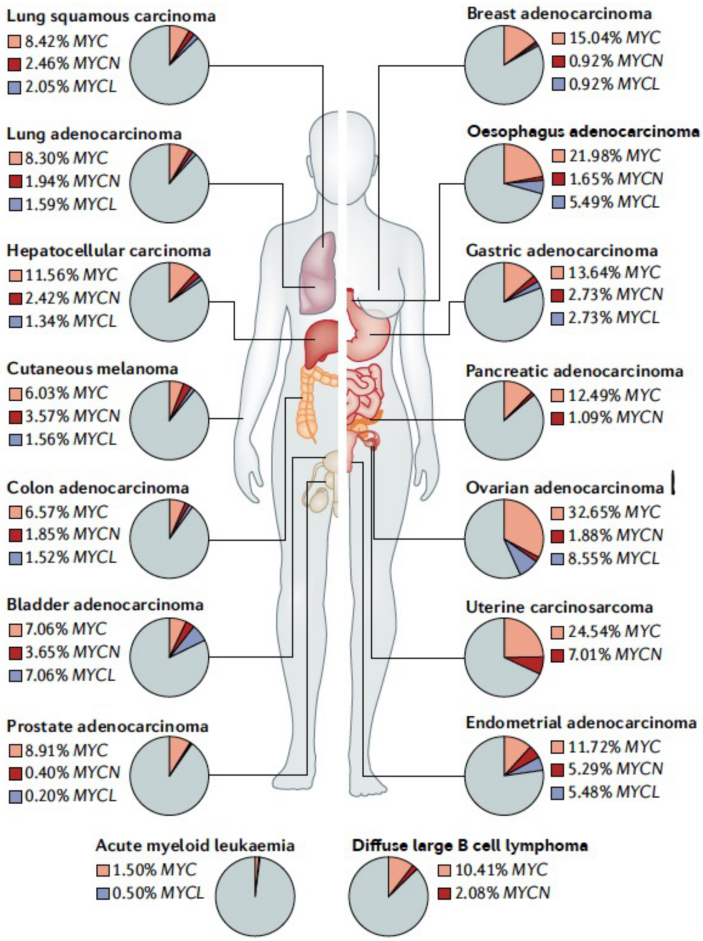

Figure 4. Prevalence of genetic alterations of MYC proteins in human cancers. Genetic alterations involving MYC and its paralogues, MYCL and MYCN, comprise gene amplification, prevalence of which is indicated in 16 major human cancer types in The Cancer Genome Atlas[179]. Image adapted from *Dhanasekaran et al., Nature Reviews Clinical Oncology, 2021* (ref. 208).

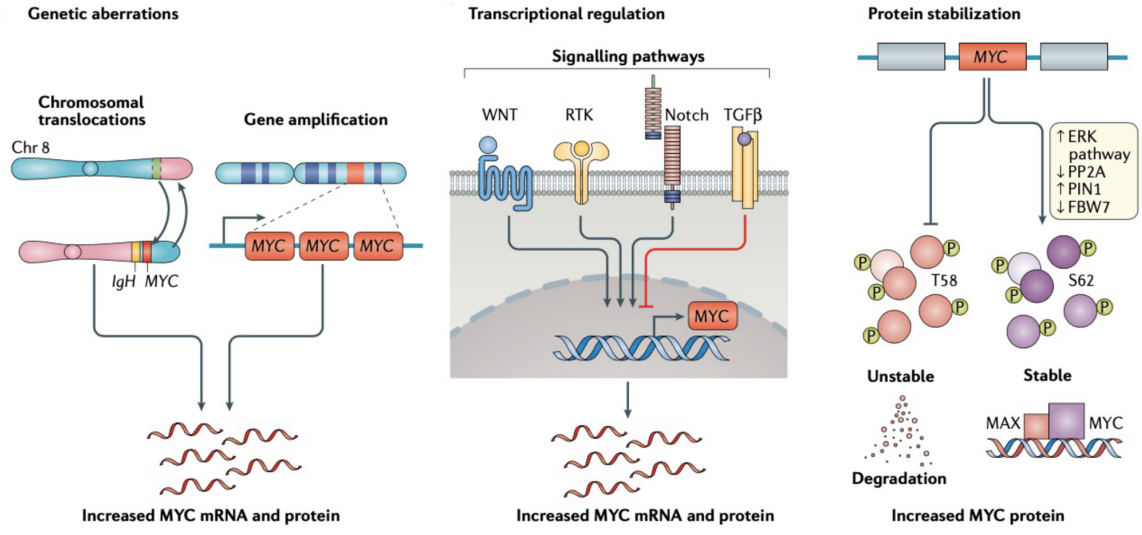

Figure 5. Schematic representation of the main mechanisms of MYC activation in cancer. MYC-mediated cell transformation is generally due to its elevated expression level which can be observed through either genomic aberration (such as gene amplification or specific chromosomal translocation, left), alteration of upstream regulatory pathways, that amplify MYC expression (center) or post-translational modifications of the MYC protein, such as phosphorylation of S62 which promote stabilization of MYC[208]. Image adapted from *Dhanasekaran et al., Nature Reviews Clinical Oncology, 2021* (ref. 208).

1.1.7 Direct targeting of MYC in cancer

Preclinical models of MYC-driven cancers showed that MYC inactivation can induce sustained tumor regression, a phenomenon referred to as oncogene addiction[209], mediated by both cell-autonomous and systemic mechanisms – the latter dependent on the host immune system and tumor microenvironment[182,210,211]. The specific mechanisms that lead to tumor involution depends on the tissue and genetic context. For example, MYC inactivation induces cell death, senescence and apoptosis in preclinical models of T cell acute lymphoblastic leukemia[182], bone differentiation on osteosarcomas[210], and cellular dormancy in lung adenocarcinoma, hepatocellular or renal cell carcinoma[212–214]. *MYC* oncogene addition can be present also in tumors that are not originated by MYC alterations, as for $KRAS^{G12D}$- or SV40-driven tumors[215].

The above observations indicated that MYC is involved not only in tumor initiation but also in tumor maintenance[180]. This view, coupled with the occurrence of widespread alterations of MYC activity in different tumors, makes targeting MYC one of the most appealing approaches for treating human cancer. However, for many years MYC has been considered undruggable, mainly due to its nuclear localization, intrinsically disordered structure, lack of a defined pocket for ligand binding site as well as its essential physiological function for the maintenance of normal tissue[216]. Despite decades of efforts towards the identification of a pharmacophore capable of overcoming these difficulties, no specific MYC inhibitor has reached the clinic yet. To overcome this issue, other efforts aimed at suppressing MYC activity by interfering with its production or function (Figure 6).

Targeting MYC transcription. MYC expression is regulated by multiple factors, such as bromodomain proteins, whose pharmacological inhibition causes down-regulation of MYC and of its target genes[217,218]. In particular, the bromodomain protein 4 (BRD4) is a transcriptional and epigenetic regulator with histone acetyltransferase activities that induces transcription of key proto-oncogenes like *MYC*. Very recently, it was also reported that BRD4 directly phosphorylates MYC, leading to MYC ubiquitination and degradation[219]. A selective small-molecule

inhibitor of the BRD4 bromodomain, JQ1, caused cell cycle arrest and cellular senescence in three murine models of multiple myeloma[218]. Significant antitumor activity was also reported in xenograft models of Burkitt's lymphoma and acute myeloid leukemia[217] and in three neuroblastoma models, where a robust correlation between *MYCN* amplification and sensitivity to bromodomain inhibition was observed[220]. However, bromodomain proteins control a plethora of other genes and their inhibitors are far from acting in a MYC-specific manner[129,221]. Moreover, in case of BRD4 inhibitors, this strategy would be limited to those cancer cases in which BRD4 is the predominant regulator of MYC transcription, and may be ineffective in a subset of tumors with *MYC* gene amplification or protein stabilization[222].

CDK9, the catalytic subunit of p-TEFb, is associated with BRD4 and is one of the major components of the MYC transcription regulatory complex[38,223,224]; indeed, its suppression leads to the abrogation of MYC and MYC-dependent transcriptional programs, resulting in tumor regression in MYC-driven hepatocellular carcinoma and B cell lymphomas[225,226].

As a super-enhancer-associated oncogene, MYC transcription is also dependent on CDK7 activity in addition to BRD4[227]. The CDK7 inhibitor THZ1 has been reported to have anti-proliferative efficacy in a wide-ranging models of cancer or cancer cells, including (i.) pre-clinical models of small cell lung cancer with high MYC expression[228], (ii.) neuroblastoma cells and a mouse model of high-risk neuroblastoma, where THZ1 selectively disrupts the transcription of amplified MYCN, resulting in significant global repression of *MYCN*-dependent transcriptional amplification and tumor regression, without toxicity[227] (iii.) hepatocellular carcinoma with high MYC expression, where THZ1 treatment significantly impaired tumor growth[229], (iv.) patient-derived xenografts models of ovarian cancer patients, where administration of THZ1 induces significant tumor growth inhibition and MYC expression abrogation[230].

Finally, MYC transcription can be effectively reduced with small molecules that alter the topology of the DNA upstream of the *MYC* gene in order to stabilize the *MYC* G-quadruplex, thus repressing its transcription[231,232].

Targeting MYC translation and protein stability. Decreasing MYC synthesis or altering its stability has emerged as another possible approach for targeting MYC. For example, inhibitors of the PI3K-AKT-mTOR signaling pathway can block MYC translation[233], and inhibition of the translation initiator eIF4A by silvestrol can reduced MYC synthesis and block tumor growth[234] by acting on both 5' cap- and IRES-dependent translation. Indeed, MYC can be translated through both mechanisms, with IRES-dependent translation in presence of ER (endoplasmic reticulum) stress, mediated by hnRPA1 and Rps25[86]. The blockage of hnRNPA1 binding to the MYC IRES induces toxicity only in ER-stressed cells, suggesting that it might be a good therapeutic candidate[86].

Another approach has been tested by delivering *MYC* small interfering RNA (siRNA)[235] molecules with different approaches (such as nanoliposomes)[236], although a poor pharmacokinetic ensues to be the limiting development factor. Antisense oligonucleotides have been used specifically against the *MYC* mRNA in primary transgenic mouse model of hepatocellular carcinoma and found to impairs tumor progression as well as induce immune response[237], as well as in prostate cancer, where they led to hydrolysis of the MYC mRNA by RNase H activity[238] . A neutral antisense phosphorodiamidate morpholino oligomer (PMO) was shown to specifically inhibit MYC expression in multiple solid tumors, such as lung and prostate cancer[239,240].

Most noteworthy here, IGF2BP1 and its four associated factors (HNRNPU, SYNCRIP, YBX1, and DHX9) are essential to ensure stabilization and translation of the *Myc* mRNA[80]. Depletion of polyamines by inhibition of ornithine decarboxylase increased the levels of CELF1 which binds to 3'-untranslated region (UTR) of *Myc* mRNA and repressed MYC translation without affecting total *Myc* mRNA levels by competing with ELAVL1 (or HuR), which binds the same region but induces the opposite process[241].

Finally, inhibitors targeting factors involved in MYC protein stabilization can induce its proteasomal degradation, with potential therapeutic effects. For example, Aurora kinase inhibitors allow N-MYC protein degradation without systemic toxic effect[242], and inhibitors of PLK1, which regulates FBW7 for MYC ubiquitination, induce potent apoptosis of MYCN-amplified neuroblastoma and lung cancer cells[243]. Moreover, specific protein degraders or proteolysis-targeting chimaeras (PROTACs) are emerging as a promising strategy to directly and specifically degrade transcription factors such as BRD4[244], albeit MYC-specific PROTACs are still to be developed.

Targeting the MYC-MAX interaction. An alternative to the depletion of MYC levels is to target the interaction between MYC and its obligate partner MAX. Numerous small molecule inhibitors have been developed in order to inhibit MYC/MAX dimerization or DNA binding, or alternatively stabilize the monomeric form of MAX, although their therapeutic utility has so far been limited by poor bioavailability, rapid metabolism, inadequate target site penetration and unclear off-target activities[245,246]. Alpha-helix mimetics, which do not induce the dissociation of MYC-MAX heterodimerization but prevent their binding to DNA, have also shown encouraging effects[247].

A successful alternative has been the development of Omomyc, which to date is the only promising candidate to have entered clinical trials[248]. Omomyc is a mutant form of the MYC protein with an altered leucine zipper, which dimerizes with wild type MYC, while MYC cannot homodimerize. The forming dimers bind to DNA with low affinity, resulting as dominant negative of MYC, hence impairing MYC-regulated transcription[249,250]. Of note, Omomyc selectively binds to MYC, N-MYC, MAX and MIZ-1 but no other HLH proteins. While preventing MYC binding to promoter and transactivation of target genes, Omomyc may maintain MYC/MIZ-1-mediated activity[251]. The effects of Omomyc are reduced proliferation and increased apoptosis, particularly in MYC over-expressing cells[252], while toxic effects were minor and reversible[253]. In different preclinical models of MYC driven tumors, Omomyc showed efficacy and promising effects[215,247].

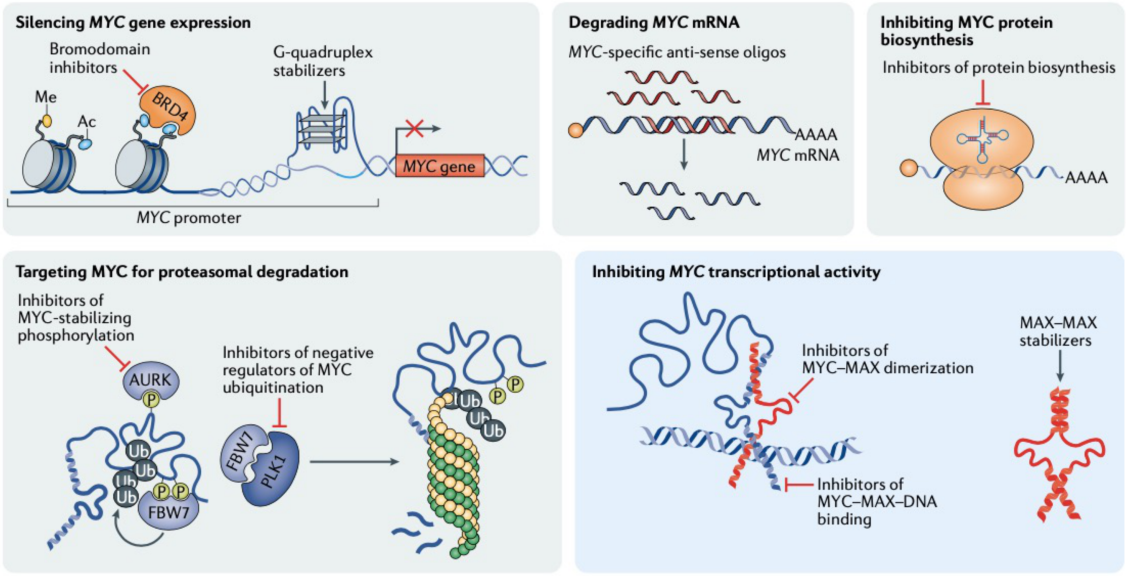

Figure 6. Therapeutic strategies to directly target MYC. Direct targeting of MYC can be exploited by interfering with MYC transcription at DNA level to silence its expression, by inducing degradation of MYC mRNA, by inhibiting MYC translation, by inducing MYC proteasomal degradation or finally by blocking MYC-MAX heterodimerization or its binding to DNA[208]. Image adapted from *Dhanasekaran et al., Nature Reviews Clinical Oncology, 2021* (ref. 208).

1.1.8 Indirect targeting of MYC: synthetic lethality as therapeutic strategy

In the context of cancer cells, MYC-mediated activation of proteins and pathways required for survival of the oncogene-addicted cells generates, as consequence, different cellular changes and dependency conditions which are not present in normal cells. The concept of "synthetic lethality" was first introduce by Dobzhansky in 1946 and is defined by the deleterious phenotype achieved by perturbing two genes in combination, but by neither individually[254]. This definition has been then extended in the context of cancer for the study of how particular oncogenic mutations may sensitize tumor cells to those therapies targeting synthetic-lethal factors, in order to avoid severe toxic effects on normal tissues. A classic synthetic lethal gene interaction in cancer therapy is the inhibition of poly (ADP-ribose) polymerase (PARP) in BRCA-deficient tumors, based on the failure of the targeted cells to repair damaged DNA[255–257].

Almost 20 years ago, Wang et al. proposed the concept of MYC-mediated synthetic lethality, induced by TRAIL- and death receptor 5 (DR5)-agonists, taking advantage of MYC's intrinsic ability to prime cells to apoptotic stimuli[258–260]. Of note,

this synthetic lethal interaction was recently confirmed in human breast cancer cells and their brain-metastatic derivatives, providing important new therapeutic options[261]. The Wang study first suggested that MYC-dependent tumor cells might be eliminated by targeting partner oncogenes of MYC that are required for survival of the MYC-addicted cells, as a new approach to selectively eradicate MYC-driven tumors (Figure 7). In this regard, functional genomics approaches with either siRNA/shRNA-based knockdown or sgRNA-mediated knockout, have been employed in synthetic lethal screens in order to identify critical MYC effectors[262].

The screening approach. A number of screens have been performed in cells with normal or elevated levels of MYC to compare the phenotypic and molecular responses between the two conditions and identify MYC vulnerabilities. Among these, three put the basis for the development of our project:

1. Toyoshima et al.[263] used a high-throughput approach with siRNAs designed to target thousands of druggable genes and miRNAs, and compared the effects of silencing those targets in MYC-overexpressing fibroblasts and in their isogenic controls. Genes that showed synthetic lethality with MYC-overexpression were involved in cellular pathways known to be regulated by MYC: cell cycle, DNA damage repair, apoptosis, senescence, ribosome biogenesis, transcription and transcriptional elongation, chromatin modification and metabolism. Pescadillo homolog 1 (*PES1*), cat eye syndrome chromosome region candidate 2 (*CECR2*) and casein kinase 1 epsilon (*CSNK1)* were validated with a major focus on *CSNK1*, which encodes the CK1**ε** protein, a regulator of DNA replication, cell cycle and circadian rhythm, the expression of which correlated with MYC in different human cancers. They further validated the synthetic lethality through *CSNK1* knockdown in MYCN-amplified glioblastomas[263].
2. Huang et al.[224] performed a screen with shRNA targeting 442 genes for which small molecule inhibitors were already present, in a MYC-driven hepatocellular carcinoma characterized also by p53 loss. The kinase component of the p-TEFb complex, CDK9, which favors RNA polymerase

II pause-release and elongation, was identified as essential for the sustainment of MYC overexpressing cells[224].

3. Kessler et al.[264] ran another synthetic lethal screen that identified SAE2, a SUMO-activating enzyme, as a crucial factor in MYC-hyperactivated cells. Knockdown of SAE2 induced spindle defects, aneuploidy and consequent cell death in MYC-overexpressing cells only, owing to the absent SUMOylation-mediated transcription of genes involved in the assembly and maintenance of the mitotic spindle[265]. Subsequently, MYC-mediated SUMOylation was further confirmed to be a therapeutic vulnerability for B-cell lymphoma[266]. Another recent study reported that MYC amplification in pancreatic ductal adenocarcinoma increases the sensitivity to pharmacological SUMO inhibition[264].

Other RNAi-based screens targeting kinases revealed additional MYC-dependent vulnerabilities. In particular:

i. Pharmacological inhibition or knockdown of PRKDC, which directly modulates MYC expression and plays a key role in DNA damage response (DDR), induced cell death in MYC-overexpressing human lung fibroblasts or cancer cell lines[267].

ii. Inhibition of AMPK-related kinase 5 (ARK5) – which regulates splicing[268] and many aspects of cellular metabolism by the modulation of AMPK, the inhibition of mTORC1 downstream signaling (hence protein synthesis), the maintenance of mitochondrial respiration and glutamine metabolism – leads to the loss of ATP production and the activation of cell death programs in MYC-overexpressing cells[269].

iii. Knockdown of glycogen synthase kinase 3β (GSK3ß) – which plays a central role in a wide variety of physiological and pathological processes and phosphorylates MYC for its recognition by the E3 ubiquitin ligase component and tumor suppressor FBW7 – potentiates TNF-related apoptosis by stabilizing MYC and increasing the expression of the TRAIL

death receptor ligand, DR5, which activates the extrinsic apoptotic pathway[270].

iv. The pharmacological inhibition of PIM1 in human-derived aggressive breast cancer cells with elevated MYC expression and in MYC-driven breast cancer, impairs cell growth by restoring the function of the endogenous cell cycle inhibitor, p27[271]. Three different PIM inhibitors, have been in use so far in clinical trials for the treatment of lymphoma, prostate cancer, acute myelogenous leukemia or multiple myeloma[272].

A genome-wide CRISPR-Cas9 screen of MYCN-amplified neuroblastoma showed a preferential dependency on genes encoding the polycomb repressive complex 2 (PRC2) components EZH2, EED, and SUZ12. Genetic and pharmacological suppression of EZH2 impaired neuroblastoma growth both *in vitro* and *in vivo*[273].

Finally, an *in vivo* genetic screen performed in our laboratory in MYC-driven lymphoma identified a dependency on the mitochondrial ribosomal protein PTCD3, a regulator of mitochondrial translation for energy metabolism, which depletion led to a reduction in the abundance of the mitochondrial respiratory chain complexes and impedes cellular growth[274]. This finding provided promising therapeutic potential in pre-clinical models of aggressive, MYC/BCL2-driven double-hit lymphoma[275].

Besides the aforementioned screens, similar findings were achieved through directed gain- or loss-of-function studies on MYC target genes involved in different biological processes. Some of the studies will be described below.

Targeting the cell cycle and the DNA damage response. The kinases Aurora A and B, involved in the regulation on the mitotic spindle, have been reported to be necessary in MYC-dependent cells and tumors in several studies. Aurora kinase genes are often amplified in human cancers[276] and their overexpression is a hallmark of MYC-driven B-cell lymphoma, in mice and humans[277]. Treatment with a selective Aurora kinase inhibitor impairs mitosis and triggers mitotic arrest, polyploidy, and ultimately apoptosis, in MYC-driven lymphomas, either *in vitro* or *in vivo*. Another Aurora kinase inhibitor selectively induces apoptosis and

autophagy in MYC-overexpressing cells and is effective against MYC-driven B-cell and T-cell lymphomas[278]. Furthermore, MYCN, stabilization of which is promoted by its interaction with Aurora A[33], is genetically amplified and constitutes a typical driver mutation for different human neuroendocrine tumors, like neuroblastomas. The treatment with two Aurora A kinase inhibitors can interrupt the N-MYC/Aurora A interaction, leading to FBXW7 ubiquitin ligase-mediated N-MYC degradation and consequent N-MYC-dependent transcription inhibition, tumor regression and prolonged survival in N-MYC-driven neuroblastoma mouse models[279]. Pharmacological inhibition of Aurora A has the potential to destabilize MYC in other cancer types, like hepatocellular carcinoma, small cell lung cancer and medulloblastoma, where degradation of MYC leads to the suppression of tumor growth and prolonged survival of tumor-bearing mice[280–282]. Aurora kinase inhibitors are now under investigation in several clinical studies for different MYC-driven cancer types, with different therapeutic approaches[283–287].

Excessive expression of MYC is known to provoke replicative stress and the activation of DDR, mediated by ATR and ATM that, in turn, activate the DNA damage transducers CHK1 and CHK2, respectively[134,288]. The reduction of ATR levels delays the development of MYC-induced lymphomas or pancreatic tumors[289] as well as RNAi-based silencing and pharmacological inhibition of CHK1 using different inhibitors induce apoptosis in lymphoma cells and tumor regression of MYC-driven lymphomas and neuroblastoma[289–292]. Moreover, the dual CHK1/CHK2 inhibitor induces apoptosis *in vitro* and delays tumor progression of transplanted lymphoma cells *in vivo*[293]. In particular, while MYC regulates CHK2, MYC-overexpressing cells are not dependent on CHK2 for their survival, since its depletion induces polyploidy that actually protects tumor cells from DNA damage. However, CHK2 deficiency synergizes with PARP inhibitors, which combinatorial treatment elicits a lethal response in MYC-overexpressing cells[293].

Following from the above, an interesting therapeutic synthetic lethal approach could address the efficacy of the combined inhibition of Aurora kinase A and ATR, given the transcription-independent role of MYCN in preventing R-loop formation

when interacting with Aurora A, thus blocking replication stress-induced DNA damage and facilitating cell proliferation in a mouse model of neuroblastoma[294].

Yet another potentially actionable interaction is provided by the observation that MYC regulates cell cycle progression by modulating the expression or activity of many cyclin-dependent kinases (CDKs) and CDK-inhibitory proteins, which fine-tune the transition from one cell cycle phase to the other[6,14,131]. Different studies show that the pharmacological inhibition or genetic ablation of certain CDKs can impair the growth of cells with deregulated MYC activity. Purvalanol A-mediated inhibition of CDK1, whose activity is positively regulated by MYC to stimulate cell progression, results in apoptosis in MYC-overexpressing cells and is beneficial for mice harboring MYC-overexpressing lymphoma[295] or breast cancer[296]. Unlike CDK1, CDK2 is not essential for mouse development, owing to the function compensation by other CDKs[297] and its loss sensitizes to MYC-induced senescence and delay of lymphomagenesis *in vivo*, pointing to CDK2 as a possible target[298,299].

Finally, other CDK inhibitors have been evaluated in clinical trials[300]; among these, Dinaciclib was effective against aggressive MYC-driven B-cell lymphoma *in vivo*[225], where it caused downregulation of the anti-apoptotic factor MCL1; a similar effect was also described in multiple myeloma upon treatment with Seliciclib, which inhibits CDK2, CDK7 and CDK9[301].

Targeting apoptosis. Evasion of cell death is considered essential for tumorigenesis and cancer cell survival hence many cancers show deregulated expression of pro-apoptotic or pro-survival members of the BCL-2 protein family, which comprise the major regulators of intrinsic apoptotic pathway[177]. BCL-2-selective inhibitor venetoclax have been approved by the FDA and many regulatory authorities worldwide for many different tumor types such as a number of haematological malignancies[302]. In MYC-driven diffuse large B cell lymphomas (DLBCLs), while the response rates of R-CHOP (rituximab plus cyclophosphamide, doxorubicin, vincristine, and prednisone) alone are poor, the combination of Venetoclax with R-CHOP recently showed potential for improved efficacy, supporting further investigation of venetoclax in for this particular cancer type[303].

Furthermore, inhibition of mitochondrial translation by the antibiotic tigecycline synergizes with venetoclax *in vitro* by killing human cells of MYC/BCL2 "double hit lymphoma" – a subtype of DLBCL characterized by both chromosomal rearrangements of MYC and BCL2 which leads to their overexpression – and revealed strong antitumor effects in mice engrafted with either the same cell lines or a patient-derived xenograft[275]. Additionally, in MYC-driven lymphomas where high BCL-2 expression is prevalent, such as in double hit lymphomas and in "double expressor lymphomas" – which is characterized by high co-expression of MYC and BCL2 without underlying chromosomal rearrangement – venetoclax synergize with BET inhibitors leading to a reduction in tumour burden and prolonged survival of xenograft-bearing mice[304]. Finally, high level of MCL1 has been found in diverse cancer types and its overexpression, coupled with high expression of MYC, can accelerate lymphomagenesis. It has been found that MYC-driven acute myeloid leukemia and lymphomas are rapidly killed upon inducible genetic deletion or blockade of MCL-1, indicating MCL-1 as critical for MYC-driven tumorigenesis[301,305].

Targeting transcription. As already mentioned, MYC controls multiple aspects of transcription, from initiation to elongation, by interacting with key proteins and co-factors[14,306]. The recruitment of MYC itself to chromatin is facilitated by interaction with factors such as WDR5[48], which may provide additional opportunities for therapeutic intervention. Indeed, the use of small-molecule antagonists of WDR5 reduces MYCN-WDR5 complex formation and leads to growth suppression in MYCN-dependent neuroblastoma cells[307]. Genetic disruption of the MYC-WDR5 interaction elicits tumor regression also *in vivo*[49] and, very recently, a novel WDR5 antagonist has been described as a potential starting point for therapeutics, given its ability to inhibit proliferation in MYC-driven cancer cells[308].

DPY30 is another component of a histone modifier complex reported to be important for effective binding of MYC to its genomic targets and frequently amplified in human cancers such as in Burkitt lymphoma[309]. DPY30 promotes the expression of endogenous MYC and its partial loss significantly suppressed MYC-

driven lymphomagenesis[309]. Recently, a peptide-based therapeutic approached has been developed to bind DPY30 and inhibit its activity, resulting in impairment of the growth of diverse MYC-dependent hematologic cancer cells, suggesting DPY30 as potential cancer target[310].

The histone acetyltransferases P300/CBP and GCN5 are MYC transcriptional co-factors. In chronic myeloid leukemia cells, the bromodomain inhibitor CBP30 can displace CBP and P300 from MYC binding sites at enhancers, diminishing the levels of histone acetylation at these regulatory regions and consequently the expression level of crucial genes, leading to the accumulation of cells in the G0/G1 phase of the cell cycle[311]. Thus, inhibition of P300/CBP bromodomains represent a therapeutic potential, owing to the interference with MYC transcription programs but also the antitumor activity *in vivo* in an acute myeloid leukemia tumor model[312]. GCN5 was found upregulated in mouse and human non-small cell lung cancer cells, where its depletion reduces c-MYC expression and cell proliferation while inducing necrosis or apoptosis, therefore representing a novel target for inhibition of non-small cell lung cancer growth and progression[313]. The same authors reported that GCN5 was overexpressed in Burkitt's lymphoma and its inhibition downregulates MYC target genes, causing reduction of viability and proliferation in Burkitt lymphoma cell lines[314].

Other epigenetic modifiers, such as histone deacetylases (HDACs) are promising therapeutic targets for MYC-driven cancers[315–317]. The combination of HDAC and DNA methyltransferase inhibitors in non-small-cell lung cancer cell lines result in the suppression of MYC signaling accompanied by activation of interferon **α**/ß-based transcriptional program, upregulation of the antigen presentation machinery and CCL5, a T cell chemoattractant; in line with these *in vitro* data, the same treatment in mouse models led to rescue of tumor immune evasion and modulation of T cell exhaustion state towards memory and effector T cell phenotypes[318].

Targeting metabolism. MYC is a key regulator of cellular and a number of metabolic factors, receptors or enzymes may provide therapeutic opportunities in this context[136,137,319,320]. In particular, MYC-mediated remodeling of cancer

metabolism leads to a dependency on the Warburg effect, or aerobic glycolysis (i. e. preferential fermentation of glucose into lactate even in the presence of oxygen and fully functioning mitochondria), as well as glutaminolysis as key bioenergetic pathways to sustain tumor growth[136,214,319]. High expression of glutaminase (GLS), a MYC target gene, is present in ovarian cancer, in which the deprivation of glutamine, knockdown of GLS or the treatment with GLS inhibitors induce a robust production of reactive oxygen species and sensitive cancer cells to the platinum-based therapy, owing to the incapacity to overcome oxidative stress and DNA damage . Similarly, MYC-driven models of liver and pancreatic cancer showed that the tumours are dependent on lactose dehydrogenase A activation, which catalyzes the conversion of pyruvate to lactate, to sustain anerobic glycolysis[322,323]. Finally, besides glycolysis, MYC-overexpressing cells also show enhanced dependency upon mitochondrial activities, including transcription, translation and Oxidative Phosphorylation (OxPhos)[274,324,325]: interfering with these processes sensitizes MYC-driven lymphomas to apoptosis, and provides therapeutic synergy with BH3-mimetic compounds (which inhibit anti-apoptotic BCL2-family members)[275,325].

Targeting RNA processing. Among the discrete functional classes of genes regulated by MYC in different tissues and cancer types, the most recurrent includes all levels of RNA processing (splicing, capping, polyadenylation, turnover and modifications), in line with the notion that MYC is a key player in the regulation of these events[15,176].

Splicing in particular emerged as a critical process in MYC-driven tumors, in several independent studies. First, a genome-wide synthetic-lethal screen led to the identification of BUD31, which the authors then showed to be a component of the core spliceosome[175]; in line with this finding, additional components of spliceosome assembly and catalysis including SF3B1 (U2 snRNP), U2AF1 (U2-related splicing factor), EFTUD2 (U5 snRNP), and SNRPF (core Sm protein found in every snRNP complex) were also essential to tolerate oncogenic MYC. In the same study, genetic or pharmacological inhibition of the spliceosome *in vivo* impairs

survival and tumorigenicity of MYC-dependent breast cancers[175]. Second, MYC activation in lymphomas promotes the expression of the core genes of snRNP assembly, such as the arginine methyltransferase PRMT5, suppression of which compromises splicing fidelity by inducing aberrant intron retention or exon skipping events, resulting in delayed lymphomagenesis in Eμ-*myc* mice[154]. Of note, PRMT5 is a pre-mRNA-processing enzyme required also for translation initiation[326]. Third, MYC overexpression can sensitize cancer cells to the suppression of U2 snRNP splicing with SF3B inhibitors[327]. Fourth, a MYC-induced splicing regulator, PTBP1, is critical for the growth of N-MYC-driven neuroblastoma[328]. Fifth, hyper-activation of MYC can render cells sensitive to inhibition of the CLK2 kinase, which has been linked to alternative splicing[329]. Sixth and finally here, a recent study showed that splicing-targeted therapies, to which many tumors with RNA splicing deregulation are sensitive[154,175,330–333], are effective in MYC-driven triple-negative breast cancer because of the accumulation of mis-spliced mRNAs[334] with double-stranded structures, which trigger antiviral signaling and extrinsic apoptosis[335].

Besides splicing, RNA turnover is also indirectly regulated by MYC, which suppresses the expression of TTP/ZFP36, an RBP involved in mRNA stabilization through the AU-rich elements. The restoration of TTP levels in MYC-driven lymphoma models impaired tumor growth and maintenance[150].

Targeting protein synthesis. As introduced earlier, besides RNA Polymerase II, MYC also regulates transcription by RNA Polymerases I and III, which produce the rRNA and tRNA species required for ribosome assembly and function[336]. Interfering with ribosome biogenesis and protein synthesis, processes that are highly active during oncogenic MYC activation, may thus represent an interesting therapeutic strategy. For example, inhibition of Pol I, with subsequent nucleolar disruption and P53-mediated apoptosis, was effective against MYC-driven lymphomas[337,338]. The combination of inhibiting Pol I with ATR, suppression of which showed encouraging results in MYC-driven cancer with high level of replicative stress[289], also exhibited a potentiated effect[339]. Furthermore, the reduction of the dosage of different

ribosomal proteins provided to be a successful strategy for targeting MYC-driven tumors[340,341].

The PI3K/AKT/mTOR axis is a key regulator of translation and is frequently activated in human cancers, such as in MYC-driven B-cell lymphomas, where the downstream effector EIF4E, a translation initiation factor, has been found to mediate tumorigenesis and also a synthetic lethal effect upon depletion[342–346]. Many inhibitors of mTOR and PI3K are under clinical trial, and some clinically approved, owing to the synthetic lethal effect with abnormal MYC activation in lymphoma cells[233,347–349].

Targeting immune pathways. Finally, recent observations revealed the possibility of exploiting MYC-induced alterations of immune surveillance to treated MYC-driven cancers[178]. Indeed, MYC can modulate the transcription of immune factors and pathways and the restoration of immune responses mediated by cytokine administration is effective against specific MYC-driven mouse tumors[350], as also reported with restoration of NK cell-mediated immune surveillance[351] or immune-checkpoint inhibition[352]. Moreover, direct inhibition of MYC had a synergistic effect with anti-PD-1 antibodies in mouse MYC-driven prostate cancer[353], and the combination of JQ1 (which targets BRD4 and blocks MYC expression) with anti PD-L1 exhibited a promising synergy in pancreatic ductal adenocarcinoma[354]. Hence, MYC expression might predict response to immunotherapy, and the latter may be further potentiated by targeting MYC or MYC-regulated pathways.

Figure 7 shows a summary of the aforementioned different therapeutic strategies to target MYC and its liabilities.

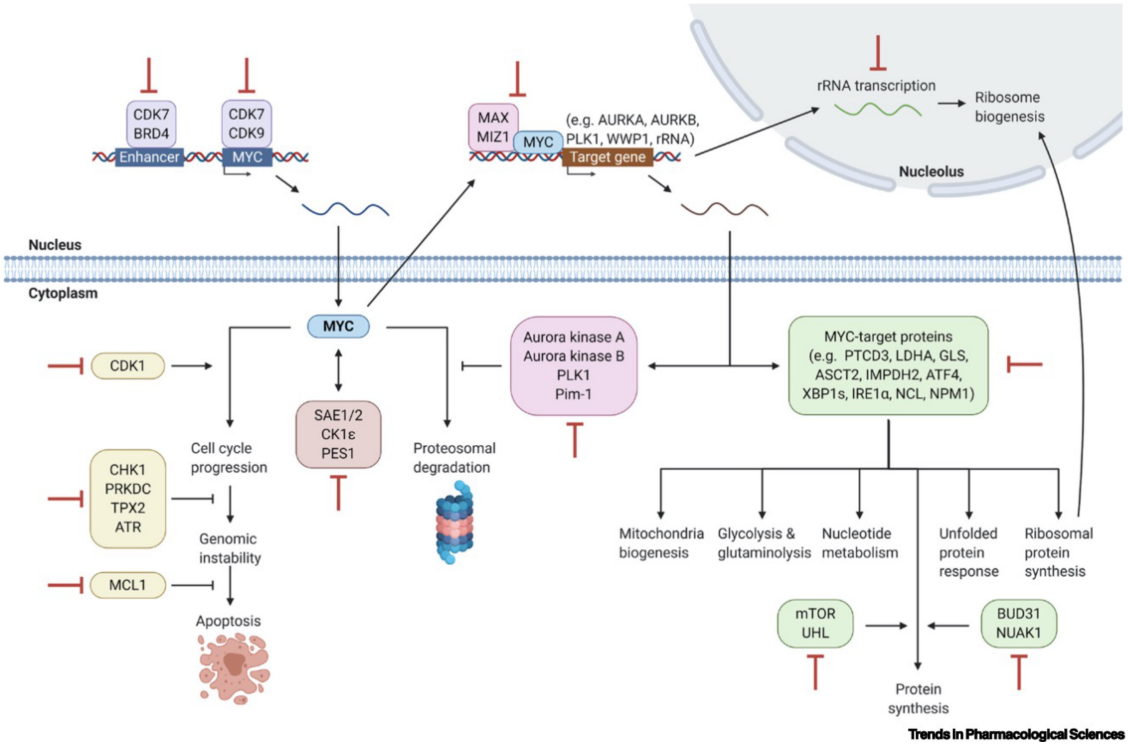

Figure 7. Schematic representation of different therapeutic strategies to target MYC or MYC functions. Examples of MYC targetable vulnerabilities are represented by proteins that regulates MYC expression (in violet), MYC transcription function (MAX and MIZ1), MYC protein stability (in pink), MYC-mediated cell cycle, genome stability and apoptosis regulations (in yellow), MYC-mediated cellular metabolism, protein synthesis and RNA processing (in green). Other independent synthetic lethal interactors are SAE1/2, CK1e and PES1. Many other factors are not shown here but demonstrated to be synthetic lethal genes with MYC overexpression (see main text). Image adapted from *Thng et al., Trends in Pharmacological Sciences, 2021* (ref. 349).

1.1.9 *In vivo* and *in vitro* models for MYC studies

The Eμ-Myc mouse model. Deregulated MYC expression is associated with diverse lymphoid tumors. Human Burkitt's B-cell lymphoma, for example, originates from the t(8;14) translocation, which juxtaposes the immunoglobulin heavy (IgH)-chain locus to an upstream region of the c-*MYC* gene. While the *MYC* coding sequence remains intact, this translocation leads to its deregulated expression under the control of the IgH enhancer, unleashing its potent oncogenic activity[355]. Remarkably, analogous translocations events were observed in murine lymphoid tumors: one of these rearrangements, originating in a spontaneous mouse plasmacytoma[356] was used to construct the transgenic mouse line Eμ-Myc[181], which develops aggressive B-cell lymphomas with rapid onset and high penetrance. In these mice, the Eμ enhancer drives overexpression of MYC in B-cells, the expansion of Pro/Pre-B cells which eventually stop their differentiation[357] and finally, after

accumulation of secondary mutations[358], the development of B-cell tumor around 4 months of age[181]. Lymphoma cells massively infiltrate lymph nodes, spleen and thymus. Isolated primary tumors can be expanded *in vitro*, infected with suitable vectors for over-expression or suppression of selected genes, and transplanted back into recipient animals: owing to these features, Eμ-Myc mice have become one of the most tractable and widely used models for genetic studies and screens in MYC-driven lymphoma, as exemplified by a plethora of studies, including work from our own lab[274].

The MycER™ model. Intracellular proteins can be functionally converted to become hormone-dependent by fusing their coding sequence with the hormone-binding domain (HBD) of steroid receptors: this approach was used to generate conditional forms of diverse proteins, including transcription factors or kinases[359]. The HBD of the human estrogen receptor (ER) in particular has been the most widely used as a heterologous regulatory domain, owing to the fact that the majority of cell types do not express endogenous ER. One of the proteins that was successfully fuser to the ER was MYC, with the early demonstration the ER moiety endowed the fusion protein (MycER) with conditional biological activity[360,361].

While this initial version of MycER allowed unprecedented control of MYC activity, it suffered from two major caveats: (i.) ER possesses an inherent ligand-dependent transactivation activity, which contributes to the total transcriptional activity of the fusion protein; (ii.) culture media and serum contain phenol red (a weak ER agonist) and estrogens, respectively, conferring leakiness to the system[362]. To avoid this problem, Littlewood and colleagues used a mutant form of murine ER (G525R) that cannot bind oestrogen but rather the synthetic steroid 4-hyfroxytamoxifen, and lacks an inherent transactivation function[363]. The authors created a switchable form of the c-MYC protein, MycER™, and validated the effects of MYC activation[363]. This model has been extensively used as tool for investigation for the biological function of MYC in both cultured cells (including the present study) and transgenic animals[362].

1.2 RNA Binding Proteins (RBPs)

1.2.1 RBPs in cancer

RBPs constitute 7.5% of the products of protein-coding genes and coordinate the entire life of RNA molecules, from synthesis to degradation[364]. RBPs bind to diverse classes of RNAs, such as ribosomal RNAs (rRNA), messenger (mRNA), small nuclear RNA (snRNA), small nucleolar RNA (snoRNA), transfer RNAs (tRNAs) and non-coding RNAs (ncRNAs). However, about half of the RBPs exert their function by binding to mRNA and regulating its fate[364] while 11% is constituted by ribosomal proteins[364].

RBP-mediated mRNA regulation comprises its transcription, processing, localization, modification, export, stabilization, translation and degradation (Figure 8), hence is not surprising that alterations in RBPs (i. e. deregulated expression or mutation) might lead to various diseases, including diabetes, cardiovascular and neurodegenerative disorders, and cancer[365–367]. RBPs can interact with structural RNA species (e.g. rRNAs, snRNAs) to form ribonucleoprotein (RNP) complexes, which regulate specific steps (i. e. maturation, processing, transport, etc…) in the life cycle of a variety of target RNAs. RNPs and RBPs also act as chaperones by preventing misfolding, incomplete processing and aggregation, and facilitating the partitioning of RNA targets in their correct subcellular locations. Consequently, the abundance and composition of RBPs contribute to all facets of RNA regulation[368,369].

The 1,542 human RBPs that were registered are characterized by ca. 600 structurally distinct RNA-binding domains (RBDs), which were found to frequently occur in multiple repeats or in combination with other RBDs, most luckily in order to increase sequence specificity and affinity with target RNAs. RBDs are highly conserved across bacteria, archaea and eukaryotes, a further indication of their fundamentally conserved roles in coordinating RNA homeostasis and regulation at the post-transcriptional level[364]. Some of the RBD classes have been studied for decades and relatively well understood, although RBDs are extremely heterogeneous and can be difficult to classify[364]. Known RBDs include the RNA-

recognition motif (RRM), double-stranded RBD (dsRBD), K homology (KH) domain, arginine-glycine-glycine (RGG) motif, cold-shock domain (CSD), zinc fingers (ZnF) and others[370]. Others remain to be characterized, given that hundreds of RBPs lack known RNA-binding domains[371].

RBP expression is tightly regulated, as alterations in this equilibrium can cause changes in RNA metabolism, transcriptome and proteome profiles, with potentially dire consequences on cellular homeostasis[372]. Indeed, dysregulated expression of some RBPs has been shown to be implicated into different diseases, such as cancer[371,373]. Furthermore, tumor cells express mRNA-binding proteins (mRBPs) and ribosomal proteins at higher levels than normal tissues, owing to the increased demand for continuous transcription and protein synthesis[15,374]. Numerous studies showed that RBPs can control multiple cancer traits by regulating critical groups of genes[366,375]. For example, overexpression of the mRNA 5' cap-binding protein eIF4E can induce cell transformation[376] and the treatment of antisense oligonucleotides against eIF4E resulted effective to block tumor growth[377]. Loss of function mutations in DICER1, involved in microRNA maturation, occurs in many different tumor types, pointing to a wide role of this RBP in tumor suppression[378]. Another example is the splicing factor SRSF1 (or SF2/ASF), which is genetically amplified in various human cancers, and promotes tumorigenesis through alternative splicing of the tumor suppressor BIN1 and the kinases MNK2 and S6K1[379]. Negative Elongation Factor E (NELFE) was also reported to promote hepatocellular carcinoma by increasing MYC signaling and selectively modulating MYC-associated genes[380]. During the last years, a compendium of RBPs involved in cancer has been laid out by different studies, pointing to RBPs as promising targets for cancer therapy[366,375,381]. From these findings, it is clear that RBPs are involved in different key processes in tumorigenesis, such as energy metabolism, immune surveillance, genome stability and others (Figure 9)[375,382].

Figure 8 (next page). Schematic overview of the main RBPs and RBP-regulated pathways. RBPs cand bind to different species of RNAs and regulate their biogenesis, decay and function: tRNAs, ribosomal RNAs, small nuclear RNAs (snRNAs), small nucleolar RNAs (snoRNAs), mRNAs, microRNAs (miRNAs), PIWI-interacting RNAs (piRNAs) and long non-coding RNAs (lncRNAs). **(a)** tRNAs are transcribed by RNA polymerase III (Pol III); processed and modified by different enzymes. **(b)** The 5S rRNA is transcribed by Pol III while 28S, 18S and 5.8S rRNAs are transcribed by Pol I as one transcript. The precursors are processed by RNA exonucleases, endonucleases and RNPs and guided as well as modified by snoRNPs. rRNAs are assembled together with ribosomal proteins within the nucleus and transported to the cytoplasm for maturation into functional ribosomes. **(c)** Most snRNAs are transcribed by Pol II, capped and processed in the nucleus and then exported to the cytoplasm, where they are methylated and assemble into snRNP, which are re-imported into the Cajal body (CB) within the nucleus for final processing and assembly. Mature snRNPs form the core of the spliceosome. **(d)** snoRNAs and small Cajal body-specific RNAs (scaRNAs) are processed from mRNA introns, capped and modified before they assemble into snoRNPs or scaRNPs. snoRNPs and scaRNPs carry out methylation and pseudouridylation of rRNAs, snoRNAs and snRNAs, or function in rRNA processing. **(e)** mRNAs are transcribed by Pol II, capped, spliced, edited and polyadenylated in the nucleus and then exported into the cytoplasm, all through the activity of different RBPs, which than regulate correct translation and monitor stability, decay and localization. Finally, RBPs can also shuttle mRNAs among actively translating ribosomes, stress granules and P bodies. **(f)** miRNAs are either transcribed from separate genes by Pol II as long primary miRNA (pri-miRNA) transcripts or expressed from mRNA introns and processed into hairpin pre-miRNAs in the nucleus. After transport into the cytoplasm, they are processed and incorporated into Argonaute (AGO) proteins which guides them to partially complementary target mRNAs to recruit deadenylases and repress translation. **(g)** piRNAs are ~28-nucleotides-long, germline-specific small RNAs directly processed and assembled from long, Pol II-transcribed precursor transcripts, whereas secondary piRNAs are generated by the cleavage of complementary transcripts by PIWI proteins. Mature piRNAs form complexes with PIWI proteins (piRNPs) which silence transposable elements. **(h)** Most lncRNAs are transcribed and processed in a similar way to mRNAs and direct proteins to specific gene loci, where they recruit chromatin modification complexes and induce transcriptional silencing or activation. **(i)** Misprocessed RNAs are recognized by several RNA surveillance complexes in the nucleus and cytoplasm and degraded. Image and legend adapted from *Gerstberger et al., Nature Reviews Genetics, 2014* (ref. 364).

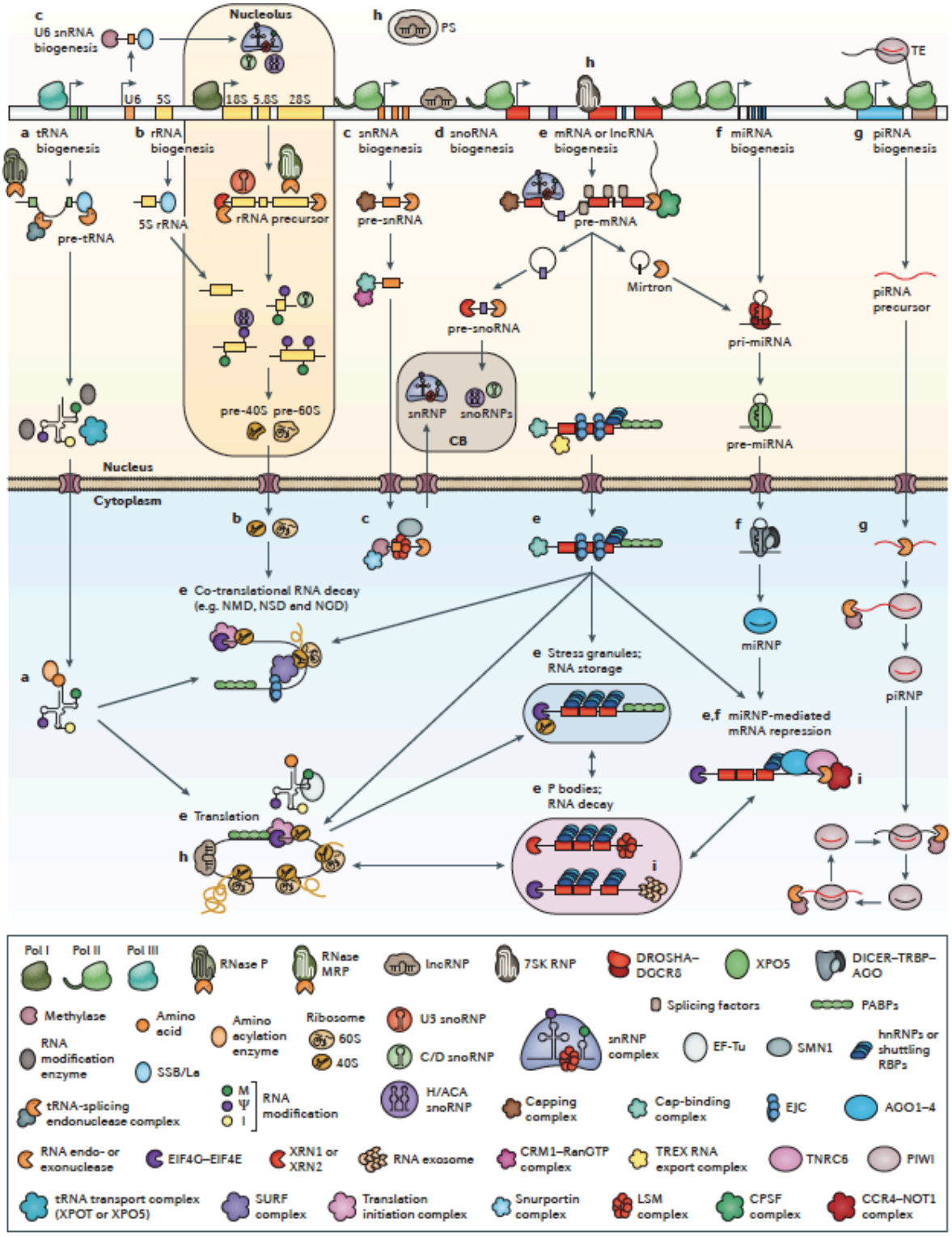

Figure 8. Schematic overview of the main RBPs and RBP-regulated pathways. See the legend in the previous page.

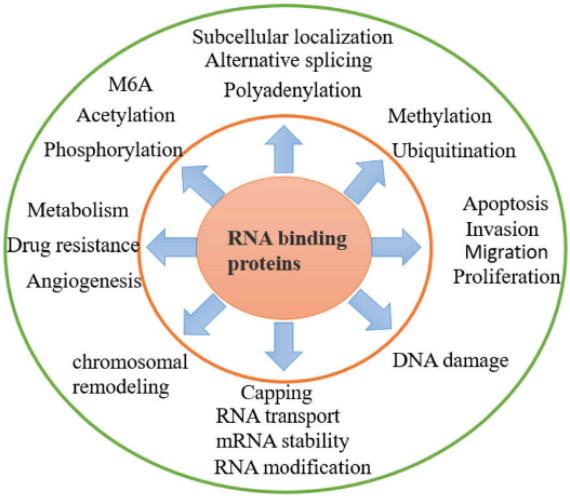

Figure 9. RBPs controlled processes in tumor cells. Pool of molecular and biological processes modulated by different RBPs in cancer as emerged from different studies[366,375,381]. Image adapted from *Qin et al., Journal of Hematology and Oncology, 2020* (ref. 375).

1.2.2 RBPs in mRNA decay

Pathways of mRNA decay are various and encompass non only mRNA turnover mechanisms, which lengthen or shorten mRNA half-life for the purpose of changing the abundance of functional proteins, but also surveillance mechanisms involved in quality control, eliminating aberrant mRNAs whose translation would produce potentially toxic proteins[383]. These processes constitute a fundamental layer of regulation of gene expression as almost half of the changes in RNA abundance in response to a particular signals occurs at the level of mRNA stability[384].

mRNA turnover. Deadenylation-dependent mRNA decay is the main eukaryotic pathway which occurs when the 5′ 7-methilguanoside cap or the 3′ polyadenylated tail are compromised hence unable to protect the transcript from exonuclease activities or when mRNA is cleaved internally by endonucleolytic attack[384,385]. This process starts upon poly(A)-tail shortening (deadenylation), that in eukaryotes can be mediated by several deadenylases, including PAN2–PAN3, CCR4–NOT and PARN, each with unique properties. Destruction of mRNA can be achieved by two redundant pathways which occurs in the two opposite directions, including (i.) removal of the 5′ cap, mediated by the dimer of DCP1 and DCP2 decapping enzymes which allows digestion of the mRNA in the 5′ to 3′ direction by the

exoribonuclease XRN1, and (ii.) exonucleolytic 3′ to 5′ degradation by the exosome complex (Figure 10)[384,385].

Other less common mRNA decay pathways occur for specific targets, for example deadenylation-independent mRNA decay found in *S. cerevisiae*, and the endoribonucleolytic pathway, which relies on the endonucleolytic cleavage by several identified endonucleases and degradation of the resulting fragments from the break by the aforementioned exonucleases (Figure 10)[384].

Factors of the 5′->3′ decay pathway can be found in granular cytoplasmic foci, named "P bodies", with other components of deadenylation, decapping, nonsense-mediated decay and miRNA-mediated decay. P bodies are dynamic sites for mRNA turnover and storage of those mRNA that cannot be immediately degraded, and can serve to compartmentalize mRNAs targeted for decay in order to prevent their association with ribosomes[386].

mRNA surveillance. Surveillance mechanisms are part of mRNA decay pathways and serve as sensor of faulty mRNAs which need to be degraded in order to prevent the synthesis of potential toxic proteins. These pathways include non-stop decay, no-go decay and the most studied nonsense-mediated decay, which will be introduced in a separate section below[384,385].

Non-stop decay occurs in case of missing stop codon, which allow ribosomes to continue translation along the polyA tail, by displacing the polyA-binding proteins (PABP), where the ribosome then stalls and binds to Ski7 and eRF3 proteins. These factors permit the release of the stalled ribosome, deadenylation and finally recruitment of exosome for degradation, or XRN1 in the absence of Ski7 (Figure 10)[384,387].

No-go decay is a less well-known pathway that targets faulty transcripts with stalled ribosomes due to strong RNA structures. As above, XRN1 and the exosome mediate the degradation of the RNA fragments resulting from an endonucleolytic cleavage near the stalled site (Figure 10)[384,387,388].

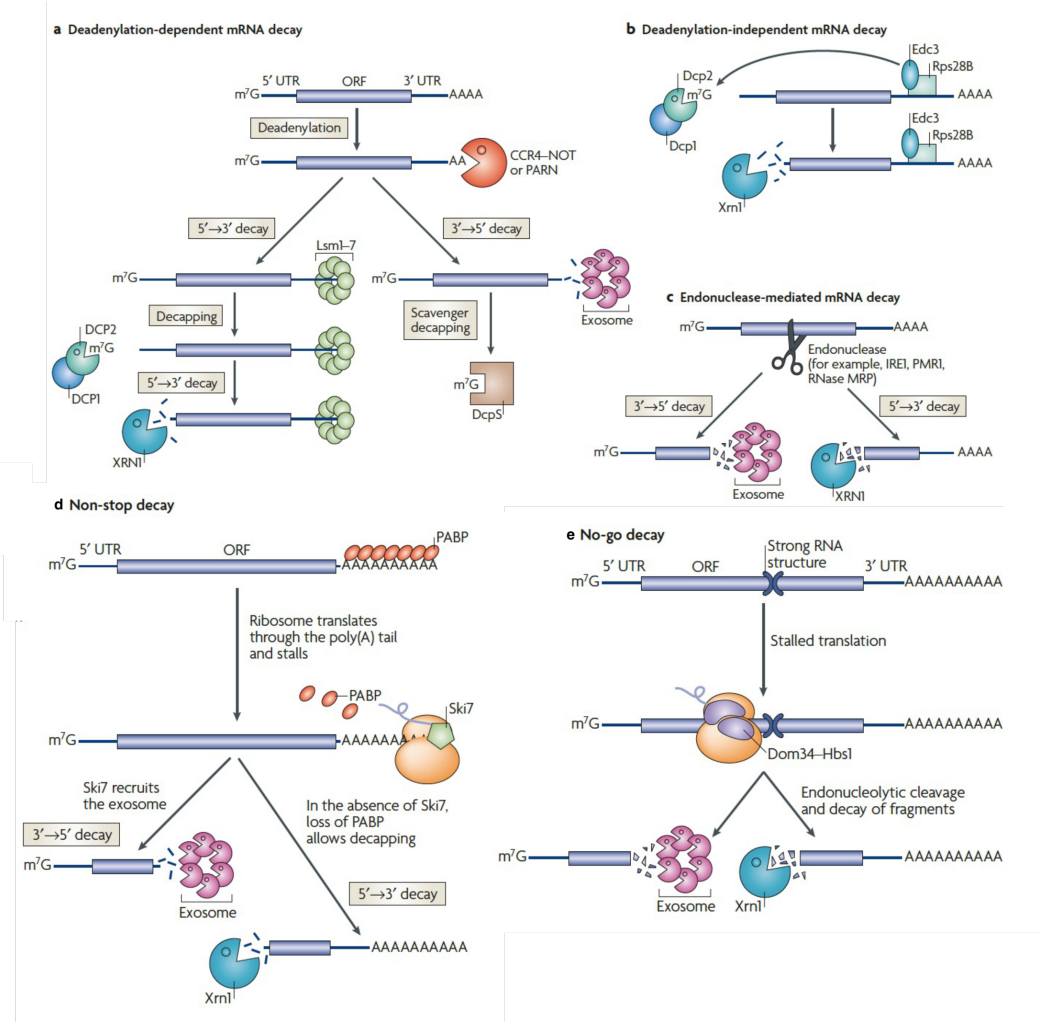

Figure 10. Pathways of mRNA decay and surveillance. (a) The majority of mRNAs are degraded through the deadenylation-dependent pathway, which comprises a starting step of removal of the poly(A) tail by carbon catabolite repressor protein 4 (CCR4)–NOT or PARN and two redundant mechanisms that degrade the mRNA. 5′→3′ decay is mediated by the DCP1–DCP2 decapping complex which leaves the mRNA subject to decay by the 5′→3′ exoribonuclease XRN1. Alternatively, the deadenylated mRNA can be degraded in the 3′→5′ direction by the exosome, with the remaining cap structure being hydrolysed by the scavenger-decapping enzyme DcpS. **(b)** In *S. cerevisiae*, deadenylation-independent pathway comprises the recruitment of a decapping machinery followed by the XRN1-mediated mRNA degradation. **(c)** Endonuclease-mediated mRNA decay initiates with internal cleavage of the mRNA, which generates two fragments which are degraded by XRN1 and the exosome. **(d)** Stalling of ribosomes at the 3′ end of the mRNA, after traversing the poly(A) tail and displacing poly(A)-binding protein (PABP) occurs when stop codon is missing. This scenario activates the so-called non-stop decay which implies the release of the transcript by the SKI7 adaptor proteins which also recruits exosome that degrades the poly(A) tail and mRNA body. In *S. cerevisiae*, in absence of SKI7, the displacement of PABP by the translating ribosome renders the mRNA susceptible to decapping and 5′→3′ decay by XRN1. **(e)** When ribosomes stall within the coding region for a strong secondary structure for example, endonucleases induce the release of the ribosome by cutting near the stall site the transcript which fragments become exposed to XRN1 and exosome activities. Image adapted from *Garneau et al., Nature Reviews Molecular Cell Biology, 2007* (ref. 384).

1.2.2.1 Nonsense-mediated decay

The most studied mRNA quality control pathway is nonsense-mediated decay (NMD)[389–391]. This surveillance mechanism is highly conserved among eukaryotes[392] and has evolved to eliminate faulty mRNAs with a premature termination codon (PTC). PTC-harboring transcripts can arise from inefficient transcription which leads to point mutations or frame-shifts owing to the insertion or deletion of nucleotides, and if translated could lead to the synthesis of truncated proteins with anomalous functions. Moreover, NMD can protect cells from heterozygous mutations that introduce PTCs in the corresponding mRNA, which may potentially produce dominant-negative proteins, although this mechanism may concomitantly cause disease due to haploinsufficiency[391].

Studies on different model systems suggested that NMD acquired a more critical role during evolution: while *S. cerevisiae* and *C. elegans* are viable without a functional NMD[393,394], key factors of this pathway display essential features in vertebrates, in particular for embryonic viability and for hematopoietic stem and progenitor cells[395–397]. Moreover, NMD factors were found to be important in mammals during spermatogenesis, liver development, neural and hematopoietic differentiation[389,398]. This gain of essentiality in complex organisms denotes an expansion of NMD functions from quality control to other regulatory mechanism. Indeed, the second fundamental role of NMD is the physiological regulation of transcripts that normally harbor a PTC[391], which have been estimated to cover the 20-40% of mammalian transcriptome, highlighting an important role of NMD in the control of gene expression[399]. For example, NMD in involved in the degradation of stress-related transcripts such as *Atf4* in unstressed, physiological conditions, thus contributing to normal cellular homeostasis. *ATF4* encodes a transcription factor that is active during the integrated stress response: its mRNA contains an upstream open reading frame with a PCT which targets the transcript for NMD-mediated degradation in normal conditions, while the reading frame encoding ATF4 is NMD-insensitive, and thus favored in stress condition[400,401]. Moreover, NMD can be physiologically coupled to alternative splicing for gene regulation: tissue-specific

inclusion of a PTC-bearing exon in a transcript can lead to its degradation, hence to gene silencing in that tissue[402].

In vertebrates, NMD is structured as a branched pathway in which different branches either regulate distinct sets of transcripts with particular features or are activated by diverse sets of factors (see below), to converge all on a common decay mechanism. Indeed, apart for PTCs, NMD can also be activated by the presence of other particular features on the mRNA, such as long 3′-UTRs, the presence of the exon-junction complex (EJC) at least 50 nucleotides downstream of stop codons, upstream open reading frames (as for *Atf4)* or 3′-UTR introns (Figure 11)[403]. In all of these conditions, NMD can be activated to induce translation termination and transcript degradation. For historical reasons, PTCs generally refers to all termination codons that trigger translation termination and NMD, including those that are not "premature" (e.g. those present in long and structured 3'UTR), because they were originally identified in transcripts with truncated open reading frames[391].

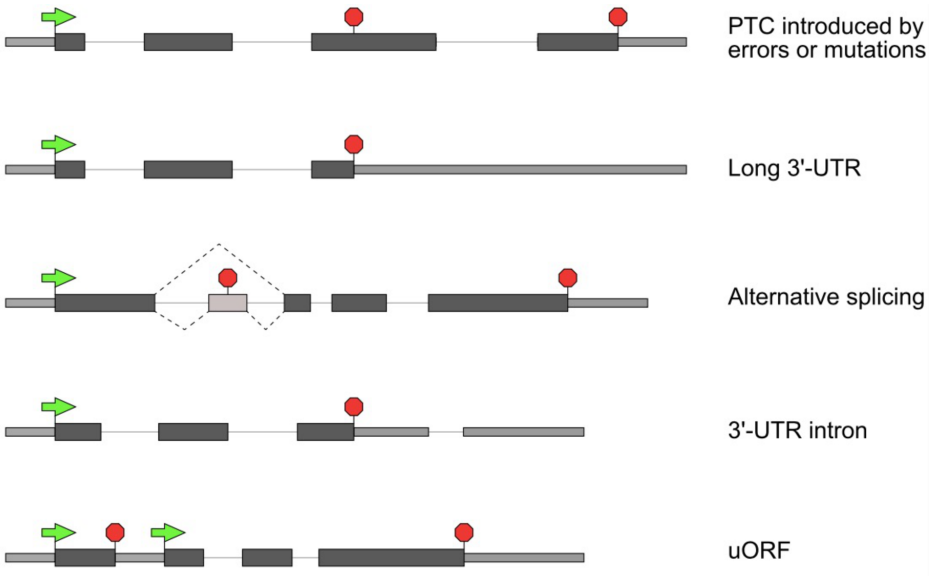

Figure 11. Features of NMD sensitive transcripts. Dark boxes: coding region; lighter and tinner boxes: untranslated regions; lines: introns; green arrows: start codons; red stop-signs: stop codons. Image adapted from *Yi et al., Trends in Genetics, 2021* (ref. 403).

In all of the aforementioned scenarios, mammalian NMD occurs during the first rounds of translation of mRNA which required to be associated with the nuclear cap-binding complex (CBC) or, when replaced, by cytoplasmic cap-binding protein

EIF4E[404]. The CBC is composed by CBC20 (or Nuclear Cap Binding Protein Subunit 2 - NCBP2) and CBC80 (or NCBP1), which remain bound to the mRNA 5′-cap after transcription and during mRNA export to the cytoplasm, and are involved in the recruitment of ribosomes for the first rounds of translation[405]. Recognition of a PTC-containing mRNA as an NMD substrate strictly requires operating ribosomes, and therefore active translation, inhibition of which also causes NMD blockade[390]. At the core of the branched NMD pathway there is a conserved ATP-dependent RNA helicase, upstream frameshift 1 protein (UPF1), which together with UPF2 and UPF3B (or UPF3X) recognizes PTC-containing transcripts and activate the pathway[399]. Indeed, UPF1 is considered to be the principal NMD factor, because it is central to most (if not all) steps. UPF1 bind promiscuously and transiently to all transcripts, whether or not targeted by the NMD, in a manner dependent on its ATPase and helicase activities[391]. Work in *Drosophila* has shown that UPF1 co-transcriptionally binds to transcripts and this is required for the release of mRNAs from gene loci[406]. Recognition of the PTC by the NMD pathway specifically requires the recruitment of UPF1 to the terminating ribosome and assembly of UPF proteins[389]. It has also been shown that the presence of the CBC and the UPF1-CBP80 interaction ensure a more efficient UPF1 binding to PTC-containing mRNA[407].

Of the NMD branches, the best-characterized is the exon-junction complex (EJC)-dependent NMD which occurs in case of a PTC at least 50 nucleotides upstream of an EJC. The EJC is a protein complex that is deposited onto newly synthesized and spliced mRNAs ~20–24 nucleotides upstream of the resulting exon−exon junctions. A PCT upstream of the EJC is typically due to transcription errors or mutations[383,389,391,403,405] and its presence leads to an inefficient translation termination which cause NMD activation. Indeed, efficient translation termination prevents NMD and occurs when the normal termination codon (TC) is in proximal to the 3′ poly(A) tail and when the eukaryotic release factor complex eRF1–eRF3 interacts with the TC and with the ribosome. The 5′ cap is associated with either the CBC during the pioneer round of translation or eIF4E in subsequent rounds of

translation, and binds to the eukaryotic translation initiation factor 4G (eIF4G). This binding contributes to normal termination by promoting the eIF4G interaction with the cytoplasmic poly(A)-binding protein (PABPC), thus creating a circular conformation of the mRNA (Figure 12a) and preventing UPF1 from interacting with eRF3 when the TC is proximal to the 3′ and/or the 5′ end of the mRNA (Figure 12a). Unlike normal termination, the presence of a EJC downstream to the PTC hinders the proximity of the terminating ribosome with the extremities of the transcript and NMD occurs: UPF1 interact with eRF3, thereby recruiting UPF2 and/or UPF3B through the EJC (Figure 12b). Consequently, UPF1 recruits DHX34, SMG1, SMG8 and SMG9, hence assembling the NMD-activating complex. DHX34 leads to the dissociation of eRF1 and eRF3 and to translation termination with the release of the ribosomal subunits and the nascent peptide. This step facilitates the interaction among UPF2, UPF3B and EJC and the consequent binding between UPF2 and UPF1, already associated with DHX34, SMG1, SMG8, and SMG9. However, it has been shown that UPF2 or UPF3B are not essential for the activation of NMD and may have redundant roles. The binding of UPF2 to the amino-terminal domain of UPF1 promotes its phosphorylation in both terminal domains, mediated by the SMG1 kinase. This step is essential for the recruitment of downstream factors which initiate mRNA degradation: the endonuclease SMG6, which realizes the cleavage; the SMG5-SMG7 dimer, which recruits the deadenylation complex CCR4-NOT; the proline-rich nuclear receptor co-activator 2 (PNRC2), which recruits the decapping complex DCPC (Figure 12c). As for all the typical pathway of mRNA decay (see previous section), endonucleolytic cleavage, decapping and deadenylation are followed by complete mRNA degradation by 5′–3′ and 3′–5′ exonucleolytic activities of XRN1 and the exosome, respectively. Finally, SMG5 and/or SMG7 interacts with the PP2A phosphatase which in turn dephosphorylates UPF1, a necessary step to ensure recycling of UPF1[389,391,403,405].

As mentioned above, the core proteins of the NMD pathway are UPF1, UPF2, and UPF3B[399]; however, differently from yeast, UPF3B and perhaps UPF2 may not be necessary for suppression of all NMD-targeted mRNAs in mammals[403]. Indeed,

apart for the aforementioned EJC dependent pathway, NMD includes the UPF3B-independent (UPF2- and RNPS1-dependent), the UPF2-independent (UPF3B- and CASC3-dependent) and the SR-protein-stimulated (EJC-independent) branches[403]. Moreover, the abundance of UPF1 in human cells is ~10-fold higher than UPF2 and UPF3B[408], suggesting that UPF1 might be involved in other pathways. In line with this, UPF1 has been found to function as an E3-ubiquitin ligase that represses myogenesis[409]. More importantly, besides NMD, UPF1 is involved in a series of distinct RNA decay pathways, including Staufen1-mediated mRNA decay (SMD), replication-dependent histone mRNA decay (HMD), glucocorticoid receptor-mediated mRNA decay (GMD), Regnase1-mediated mRNA decay (RMD), Tudor-staphylococcal/micrococcal-like nuclease-mediated microRNA decay (TumiD) and TRIM 71-mediated decay (TRIM71-MD)[405,410]. Of note, other NMD factors also participate to these pathways with an intricate level of overlap between effectors and substrates, raising the question of whether these decay pathways can truly be distinguished from each other, or if they should be considered as a cloud-like pool, whose components may differ in different cell types, physiological situations and stage of development[410]. Furthermore, the distinctive proteins that take part of NMD branched pathways are also involved in other mRNA decay pathways, translation termination or splicing[403].

A final consideration here regards SMG6 and SMG5-SMG7, the redundancy and target specificity of which are not completely comprehended. Transcripts with a PTC or a long 3'UTR showed more sensitivity to the SMG6 route, suggesting a specific distinction among mRNA substrates and independent branches of NMD[403]. However, a very recent paper demonstrated that the loss of the SMG5-SMG7 dependent pathway also hindered the SMG6 branch, which indicates an unexpected functional connection between the final steps of NMD, and led to a complete NMD inhibition[399]. Moreover, the same authors showed that SMG5 could substitute SMG7 functions and individually activate NMD in its absence, revealing that the presence of either SMG5 or SMG7 is sufficient to support SMG6-mediated cleavage of NMD targets.

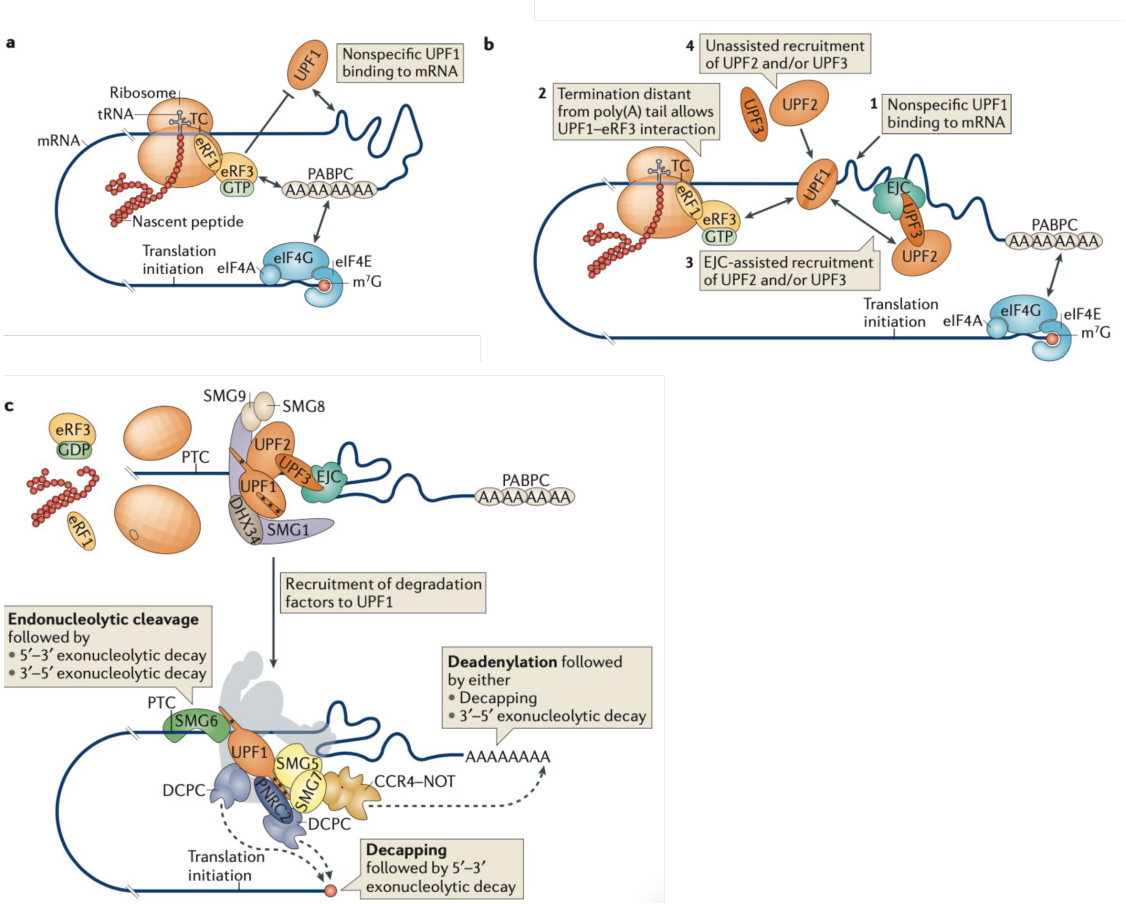

Figure 12. Normal translation termination versus EJC-dependent branch of NMD. (a) Main factors involved in the efficient termination of translation and visual representation of the conformation of the mRNA bound to all of them. **(b)** Presence of a termination codon (TC) upstream of the EJC, which refers to the PCT, impedes efficient translation termination and induce the first assembly of the NMD-activating complex through the depicted temporal sequence of events. **(c)** Once the NMD-activating complex is assembled, recruitment of different factor involved in the promotion of mRNA degradation occurs as shown. Main details in the text. Image adapted from *Lykke-Anderson and Jensen, Molecular Cell Biology, 2015* (ref. 389).

AIM

Understanding and targeting MYC dependencies might provide new therapeutic strategies against MYC-driven tumors. Here, prompted by multiple observations connecting MYC to RNA biology, we aimed to identify novel synthetic lethal interactions between MYC and RNA binding proteins (RBPs). Our data reveal that MYC activations renders cells dependent upon nonsense-mediated RNA decay (NMD), pointing to this pathway as a possible therapeutic target, and warranting further dissection of the underlying mechanisms.

2. Materials and Methods

2.1 Generation of murine sgRNA and shRNA lentiviral libraries

The design and construction of the sgRNA and shRNA libraries were achieved in collaboration with Johannes Zuber's laboratory, as previously described[411,412]. For detailed description of the library composition, see Table S1. Our libraries target 730 RBP-coding genes that were chosen according the following criteria:

- 318 RBPs were selected from *Sebestyén et al.*[373] on the basis of their elevated expression in different tumor types, owing to a copy number gain in the top 5% of a specific tumor of the study, $\log_2$FC (fold change) > 0 and q-value < 0.05);
- 452 RBPs from *Dang et al.*[380] as differentially upregulated in hepatocellular carcinoma compared to control samples, as defined in the study;
- 94 RBPs which emerged as candidates from MYC synthetic-lethal screens[224,263,413], albeit not yet validated.

For each target, we selected six different shRNAs and sgRNAs from previously published libraries[411,412], yielding a total complexity of about 4500 shRNAs/sgRNAs in each library. This number comprises also 47 negative controls (non-essential genes) and 23 positive controls, of which 10 are published MYC synthetic lethal genes (which are *Brd4*[414], *Bud31*[175], *Cdk2*[299], *Cdk9*[224], *Cecr2*[263], *Csnk1e*[263], *Pes1*[263], *Prmt5*[154], *Sae2*[265], and *Sf3bp1*[175]) and 13 are essential genes (*Dnmt1*, *Mcm6*, *Myc*, *Pcna*, *Plk1*, *Pola1*, *Psma1*, *Psmb1*, *Rpa1*, *Rpa3*, *Rpl15*, *Rrm1* and *Top2a*, from Zuber personal communication).

2.2 Gene ontology analysis

Selected genes of our libraries was subject to gene ontology analysis throughout the ShinyGO online tool (v0.66)[415] with allows an enrichment analysis based on hypergeometric distribution followed by FDR correction. As output, a hierarchical clustering tree summarizing the correlation among significant pathways of biological processes is created (see Figure 14).

2.3 Cell lines

The 3T9 cell line expressing MycER^{TM} (see paragraph 1.1.9) was previously generated as clonal population[416] (indicated as 3T9^{Mycer}) and was grown in DMEM medium supplemented with 10% serum, 1% penicillin/streptomycin and 2mM L-Glutamine. 3T9^{Mycer} cells were treated with 50nM 4-hydroxytamoxifen (OHT) for MycER^{TM} activation[363] for the time indicated in the Figures or legends.

The FL5.12 cell line (RRID: CVCL_0262) was grown in RPMI 1640 medium supplemented with 10% serum, 1% penicillin/streptomycin, 2mM L-Glutamine, 50μM β-mercaptoethanol, 10% WEHI-3B conditional medium as IL-3 source for survival[417]. FL5.12^{Mycer} cells were originated after infection with the *MSCV-MycER-IRES-BleoR* retroviral vector (see below, Plasmids and cloning) and selection for 10 days with 800μg/ml Bleomycin. For MycER^{TM} activation, FL5.12^{Mycer} cells were treated with 100nM OHT for the indicated times.

3T9^{Mycer} and FL5.12^{Mycer} cells where infected with the lentiviral vector *EFIas-Cas9-P2A-BFP-P2A-BlastR* for constitutive expression of Cas9 and selected for 10 days with 2.5μg/ml and 10μg/ml Blasticidin, respectively. All experiments involving CRISPR/Cas9 were performed in clonal populations, derived from either 3T9$^{Mycer/Cas9}$ or FL5.12$^{Mycer/Cas9}$ cells by sorting the brightest BFP-positive cells and seeding 1 cell per well in a 96-well plate, with a BD FACSMelody™ Cell Sorter. Sorted cells were kept in culture with 100μg/ml Gentamicin for one week. Clonal populations were expanded by serial passages and some of them subjected to biological characterization (see Figure 16) which allowed us to select clone 4 of 3T9$^{Mycer/Cas9}$ and clone 3 of FL5.12$^{Mycer/Cas9}$ cells to be employed for screening, technical validation and biological characterization. Where applicable, selection of cells infected with *hU6-sgRNA-EFIas-Thy1.1-P2A-NeoR* (for sgRNA expression) or *SFFV-GFP-mirF-shRNA-PGK-NeoR* (for shRNA expression) vectors was performed with 800ug/ml of Neomycin in both cell lines for the indicated times. For all experiments (including the screens), 3T9 and FL5.12 cells were split every two days and every day, respectively, both at a 1:4 dilution in order to keep all cultures sub-confluent

and in a logarithmic growth state. OHT was added to the fresh medium during cell splitting or dilution to ensure constant concentration.

To derive Eμ-*myc*/Cas9 lymphomas, Eμ-*myc*/Rosa26*Cas9* mice[418] were monitored for lymphoma development (by peripheral lymph node palpation 3 times a week): tumors were dissected, and cells were placed in culture and stabilized as previously described[419]. Lymphoma cells were maintained in a 50:50 mixture of DMEM and IMDM, 10% serum, 2mM L-glutamine, 1% penicillin/streptomycin, 50μM **β**-mercaptoethanol and 1% non-essential amino acids.

2.4 Plasmids and cloning

For expression of MycER^{TM} in FL5.12 cells, we constructed the retroviral vector *pMSCV-MycER-IRES-BleoR* (Figure 15A). Specifically, we started from *pMSCV-IRES-GFP* (#20672, Addgene) where the GFP cassette, flanked by NcoI and ClaI sites, was replaced by the BleoR cassette from *pMSCV-BleoR* (#75088, Addgene). The MycER^{TM} cassette[363] was recovered from a pBabe retroviral vector (Figure 15B) digested with EcoRI-HF (#R3101S, NEB), gel-purified and ligated into EcoRI-digested *pMSCV-IRES-BleoR* (the EcoRI site being located before the IRES element).

For the expression of Cas9 in FL5.12^{Mycer} and 3T9^{Mycer} cells, we used the lentiviral vector *EFIas-Cas9-P2A-BFP-P2A-BlastR* (Figure 15C; a gift from Johannes Zuber)[412]. For the expression of sgRNAs, we used the lentiviral vector *hU6-sgRNA-EFIas-Thy1.1-P2A-NeoR* (sgETN, a gift from Johannes Zuber)[412], without the deep-seq primer binding site (PBS Nras LSL primer binding site), present in the sgRNA library vector (Figure 17, bottom) and required for sequencing. We cloned the sgRNAs by first annealing complementary synthesized sgRNAs of 18-, 19- or 20mers, flanked by two BsmBI sites for cloning into the sgETN vector. Oligonucleotide annealing was coupled with 5'-end phosphorylation with PNK (#M0201S, NEB), with incubation at 37˚C for 30 minutes, 95˚C for 5 minutes, followed by a ramp down to 25˚C (5˚C/min). The sequences used for individual sgRNAs were the same as in our

library[412], except for those targeting NMD factors, and listed in Table 1. The sgETN backbone was digested with BsmBI (#R0739, NEB), gel-purified and ligated with the annealed oligonucleotides.

For sgRNA expression in mouse-derived lymphoma cells, we used the retroviral vector *MSCV-pU6-(BbsI)-CcdB-(BbsI)-Pgk-Puro-T2A-BFP* (Addgene # 86457; Figure 29A), that we cloned by using the same annealed sgRNA oligonucleotides and protocol as for cloning into sgETN. The only difference is given by the BbsI digestion of the backbone, which produces ends matching with those of BsmBI digestion.

For the expression of shRNAs, we used the same lentiviral vector as for the shRNA library, *SFFV-GFP-mirF-shRNA-PGK-NeoR* (Figure 17, top; a gift from Johannes Zuber). The 97-mer oligonucleotides coding for the shRNAs used in this study are listed in Table 2[411,420]. Synthetic oligonucleotides were PCR amplified, using the primers miRF-Xho-fw (5'-TGAACTCGAGAAGGTATATTGCTGTTGGCAGTGAGCG-3') and miRE-EcoOligo-rv (5'-TCTCGAATTCTAGCCCCTTGAAGTCCGAGGCAGTAGGC-3'), in order to generate flanking XhoI- and EcoRI-sites. Both insert and backbone were digested with EcoRI-HF (#R3101S, NEB) and XhoI (#R0146S, NEB) and gel-purified before ligation.

For the generation of stable knock-out clones, cells were electroporated with two plasmid co-expressing the Cas9 gene and two different sgRNAs. The plasmid used for this purpose is *pX458_pSpCas9(BB)-2A-GFP* (Figure 32B). The couple of sgRNAs used for each gene knock-out are listed in Table 3. Cloning of the sgRNAs into this plasmid was performed as for the other sgRNA-expressing vectors, through BbsI-mediated digestion.

All described plasmids are listed in Table 4 with the corresponding internal code number.

All described gel purifications were performed by using the Wizard® SV Gel and PCR Clean-Up System kit, by following manufacturer's protocol. All described ligation steps were performed using T4 DNA ligase (#M0202S, NEB) and associated

T4 ligase buffer. Cloned regions were always sequenced by automated Dye-Terminator Sequencing (Sanger Sequencing).

All illustrated maps were generated by SnapGene® Viewer software.

sgRNA sequence	Gene		sgRNA sequence	Gene
GAAGATGGGCGGGAGTCTTC	Rosa26		GAAGCAGACGCAGAAGAACA	Dhx36 (#3)
GGGCCGGTCGATATACTG	Rpa3		GCGAGAACGTGACCAAGG	Khsrp (#1)
GTAGCGACCGCAACATAGGA	Myc		GAAGAGTATAGGGTTCCGGA	Khsrp (#2)
GTACTCGCTGAGTTCCACGT	Ncbp2 (#1)		GGCTCCCAGAACACAAATG	Khsrp (#3)
GATATAAAGAAGATCATCA	Ncbp2 (#2)		GATGTTGCTTGAAGTCCGGA	Tnpo1 (#1)
GAGGACTACGATGCTGGAAG	Ncbp2 (#3)		GATGTGCAGCATGAGCGCCT	Tnpo1 (#2)
GAAGTACCGAAAAGAGCAG	Noc3l (#1)		GGGGATCATGATGTTGAGA	Tnpo1 (#3)
GACGTGCAGCAAGAAGAGG	Noc3l (#2)		GGGCGGAATGAATGATGACG	Zc3h4 (#1)
GAAGCTGAAGAAGAGCAATG	Noc3l (#3)		GGACAAGAGAGGAGTCGGA	Zc3h4 (#2)
GGTCAAGAAGTCTGATGTGG	Hnrnpc (#1)		GCACCACAGCGACTCTGAGG	Zc3h4 (#3)
GTGGGCTGCTCTGTGCATAA	Hnrnpc (#2)		GAGGCTGGCTACTTCAATG	Acaa2
GGTGGTCAAGAAGTCTGATG	Hnrnpc (#3)		GAAACTGGAGGTCAACGAGG	Ptrf
GAACTTCGAGGAAGATGAAG	Upf1 (#1)		CAAAGTTGCGAACCCCATT	Smg1 (#2)
GTGGTTCTGCAATGGCCG	Upf1 (#2)		TCGTATTCGACAGGCCTTT	Smg1 (#3)
GCTAGCTGAGCTGAACTTCG	Upf1 (#3)		CTCAAAGGACACTTCCGAC	Smg5 (#2)
GCTATCCTGCCAGAACTTGG	Xrn1 (#1)		AACCTTGGTCTAACCAACG	Smg5 (#3)
GAAGGAGAGCATAAAATCA	Xrn1 (#2)		CGATAATGGATGTCGCCGG	Smg6 (#2)
GATGCGCTGCCTCTTCTTTA	Xrn1 (#3)		CGGCGCCAGGATCGGGCCA	Smg6 (#3)
GAGAGAGTGGCCACAGAAA	Dhx36 (#1)		ACTCAGGTATACATGACCG	Smg7 (#2)
GAGAGAGTGGCCACAGAA	Dhx36 (#2)		AGCCCTCTTCGAGAGAAGT	Smg7 (#3)

Table 1. List of used sgRNA sequences for competition assays.

97-mer	Gene
TGCTGTTGACAGTGAGCGCAGGAATTATAATGCTTATCTATAGTGAAGCCACAGATGTATAGATAAGCATTATAATTCCTATGCCTACTGCCTCGGAATTC	Renilla (Ren.713)
TGCTGTTGACAGTGAGCGCGCGACTCCTATAATTTCTAATTAGTGAAGCCACAGATGTAATTAGAAATTATAGGAGTCGCTTGCCTACTGCCTCGGA	Rpa3 (Rpa3.455)
TGCTGTTGACAGTGAGCGCACGACGAGAACAGTTGAAACATAGTGAAGCCACAGATGTATGTTTCAACTGTTCTCGTCGTTTGCCTACTGCCTCGGA	Myc (Myc.1891)
TGCTGTTGACAGTGAGCGCCCCGATGAAATTCTATACACATAGTGAAGCCACAGATGTATGTGTATAGAATTTCATCGGGTTGCCTACTGCCTCGGA	Noc3l #2 (Noc3l.1860)
TGCTGTTGACAGTGAGCGAAGCACCATAGTTGAAAGCAAATAGTGAAGCCACAGATGTATTTGCTTTCAACTATGGTGCTGTGCCTACTGCCTCGGA	Noc3l #3 (Noc3l.2925)
TGCTGTTGACAGTGAGCGCTGATGTCATTGAAGAATGTAATAGTGAAGCCACAGATGTATTACATTCTTCAATGACATCATTGCCTACTGCCTCGGA	Rbm39 #1
TGCTGTTGACAGTGAGCGAAGATGTGAGAATGATTTCTGATAGTGAAGCCACAGATGTATCAGAAATCATTCTCACATCTCTGCCTACTGCCTCGGA	Rbm39 #3
TGCTGTTGACAGTGAGCGATGACAGTGATGATGAATACGATAGTGAAGCCACAGATGTATCGTATTCATCATCACTGTCACTGCCTACTGCCTCGGA	Srrt #2
TGCTGTTGACAGTGAGCGATCCTGCATTGCTACATCAGTATAGTGAAGCCACAGATGTATACTGATGTAGCAATGCAGGAGTGCCTACTGCCTCGGA	Srrt #3
TGCTGTTGACAGTGAGCGAACCCTTTGTTACTCAAAGTAATAGTGAAGCCACAGATGTATTACTTTGAGTAACAAAGGGTCTGCCTACTGCCTCGGA	Yhtdf2 #1
TGCTGTTGACAGTGAGCGACGAACTGGAAGAAAATTTTTATAGTGAAGCCACAGATGTATAAAAATTTTCTTCCAGTTCGGTGCCTACTGCCTCGGA	Yhtdf2 #2 (Ythdf2.2662)
TGCTGTTGACAGTGAGCGAACCGTTCCATTAAGTATAATATAGTGAAGCCACAGATGTATATTATACTTAATGGAACGGTGTGCCTACTGCCTCGGA	Yhtdf2 #3
TGCTGTTGACAGTGAGCGAAGCCCAGAACTTCTATGAGAATAGTGAAGCCACAGATGTATTCTCATAGAAGTTCTGGGCTGTGCCTACTGCCTCGGA	Zc3h4 #3

Table 2. List of used shRNA sequences for competition assays.

sgRNA sequence	Gene
TGCAGCATACCTGCAGGCGT	Upf1 (#4)
CAGCCCCATTTTGCAAGATG	Upf1 (#5)
TTCTCTCTAGGTTGGACCAG	Upf1 (#6)
TTTCAGGTTTGGTTAGTGTG	Upf1 (#7)
TATGTAAATGAGGTAGATGA	Xrn1 (#4)
GCAGCACTCTAATAAATGGA	Xrn1 (#5)
ATGTTGGTCATCTCTTAAGT	Smg7 (#4)
GAAGTCAGAAACACCCCACT	Smg7 (#5)

Table 3. List of sgRNA used for the generation of stable knock-outs.

Plasmid name	Internal code
pBabe-MycER-BleoR	2465
pMSCV-BleoR	3267
pMSCV-IRES-GFP	2102
pMSCV-IRES-BleoR	3317
pMSCV- MycER-IRES-BleoR	3318
EFIas-Cas9-P2A-BFP-P2A-BlastR	3324
hU6-sgRNA-EFIas-Thy1.1-P2A-NeoR	3322
MSCV-pU6-(BbsI)-CcdB-(BbsI)-Pgk-Puro-T2A-BFP	3336
SFFV-GFP-mirF-shRNA-PGK-NeoR	3323
pX458_pSpCas9(BB)-2A-GFP	3074

Table 4. List of plasmids used throughout this study with the corresponding internal code.

2.5 Screening procedures: library production, transduction and passaging

For viral packaging of our libraries, we co-transfected ca. $6x10^6$ HEK-293T cells (in 20 10cm-dishes) with 10µg of DNA from each of the pooled sg- or sh-RNA library, 5µg of DNA from pMD2.G plasmid (#12259, Addgene) for VSV-G envelope expression and 5µg DNA from psPAX2 plasmid (#12260) for Pol and Gag packaging protein expression, using Lipofectamine™ 3000 transfection reagents with the manufacturer's protocol (L3000001, ThermoFisher). Viral supernatants were harvested 48h post transfection, pooled (yielding ca. 100 ml in total for each library), cleared of cellular debris by filtration through a 0.45µm PES filter (VWR) and stored at -80°C. Virus titration was performed by infecting either $3T9^{Mycer/Cas9*}$ or $FL5.12^{Mycer/Cas9*}$ cells with different dilutions and scoring either GFP (for the shRNA library) or CD90.1 (sgRNA library) positivity by flow cytometry on the next day. Screens were performed in triplicates as depicted in Figure 19D: for each technical replicate, at least 30 million cells were transduced at MOI (multiplicity of infection) <0.2 to ensure single viral integration in at least 4,5 million cells, thus maintaining a 1000x library representation. For infection, aliquots of viral supernatant were thawed, diluted in medium, supplemented with 2µg/ml polybrene (Merck Millipore) and either added directly to $3T9^{Mycer/Cas9*}$ cells, or used for spin infection of $FL5.12^{Mycer/Cas9*}$ cells. 24h after infection, we determined the efficiency of

transduction (below <20%) by flow cytometry; on the same day, we initiated antibiotic selection of the infected cells with 800ug/ml of neomycin, which was maintained for either 6 days (for 3T9$^{Mycer/Cas9*}$ cells) or 4 days (for FL5.12$^{Mycer/Cas9*}$ cells). After selection, parallel cultures of the same cells were treated or not with OHT, and kept in a sub-confluent state for the whole duration of the screen, by routinely splitting 3T9$^{Mycer/Cas9*}$ cells every 2 days or diluting FL5.12$^{Mycer/Cas9*}$ cells every day, until reaching a total of 12 population doublings. Cells were sorted at the described time points with the BD FACSMelody™ Cell Sorter, according either to GFP positivity (for shRNA expression) or to combined CD90.1 and BFP positivity (for sgRNA and Cas9) upon anti-CD90.1 immunostaining. 5 million cells were sorted from each replicate sample. For FL5.12$^{Mycer/Cas9*}$ screens only, 30 million cells were harvested and collected the day after infection for the "Post Infection" sample.

2.6 Genomic DNA extraction and NGS library preparation

Genomic DNA (gDNA) was extracted from cells collected the day after infection (for FL5.12$^{Mycer/Cas9*}$ screens only), after selection and after 12 population doublings in the two conditions (with and without OHT). gDNA extraction from at least 4.5 million cells per sample was performed with the NucleoSpin® Tissue kit (# 740952, Macherey-Nagel) following the manufacturer's protocols and using two or three columns per sample. Extracted gDNA of each sample was completely used for PCR reactions in multiple parallel reactions, each of them containing1µg as template.

NGS libraries from the samples of the sgRNA screens were generated by two rounds of PCR amplification: as depicted in Figure 20, primers of the first PCR bind the sgETN-Library vector at a unique and optimized primer binding site seated the start of the U6 promoter and the reverse primer, harboring a unique barcode for each sample, binds a downstream fragment of the sgRNA sequence. First-round PCR reactions contained 50µl of 1µg of template, 1× AmpliTaq Gold buffer, 2mM $MgCl_2$, 0.2mM dNTPs, 0.2µM of each primer and 1.2U AmpliTaq Gold (Applied Biosystems), and were run using the following cycling parameters: 95 °C for 10 min; 25 cycles of 95 °C for 30 s, 57 °C for 45 s and 72 °C for 30 s; 72 °C for 7 min. PCR

products were pooled and concentrated with NaOAc (1/10 of volume) and cold ethanol (2 volumes), purified on a 3% agarose gel (QIAquick gel extraction kit, Qiagen) and completely used for the second-round PCRs, performed in multiple parallel reactions, each of them containing 10ng as template. The cycling parameters of the second PCR differed for the number of cycle (4 instead of 25) and the annealing temperature (62 °C instead of 57 °C). Second-PCR products were pooled, purified first with the QIAquick PCR Purification Kit and then again through gel. Diluted DNA was quantified using the Qubit™ dsDNA Assay kit (Invitrogen) and quality-checked with the Agilent 2100 Bioanalyzer (Agilent Technologies).

NGS libraries of the shRNA screen samples were generated by PCR amplification of shRNA guide strands using primers that harbor a barcode sequence and the standard Illumina adapters:

- Fw CAAGCAGAAGACGGCATACGAXYXYTAGTGAAGCCACAGATGT, where XYXY is the barcode;
- Rv AATGATACGGCGACCACCGATGGATGTGGAATGTGTGCGAGG.

PCR reactions contained 0.5µg template, 1× AmpliTaq Gold buffer, 0.8mM of each dNTP, 0.3µM of each primer and 3U AmpliTaq Gold, which were run using the following cycling parameters: 95 °C for 10 min; 28 cycles of 95 °C for 30 s, 52 °C for 45 s and 72 °C for 60 s; 72 °C for 7 min. PCR products were pooled, concentrated as before and purified on a 3% agarose gel. Again, DNA was quantified with Qubit and checked with the Bioanalyzer.

Libraries were sequenced using the standard Illumina primers. To provide a sufficient baseline for detecting shRNA/sgRNA depletion in experimental samples, we aimed to acquire >1,000 reads per shRNA/sgRNA. In practice, this depth of coverage required ~10 million reads per sample to compensate for disparities in shRNA/sgRNA representation inherent in the pooled plasmid preparation.

2.7 Data analysis

Illumina-NGS reads were identified, mapped and demultiplexed based on the barcode sequence of each sample. Before analysis, read counts were normalized

to library size. Correlation among samples was calculated with the "heatmap.2" function of the "gplots" package of the R software[421]. Analysis of the positive and negative controls (essential and neutral genes, respectively) was achieved by calculating the ratio of the reads for each sgRNA or shRNA in a given sample with the corresponding reads in the library pool. To compared the distribution of shRNA/sgRNA inserts among samples we employed normalized reads as input data for the MAGeCK algorithm, as described[422–424]. Briefly, in order to rank screening hits by consistent enrichment among multiple shRNA or sgRNAs targeting the same gene, a beta score was calculated for each gene. Furthermore, the FluteMLE[424] feature of the MAGeCK tool performed a normalization of beta scores to exclude possible bias derived from different proliferation rate among samples. To do so, we used considered the beta scores of 167 annotated essential genes of our libraries that were present in the list of 625 genes identified by the same authors in different CRISPR/Cas9 screen studies[425–432]. The beta scores of all genes of the screens were thus normalized based on the median beta score of the 167 essential genes with the assumption that they were equally negatively selected among samples.

Beta score distribution plots were produced with GraphPad Software (Version 9.1.2). Scatter plots of beta scores were produced with the "plot" function of R software. Criteria for hits filtering are described in the text. Venn diagrams were produced by an interactive online tool for comparing lists with Venn's diagrams[433].

2.8 Flow Cytometry

For cell cycle analysis, replicating DNA was metabolically labeled with a pulse of 30nmol/L BrdU (B9285, Sigma) added to the culture medium for 15 minutes (3T9 cells) or 5 minutes (FL5.15 cells). Cells were fixed by adding 2 volumes of cold ethanol (dropwise) and washed once in PBS with 1% BSA. DNA was denaturated with 1ml of 2N HCl for 20 minutes, followed by neutralization with 3ml of 0.1M $Na_2B_4O_7$ pH 8.5. After two washes, the cells were incubated for 1 hour at room temperature with anti-BrdU (347580, Becton Dickinson, at 0.4 μg/ml, protected

from light) and then, after washing, with an AF-488-conjugated anti-mouse secondary antibody (#715-545-150, Jackson ImmunoResearch). Finally, a solution of 2.5 μg/ml Propidium Iodide (PI) and 250 μg/ml of RNaseA in PBS) was added for overnight staining before flow cytometer acquisition.

Measurement of the fraction of dead cells was performed by adding a final concentration of 2μg/ml of PI to cells at the indicated time points and direct flow cytometric detection of PI-positive cells, without washing.

For competitive proliferation assays, cells were harvested at the indicated time points, and directly analyzed by flow cytometry for either GFP positivity (for shRNAs in FL5.12 cells: see map in Figure 17, top) or BFP (for sgRNAs in lymphoma cells: see Figure 29A). For sgRNA competition assays in FL5.12 and 3T9 cells (Figure 17, bottom), cells were first washed with MACS buffer (PBS, 2mM EDTA, 0.5% BSA) and then stained in 50μl of MACS buffer containing 1:200 dilution of specific fluorochrome-conjugated antibodies: BB700, APC or APC-eFluor® 780 Rat Anti-Mouse CD90.1 (Clone: HIS51, eBioscience™), for 15 minutes at 4°C in the dark. Before flow cytometer acquisition, cells were washed again and resuspended in PBS for analysis of CD90.1 and BFP positivity.

Growth curves were generated after automatic cell counting of PI negative cells with MACSQuant® Analyzer at the indicated time points. The proliferation index was calculated by dividing the values of OHT-treated sample by their untreated counterpart.

Samples were acquired with the MACSQuant® Analyzer 10 Flow Cytometer (Miltenyi Biotec) or BD FACSCelesta™ Flow Cytometer. FACS data were then analyzed with the BD FlowJo™ Software. All plots were created with the GraphPad Software (Version 9.1.2).

2.9 RT-qPCR

Total RNA was extracted by using the Quick-RNA™ MiniPrep RNA extraction kit (#R1054, Zymo Research) according to the manufacturer's protocol. cDNA was produced using the reverse transcriptase ImPromII™ Reverse Transcription System

(#A3800, Promega). 10ng of cDNA were used for Real-time PCR reactions with the Applied Biosystems™ Fast SYBR™ Green Master Mix (#4385612 Applied Biosystems™). The primers for the murine genes analyzed in this study are listed in Table 5. To analyze the relative changes in gene expression we used the $2^{-\Delta\Delta CT}$ algorithm, with *Tbp* as housekeeping gene. All bar plots were created with GraphPad Software (Version 9.1.2).

Gene	Fw primer	Rv primer
Myc	TTTTTGTCTATTTGGGGACAGTG	CATCGTCGTGGCTGTCTG
Reep6	GTGCAATGTCATCGGATTTG	TTGCCCGCGTAGTAGAAAG
Rrp9	AGAGACCGCACAGGAAAAGA	ACTTCTGCAACCTGCCTCTC
Noc3l	CTGACGTGCAGCAAGAAGAG	TCCTTCCTGGGGTCTTCAA
Rbm39	CTGGCCAACGAGTTTTAGGA	AGGTCCAGCACTTCCCTTTT
Srrt	GCTCACAAAGACGAGGAGTG	AGGGACAGGAACACCTTCAG
Ythdf2	GATCCGAGAGCCATGTCG	TCCATCCTTTTGATGCACAG
Zc3h4	GCAAGGGCGGAATGAATGAT	CACAACTCTCGCTTCTTCGG
Tbp	TAATCCCAAGCGATTTGCTG	CAGTTGTCCGTGGCTCTCTT

Table 5. Murine primers used for the qPCR of this study.

2.10 Western Blotting

Protein extraction was carried out by resuspending $3x10^6$ to 10^7 cells in Lysis buffer (300mM NaCl, 1% NP-40, 50mM Tris-HCl pH8.0, 1mM EDTA) supplemented with fresh protease inhibitors (CompleteTM Mini Protease Inhibitor Cocktail, #11836153001 Roche-Merck) and phosphatase inhibitors (PhosSTOPTM, #4906845001, Roche-Merck). Following resuspension, cell lysates were sonicated for 10 seconds, cleared by centrifugation at 13000 rpm for 15 minutes at 4°C and quantified by Bradford assay (#5000006, Bio-Rad Protein Assay). Upon quantification and addition of 1/6 volume of 6X Laemmli buffer (375mM Tris-HCl, 9% SDS, 50% glycerol, 9% ß-mercaptoethanol and 0.03% bromophenol blue), samples with 20µg of each lysate were boiled (5 minutes at 95°C), electrophoresed on 4-15% gradient pre-cast polyacrylamide gels (Bio-Rad, #5678084) and

transferred to a methylcellulose membrane (Bio-Rad, #1704271) with a Trans-Blot® SD Semi-Dry Transfer apparatus (BioRad, #1704150; transfer at 0.3 A, 30 min). Membranes were then blocked with 5% milk in TBS-T (10mM Tris-HCl, 100mM NaCl, 0.1% Tween at pH7.4) for 30 minutes, incubated overnight at 4°C with the indicated primary antibodies (listed below), washed three times for 5 minutes with TBS-T and then incubated at room temperature for 1 hour with the corresponding secondary antibodies. After subsequent washes in TBS-T, imaging was performed with enhanced chemiluminescence (ECL) detection kit (Bio-Rad, Hercules, CA, USA) followed by analysis with ChemiDoc XRS+ imaging system and Image Lab Software (Bio-Rad). The primary antibodies used in this study were the following: MYC (Y69, ab32072, Abcam), VINCULIN (V9131, Sigma), XRN1 (sc-165985, Santa Cruz), UPF1 (ab109363, Abcam), ACTIN (A4700, Sigma-Aldrich), γH2AX (05-636, Merk Millipore) and H3 (ab1791, Abcam), SMG7 (A302-170A, Bethyl Laboratories). The secondary antibodies were Goat Anti Mouse IgG (H+L) HRP (#170-6516, Bio-Rad) or Goat Anti Mouse IgG (H+L) HRP Conjugate (#926-32211, LI-COR).

2.11 Generation of stable knockout clones

FL5.12^{Mycer} cells were electroporated with ca. 0.5μg each of two sgRNA-Cas9-co-expressing plasmids (see Figure 32 for details). The sgRNAs expressed by each plasmid are listed in Table 3 and visualized in Figure 32C. The sequences targeted by the pair of sgRNAs in each locus were ca. 100bp apart, in order to allow efficient detection of the deleted product by PCR. For each targeting gene, 0.4x10^6 cells were subjected to 4 parallel electroporations with the plasmid pair by using the Neon™ Transfection System 10μL Kit (MPK1025, Invitrogen). The setting of the electroporation apparatus was as follows: 1550 pulse Volts; 20 milliseconds of pulse width; 1 total pulse. Following electroporation, cells were plated in 500μL fresh medium without antibiotics. The day after cells were diluted and on the second day single GFP positive cells were sorted onto 96-well plates, in order to generate clonal populations. The medium for sorted cells contained 100μg/ml gentamycin. Clonal populations were expanded by serial passages and screened by PCR.

2.12 Knockout validation of clones

Following the paired sgRNA transfections for targeted knockouts (see above, section 2.11), sorted cells and the resulting cell clones were tested by PCR for the presence of the deleted gene (which generate a smaller PCR product) and absence of the original wild-type allele, thus ensuring bi-allelic targeting. DNA from clonal cell cultures and sorted cells (as control for efficient gene deletion), was extracted with QuickExtract™ DNA Extraction solution (QE09060, Epicentre), by adding 20µl of the solution to 20µl of cell volume, mixing and then incubating for 5 minutes at 95 °C. PCR reactions were performed with 4µl of cell lysate, 2mM $MgCl^2$, colorless 1xGoTaq® Flexi Buffer (M890A, Promega), 0.8mM dNTPs, 0.5µm of each primer, 0.6U of GoTaq® G2 Hot Start Polymerase (M7408, Promega). Primers used for PCR reactions of hit-depleted clones are listed in Table 6 and depicted in Figure 20C as "PCR screen Fw" and "PCR screen Rv".

PCR cycling parameters were the following: 98 °C for 3 min; 55 cycles of 98 °C for 30 s, 58 °C for 45 s and 72 °C for 50 s; 72 °C for 10 min. The WT and KO PCR products were visualized through 1% agarose gel for detection of gene deletion: biallelic deletion was assessed by the presence of a single, smaller band. PCR products of the putative deleted gene were gel-purified (Wizard® SV Gel kit) and then sequenced by automated Dye-Terminator Sequencing (Sanger Sequencing). Alignment of the sequenced PCR products with wild type gene was performed with EMBOSS Needle - Pairwise Sequence Alignment – EMBL-EBI online tool[434].

Gene	Fw primer	Rv primer
Upf1	GAGGAGCACGGGATTCAGTA	GTCAACCAGGAGAGAGCCAT
Xrn1	GTGCACCAGAAGAAACGACA	CCAATGAGGCTGCTGGTTT
Smg7	GCTGTGAAGCTAGACCTGGA	GGGGTCAATGAGAAGGCTGT

Table 6. Murine primers used for PCR detection of depletion of indicated genes.

2.13 Statistical tests

P-values were calculated by a Student's Unpaired t-test and Welch correction, where each group was characterized by an individual variance. Comparisons among groups are described in the figure legends, together with the number (N) of replicate experiments. Mean values and SEM (standard error of the mean) are shown for each experiment.

3. Results

3.1 Lentiviral sh- and sgRNA libraries

In order to identify RNA Binding Proteins (RBP) necessary for the growth of MYC-overexpressing cells, we set up a series of genetic dropout screens, based on both RNA interference and CRISPR/Cas9 technologies, which allow the detection of genes whose loss of function affects cell proliferation and viability[435,436], as illustrated in Figure 13. Firstly, we designed lentiviral shRNA and sgRNA libraries (Table S1) targeting 730 known RBPs, alongside 23 positive controls (13 essential genes and 10 RBPs with validated synthetic-lethality with MYC overexpression) and 47 negative controls (non-essential genes). The RBPs included in our libraries were chosen on the basis of their high expression in different tumor types[373,380] or because they emerged from MYC synthetic lethal screens[224,263,265], albeit not yet validated (Table S1). The selected RBPs are involved in mRNA maturation, ribonucleoprotein biogenesis, translation, RNA transport, localization and degradation, as also corroborated by gene ontology analysis of the library composition (Figure 14). Such results reveal that splicing factors are highly represented, although we filtered most of these out from the libraries as the design stage, owing to the known synthetic lethal interactions between splicing impairment and MYC overexpression[175,176,335] (see "Targeting RNA processing" in section 1.1.8 of Introduction). The design of the shRNA and sgRNA inserts and the construction of both libraries were achieved by Arianna Sabò in our group, in collaboration with Johannes Zuber's laboratory, based on previously described procedures[411,412]. In particular, for each target, we designed and cloned six different shRNAs and sgRNAs, with sequences selected from previously published libraries[411,412], yielding a total complexity of about 4500 shRNAs/sgRNAs in each library.

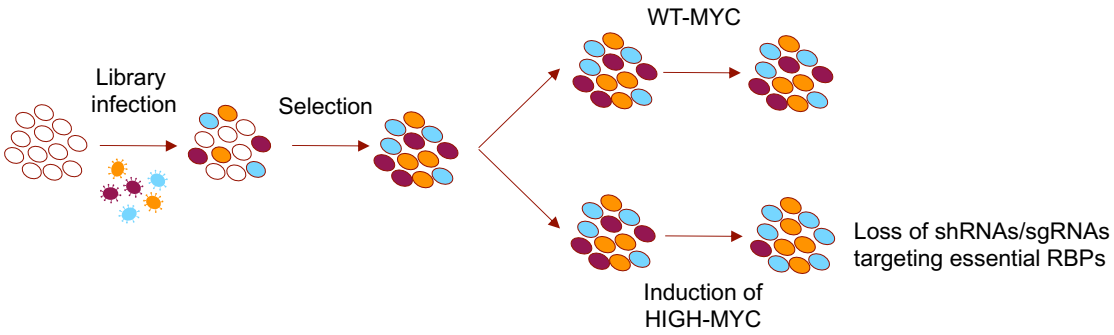

Figure 13. Schematic representation of the dropout screens. Cells are infected with a library of sgRNAs or shRNAs targeting genes of interest and selected; selected cells are divided into two groups, one with a wild-type level of MYC activation ("WT-MYC") and the second with high MYC level ("HIGH-MYC"), and kept in culture. At the end of the experiment those cells infected with sgRNAs or shRNAs targeting a required gene for the survival of HIGH-MYC cells will be lost withing the population. As readout, NGS is used to compare the distribution of sgRNA or sgRNA in WT- and HIGH-MYC conditions at the end of the experiment relative to the starting point.

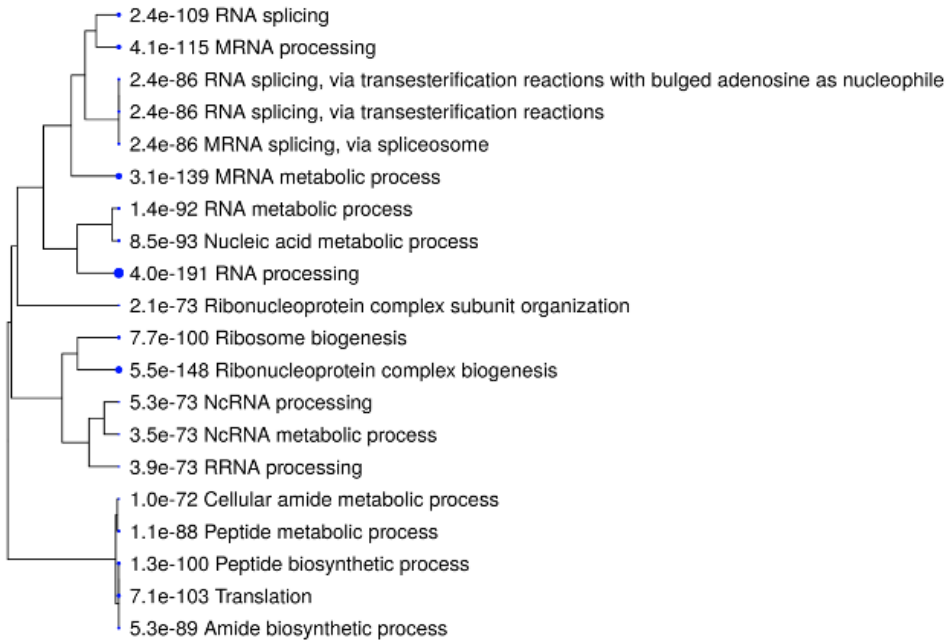

Figure 14. Gene ontology analysis of the selected RBPs. Top 20 pathways enriched by gene ontology analysis of the RBPs included in our libraries, based on the ShinyGO online tool (v0.66)[415]. The results are displayed as a hierarchical clustering tree summarizing the correlation among significant pathways or biological processes. Pathways with many shared genes are clustered together and bigger dots indicate more significant P-values.

3.2 Establishment of the cellular models for the screens

We decided to perform the screens in cell lines in which we could modulate MYC levels in order to identify vulnerabilities that are specific of MYC-overexpressing cells, as opposed to their normal counterpart. As a tool for conditional MYC activation, we used retroviral vectors expressing a chimeric MycER^{TM} fusion protein (Figure 15A, B), which is kept inactive in cells, but can be post-translationally

activated by 4-hydroxytamoxifen (OHT) administration[363]. The cellular models that we choose for the screens are two murine cell lines: 3T9 fibroblasts, for which we already had detailed information on the transcriptional effects of acute MycER^{TM} activation[58,416], and the B-cell progenitor line FL5.12, which represents a more suitable model to address MYC function in B-cell lymphomagenesis, also used to study other pharmaco-genetic interactions in our laboratory[325]. For our CRISPR/Cas9 screens, we infected both cell lines with a lentiviral vector driving constitutive expression of Cas9 (Figure 15C), generating 3T9$^{Mycer/Cas9}$ and FL5.12$^{Mycer/Cas9}$ cells.

In order to eliminate clonal variability as a confounding factor in our screens, we generated a number of clonal populations for both cell lines by deriving BFP-positive (Cas9-expressing; Figure 15C) single-cell clones (Figure 16A) and monitoring MycER^{TM} activity in a subset of these clones. In particular, we assessed the transcriptional activity of MycER^{TM} after 24h of OHT treatment by measuring the activation of two known MYC target genes (*Reep6* and *Rrp9*)[416] at the mRNA level, as well as the auto-regulatory suppression of the endogenous *Myc* mRNA and protein[75] (Figure 16B,C). Flow-cytometric analysis of cell cycle phases in BrdU-labeled cells revealed an increase in the percentage of S-phase cells – most often at the expense of G1 - following MycER^{TM} activation (Figure 16D), indicating accelerated cell cycle progression. In the same conditions, Propidium Iodide (PI) staining revealed no substantial increase in cell death upon MycER^{TM} activation (Figure 16E), owing most likely to the presence of survival factors in the culture medium[159,437]. Although the above experiments showed similar effects among clones and the bulk (polyclonal) population (Figure 16), we selected one clone per cell line to be used in our screens: clone 3 for FL5.12 cells and clone 4 for 3T9 cells, hereafter FL5.12$^{Mycer/Cas9*}$ and 3T9$^{Mycer/Cas9*}$ for simplicity.

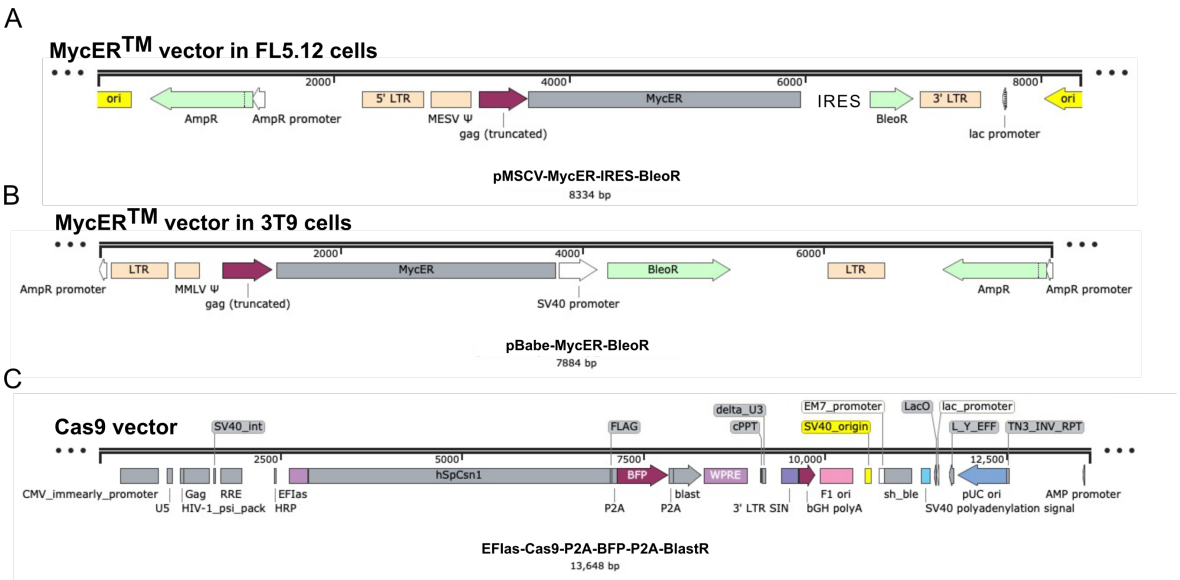

Figure 15. Structure of MycER™- and Cas9-expressing vectors. (A, B) Maps of the retroviral vectors used to express the MycER™ fusion protein (here, MycER) in FL5.12 and 3T9. BleoR: bleomycin resistance. **(C)** Map of the lentiviral vector used to allow the constitutive co-expression of Cas9, BFP and Blasticidin resistance (blast), linked by P2A self-cleaving peptide sequence.

Figure 16 (next page). Characterization of 3T9$^{Mycer/Cas9}$ and FL5.12$^{Mycer/Cas9}$ clones. (A) Flow cytometric profiles of BFP intensity for 5 clones originating from 3T9$^{Mycer/Cas9}$ (left) and 4 clones from FL5.12$^{Mycer/Cas9}$ cells (right). Parental 3T9^{Mycer} and FL5.12^{Mycer} cells (without Cas9 expression) were used as negative controls. **(B)** Variations in endogenous *Myc*, *Reep6* and *Rrp9* mRNA levels in the indicated cells following 24 hours of OHT treatment (100nM in FL5.12 cells, 50nM in 3T9 cells). mRNA expression levels were normalized to *Tbp* as housekeeper, and are expressed as fold-change relative to the untreated condition. **(C)** Western blot analysis of MycER™ (97kDa) and endogenous MYC (57kDa) in 3T9$^{Mycer/Cas9}$ bulk population and clone 4, in the indicated cells, treated as in (B). Vinculin is shown as loading control. Note that for the 3T9 line we used bulk 3T9$^{Mycer/Cas9}$ cells as the only control, since the parental 3T9^{Mycer} population was already clonal[416]. **(D)** Cell cycle analysis with or without OHT treatment, as in (B). Prior to harvesting, cells were pulsed with 30nmol/L BrdU (15 min. for 3T9; 5 min. for FL5.1), followed by fixation, BrdU and PI (DNA content) staining and flow-cytometric profiling. The percentage of cells in each phase of the cell cycle was measured through the gating strategy illustrated in the representative gates on the right: debris in the bottom left corner were excluded with forward versus side scatter (FSC vs SSC) gating; doublets deviating from the diagonal were excluded with PI-area versus -height scatter (PI-A vs PI-H) gating; cells in each cell cycle phases were gated according to the intensity of BrdU (y-axis) and PI (x-axis). **(E)** Percentage of apoptotic (PI positive) cells in the same conditions as in (B), measured by FACS following addition of 2µg/ml PI to the cultures. Representative gates are shown on the right: debris were excluded as in (D) and dead cells were gated according to the intensity of PI (y-axis) in function of FSC (x-axis). The phenotypic assays shown here, aimed at selecting the clones for subsequent screens, were performed as single measurements (N=1).

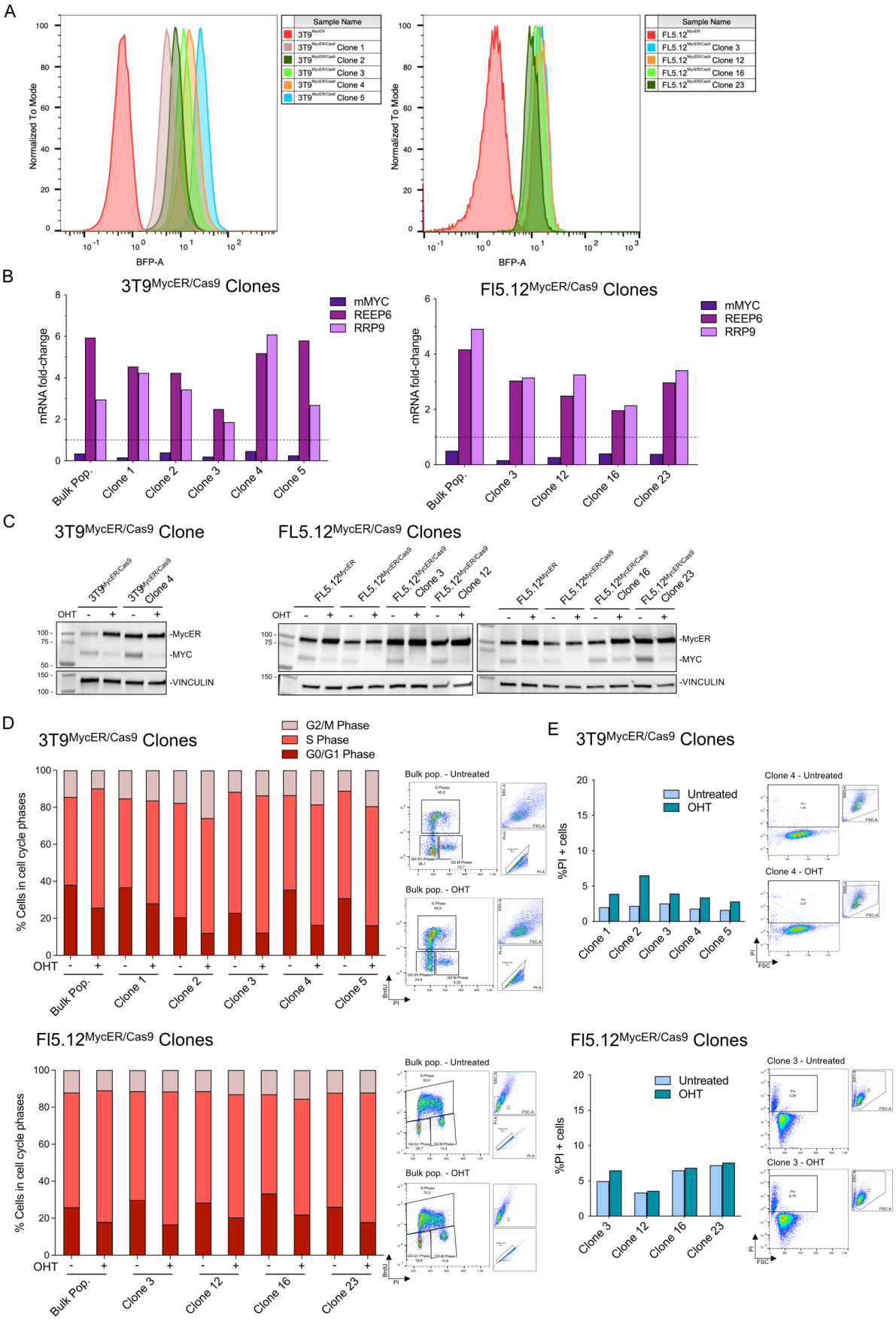

Figure 16. Characterization of 3T9$^{Mycer/Cas9}$ and FL5.12$^{Mycer/Cas9}$ clones. See the legend in the previous page.

3.3 Functional evaluation of the targeting vectors in competitive proliferations assays

As an additional control, we assessed the efficiency of the shRNA- and sgRNA-expressing vectors used for our libraries (Figure 17) in the conditions used for screening. Toward this aim, we subcloned shRNAs or sgRNAs targeting *Renilla* luciferase as a negative control (neutral impact) and *Rpa3* as an essential gene: the resulting constructs were transduced in FL5.12$^{Mycer/Cas9*}$ or 3T9$^{Mycer/Cas9*}$ cells, and the infected cell populations subjected to a competitive proliferation assay allowing to score the positive, neutral or negative impact of each specific insert, as depicted in Figure 18A. In practice, mixed cultures of infected and uninfected cells were serially passaged with periodic flow-cytometric analysis of the percentage of cells positive for either GFP or CD90.1 (used as markers in the shRNA and sgRNA vectors; Figure 17). As expected, the constructs targeting *Rpa3* were rapidly counter-selected, while the control vectors showed no bias, confirming their neutrality in both cell lines (Figure 18B). Based on the results of these tests, we proceeded with the screening experiments.

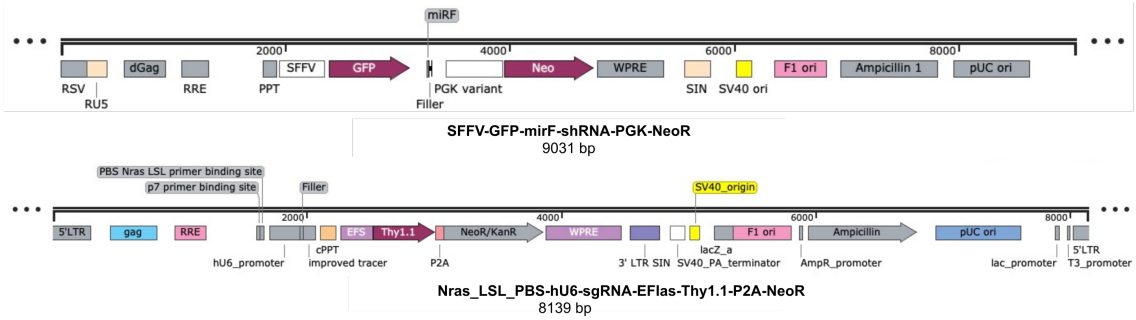

Figure 17. Structure of the library vectors. Maps of the lentiviral vector used for the construction of shRNA (top) and sgRNA (bottom) library, with Neo (or NeoR) as neomycin resistance gene for both vectors, GFP for shRNA and Thy1.1 – or CD90.1 – for sgRNA as reporter genes and Filler as the site of shRNA or sgRNA inclusion. GFP and shRNA are expressed together and are controlled by a promoter different from that of resistance gene. sgRNA expression is regulated by a promoter which differs from that of Thy1.1 and NeoR, which are expressed together and linked by the T2A self-cleaving peptide sequence.

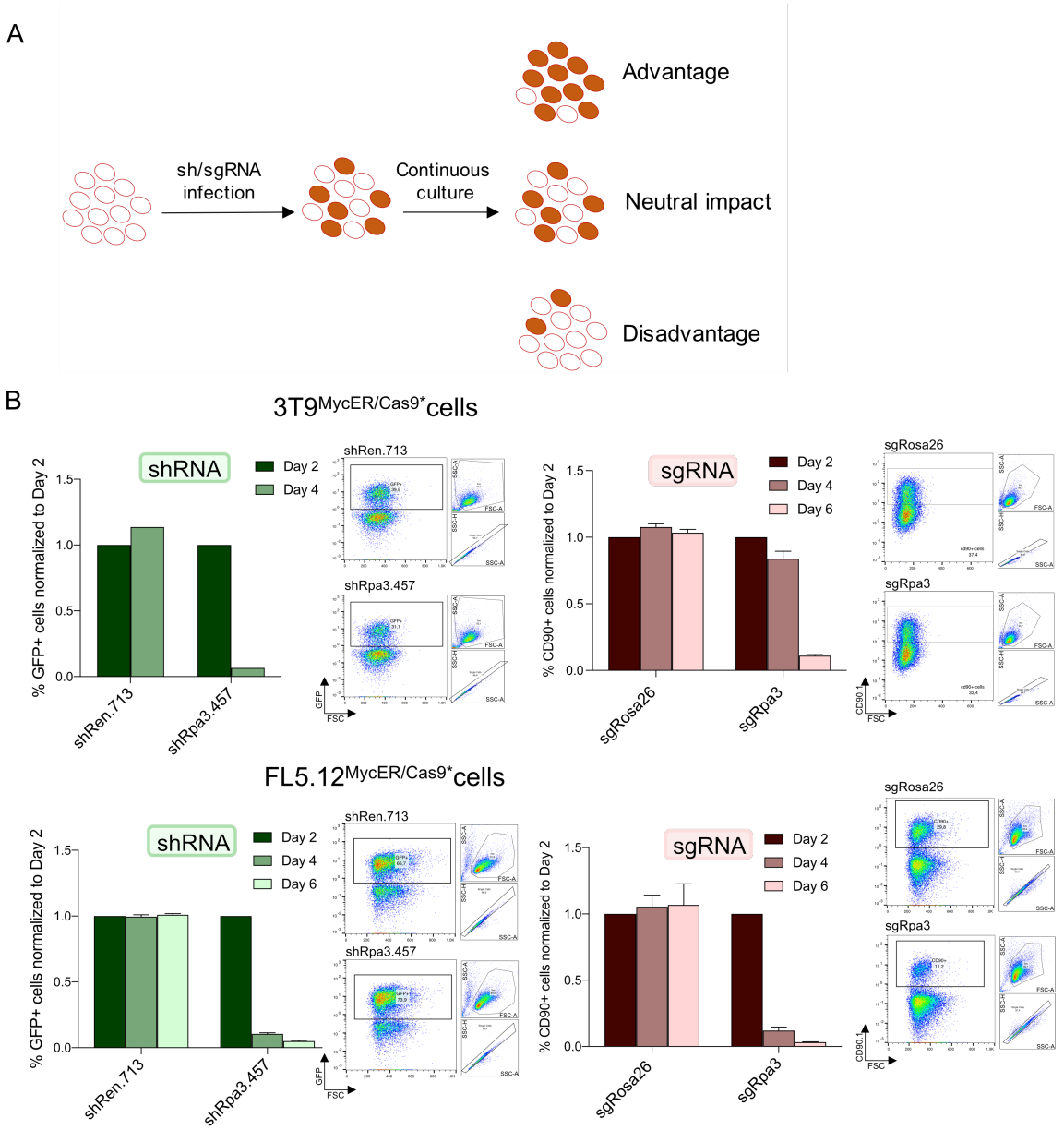

Figure 18. Competitive proliferation assays for the evaluation of knock-down and knock-out efficiency of the shRNA- and sgRNA- expressing vectors. (A) Schematic representation of competitive proliferation assay and possible outcomes: mixed cultures of infected (GFP$^+$ or CD90.1$^+$) and uninfected cells are passaged to score the percentage of GFP$^+$ or CD90.1$^+$ cells by flow cytometric analysis, as a measure of the positive, neutral or negative impact of each shRNA/sgRNA element, as indicated. **(B)** Percentage of 3T9$^{Mycer/Cas9*}$ (top) and FL5.12$^{Mycer/Cas9*}$ (bottom) cells infected with the shRNA/sgRNA elements targeting either *Renilla* luciferase, *Rosa26* or *Rpa3*, as indicated. Cells infected with sgRNAs were stained with anti-CD90.1. GFP and CD90.1 positive cells were measured by flow cytometry at each time-point and normalized to Day 2 after infection. Representative gates of indicated samples are shown for one replicate of day 2: debris in the bottom left corner were excluded with FSC vs SSC gating; doublets deviating from the diagonal were excluded with SSC-area versus -height scatter (SSC-A vs SSC-H) gating; infected cells were gated according to the intensity of GFP (shRNA) or CD90.1 (sgRNA) on the y-axis in function of FSC on the x-axis. N=1 for shRNA competition assay in 3T9$^{Mycer/Cas9*}$cells; N=2 for sgRNA competition assay in 3T9$^{Mycer/Cas9*}$ and FL5.12$^{Mycer/Cas9*}$ cells; N=3 for shRNA competition assay in FL5.12$^{Mycer/Cas9*}$ cells.

3.4 CRISPR/Cas9 screen on 3T9$^{Mycer/Cas9*}$ cells

After establishing libraries, cellular models and vectors to be employed in our screens, we decided to start with the CRISPR/Cas9 screen in 3T9$^{Mycer/Cas9*}$ cells. First, we transfected the pooled plasmids constituting the sgRNA library (hereafter pooled sgRNA library) onto packaging cells to produce the virus. We then proceed to titrate the viral supernatant by infecting 3T9$^{Mycer/Cas9*}$ cells with serial dilutions and measuring the fraction of infected CD90.1^{+} cells (Figure 19A). For the screen, our goal was to favor single-infection events, thus minimizing the probability of multiple integration events. Assuming that the infection of any given cell with a number of virus particles is a stochastic process, we applied a Poisson distribution to calculate the fraction of cells to be infected in order to meet these conditions[438]: on this basis, we estimated that by infecting ca. 20% of cells, the probability that cells would have more than 1 viral particle integration into the cellular DNA is less than 1.8% (Figure 19B). Library infections were thus carried out in triplicate with a 1:15 dilution of the virus, which was effectively transduced in ca. 15% of 3T9$^{Mycer/Cas9*}$ cells (Figure 19C). As summarized in Figure 19D, the cells were then selected with neomycin for 6 days, following which they were passaged in the presence or absence of OHT to activate MycER^{TM}, with particular care to maintain the cells continuously sub-confluent to avert possible MYC-mediated effects on proliferation rate. Moreover, to avoid stochastic loss of sgRNAs during the time in culture, we maintained a coverage of 1000 cells per sgRNA throughout the screens, by infecting, re-plating and harvesting at least 4.5 million cells per sample at each passage. Samples were harvested at the end of the selection ("Post Selection" or "PS") and after 12 population doublings (i. e. 8 days) either with OHT ("HIGH-MYC") or without it ("WT-MYC"). The collection of the cells was achieved by sorting those co-expressing BFP and CD90.1, in order to exclude cells that could have silenced either *Cas9* or the sgRNA (Figure 19E).

Following collection of all the samples, genomic DNA was extracted and used for PCR amplification of the embedded sgRNA sequences to prepare the NGS

(Next Generation Sequencing) libraries for Illumina Sequencing (Figure 20). As well, we generated NGS library from the plasmid pooled sgRNA library to be used as baseline for the analysis. The library preparation protocol was developed by the Zuber laboratory and implied two rounds of PCR amplification (Figure 20): the forward primer (*fw*) of the first PCR annealed to an optimized primer-binding site positioned just upstream of the sgRNA in the library vector, while the reverse primer (*rv*) bound downstream and introduced a 6-bp barcode, different for each sample, allowing correct calling and deconvolution of the samples in subsequent analysis. The resulting PCR products were pooled and the used for second PCR reactions with primers introducing the Illumina sequencing adapters (Figure 20). The resulting libraries were pooled again, analysed for quality check and then used for sequencing on Illumina sequencing platform NovaSeq 6000, with read length of 50bp and depth of 10 million reads for each sample. Altogether, NGS libraries were generated and sequenced for the pooled sgRNA library and the triplicates of Post Selection, WT-MYC and HIGH-MYC samples.

Having completed sample collection and sequencing, we proceed to the computational analysis of the results, with the aim to compare the distribution of the sgRNAs in the WT- and HIGH-MYC groups at the end of the experiment relative to the starting point. This step was performed by Mattia Dalsass, a bioinformatician in our group, but will be described in detail here for the sake of completeness. After sequencing, the reads of each sample were subjected to quality control, alignment and library size normalization with the use of the Empirical Analysis of Digital Gene Expression Data in R (edgeR) tool[439]. A first analysis indicated a high correlation among replicates (Figure 21A). As might also be expected, the WT- and HIGH-MYC samples, which had both undergone 12 additional population doublings (Figure 19D) were closer each-other than to the Post Selection sample and initial sgRNA library (Figure 21A). In line with this finding, the data also showed a coherent trend for the individual control sgRNAs included in the library: regardless of MycER^{TM} activation, positive controls (i. e. sgRNAs targeting essential genes) showed consistent decreases in sequenced reads, in either the WT- or HIGH-MYC

conditions relative to the Post Selection time point (Figure 21B, top); on the other hand, none of the negative controls (targeting neutral genes) underwent such depletion (bottom). Most noteworthy here, sgRNAs targeting the endogenous *Myc* gene were lost selectively in the WT-MYC but not HIGH-MYC condition, thus controlling for the ability of MycER^{TM} to compensate for the loss of endogenous MYC.

In order to properly identify sgRNAs preferentially depleted in HIGH-MYC cells, we took advantage of the bioinformatic tool MAGeCK[422–424], which follows the steps summarized in Figure 22A. This tool permits comparisons among multiple samples by calculating a unique "beta score" for each gene targeted in the library, at each stage (Post Selection, WT-MYC and HIGH-MYC), taking the starting pooled sgRNA library as baseline of the analysis. Most importantly, beta score values encompass the data from the six different sgRNAs for each gene, in the three replicates. Hence, the beta score gives a measure of the degree of selection upon gene perturbation, with positive and negative values indicating enrichment and loss, respectively: thus, genes with a negative beta score in the HIGH-MYC, lower than that in the WT-MYC and Post Selection samples, should be those that are preferentially required for proliferation of MYC-overexpressing cells.

As an additional measure, to avoid biases in hit identification derived from differences in proliferation rates - as faster growing populations would show increased depletion of counter-selected sgRNAs – the MAGeCK pipeline includes the normalization of all beta scores by those of the essential genes present in the library[424]. For this purpose, we used 167 genes present in our library among a list of 625 essential genes selected from previous sgRNA screens by the authors of MAGeCK tool[424–432]. These genes include 11 of our positive controls (*Cdk9*, *Mcm6*, *Pcna*, *Pes1*, *Plk1*, *Psma1*, *Psmb1*, *Rpa1*, *Rpl15*, *Rrm1*, *Top2a*) selected as essential genes throughout the design process of the library (see section 3.1). Indeed, this normalization corrected the general bias observed between the WT- and HIGH-MYC conditions (Figure 22B), thus warranting a more reliable calling of differentially selected genes.

We thus obtained a beta score for each targeted RBP in the sgRNA library, in each of the three conditions (Figure 22C and Table S2). Most noteworthy here, a sizeable fraction of the genes represented in our library was associated with a negative beta score in the three samples (Figure 22C), an indication that most of the genes in our library contribute to some extent to cellular fitness. In order to reliably identify synthetic-lethal interaction with MYC on top of this general trend, we applied a series of selective filtering criteria:

(i) A negative beta score in the HIGH-MYC condition, reflecting net negative selection over time.

(ii) Difference between the HIGH- and WT-MYC beta scores (indicated as $\Delta 1$) below -0.1, reflecting stronger negative selection following MycER^{TM} activation.

(iii) Difference between the WT-MYC and PS beta scores (indicated as $\Delta 2$) below 0.05, reflecting the absence of strong counter-selection in WT-MYC cells.

The resulting filtered list of 31 genes (Figure 22D, E and Table S2) comprised a number of ribosomal protein-coding genes, such as *Rpl23*, and *Rps3*, already known to be mediators of the oncogenic MYC activities[336,344,440,441], and *Huwe1*, a gene encoding an E3 ligase that regulates MYC protein stabilization and has emerged as a possible therapeutic target in MYC-dependent tumors[442–444]. Technical validations for selected hits, including *Ncbp2* (1st ranked hit), *Noc3l* (9th) and *Hnrnpc* (29th) (Figure 22D, E and Table S2) will be presented further below (section 3.6), together with the validations from the screens in FL5.12$^{Mycer/Cas9*}$ cells.

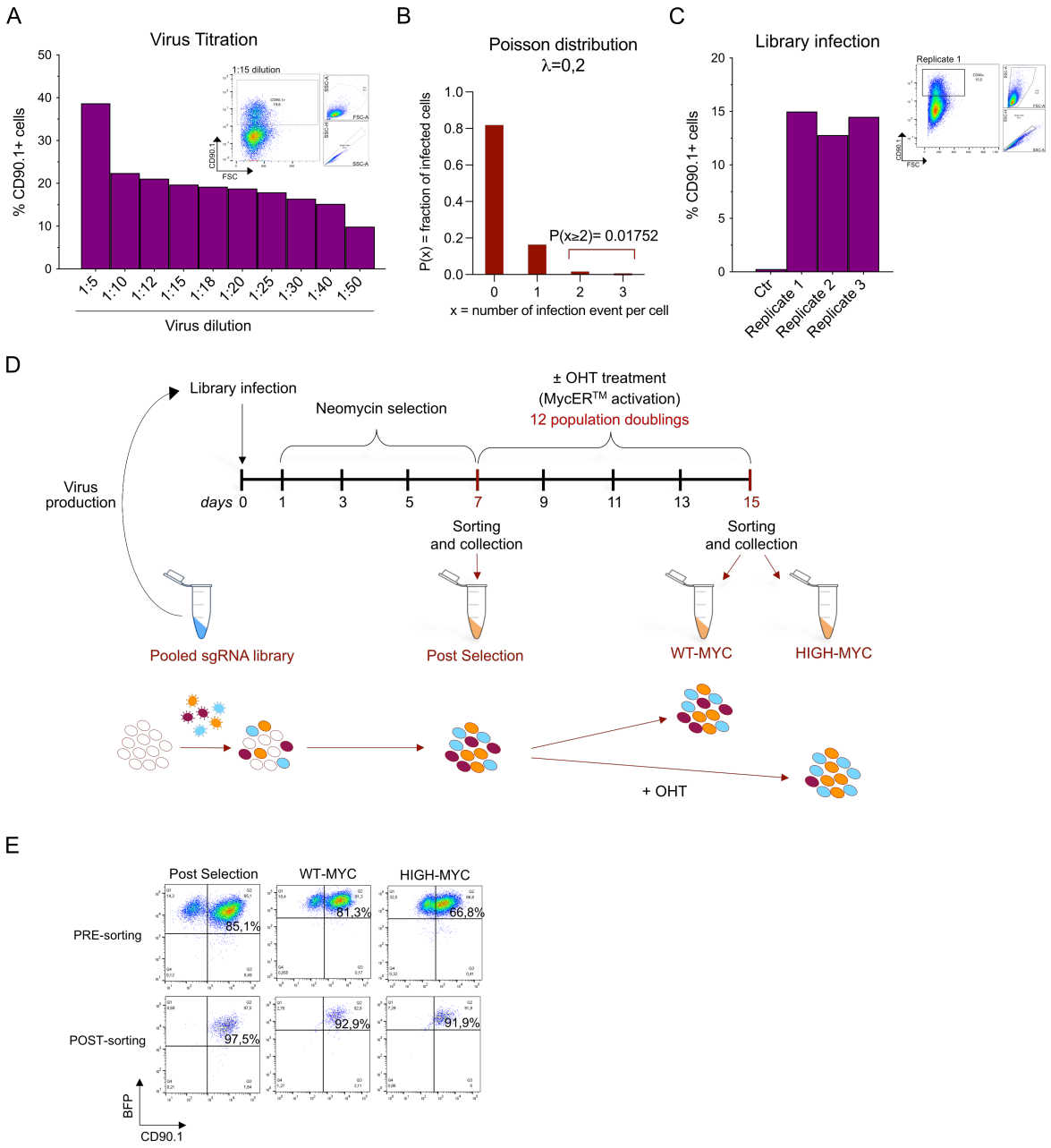

Figure 19. CRISPR screen in 3T9$^{Mycer/Cas9*}$ cells. (A) Percentages of 3T9$^{Mycer/Cas9*}$ cells infected (CD90.1^{+}) with the indicated dilutions of the pooled sgRNA library virus, stained with anti-CD90.1 and measured by flow cytometric analysis one day after infection. Representative gates as described in Figure 18B. N=1. **(B)** Poisson distribution which describe the probability of a number of events as a measure of the fraction of infected cells (on the y axis) in function of the number of infection event per cell (x axis). With $\lambda = 0.2$ as shown here (where λ is the sole parameter that define the distribution and represents the mean rate of occurrence for the event being measured), the probability of one single infection event per cell is almost 20% and that of more than one infection event per cell is less than 2%. Hence, we aimed to initiate all our screens with less than 20% of infected cells in order to ensure single infection events. **(C)** Percentage of infected CD90.1^{+} cells in the triplicate infections used for our screens. Uninfected cells were used as control. Representative gate as in (A). **(D)** Schematic overview of the sgRNA screen in 3T9$^{Mycer/Cas9*}$ cells. For a detailed description, see the text and Methods. **(E)** Representative flow cytometric analysis of one replicate for each sample (Post selection, WT-MYC and HIGH-MYC) before and after sorting cells positive for both CD90.1 and Cas9 (sgRNA and Cas9 reporters, respectively: Figures 15, 17).

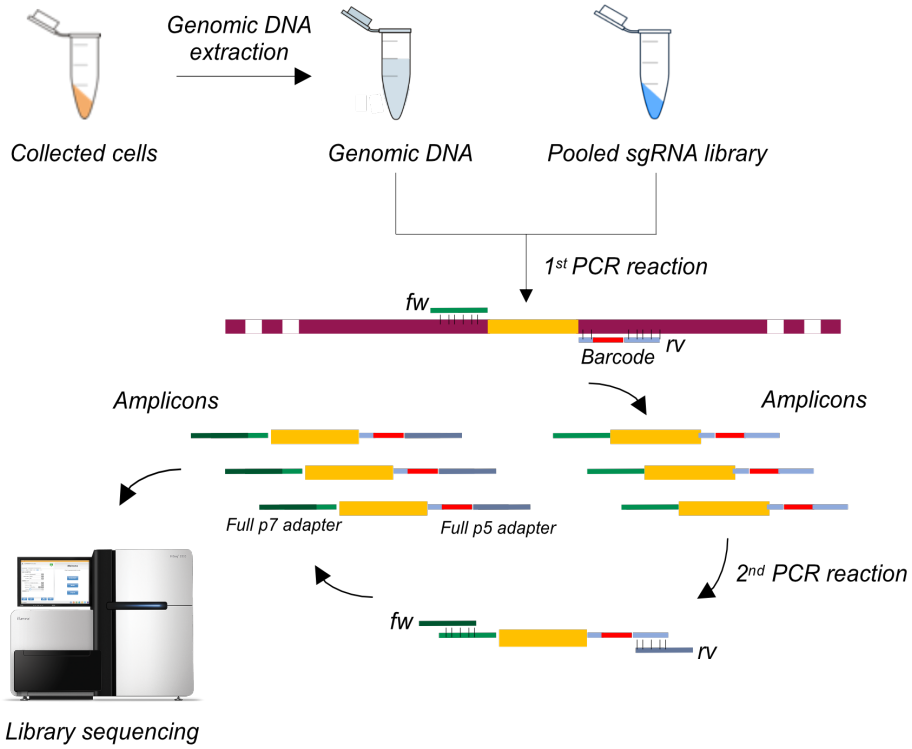

Figure 20. Scheme of NGS library preparation for Illumina sequencing of sgRNA inserts. Plasmid pooled sgRNA library and genomic DNA, extracted from sorted cells, were used as template for a first PCR amplification of the integrated sgRNA sequences. Full adapters were attached by a second PCR amplification step for Illumina-based sequencing. See text and Methods for details.

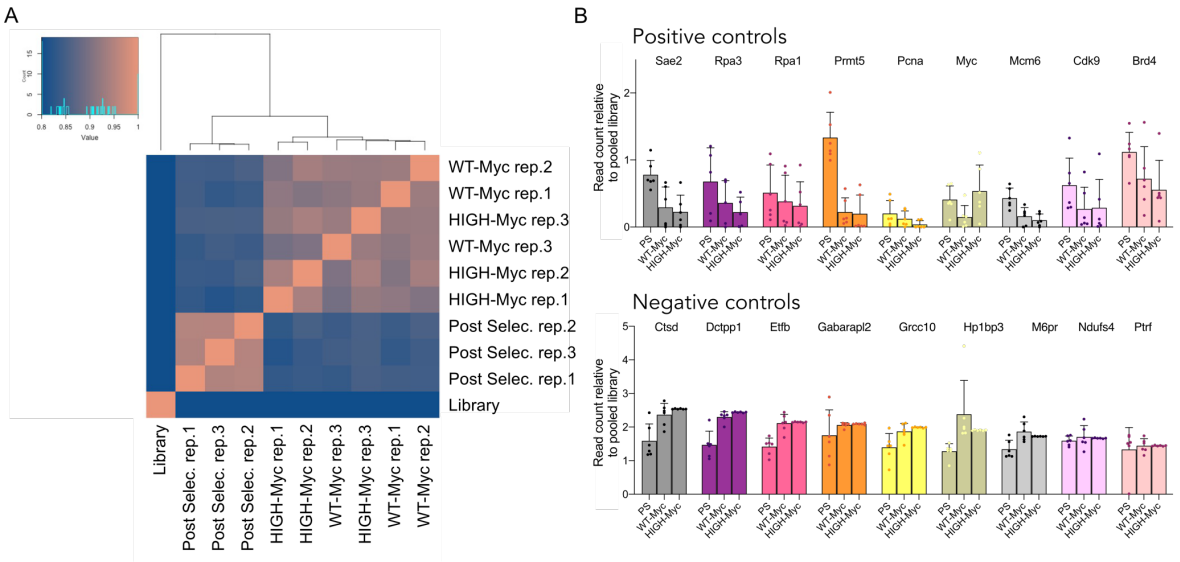

Figure 21. Quality control analysis of sequenced reads from CRISPR screen in 3T9$^{Mycer/Cas9*}$ cells. (A) Sample correlation between biological replicates of the three screening steps (Post selection, WT-MYC and HIGH-MYC; see Figure 19D). Read counts were normalized to library size and their correlation was calculated with the "heatmap.2" function of the R software. **(B)** Read counts for selected positive (top) and negative (bottom) control genes, relative to the read counts of the same genes obtained upon sequencing of the pooled sgRNA library. Each data point represents a different sgRNA targeting the same gene, with bars showing the mean ± SEM, as an indication of variability among different sgRNAs targeting the same gene.

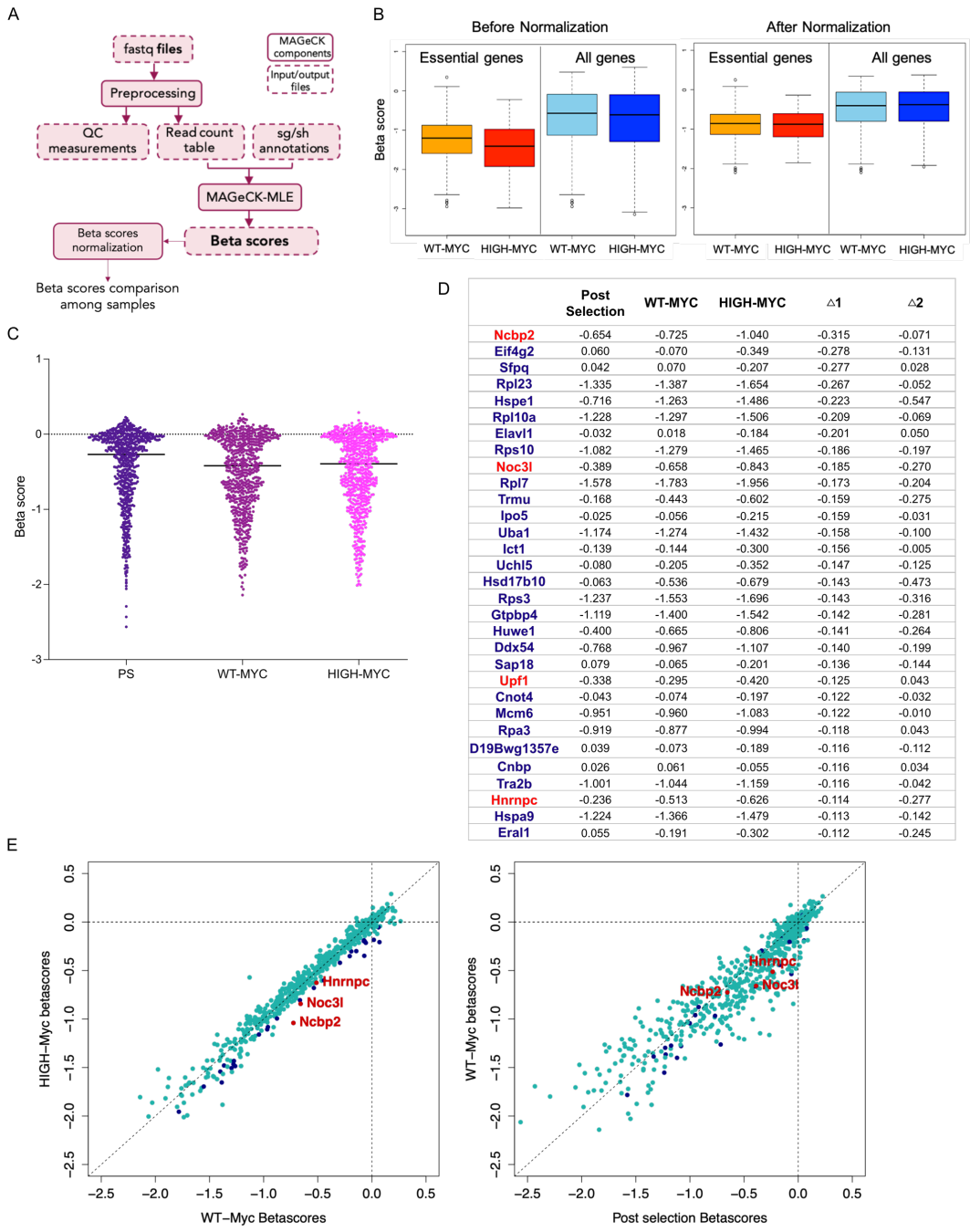

	Post Selection	WT-MYC	HIGH-MYC	Δ1	Δ2
Ncbp2	-0.654	-0.725	-1.040	-0.315	-0.071
Eif4g2	0.060	-0.070	-0.349	-0.278	-0.131
Sfpq	0.042	0.070	-0.207	-0.277	0.028
Rpl23	-1.335	-1.387	-1.654	-0.267	-0.052
Hspe1	-0.716	-1.263	-1.486	-0.223	-0.547
Rpl10a	-1.228	-1.297	-1.506	-0.209	-0.069
Elavl1	-0.032	0.018	-0.184	-0.201	0.050
Rps10	-1.082	-1.279	-1.465	-0.186	-0.197
Noc3l	-0.389	-0.658	-0.843	-0.185	-0.270
Rpl7	-1.578	-1.783	-1.956	-0.173	-0.204
Trmu	-0.168	-0.443	-0.602	-0.159	-0.275
Ipo5	-0.025	-0.056	-0.215	-0.159	-0.031
Uba1	-1.174	-1.274	-1.432	-0.158	-0.100
Ict1	-0.139	-0.144	-0.300	-0.156	-0.005
Uchl5	-0.080	-0.205	-0.352	-0.147	-0.125
Hsd17b10	-0.063	-0.536	-0.679	-0.143	-0.473
Rps3	-1.237	-1.553	-1.696	-0.143	-0.316
Gtpbp4	-1.119	-1.400	-1.542	-0.142	-0.281
Huwe1	-0.400	-0.665	-0.806	-0.141	-0.264
Ddx54	-0.768	-0.967	-1.107	-0.140	-0.199
Sap18	0.079	-0.065	-0.201	-0.136	-0.144
Upf1	-0.338	-0.295	-0.420	-0.125	0.043
Cnot4	-0.043	-0.074	-0.197	-0.122	-0.032
Mcm6	-0.951	-0.960	-1.083	-0.122	-0.010
Rpa3	-0.919	-0.877	-0.994	-0.118	0.043
D19Bwg1357e	0.039	-0.073	-0.189	-0.116	-0.112
Cnbp	0.026	0.061	-0.055	-0.116	0.034
Tra2b	-1.001	-1.044	-1.159	-0.116	-0.042
Hnrnpc	-0.236	-0.513	-0.626	-0.114	-0.277
Hspa9	-1.224	-1.366	-1.479	-0.113	-0.142
Eral1	0.055	-0.191	-0.302	-0.112	-0.245

Figure 22. Computational analysis of CRISPR screen in 3T9$^{Mycer/Cas9*}$ cells with MAGeCK tool. (A) Schematic representation of the MAGeCK analytical pipeline. Starting from processed and normalized read counts, this tool calculates a "beta score" for all the sgRNAs targeting a specific gene at each step (Post selection, WT-MYC and HIGH-MYC) using the starting pooled sgRNA library as baseline, providing a measure of the degree of selection upon gene perturbation: for further detail, see text and Methods. Figure adapted from *Li et al., Genome Biology, 2015 (ref.* 423). **(B)** Distribution of beta scores, before (left) and after (right) the normalization for essential genes in WT-MYC and HIGH-MYC groups (see text and Methods). **(C)** Distribution of beta scores in the indicated samples (PS: Post selection). The horizontal bar indicates the median value. **(D)** List of beta scores in each sample group for the 31 candidate genes passing the three selective filtering criteria: (i.) a negative beta score in the HIGH-MYC condition; (ii.) $\Delta 1 \leq -0.1$ (difference between HIGH- and WT-MYC); (iii.) $\Delta 2 \leq 0.05$ (difference between WT-MYC and PS). Genes are ranked based on decreasing $\Delta 1$ values. Hits chosen for technical validation are depicted in red. **(E)** Beta scores of all scored RBP-coding genes in the WT-MYC condition relative to either HIGH-MYC (left) or Post Selection (right). Those genes that passed our filtering criteria are depicted in blue or red, as in (D). The dashed lines mark the diagonal and the origins of each axis.

3.5 CRISPR/Cas9 and shRNA screens on FL5.12$^{Mycer/Cas9*}$ cells

Following the initial sgRNA screen in the 3T9$^{Mycer/Cas9*}$ model, we pursued the sgRNA and shRNA screens in FL5.12$^{Mycer/Cas9*}$ cells. Following the same procedure outlined above, the sgRNA and shRNA libraries were used for virus production and titration (Figure 23A), followed in both cases by infections with 1:10 dilutions, in order to obtain infection indices below 20% (Figure 23B). For these two screens we decided to collect cells also immediately after infection ("Post Infection or "PI", Figure 23C), as a better initial representation of the sgRNA and sgRNA populations to be employed as baseline for MAGeCK analysis. As FL5.12$^{Mycer/Cas9*}$ grew faster, with a doubling time of 11 hours (compared with 16h for 3T9$^{Mycer/Cas9*}$), these cells were cultured for 6 days to reach 12 population doublings, with or without OHT treatment (Figure 23C). Other samples (PS, WT- and HIGH-MYC) were collected as above, by sorting CD90.1^{+} and BFP^{+} cells for the sgRNA screen, and GFP^{+} cells for the shRNA screen (Figure 23D). NGS library preparation for the CRISPR screen was performed with 2 PCR steps, as above (Figure 20), while only one amplification step was used for the shRNA screen (see details in Methods).

Following Illumina sequencing, the CRISPR screen in FL5.12$^{Mycer/Cas9*}$ cells yielded a close clustering of the three NGS replicates in each sample, with the WT- and HIGH-MYC conditions the closest among them, and equidistant from Post Selection (Figure 24A), consistent with the data in the 3T9 screen (Figure 21A); the additional Post Infection samples clustered at a higher distance, in close proximity with the sgRNA library (Figure 24A), confirming the validity of either sample as a baseline. As above, positive control sgRNAs were generally counter-selected over time (Figure 24B, top), while negative control sgRNAs were not (bottom): in fact, the latter showed apparent increases at late steps (PS, WT- and HIGH-MYC) relative to the earliest (PI), possibly reflecting passive enrichment due to the loss of other counter-selected sgRNAs in the library.

Again, the MAGeCK pipeline was used to assign a beta score for each gene of the library in each sample (PS, WT- and HIGH-MYC), this time using PI as a baseline,

instead of the library (Figure 24C and Table S2). As seen in the 3T9$^{Mycer/Cas9*}$ screen (Figure 22C), a majority of genes also showed negative beta scores in FL5.12$^{Mycer/Cas9*}$ cells (Figure 24C). In order to identify potential vulnerabilities in MYC-hyperactivated cells only, we applied the same filtering criteria used for the initial screen, which yielded a list of 52 genes (Figure 24D, E and Table S2).

In contrast to the sgRNA screen, the shRNA screen showed less distinct clustering of the samples, with some intermingling of the PS and WT-MYC conditions (Figure 25A). Moreover, positive control shRNAs did not show significant variation over time, with either weak or absent negative selection (Figure 25B), thus revealing an appreciable limit of RNAi compared to CRISPR/Cas9-based screening, as previously reported[425,445,446]. Also, the majority of MAGeCK beta scores from the shRNA screen (listed in Table S2) presented values near zero (Figure 25C), indicating poor selection, in striking contrast with the overall negative selection observed in the two sgRNA screens (Figure 22C and 24C). This notwithstanding, we note that the distinct clustering of the HIGH-MYC and PI samples (the latter together with the pooled shRNA Library) were maintained (Figures 24A and 25A), indicating some consistency in the selective pressure exerted over the shRNA inserts. For hit identification in FL5.12$^{Mycer/Cas9*}$ shRNA screen, we applied the same beta score filtering criteria as above and obtained 100 genes (Table S2), the top 10 of which are listed Figure 25D.

By overlapping the filtered hits from the three screens we found 2 genes (*Noc3l* and *Upf1*) common to all, 3 genes (*Ncbp2*, *Ddx54* and *Cnot4*) common to the sgRNA screens in both cell lines, and 18 genes uncovered by both screening methods in FL5.15$^{Mycer/Cas9*}$ cells (Figure 26A). Next, we sought to intersect the hits emerged from our three screens with those listed - but not validated - in prior MYC synthetic-lethal screens[224,263,265]: among 94 candidate hits from these studies that were also present in our libraries, 21 scored as candidates in at least one of our screens (Figure 26B and Table S3).

For technical validation, together with the 3 hits chosen from the 3T9$^{Mycer/Cas9*}$ screen – *Ncbp2, Noc3l* and *Hnrnpc* (red in Figure 22D, E) – we selected the

following genes: *Khsrp*, *Xrn1*, *Tnpo1*, Zc3h4 and *Dhx36* from the sgRNA screen (red in Figure 24D, E), *Ythdf2*, *Srrt*, *Noc3l*, *Rbm39* and *Zc3h4* from the shRNA screen (red in Figure 25D, E), and finally *Upf1* and *Noc3l* as hits common to all three screens (red in Figure 22D, 24D, 26A and Table S2) - the latter already considered for validation from the 3T9$^{Mycer/Cas9*}$ sgRNA screen.

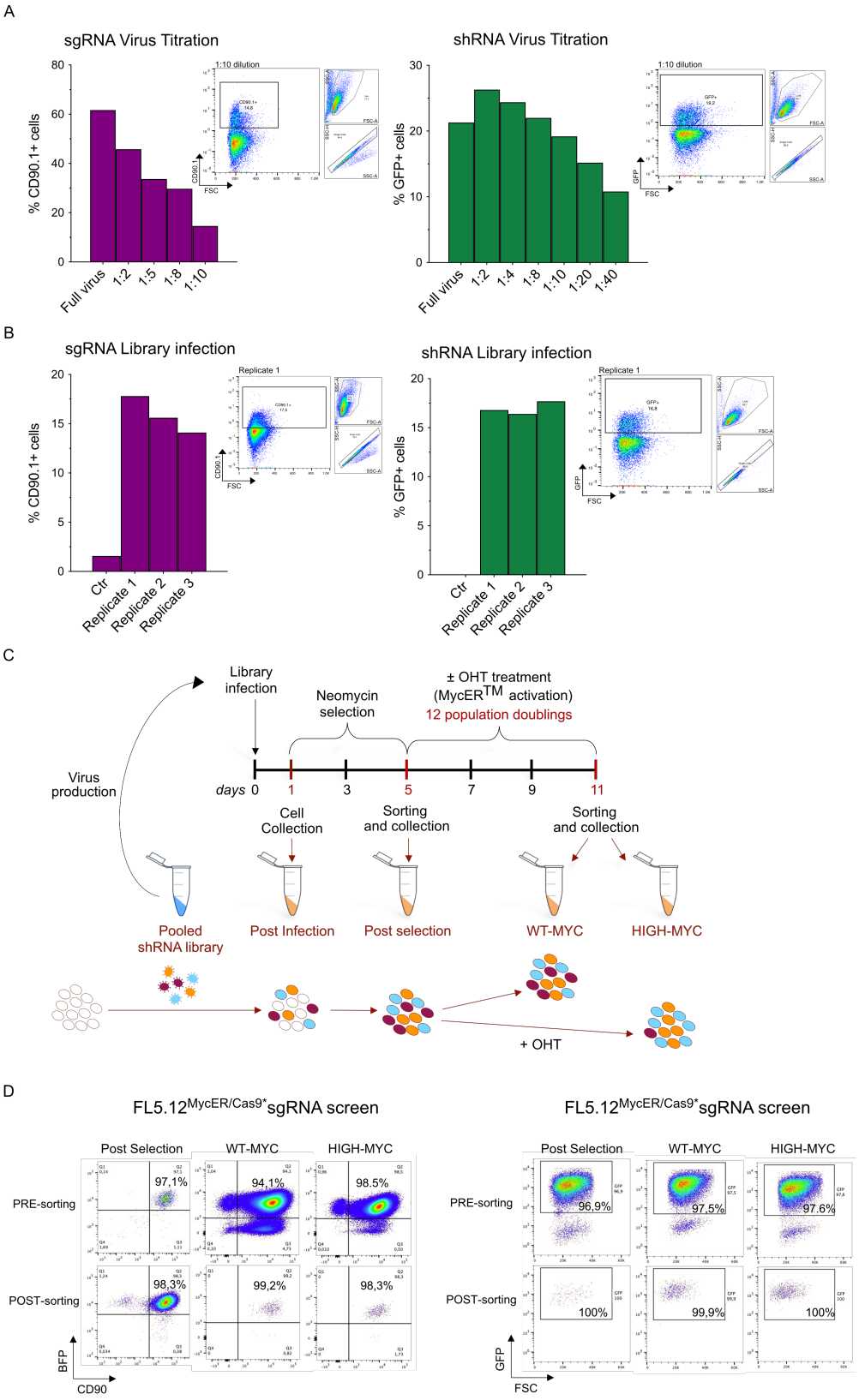

Figure 23. CRISPR/Cas9 and shRNA screen on FL5.12$^{Mycer/Cas9*}$ cells. (A) Percentages of FL5.12$^{Mycer/Cas9*}$ cells infected with different dilution of the library virus of pooled sgRNAs (CD90.1^{+}, left) or shRNAs (GFP^{+}, right), measured by flow cytometric analysis one day after infection. Representative gates as in Figure 18B. For sgRNA infection, cells were stained with anti-CD90.1. N=1. **(B)** Percentage of sgRNA (left) or shRNA (right) infected cells as in (A) of the screen triplicates. Uninfected cells were used as control. Representative gate as in (A). **(C)** Schematic overview of the sgRNA and shRNA screen in FL5.12$^{Mycer/Cas9*}$ cells. For a detailed description, see the text and Methods. **(D)** Representative flow cytometric analysis of one replicate for each sample (Post selection, WT-MYC and HIGH-MYC) before and after sorting cells for double positivity of CD90.1 (sgRNA reporter) and BFP (Cas9 positivity) for the CRISPR screen (left) or GFP^{+} (shRNA reporter) for the shRNA screen (right).

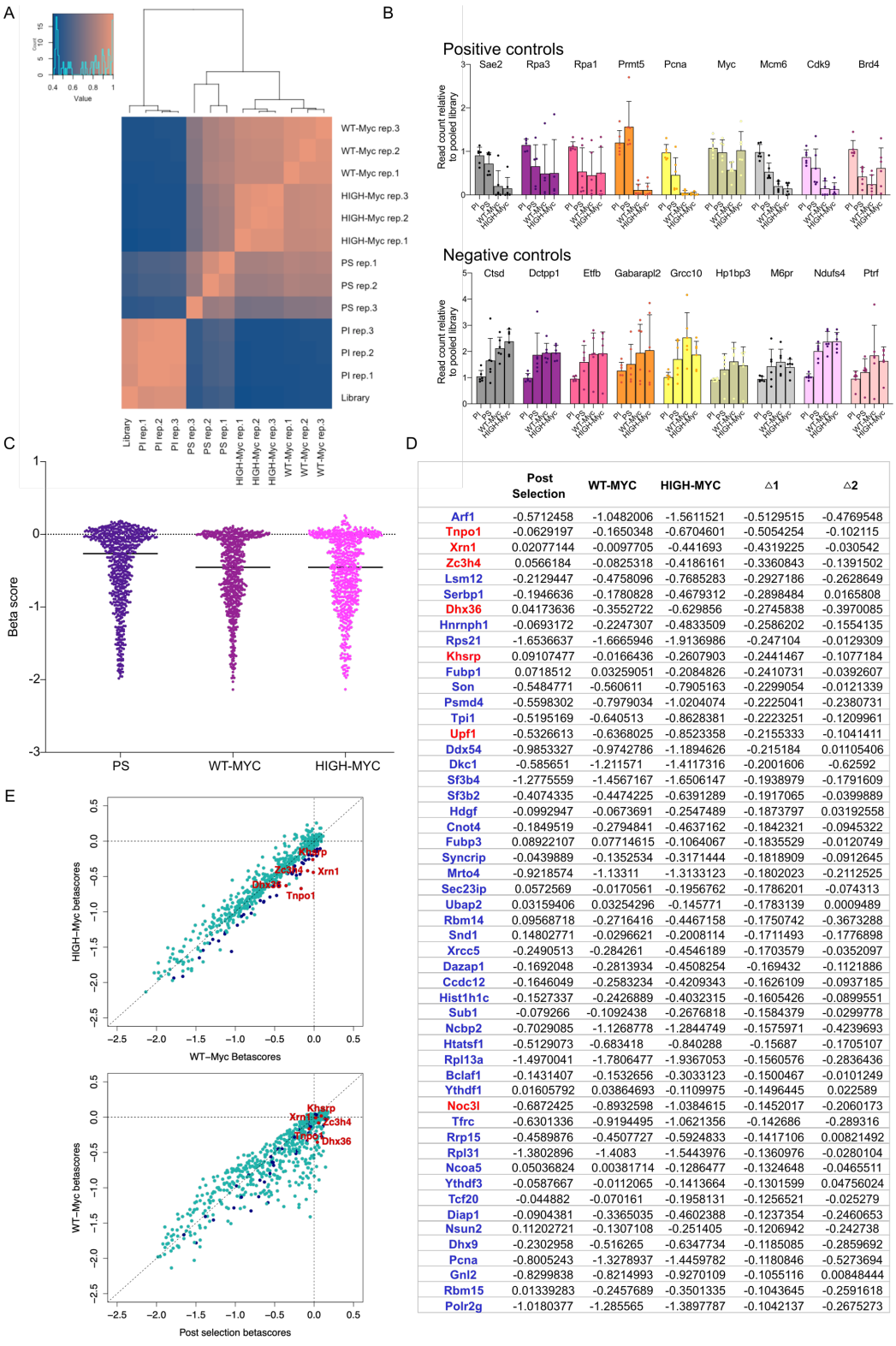

	Post Selection	WT-MYC	HIGH-MYC	Δ1	Δ2
Arf1	-0.5712458	-1.0482006	-1.5611521	-0.5129515	-0.4769548
Tnpo1	-0.0629197	-0.1650348	-0.6704601	-0.5054254	-0.102115
Xrn1	0.02077144	-0.0097705	-0.441693	-0.4319225	-0.030542
Zc3h4	0.0566184	-0.0825318	-0.4186161	-0.3360843	-0.1391502
Lsm12	-0.2129447	-0.4758096	-0.7685283	-0.2927186	-0.2628649
Serbp1	-0.1946636	-0.1780828	-0.4679312	-0.2898484	0.0165808
Dhx36	0.04173636	-0.3552722	-0.629856	-0.2745838	-0.3970085
Hnrnph1	-0.0693172	-0.2247307	-0.4833509	-0.2586202	-0.1554135
Rps21	-1.6536637	-1.6665946	-1.9136986	-0.247104	-0.0129309
Khsrp	0.09107477	-0.0166436	-0.2607903	-0.2441467	-0.1077184
Fubp1	0.0718512	0.03259051	-0.2084826	-0.2410731	-0.0392607
Son	-0.5484771	-0.560611	-0.7905163	-0.2299054	-0.0121339
Psmd4	-0.5598302	-0.7979034	-1.0204074	-0.2225041	-0.2380731
Tpi1	-0.5195169	-0.640513	-0.8628381	-0.2223251	-0.1209961
Upf1	-0.5326613	-0.6368025	-0.8523358	-0.2155333	-0.1041411
Ddx54	-0.9853327	-0.9742786	-1.1894626	-0.215184	0.01105406
Dkc1	-0.585651	-1.211571	-1.4117316	-0.2001606	-0.62592
Sf3b4	-1.2775559	-1.4567167	-1.6506147	-0.1938979	-0.1791609
Sf3b2	-0.4074335	-0.4474225	-0.6391289	-0.1917065	-0.0399889
Hdgf	-0.0992947	-0.0673691	-0.2547489	-0.1873797	0.03192558
Cnot4	-0.1849519	-0.2794841	-0.4637162	-0.1842321	-0.0945322
Fubp3	0.08922107	0.07714615	-0.1064067	-0.1835529	-0.0120749
Syncrip	-0.0439889	-0.1352534	-0.3171444	-0.1818909	-0.0912645
Mrto4	-0.9218574	-1.13311	-1.3133123	-0.1802023	-0.2112525
Sec23ip	0.0572569	-0.0170561	-0.1956762	-0.1786201	-0.074313
Ubap2	0.03159406	0.03254296	-0.145771	-0.1783139	0.0009489
Rbm14	0.09568718	-0.2716416	-0.4467158	-0.1750742	-0.3673288
Snd1	0.14802771	-0.0296621	-0.2008114	-0.1711493	-0.1776898
Xrcc5	-0.2490513	-0.284261	-0.4546189	-0.1703579	-0.0352097
Dazap1	-0.1692048	-0.2813934	-0.4508254	-0.169432	-0.1121886
Ccdc12	-0.1646049	-0.2583234	-0.4209343	-0.1626109	-0.0937185
Hist1h1c	-0.1527337	-0.2426889	-0.4032315	-0.1605426	-0.0899551
Sub1	-0.079266	-0.1092438	-0.2676818	-0.1584379	-0.0299778
Ncbp2	-0.7029085	-1.1268778	-1.2844749	-0.1575971	-0.4239693
Htatsf1	-0.5129073	-0.683418	-0.840288	-0.15687	-0.1705107
Rpl13a	-1.4970041	-1.7806477	-1.9367053	-0.1560576	-0.2836436
Bclaf1	-0.1431407	-0.1532656	-0.3033123	-0.1500467	-0.0101249
Ythdf1	0.01605792	0.03864693	-0.1109975	-0.1496445	0.022589
Noc3l	-0.6872425	-0.8932598	-1.0384615	-0.1452017	-0.2060173
Tfrc	-0.6301336	-0.9194495	-1.0621356	-0.142686	-0.289316
Rrp15	-0.4589876	-0.4507727	-0.5924833	-0.1417106	0.00821492
Rpl31	-1.3802896	-1.4083	-1.5443976	-0.1360976	-0.0280104
Ncoa5	0.05036824	0.00381714	-0.1286477	-0.1324648	-0.0465511
Ythdf3	-0.0587667	-0.0112065	-0.1413664	-0.1301599	0.04756024
Tcf20	-0.044882	-0.070161	-0.1958131	-0.1256521	-0.025279
Diap1	-0.0904381	-0.3365035	-0.4602388	-0.1237354	-0.2460653
Nsun2	0.11202721	-0.1307108	-0.251405	-0.1206942	-0.242738
Dhx9	-0.2302958	-0.516265	-0.6347734	-0.1185085	-0.2859692
Pcna	-0.8005243	-1.3278937	-1.4459782	-0.1180846	-0.5273694
Gnl2	-0.8299838	-0.8214993	-0.9270109	-0.1055116	0.00848444
Rbm15	0.01339283	-0.2457689	-0.3501335	-0.1043645	-0.2591618
Polr2g	-1.0180377	-1.285565	-1.3897787	-0.1042137	-0.2675273

Figure 24. Results from FL5.12$^{Mycer/Cas9*}$ sgRNA screens. (A) Correlation between the pooled sgRNA library and the biological replicates of all the screening steps (Post Infection, Post selection, WT-MYC and HIGH-MYC; see Figure 23C). Read counts were normalized to library size and their correlation was calculated as in Figure 21A. **(B)** Reads counts for selected positive (top) and negative (bottom) control genes, as in Figure 21B. **(C)** Distribution of beta scores in the indicated samples. The horizontal bar indicates the median value. **(D)** List of beta scores in each sample group for the 52 candidate genes passing the three selective filtering criteria, with the Δ1 and Δ2 values, as defined in Figure 22D. Hits chosen for technical validation are depicted in red. **(E)** Beta scores of all scored RBP-coding genes in the WT-MYC condition relative to either HIGH-MYC (top) or Post Selection (bottom). Those genes that passed our filtering criteria are depicted in blue or red, as in (D). The dashed lines mark the diagonal and the origins of each axis.

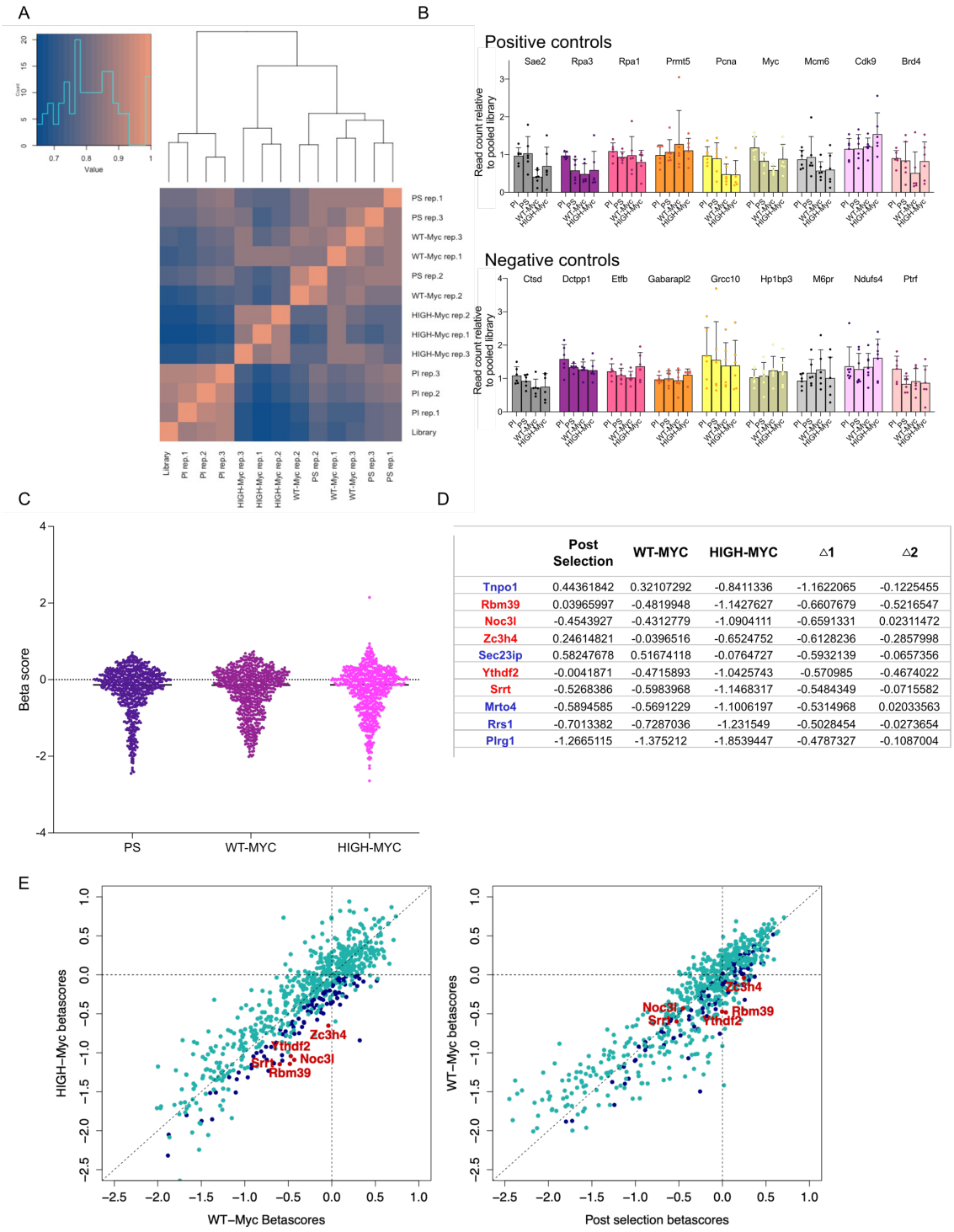

	Post Selection	WT-MYC	HIGH-MYC	Δ1	Δ2
Tnpo1	0.44361842	0.32107292	-0.8411336	-1.1622065	-0.1225455
Rbm39	0.03965997	-0.4819948	-1.1427627	-0.6607679	-0.5216547
Noc3l	-0.4543927	-0.4312779	-1.0904111	-0.6591331	0.02311472
Zc3h4	0.24614821	-0.0396516	-0.6524752	-0.6128236	-0.2857998
Sec23ip	0.58247678	0.51674118	-0.0764727	-0.5932139	-0.0657356
Ythdf2	-0.0041871	-0.4715893	-1.0425743	-0.570985	-0.4674022
Srrt	-0.5268386	-0.5983968	-1.1468317	-0.5484349	-0.0715582
Mrto4	-0.5894585	-0.5691229	-1.1006197	-0.5314968	0.02033563
Rrs1	-0.7013382	-0.7287036	-1.231549	-0.5028454	-0.0273654
Plrg1	-1.2665115	-1.375212	-1.8539447	-0.4787327	-0.1087004

Figure 25. Results from FL5.12$^{Mycer/Cas9+}$ shRNA screens. (A) Correlation between the pooled shRNA library and the biological replicates of all the screening steps (Post Infection, Post selection, WT-MYC and HIGH-MYC; see Figure 23C). Read counts were normalized to library size and their correlation was calculated as in Figure 21A. **(B)** Reads counts for selected positive (top) and negative (bottom) control genes, as in Figure 21B. **(C)** Distribution of beta scores in the indicated samples. The horizontal bar indicates the median value. **(D)** List of beta scores in each sample group for the top 10 candidate genes passing the three selective filtering criteria, with the Δ1 and Δ2 values, as defined in Figure 22D. Hits chosen for technical validation are depicted in red. **(E)** Beta scores of all scored RBP-coding genes in the WT-MYC condition relative to either HIGH-MYC (left) or Post Selection (right). Those genes that passed our filtering criteria are depicted in blue or red, as in (D). The dashed lines mark the diagonal and the origins of each axis.

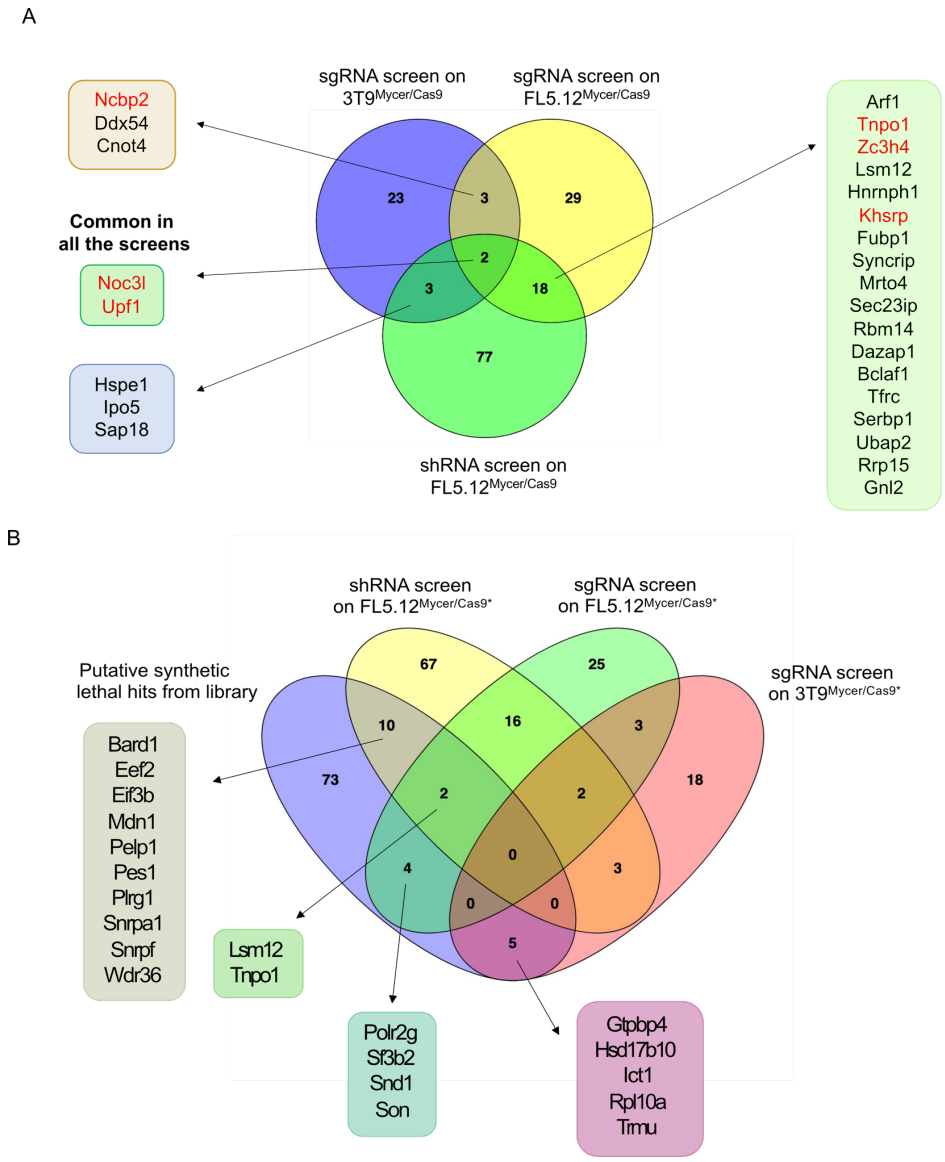

Figure 26. Common hits among the three screens. (A) Venn diagram representing the overlap between the hits identified in the three screens. Common candidates selected for validation are labeled in red. **(B)** Venn diagram showing the intersections of the hits emerged from our three screens with those listed in published MYC synthetic-lethal screens that are present in our libraries (see section 3.1 and table S1) All images were produced with an interactive online tool for comparing lists with Venn's diagrams[433].

3.6 Genetic validation of the screen results and selection of targets

The technical validation of candidate genes from our screens was pursued with competitive proliferation assays (as defined in Fig. 18A) with individual sgRNA or shRNA vectors targeting the selected RBPs (2-3 constructs each). We first validated *Ncbp2*, *Noc3l* and *Hnrnpc*, from the sgRNA screen in 3T9$^{Mycer/Cas9*}$ cells (Figure 22D, E, 26A), showing a consistent trend toward preferential loss of the targeting constructs upon OHT-treatment (i. e. HIGH-MYC) not only in the same cells (Fig.

27A) but also in FL5.12$^{Mycer/Cas9*}$ (Figure 27B), although this effect reached statistically significance only for the *Hnrnpc*-targeting vectors in 3T9$^{Mycer/Cas9*}$ cells. Of note, all constructs also showed some loss in untreated cells (Figure 27A, B), indicating a negative impact on proliferation also with endogenous MYC levels (i. e. WT-MYC). As additional controls, and as above (Fig. 18B, 21B, 24B), sgRNAs targeting *Rpa3* were counter-selected in all conditions, while those targeting endogenous *Myc* were lost selectively in untreated cells (Figure 27A, B).

We then focused on 5 among the top-ranked candidates from the sgRNA screen in FL5.12$^{Mycer/Cas9*}$ cells (*Khsrp*, *Xrn1*, *Tnpo1*, *Dhx36 and Zc3h4*; Figure 24D, E, 26A) together with *Upf1* (as common hit among the three screens). As above, most of the sgRNA constructs showed a trend toward preferential loss in OHT-treated cells: this reached statistical significance for 6 of the 15 constructs tested, including all of the sgRNAs for two genes, *Xrn1* and *Upf1* (Figure 27C). For the latter, we also confirmed the loss of the UPF1 and XRN1 proteins by western blot in infected FL5.12$^{Mycer/Cas9*}$ cells (Figure 27D).

Finally, targeting the 5 candidates selected from the shRNA screen in FL5.12 cells (*Ythdf2*, *Srrt*, *Zc3h4, Noc3l, Rbm39,* Figure 25D, E, 26A) provided the right trend for overall all targets with only one construct reaching statistical significance (shNoc3l #2), while others failed to validate (Figure 27E), in line with the modest levels of knock-down obtained with the shRNA constructs (Figure 27F).

Altogether, our validation data corroborate the higher reliability of the sgRNA technology in competitive dropout screens, and point to a number of candidates for further analysis (see Discussion). Among these, *Upf1* and *Xrn1* stand out, based both on their consistent validation with different sgRNA constructs and their possible convergence on the same biological pathway, nonsense-mediated decay (NMD; see Introduction). Based on these considerations, we decided to focus on those two genes and to extend our analyses to other components of the NMD pathway for the remainder of this work.

Figure 27(next page). Technical validations. (A) Percentage of 3T9$^{Mycer/Cas9*}$ cells infected with sgRNAs targeting either control genes (*Rosa26, Rpa3, Myc*) or the indicated candidates from the sgRNA screen. Reported values correspond to day 8 after infection and are normalized to day 2. Cells were treated or not with 50nM OHT the day after the infection and for the rest of the experiment. Values were measured after flow cytometric staining with anti-CD90.1 according to the intensity of BFP on the y-axis in function of CD90.1 on the x-axis, as shown in the representative gates of sgMyc-infected cells in the two conditions (with or without OHT) at day 2. Gating strategy for debris and doublets exclusions as in Figure 18B. N=3 for the following samples: sgRosa, sgRpa3, sgMyc, sgHnrnpc (constructs #1, #2, #3). P-values were calculated using a Student's t-test by comparing OHT-treated HNRNPC-depleted samples with their untreated counterpart (star above the brackets), or untreated HNRNPC-depleted samples with the sgRosa control (star above each bar) conditions. N=2 for the following samples: sgNcbp2 (#1, #2, #3) and sgNoc3l (#1, #2). Mean value + SEM is shown for all samples. **(B)** As in (A) but in FL5.12$^{Mycer/Cas9*}$ cells. N=2. **(C)** As in (A) for candidates from the sgRNA screen in FL5.12$^{Mycer/Cas9*}$ cells, tested in the same cells with sgRosa as unique control. N=3 for all samples. P-value was calculated as in (A). Mean value is shown + SEM for all samples. **(D)** Western blot analysis of for UPF1 (140kDa) and XRN1 (175kDa) in FL5.12$^{Mycer/Cas9*}$ cells infected with the indicated sgRNA vectors. Infected cells were collected after two or four days of antibiotic selection, as indicated. **(E)** As in (A) for candidates from the shRNA screen in FL5.12$^{Mycer/Cas9*}$ cells, using shRen.713 as neutral control. Values were measured according to the intensity of GFP on the y-axis in function of FSC on the x-axis as shown in representative gates. Gating strategy for debris and doublets exclusions as in (A). N=3 for the following samples: shRen.713, shRpa3.457, shMyc.1891, shNoc3l (#2). P-values were was calculated as in (A). N=2 for the following samples: shNoc3l (#3), shRbm39 (#2, #3), shSrrt (#2, #3), shYthdf2 (#1, #2, #3), shZc3h4 (#3). **(F)** mRNA levels of genes targeted with the indicated shRNAs were measured by RT-qPCR after two days of antibiotic selection of the infected populations. Data are normalized to *Tbp* mRNA and to control uninfected cells. N=2, mean + SEM (ns $P > 0.05$; * $P \leq 0.05$; ** $P \leq 0.01$; *** $P \leq 0.001$).

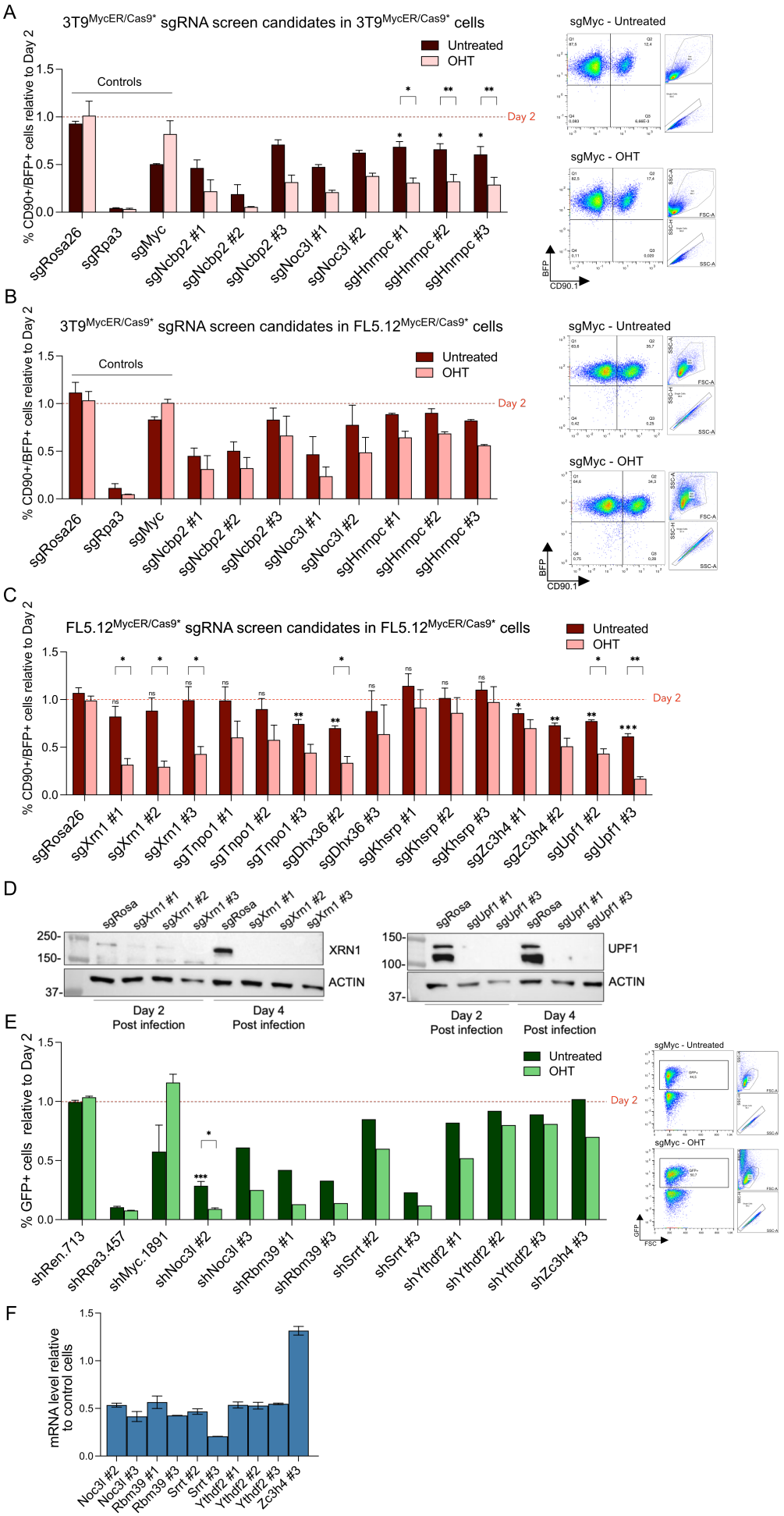

Figure 27. Technical validations. See the legend in the previous page.

3.7 UPF1 and XRN1 loss decrease cell growth and viability in MYC-overexpressing cells

Having selected XRN1 and UPF1 for follow-up characterizations, we sought to investigate the basis for their requirement in MYC-overexpressing cells. First of all, we wanted to better characterize the growth disadvantage imparted by the loss of either gene product: toward this aim, FL5.12$^{Mycer/Cas9*}$ cells were infected *de novo* with the various sgRNAs and selected with neomycin to obtain pure knock-out populations (Fig. 28A). Beside sgRosa26, two additional negative controls from our libraries (sgAcaa2, sgPtrf: see figure 21B, 24B and 25B for their read counts across the samples) were used for these experiments. Live-cell counts were determined over time for six days in cultures with or without MycER^{TM} activation. On note, OHT treatment reduced proliferation rate and augmented apoptosis already in the control populations (sgRosa26, sgAcaa2, sgPtrf; Figure 28B), revealing a basal level of MycER^{TM}-induced cell death, and thus a specific limitation of this experimental model (see below, section 3.9). This notwithstanding, the sgRNAs targeting *UPF1* and *XRN1* showed clear MYC-dependent effects. In particular, while showing no defects in population growth and apoptosis in the untreated condition, sgUpf1- and in particular sgXrn1-infected cultures showed significantly stronger impairment in cell growth upon OHT treatment (Figure 28B, left), revealed also by the proliferation index (Figure 28B, center) – defined as the ratio of viable OHT-treated cells to viable cells in the corresponding untreated control – and in dead cell counts (right), relative to the control sgRNA populations.

In order to evaluate the stability of knock-out by western blot, we collected cells at three different stages: after selection of sgRNA-infected cells (Figure 28A), after two additional weeks of culture, corresponding to the beginning of the aforementioned viability assays (Day 0; Figure 28C), and finally after two days of OHT treatment (Day 2; Figure 28C). Although incomplete, the loss of the UPF1 and XRN1 proteins in the targeted cells was confirmed by immunoblot analysis at the

different stages: while the knock-out of Xrn1 was more extensive (Figure 28A, C), the level of depletion for UPF1 appeared more variable among the three different sgRNAs (Figure 28A, C), particularly at Day 2, suggesting a possible selection of cells which have escaped the depletion, a first indication that the loss of UPF1 may be too detrimental. This could explain why sgUpf1-infected populations showed a lesser impact of OHT treatment, relative to sgXrn1. Of note, our data also revealed induction of UPF1 (but not XRN1) upon MycER^{TM} activation in control cells (sgRosa26) and further confirmation of MycER^{TM} activation was provided by the suppression of endogenous MYC levels (Figure 28C, Day 2). Altogether, these data confirmed the synthetic lethality of sgXrn1 and sgUpf1 with MycER^{TM} activation observed in validation experiments.

With the perspective of understanding the molecular pathways behind the observed synthetic-lethal phenotype, we assessed the level of the DNA damage marker γH2AX as a measure of MYC-induced genotoxic stress[447]. While γH2AX was induced upon MycER^{TM} activation in cells, as expected, this response was not augmented - but in fact suppressed in the absence of either Upf1 or Xrn1 (Figure 28C, Day 2). While these data may appear to argue against DNA damage as the cause of the increased apoptosis, it remains possible that an impaired DNA Damage Response (DDR), as measured here by γH2AX activation, may underlie the augmented lethality upon MycER^{TM} activation (see Discussion).

Ultimately, in order to extend the findings in FL5.12$^{Mycer/Cas9*}$ cells to a *bona fide* MYC-driven lymphoma, we crossed *Eμ-myc* transgenic and *Rosa26-Cas9* animals[181,418], collected lymphomas and stabilized them *in vitro* (see Methods) and infected the resulting cell lines with retroviral sgRNA-BFP constructs (Figure 29A) targeting either *Upf1* or *Xrn1*, with *Rosa26* and *Rpa3* as controls. While the percentage of sgRosa26-infected cells did not change over time, as defined by the measurement of BFP^{+} cells by FACS, sgRpa3, sgUpf1- and sgXrn1-infected cells were overgrown by uninfected BFP^{-} cells, with consistent results in the two independent lymphoma cell lines (Figure 29B). To confirm gene knock-out, we assessed the protein level of Xrn1 and Upf1 in cells infected as above and selected

with puromycin for three days: western blot analysis revealed partial loss of the protein from these populations (Figure 29C), owing most likely to a selective advantage of cells that escaped loss-of-function mutation. These results strengthen the notion that XRN1 and UPF1 are required for the fitness of MYC-overexpressing cancer cells, warranting their further characterization as potential therapeutic targets.

Figure 28 (next page). Loss of UPF1 or XRN1 impairs MYC-overexpressing cell proliferation. (A) Protein level of UPF1 (left) and XRN1 (right) in FL5.12$^{MycER/Cas9+}$ cells infected with indicated sgRNAs and selected for 3 days with neomycin. **(B)** Cells as in (A) and also infected with control genes (*Acaa2, Ptrf*) were kept in culture for 12 days and then tested for proliferation and viability assays in untreated and OHT-treated cultures (100nM OHT). Growth curve: cumulative live-cell counts over time. Values were obtained by counting PI negative cells (live cells) by flow cytometer according to the intensity of PI on the y-axis in function of FSC on the x-axis as shown in representative profiles (corresponding to sgRNA #1 for each indicated target, at day 4). Debris exclusion ad described in Figure 18B. Proliferation index: defined as the ratio of viable OHT-treated cells to viable cells in the corresponding untreated control. P-values were calculated using a Student's t-test by comparing the index of UPF1 or XRN1 depleted samples with the sgRosa control. N=3, mean ± SEM. Cell death: percentage of PI-positive cells (dead cells) in the same cultures. P-values were calculated as before by comparing OHT-treated UPF1- or XRN1-depleted samples with OHT-treated sgRNA control (ns $P > 0.05$; * $P \leq 0.05$; ** $P \leq 0.01$; *** $P \leq 0.001$). **(B)** Protein level of UPF1 (left) or XRN1(right) in the same cultures of (B) at Day 0 (day of OHT treatment) and after two days of OHT treatment (Day 2). Levels of endogenous MYC, VINCULIN (as loading control), γH2AX and total H3 (as histone loading control) were assessed only at Day 2.

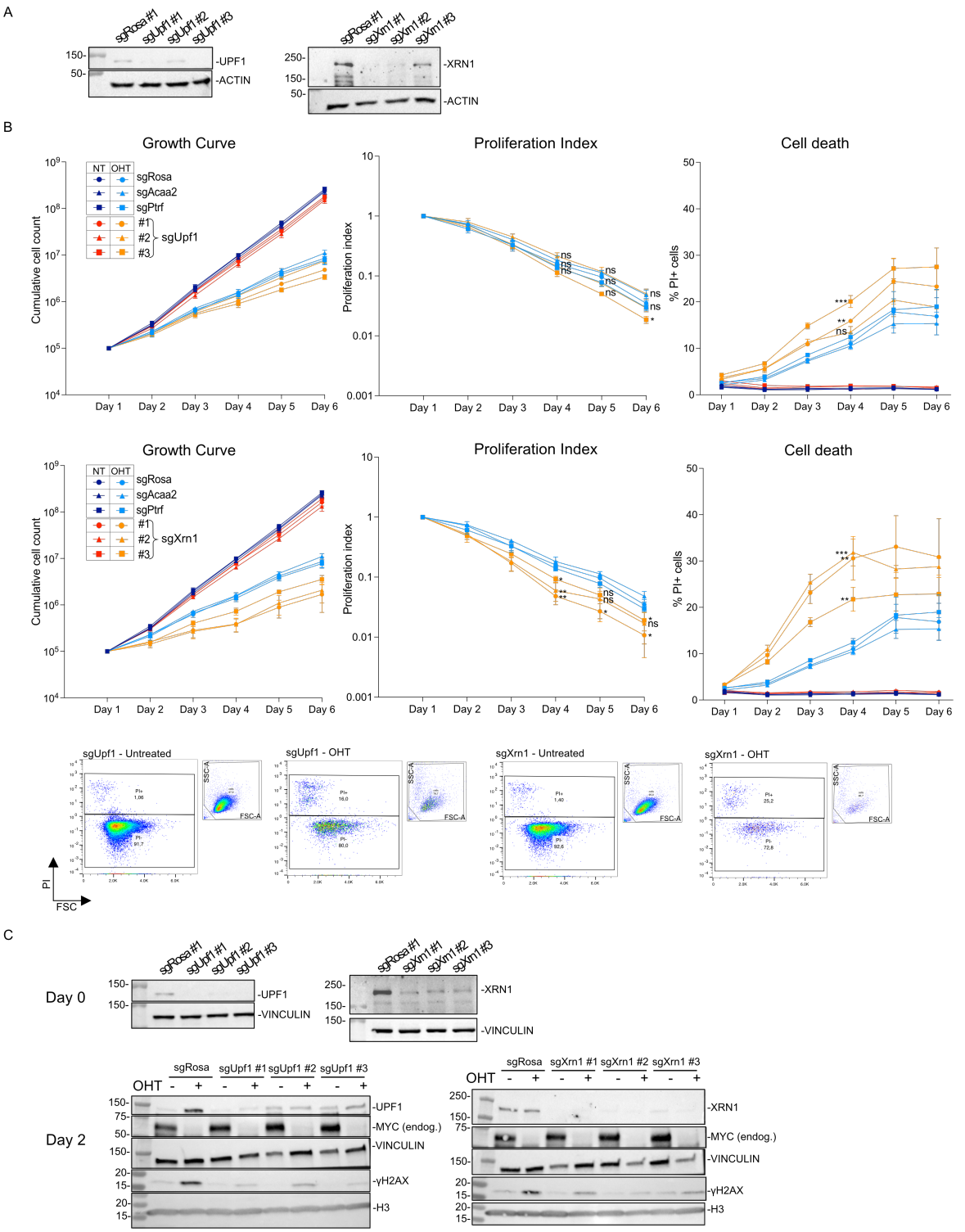

Figure 28. Loss of UPF1 or XRN1 impairs MYC-overexpressing cell proliferation. See the legend in the previous page.

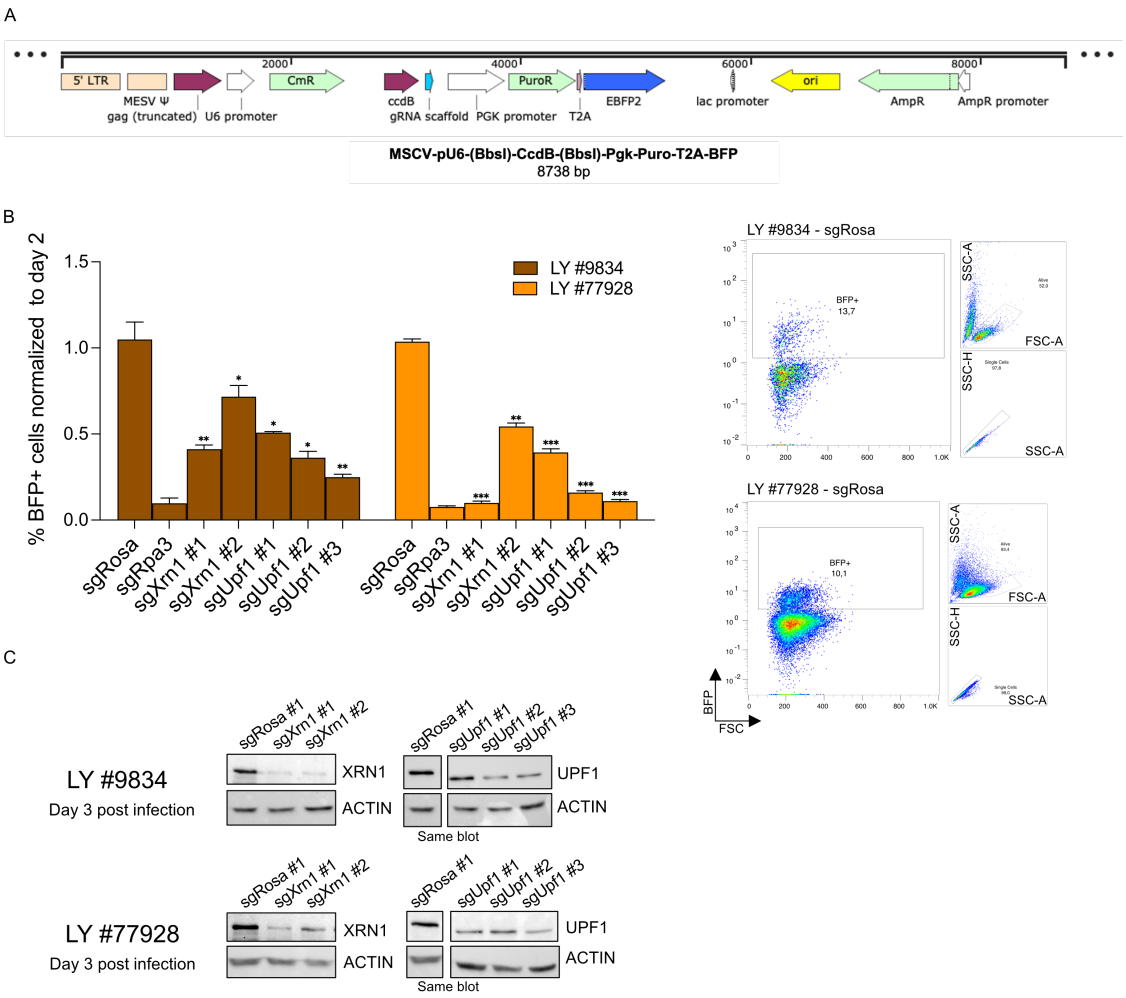

Figure 29. Validation in EμMyc cell lines. **(A)** Map of the retroviral vector used for sgRNA expression in Eμ-myc/Cas9 lymphoma cell lines, with puromycin resistance gene (PuroR) linked to the BFP reporter gene (EBFP2) through a T2A self-cleaving peptide sequence. **(B)** Percentage of BFP$^+$ cells in two lymphoma cell lines infected with sgRNAs targeting *Rosa26*, *Rpa3*, *Xrn1* or *Upf1*, as indicated. Measurements were assessed by flow cytometric analysis at day 8 after infection and normalized to those of day 2. As shown in the representative gates, values were measured according to the intensity of BFP on the y-axis in function of FSC on the x-axis as shown in representative gates. Gating strategy for debris and doublets exclusions as in Figure 18B. P-values were calculated using a Student's t-test by comparing XRN1 or UPF1 depleted cells with sgRNA control (* $P \leq 0.05$; ** $P \leq 0.01$; *** $P \leq 0.001$). N=3, mean + SEM. **(C)** Protein level of XRN1, UPF1 or ACTIN (as loading control) by western blot in two lymphoma cell lines infected with the indicated sgRNAs and selected for 2 days with puromycin.

3.8 NMD factors are required for the fitness of MYC-overexpressing cells

Considering the mutual involvement of *Upf1* and *Xrn1* in NMD, we hypothesized that MYC-overexpressing cells require this particular mRNA decay pathway to sustain oncogenic stress and cell survival. To address this issue, we infected FL5.12$^{MycER/Cas9*}$ cells with sgRNAs targeting additional NMD factors, including SMG1, SMG5, SMG6 and SMG7 (see Introduction, Figure 12), and conducted

competitive proliferation assays, as above. After eight days of culture without OHT, the populations transduced with sgRNA targeting Upf1 (used as control), *Smg1*, *Smg5*, *Smg6* or *Smg7* showed variable losses of CD90.1^{+}/BFP^{+} cells (Figure 30, untreated): most importantly, however, these losses were invariably exacerbated in the presence of OHT, in particular in SMG7-depleted cells, indicating that MycER^{TM} activation increases the dependency of these cells upon each of the NMD factors tested. As expected, the percentage of cells infected with the sgRosa26 control was unchanged regardless of MycER^{TM} activation (Figure 30). Altogether, we conclude that MYC-overexpressing cells have an increased dependency upon the NMD pathway.

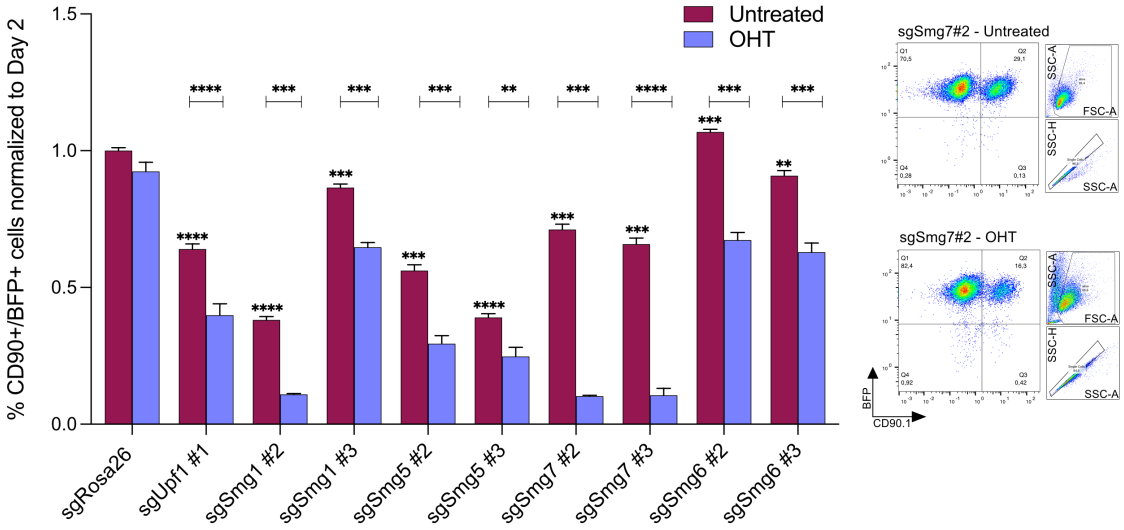

Figure 30. NMD factors loss is detrimental for Myc-overexpressing cells. Percentage of FL5.12$^{Mycer/Cas9*}$ cells infected with the indicated sgRNAs. Cells were treated or not with OHT (100nM) the day after infection. Values were measured by FACS over time and illustrated here at day 8 after infection relative to those of day 2. Representative gates corresponding to one replicate of the indicated sample at day 8. Gating strategy as Figure 27A. P-values were calculated using a Student's t-test by comparing OHT-treated samples with their untreated counterpart (stars above the brackets), or untreated samples with untreated sgRosa control (stars above each bar). ** P ≤ 0.01; *** P ≤ 0.001; **** P ≤ 0.0001; N=3, mean with SEM.

3.9 Generation of stable knock-out clones for in-depth analysis

The FL5.12$^{Mycer/Cas9*}$ cells used above are a clonal population derived from cells infected with MycER^{TM} and Cas9, both constitutively expressed in the cells. As shown in Figure 28B, these cells were sensitive to MycER^{TM} activation also when infected with control sgRNAs (although less than XRN1- or UPF1-depleted cells); hence, we wondered whether this basal toxicity was due to the infection with any sgRNA, to the constitutive expression of Cas9 in those cells, or was a feature of this particular clonal population. To answer this question, we compared the growth of different cell populations in presence or absence of OHT, including (i.) the FL5.12$^{Mycer/Cas9*}$ clone used in the above experiments, (ii.) the same clone, infected with control sgRNA vectors and selected as above, (iii.) the bulk (polyclonal) FL5.12$^{Mycer/Cas9}$ population, and (iv.) the parental FL5.12^{Mycer} cells (without Cas9 expression). Among all these populations, the FL5.12$^{Mycer/Cas9*}$ clone showed significantly enhanced OHT-induced growth suppression and cell death, whether infected or not with control sgRNAs (Figure 31A). Most noteworthy here, this clone also showed the highest levels of Cas9-associated BFP fluorescence (Figure 31B) and of the MycER^{TM} protein (Figure 31C; see also Figure 16C, clone 3), as well as a selective increase in γH2AX levels upon OHT treatment (Figure 31C). We surmise that the basal genotoxic activity of Cas9 may sensitize the cells to acute MycER^{TM} activation, explaining the intrinsic sensitivity of this FL5.12$^{Mycer/Cas9*}$ clone to OHT. While this feature did not prevent the scoring of sgRNA-associated effects in competitive growth assays, and thus also in our sgRNA screen, it significantly impacted upon absolute measurements in cell proliferation and death (Figure 28A), and might thus also impinge on the interpretation of quantitative and mechanistic studies, such as the transcriptomic profiling of the *Upf1* or *Xrn1* knock-out cells following MycER^{TM} activation.

In order to obtain a better model, suitable for in-depth mechanistic analysis, we sought to produce stable FL5.12^{Mycer} knock-out clones lacking select genes in the NMD pathway, in the absence of permanent Cas9 expression. In particular, we wanted to extend our investigations to the role of SMG7, besides XRN1 and UPF1.

As illustrated in Figure 32A, we electroporated FL5.12^{Mycer} cells with two plasmids for expression of sgRNAs targeting the gene to be eliminated, together with a vector expressing Cas9 and a GFP reporter (Figure 32B); we thus sorted GFP positive cells and proceeded with single-cell cloning, expansion and characterization. The two different sgRNAs (marked as #4 and #5 in Figure 32C) were designed to induce the deletion of about 100 base pairs comprising a portion of an exon together with a consecutive intronic fragment, resulting in the generation of deleted transcripts with frameshift mutations and premature stop codons.

Following transfection, genomic DNA was extracted from the pool of sorted cells and used for amplification with PCR primers flanking the targeted area (PCR screen Fw and Rv, Figure 32C). In our first experiment, the sgRNAs targeting *Xrn1* and *Smg7* induced a certain level of deletion (detectable as a lower band: orange arrows in Figure 33A) while those targeting *Upf1* did not allow detection of a deleted product. In line with this result, the screening of single-cell derived cultures yielded no *Upf1*-deleted clones (Figure 33B), while allowing us to score a series of candidate *Xrn1*- and *Smg7*-deleted clones (Figure 33C, D). For *Upf1,* we are currently repeating the transfection with two different pairs of targeting sgRNAs (#1 with #6, and #2 with #7, Figure 32C). For *Xrn1* and *Smg7,* we selected knock-out clones with apparent homozygous deletions based on PCR results (i. e. with a unique lower band compared to WT clones, indicated by orange arrows in Figure 33C, D) and sequenced the PCR products to genetically validate the knock-out. Figure 34A shows two examples (one for each gene) of clones showing a uniform deleted sequence, indicative of a homozygous deletion event: for the sake of clearness and time, these clones were preferred over the characterization of more complex patterns. A series of predicted WT and KO clones, selected based on the PCR screen, were then analyzed by immunoblotting of the relevant protein product, as well as of the MycER^{TM} protein, with or without OHT treatment (Figure 34B). Among the *XRN1* knock-out clones (hereafter Xrn1^{KO}), seven out of the 11 rested KO candidates (Xrn1$^{KO\#3}$, Xrn1$^{KO\#10}$, Xrn1$^{KO\#16}$, Xrn1$^{KO\#33}$, Xrn1$^{KO\#34}$, Xrn1$^{KO\#39}$ and

Xrn1$^{KO\#45}$) were negative for XRN1 and expressed the predicted form of MycER^{TM} (Figure 34B). Curiously, Xrn1$^{KO\#20}$ and Xrn1$^{KO\#29}$ still expressed the XRN1 protein, although predicted as deleted by PCR (Figure 33C), most probably due to a contamination at a later time. Finally, Xrn1$^{KO\#13}$ and Xrn1$^{KO\#24}$ showed a smaller MycER^{TM} protein, corresponding most likely to a partially deleted variant that must have arisen in the original FL5.12^{Mycer} population, where it was clearly detectable alongside the full-length MycER^{TM} protein: as a consequence, a subset of the resulting clones expressed only this truncated (and presumably OHT-independent) form and were thus discarded.

Screening of the *SMG7*-targeted clones (hereafter Smg7^{KO}) showed a faint band of the same size as SMG7: while requiring further characterization with additional antibodies, we provisionally attribute this signal to a distinct cross-reacting protein (Figure 34C). Of the six clones screened here, two Smg7$^{KO\#22}$ and Smg7$^{KO\#36}$ expressed the intact MycER^{TM} protein, while the others showed the shorter form (Figure 34C).

In conclusion, we obtained seven *Xrn1* knock-out clones and two candidate *Smg7* knock-out clones, to be potentially used for mechanistic analysis. While the nature of the *Smg7* knock-out remains to be fully ascertained, we already proceeded to an initial phenotypic analysis, as presented below.

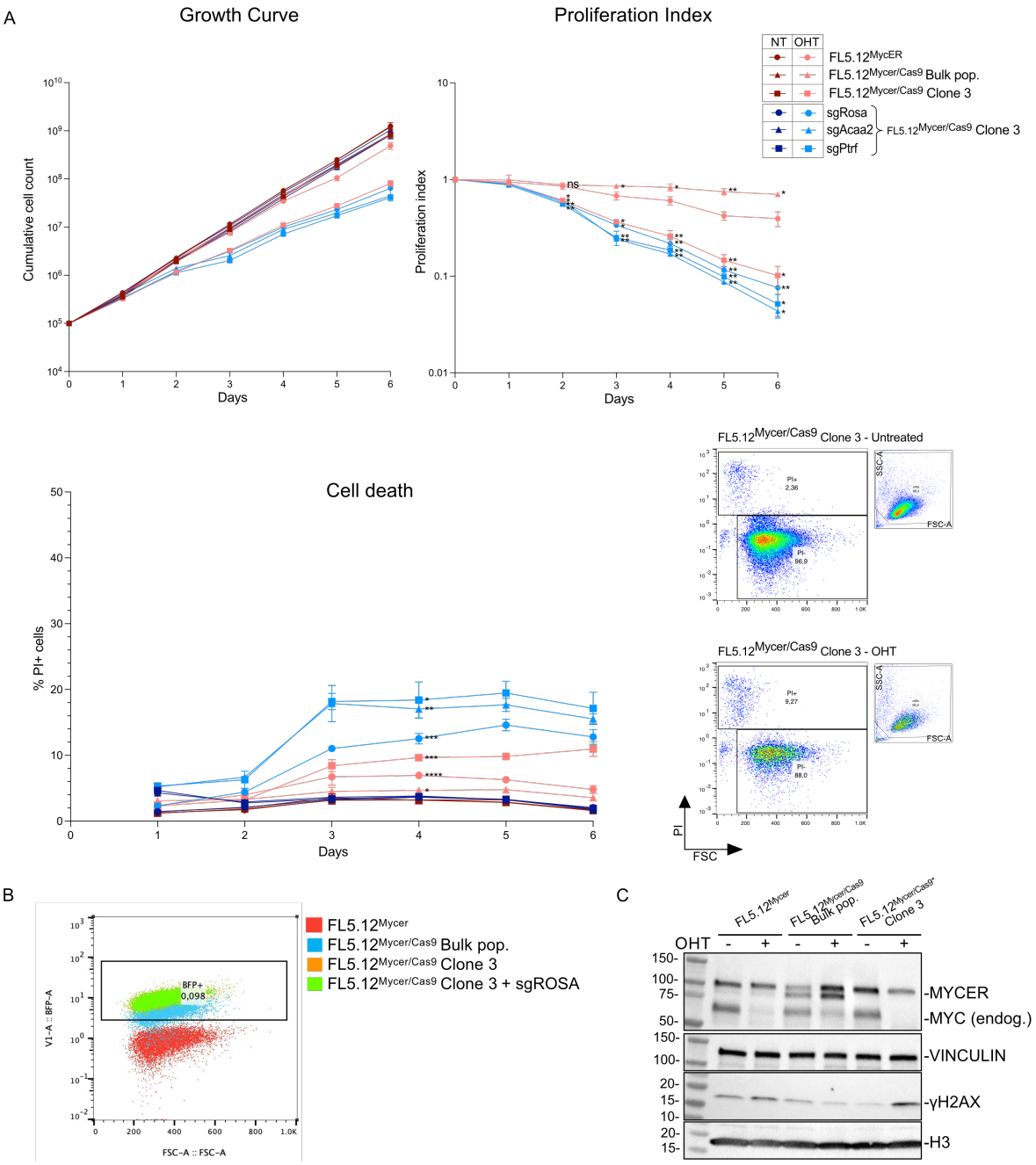

Figure 31. The FL5.12$^{Mycer/Cas9*}$ clone is sensitive to MycER^{TM} activation. (A) Growth Curves, Proliferation Index and Cell death (as defined in Figure 28) for the indicated cell populations, cultured with or without OHT (100nM). FL5.12^{Mycer}: parental cells, prior to Cas9 transduction; FL5.12$^{Mycer/Cas9}$: bulk population transduced with Cas9; FL5.12$^{Mycer/Cas9*}$: clonal population used in our screen; sgRosa, sgAcaa2, sgPtrf: FL5.12$^{Mycer/Cas9*}$ infected with sgRNAs targeting the corresponding control genes. P-values were calculated as in Figure 28A. * P ≤ 0.05; ** P ≤ 0.01; *** P ≤ 0.001; **** P ≤ 0.0001. N=3, mean + SEM. **(B)** FACS profiles showing Cas9-associated BFP intensity (Y-axis) relative to FSC (X-axis) for the indicated cell populations. **(C)** Western blot analysis of MycER^{TM}, endogenous MYC, VINCULIN (as loading control), γH2AX and total histone H3 in the indicated cells, treated or not with OHT (100nM) for 2 days.

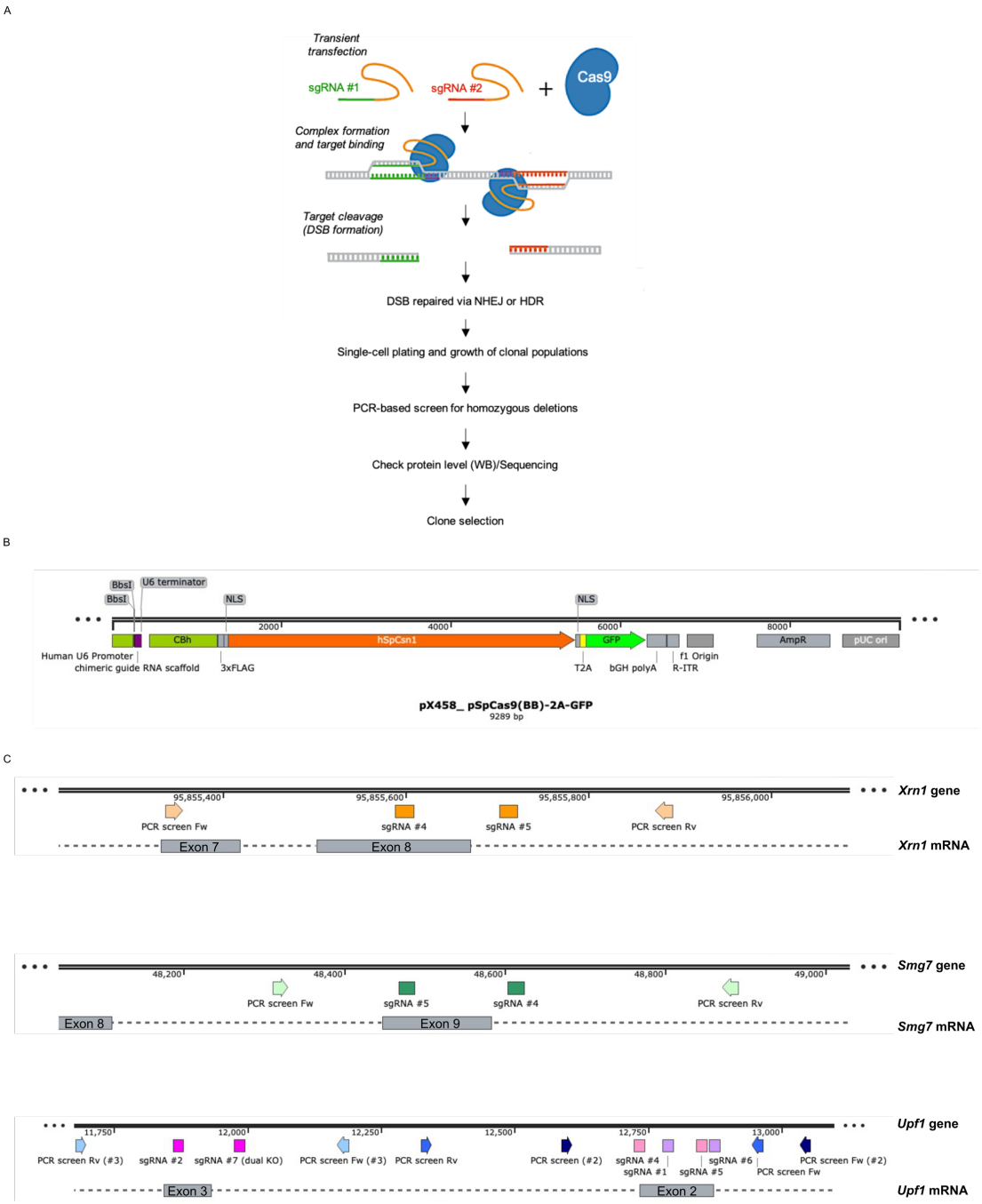

Figure 32. Strategy for generation of stable knock-out clones. (A) Schematic steps for the generation of stable knock-out clones: transient transfection of Cas9 and two different sgRNA constructs leads to two double-strand breaks (DSBs)[448,449] which in this case allow the deletion of a portion of the gene. DNA ends are repaired by non-homologous end joining (NHEJ), which is prone to introduce indel errors or homologous recombination (HR)[449]. Transfected single cell are seeded in 96-well plates to generate clonal populations and a PCR-mediated screen is performed to identify clones with homozygous deletion of the gene. Western blot and sequencing of the PCR products are performed to confirm knock-out and select suitable clones. **(B)** Map of the Cas9- and sgRNA-expressing vector used for electroporation of FL5.12^{Mycer} cells. The sgRNA and Cas9 coding sequenced are under the control of two different promotors. Cas9 is linked to the GFP reporter gene by T2A self-cleaving peptide sequence. Main features of the vector are reported. **(C)** Maps of the sgRNA target regions of *Xrn1*, *Smg7* and *Upf1* genes relative to each target exons. Primers used for the PCR-based screen are indicated as "PCR screen Fw" and "PCR screen Rv".

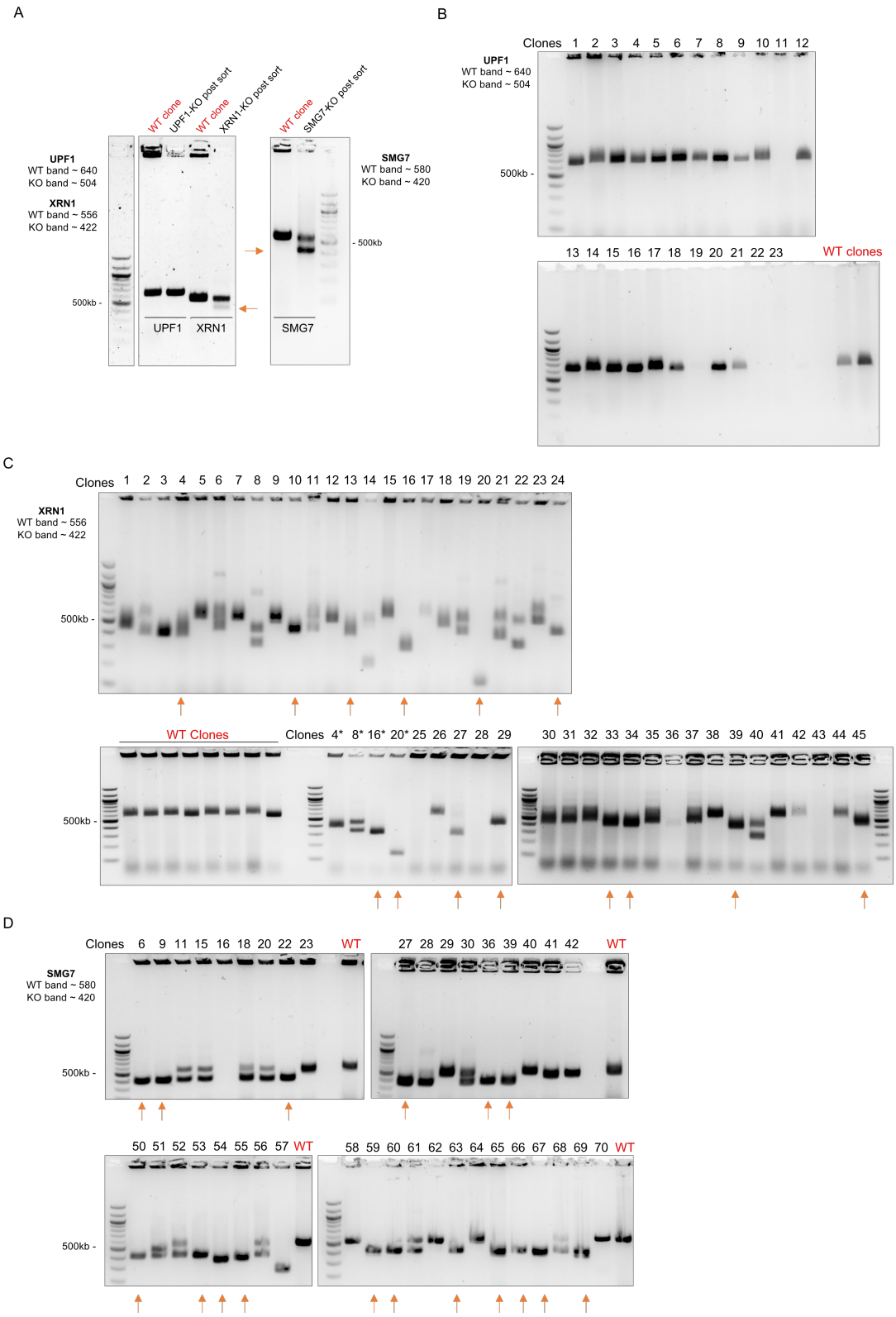

Figure 33. PCR screen for knock-out clone selection. (A) Agarose gel electrophoresis image showing PCR product of WT clones (produced by mock-transfection) and sorted cells (showed as "post sort") after electroporation with plasmids described in Figure 32 to generate *Upf1*, *Xrn1* or *Smg7* knock-out cells. See methods for full description. Expected band size for each gene deletion or wild type is indicated. Orange arrows refer to PCR products of the deleted gene. **(B)** As in A, for 23 clones generated after sgUpf1 electroporation. Two different WT clones (in red) were used as control. Indication of the expected band size for WT or KO products is shown. **(C)** As in A, for 45 clones generated after sgXrn1 electroporation. PCR for clone 4, 8, 16, 20 (indicated with a *) was performed twice. Eight different WT clones (in red) were used as control. Orange arrows indicate those clones that show apparent biallelic deletion of the gene. **(D)** As in A, for 39 clones generated after sgSmg7 electroporation. One WT clone (in red) was used as control. Orange arrows as in (C).

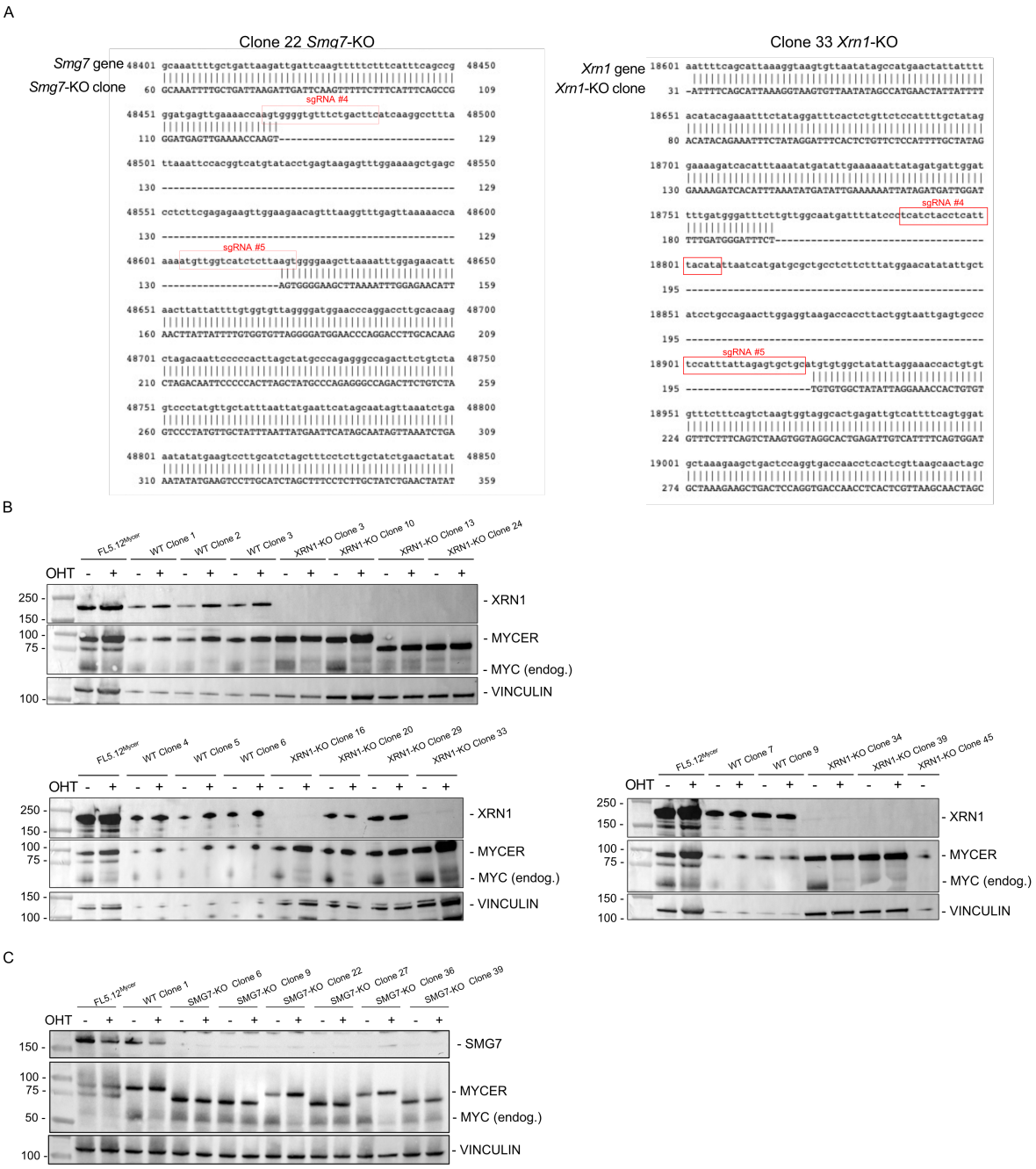

Figure 34. Validation of knock-out clones. (A) Representative alignments of the PCR products of knock-out clones (see Figure 33) of *Smg7* (left) or *Xrn1* (right) with the indicated WT gene sequence. Red boxes indicate of the target sequences for the sgRNAs used for the knock-out. Alignment was performed by using the EMBOSS Needle - Pairwise Sequence Alignment - EMBL-EBI online tool[434]. (B) Western blot analysis of XRN1, MycER^{TM}, endogenous MYC and VINCULIN (as loading control) in FL5.12^{Mycer} cells, WT clones or the indicated *Xrn1* KO clones, treated or not with OHT 100nM for 72 hours. (C) As in B, in *Smg7* KO clones.

3.10 Stable loss of XRN1 or SMG7 is detrimental in MYC-hyperactivated cells

Having obtained the aforementioned *Xrn1*- and *Smg7*-targeted cell clones, we characterized their response to OHT, to further validate the synthetic lethality of *Xrn1* and *Smg7* loss with MycER^{TM} activation. For this purpose, we monitored cell growth and apoptosis in three Xrn1-mutant (Xrn1$^{KO\#10}$, Xrn1$^{KO\#16}$, Xrn1$^{KO\#33}$) and two Smg7-mutant lines (Smg7$^{KO\#22}$ and Smg7$^{KO\#36}$), with a WT clone as control. While the *Xrn1* knock-out clones grew slightly slower than the WT control, they showed a marked sensitization to OHT treatment, which strongly suppressed proliferation and enhanced apoptosis (Figure 35A). Of note, one particular clone (Xrn1$^{KO\#10}$) showed a higher basal level of cell death in the absence of OHT, which could also explain the stronger effect of OHT treatment (Figure 35, right). The two other clones (Xrn1$^{KO\#16}$ and Xrn1$^{KO\#33}$), while showing marginally higher – yet statistically significant – levels of cell death in the untreated condition, showed a robust increase after MycER^{TM} activation (Figure 35B). Similar results were observed in Smg7$^{KO\#22}$ and Smg7$^{KO\#36}$ (Figure 35C, D).

Altogether, the above data formally confirm the requirement of XRN1 and SMG7 in MYC-overexpressing cells. Most importantly, the availability of stable KO clones will allow us to proceed with thorough molecular and genomic analyses, toward a deeper mechanistic insight into the role of NMD in MYC-overexpressing cells.

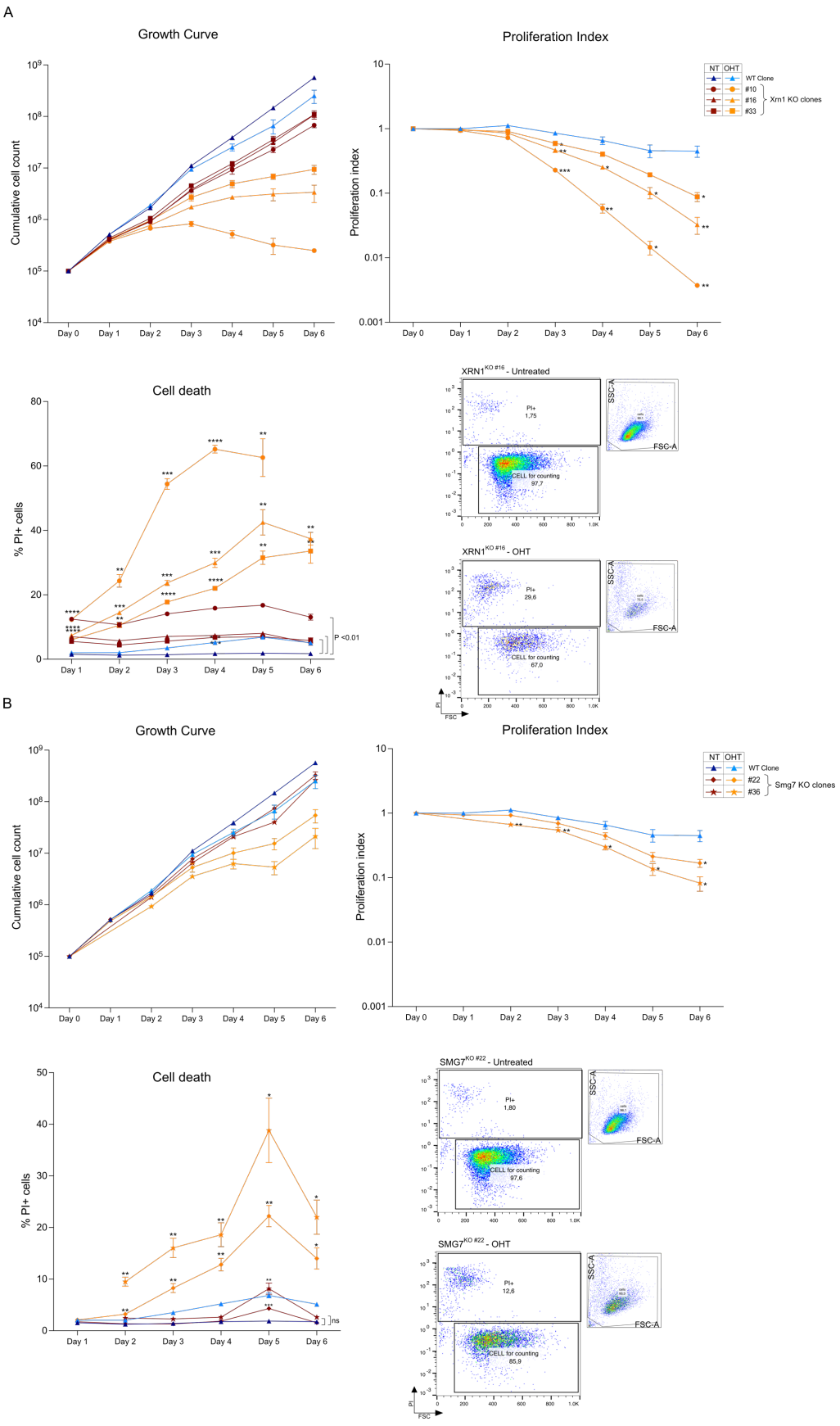

Figure 35. Characterization of stable Xrn1- and Smg7-knock-out clones. (A) Growth Curves, Proliferation Index and Cell death (as defined in Figure 28) for WT or indicated Xrn1 KO clones in untreated and OHT-treated cultures (100nM). Representative gates of one replicate of the indicated sample at day 4. P-values were calculated as in Figure 28A and for cell death values also by comparing untreated KO sample with untreated WT cells. ns $P > 0.05$; * $P \leq 0.05$; ** $P \leq 0.01$; *** $P \leq 0.001$; **** $P \leq 0.0001$. N=3, mean + SEM. **(B)** As in A, but in *Smg7* KO clones.

4. Discussion

4.1 Screening for synthetic lethal RBPs in MYC-overexpressing cells

The MYC transcription factor was one of the first identified oncogenes and represent a master regulator of cell growth and proliferation, as well as a potent tumor driver[14]. MYC is the mediator of many upstream signal transduction pathways which are integrated and converted into downstream prompts through MYC-mediated transcription of a diverse set of biological programs (see section 1.1.5). The processes regulated by MYC also embody the key pathways required for tumorigenesis, such as cell cycle, metabolism, cell stemness, the modulation of immune responses and many other cellular activities[6,15,136,178]. In non-transformed cells, these processes are finely tuned by regulation of MYC at multiple levels, from RNA synthesis to protein degradation[30,90]. When such regulation is distorted, MYC can alter many pathways and promote cell transformation. Oncogenic activation of MYC can occur in multiple manners, including genomic alterations, in particular when *MYC* gene is translocated in a different chromosome or amplified, the latter representing the most common feature of MYC-driven human tumors[6,7,14,179].

Despite the indubitable role of MYC in cancer development and maintenance, it remains still undrugged. Indeed, developing clinical inhibitors have been a particular challenge owing to MYC intrinsically disordered nature and lack of a binding pocket, coupled with potential toxic side effects in normal proliferating tissues. However, in the last years we have witnessed to successful preclinical studies of the direct MYC inhibitor Omomyc, with clinical trials just started, that offers exciting clinical prospects for treating MYC dependent cancers[248].

Among all the US Food and Drug Administration (FDA)-approved therapies for MYC-dependent cancers, there are inhibitors that target vulnerabilities of MYC, such as mTOR (everolimus, sirolimus, and tesirolimus) and of IMPDH (mycophenolic acid). Moreover, recent development against additional MYC synthetic lethal targets have successfully progressed to clinical trials, with many drugs in phase II

of clinical trials and few other is phase III[349]. Hence, targeting MYC synthetic lethality has made interesting progresses and represents a promising strategy against MYC-dependent tumors. In fact, identifying downstream effectors or dependencies of MYC in tumorigenesis has become a focus of investigation for many research groups and an important step toward the development of strategies to selectively target MYC-dependent tumors[136,216,450], as exemplified in our own group with the targeting of mitochondrial activities[275,419,451].

In this work, we decided to explore MYC synthetic lethal interactions by focusing on a particular category of genes, which encode RNA binding proteins (RBPs). Indeed, RBPs, identification and characterization of which are increasing in numbers in the recent years[364,452], mediate a correct functioning of cell by post-transcriptionally regulating processing, maturation, localization and modification of all RNA molecules. Our groups and others showed that RBPs belong to the core set of genes that are upregulated upon MYC oncogenic activation in different systems[125,127,128,144,416] and a number of RBPs involved in splicing[154,175,335] and translation[340,346,453] have been shown to be synthetic lethal with MYC, and/or to play a critical role in MYC-induced tumorigenesis. Thus, by directly or indirectly modulating RBP activities and/or expression, oncogenic MYC may have a wider impact on post-transcriptional processes, which can represent important intervention elements for future therapeutic development[176]. Hence, our study aimed the identification of those RBPs that are specifically required for the growth of MYC-overexpressing cells, which may also constitute actionable cancer liabilities.

Toward this goal, we took advantage of high-throughput genetic screening approaches combined with Next Generation Sequencing (NGS), a powerful tool that can allow the identification of genes whose loss of function affects cell proliferation and viability[435,436] (Figure 13). We have thus set up reverse-genetic dropout screens, based on both RNA interference (RNAi) and CRISPR/Cas9 technologies. This double approach was chosen in order to overcome the limits of each technique: genes whose products are functioning also at low expression levels may show no- or little phenotype upon knockdown, and might thus fail to score in

shRNA-based screen, while genes that are essential for cell viability might be missed as synthetic-lethal with MYC when using sgRNAs. Hence, knockout and knockdown together might provide a deeper comprehension of biological processes. These approaches allowed in the past to identify a number of MYC-synthetic lethal genes (see section 1.1.8) and successfully test available compounds against their protein products in pre-clinical contexts[224,229,263,265,267,269–271,273,414,419,454,455]. This method, besides having generated insights on novel and unexpected targets against MYC-driven tumors, can provide a deeper understanding regarding MYC functions and, in our case, MYC's role at the post-transcriptional level, a still under-investigated layer of regulation.

For our project, we selected 730 RBPs to be challenged in shRNA and sgRNA screens, based on their high gene expression and/or amplification levels in different tumor types from TGCA studies[373,380], or because they had emerged as candidates – albeit not characterized further - in prior MYC synthetic lethal screens[224,263,265] (Table S1, Figure 14). On note, we chose not to include several splicing factors within our libraries owing their well-known synthetic lethal interaction with MYC overexpression[154,175,335], although we included some of them as positive controls in our libraries (e. g. PRMT5, BUD31, SF3BP1)[154,175,335]. The long-standing expertise of our collaborators in Johannes Zuber's laboratory in RNAi and CRISPR techniques warranted accurate design and development of the libraries, the supply of the respective lentiviral vectors, as well as optimized protocols[411,412,414,420,456] and counseling at multiple steps, providing precious input toward the accurate preparation of the NGS libraries, proficient execution of the screens and technical validations in our laboratory.

Our screens were performed in FL5.12 and 3T9 cell lines engineered to express the chimeric protein MycER^{TM} protein, which conditionally translocates into the nucleus and exerts its function upon addition of OHT[363]. While 3T9 fibroblasts provided a well-characterized model system in our laboratory, with extensive data on the transcriptional effects of acute MYC activation[58,416], the B-cell progenitor line FL5.12 represented a more suitable model to address MYC function in B-cell

lymphomagenesis, and were used to study other pharmaco-genetic interactions in our laboratory[451]. For both cell lines, we generated clonal populations in order to remove clonal variability due to different numbers of MycER^{TM} and Cas9 gene integration events, which would have constituted a possible confounding factor in our screens. We evaluated MycER^{TM} activation mediated by OHT treatment on the selected clonal cells for both cell line by assessing transcription of target gens and cell cycle stimulation. Furthermore, we also ensured that the level of this activation would not induce an elevate level of apoptosis, which could have represented a major confounding factor in a drop-out screen (Figure 16).

Before screening, we performed a functional evaluation of the vectors to be employed (Figure 17) by conducting a number of competitive proliferation assays. These tests allowed us to clearly attest the presence of positive, negative or neutral selection of a cell population co-cultured with a second one: in this setting, deletion or silencing of an essential gene in experimental cells (identified by the sgRNA- or shRNA-associated reporter) leads to the counterselection of targeted cells and consequent positive selection of control cells (Figure 18). A similar approach was employed for the screens: cells expressing different sgRNA/shRNA grown as a large pool in order to identify, via NGS, the sgRNA/shRNA inserts that were lost selectively in MYC-overexpressing (HIGH-MYC) cells relative to their normal counterpart (WT-MYC) (Figure 13, 19D).

For a good execution of screens and to guarantee reliable data we further adopted several important precautions: a low MOI when infecting target cells with the library, to warrant a single sgRNA/shRNA integration event per cell (Figure 19B); maintenance of a high coverage, with a 1000x library representation throughout the all the steps of the screens (infection, cell collection and subculturing); sorting of cells that were functionally expressing the sgRNA/shRNA reporter (Figure 19E, 23D); NGS sequencing of ca. 10 million reads per sample in order to acquire at least 1000 reads per sgRNA/shRNA and to gain sensibility for shRNA/sgRNA representation among samples; optimized protocols for more specific NGS library preparation, such as two rounds of PCR-based amplification of integrated sgRNA

coupled with gel-purifications (see Methods and Figure 20). Following these expedients, we noticed a technically good performance of the screens, as controlled by the analysis of NGS read counts: high correlation levels among replicates (Figures 21A, 24A, 25A) as well as a good level of sgRNA-mediated knock-out of the positive controls in both cell lines (Figures 21B, 24B). By contrast, we could not detect an appreciable level of silencing of positive controls in the shRNA screen performed on FL5.12 cells (Figure 25B).

To better quantify the distribution of the sgRNAs and shRNAs within the samples in the different conditions and stages of the screen and for an accurate identification of depleted genes in HIGH-MYC condition, rather than simply statistically comparing the fold change of read counts, we took advantage of the MAGeCK tool[422,423,457]. This analytical tool has been widely used in CRISPR and RNAi screens (Figure 36) and has proven to perform better than other methods, allowing the simultaneous identification of positively and negatively selected genes, taking in consideration multiple samples (more than two) and experimental conditions within the same analysis[422,423,457]. In particular, MAGeCK integrates read counts of the various sgRNAs or shRNAs targeting the same gene in different replicates, and calculates a unique "beta score", reflecting the selective pressure exerted on this gene in each experimental sample (i. e. treatment and time-point) relative to the starting condition. Remarkably, MAGeCK automatically calculates beta scores taking into account the trend of negative controls (i. e. known neutral genes), and allows the investigator to normalize for differences in growth rates between the two conditions, averting false-positive calls due merely to differences in population doublings – as might have happened here in MYC-overexpressing cells relative to their normal counterpart.

In our screens, the aim was to detect genes that show synthetic lethality with MYC overexpression, whose suppression confers negative selection (and thus a negative beta score) in the HIGH-MYC condition, and not – or less so – in WT-MYC cells. Most noteworthy here, none of the genes targeted in our CRISPR libraries showed a negative beta score exclusively in the HIGH-MYC condition; this was

largely owing to the fact that most of these genes were critical for cellular fitness, thus showing negative beta scores already in the WT-MYC controls (Figure 22C, 24C). Nonetheless, a series of filtering criteria allowed to identify genes that imposed significantly stronger counter-section in HIGH- vs. WT-MYC cells, hence defining *bona fide* synthetic lethal interactions (Figure 22D, 24D). Of note, this screening approach cannot allow the identification of synthetic lethal genes which function, upon depletion, is rescued by redundant factors of same pathway, paralogs or pseudogene products, as well as by the activation of rescue pathways.

Next, we performed the shRNA screen on FL5.12 cells with the hypothesis that it would have ensured a better resolution of genes that are essential only in the HIGH-MYC condition only, owing to the fact that knock-down would show less deleterious effects on cell fitness compared to knock-out. However, we could not obtain strong data, most likely due to the weak and variable efficiencies in gene silencing inherent to shRNAs (as also exemplified by the analysis of the positive controls in our libraries: see above): indeed, the median value of all beta scores was near zero in all samples (Figure 25C). For these reasons, we decided not to go further with the use of RNAi-based technology and did not perform the shRNA screen in 3T9 cells.

The filtered lists of MYC-synthetic lethal hits that emerged from the CRISPR screens included a series of logical candidates. In particular, the 31 candidates identified in 3T9 cells (Figure 22D) comprised a number of ribosomal protein-coding genes, such as *Rpl23* and *Rps3*, already known to be mediators of oncogenic MYC activities[336,344,440,441]. We also identified *Huwe1*, encoding an E3 ligase that regulates MYC protein stabilization and whose inhibition has emerged as a therapeutic strategy for targeting MYC-dependent different tumors[442–444], and *Tra2b* which was recently shown to be regulated by MYC and to have a role in metastasis in breast cancer, where its levels correlate with patient survival[458]. The 52 candidates identified in FL5.12 (Figure 24D) included MYC-regulated genes, such as *Dkc1*[459],*Hnrnph1*[460], *Ythdf1*[461], *Trfc*[462] and various ribosomal proteins.

Of note, although the aforementioned factors were functionally connected with MYC, their synthetic lethal interaction with MYC overexpression remained to be

established: hence, our results add important insight and warrant further investigations about the requirement of those gene products in MYC-driven tumors. Most importantly here, the above genes highlight the validity of our screens, providing further confidence about the other identified candidates.

When integrating the results of our three screens, we obtained 5 common hits from the two CRISPR/Cas9 screens, 20 common from the two FL5.12 screens and in particular 2 common from all the screens: *Nocl3* and *Upf1* (Figure 26A). Furthermore, by ranking the hits according to the most negative degree of selection in MYC-overexpressing cells, compared to the normal cells, we found that *Noc3l* was among the top 10 hits in the two sgRNA-based screens, whereas *Tnpo1* and *Zc3h4* were highly ranked in the two FL5.12 screens.

Altogether, the aforementioned results provided us a positive indication about the quality of our screens, and allowed us to move on to the next step of technical validation, for which we selected a number of hits among the top-10 scored genes of each screen, taking into consideration also their functions and possible connection with MYC oncogenic activities. In particular, we selected the following genes:

- From the CRISPR/Cas9 screen in 3T9 cells: *Ncbp2*, *Noc3l* (which was common to all screens) and *Hnrnpc*.
- From the CRISPR/Cas9 screen in FL5.12 cells: *Tnpo1*, *Xrn1*, *Zch34*, *Dhx36*, *Khsrp* (or *Fubp2*) and the two common genes *Noc3l* and *Upf1* – event though not scored as top hits.
- From the shRNA screen in FL5.12 cells: *Rbm39*, *Noc3l*, *Zc3h4* (which was a top-hit in the sgRNA screen as well), *Ythdf2* and *Srrt* (or *Ars2*).

For technical validation we decided to employ the same competitive proliferation assays that we first used for functional evaluation of the sgRNA and shRNA vectors. Moreover, this assay technically mimicked the competitive nature of the screen with one main difference: while during the screen cells infected with different sgRNAs were competing each other, in this case we have only two competitive populations represented by cells expressing the selected sgRNA, in competition with

uninfected normal cells. Most noteworthy here, and in line with the observations made in the primary screens, almost all of the selected hits conferred a competitive disadvantage already before MycER^{TM} activation, i. e. in control WT-MYC cells; this notwithstanding, this effect was significantly increased upon MycER^{TM} activation, validating the synthetic lethal calls made in the screen. Depletion of *Dhx36* and *Tnpo1* showed a statistically significant effect with only one construct and the loss of *Khsrp* did not induce any significant impact on cell fitness. However, the biological replicates of such experiments showed a trend similar to the other tested samples, an indication that increasing the number of experiments could provide more consistent data. Furthermore, gene silencing also displayed a major detrimental effect when MYC was activated compared to normal condition, although the level of knock-down was poor as that observed during the shRNA screen (Figure 27F). Overall, the above experiments show a high level of validation for most – if not all – of the tested sgRNA-targeted candidates – allowing for the fact that statistical significance may only be reached with a larger number of validation experiments. We also observed consistent trends for shRNA-targeted hits, for which the data are less conclusive and will require alternative validation strategies (e. g. silencing via CRISPRi). We surmise that all the selected hits possibly warrant follow up investigations, in consideration of their cellular functions and possible contribution to MYC oncogenic activities, which will be briefly discussed below.

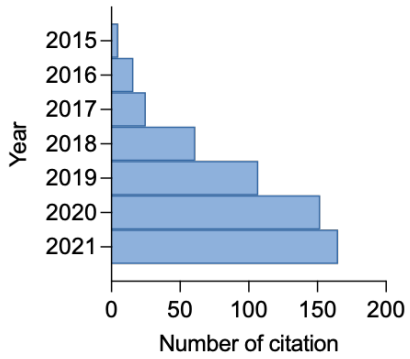

Figure 36. Increasing employment of MAGeCK tool for the analysis of CRISPR/Cas9 screens. Number of citations per year of Li et al., Genome Biology, 2014 (ref. 422) in which the MAGeCK tool was first described. PubMed® data (Cited In for PMID: 25476604).

4.2 Biological functions of the identified RBPs

Most importantly for this study, and as described later in further detail, two of our high confidence validated genes were UPF1 and XRN1. UPF1 (Upstream frameshift 1) is an ATP-dependent RNA helicase and a key factor in nonsense-mediate decay (NMD)[403,405,463,464] and other decay pathways[405], whereas XRN1 is the processive exoribonuclease that catalyzes the final 5'-3' degradation step of multiple mRNA decay pathways, including NMD[384,465,466].

Among other validated sgRNA targets, NCBP2 (or CBP20) together with NCBP1 form the heterodimeric cap-binding complex (CBC) that binds to the 5' cap structure of all nascent RNA Polymerase II transcripts and participates to most - if not all - subsequent RNA processing events by interacting with- and recruiting other RBPs, thereby ensuring a dynamic integration of these processes[467]. Under steady state conditions, NCBP2 appears not to be essential, owing to the presence of the partially redundant factors NCBP1 and NCBP3[468]: we surmise that MYC activation may lead to a major requirement of NCBP2 to fully guarantee a correct performance of all the RNA processes during massive MYC-induced RNA synthesis.

Few data are available on NOC3L (or FAD24), described as a regulator of adipogenesis and DNA replication which localizes within nuclear speckles, domains enriched in pre-mRNA splicing factors which allowed us to speculate about a possible involvement in splicing[469,470]. Related to cancer, NOC3L was reported to inhibit H-RAS-mediated transformation by repressing NF-kB activity[471]. In yeast, the homolog Noc proteins are required for correct ribosome biogenesis[472], of which MYC is a known regulator[336]. Noc3p in particular also contains a basic helix-loop-helix (bHLH) motif and two bipartite nuclear localization signals, and was found to be essential for initiation of DNA replication[473]. Which of these activities – if any – contributes to the phenotypes scored in our work remains to be investigated.

TNPO1 (Karyopherin-b2 or Transportin) is a nuclear import receptor[474] with RNA-binding capacity which has been found involved in different processes[475] such as participation in virus uncoating, ciliary transport and modulation of phase separation properties of aggregation-prone proteins[476].

ZC3H4 is an RNA-binding zinc finger protein recently found to form a complex with WDR82, with which it controls an early transcription termination checkpoint activated by the inefficiently spliced first exon of long non-coding, spliced and poly-adenylated enhancer transcripts (elncRNAs) hence regulating extragenic transcription[477].

RBM39 is a splicing regulator which emerged from a CRISPR screen in acute myeloid leukemia, as a factor required to maintain correct exon inclusion and intron exclusion of HOXA9 target genes[478], an interesting scenario that may be conveyed to splicing requirements in MYC-driven tumors.

The DEAH-box helicases DHX36 (also known as RHAU and G4R1) appears to be a multifunction protein: it was originally identified as a regulator of mRNA stability, binding to AU-rich element in the 3' untranslated region, but was further found to be localized mainly in the nucleus and to localize in nuclear speckles. Moreover, DHX36 has guanine quadruplex (G4) resolvase activity on both DNA and RNA substrates, a unique characteristic among RNA helicases, and play a critical role in translation initiation. At the biological level, it has been implicated in essential roles in heart development, hematopoiesis, and embryogenesis[479,480].

The single-stranded nucleic acid binding protein KHSRP modulates RNA life and gene expression at various levels like splicing an mRNA decay and controls important cellular functions as proliferation, differentiation, metabolism and response to infectious agents[481].

Finally, it is noteworthy here that two of the RBPs that emerged as candidates in our 3T9 CRISPR screen, ELAVL1 (or HuR)[482] and HNRNPC[483], were reported to be involved in post-transcriptional regulation of the *MYC* mRNA; similarly, SYNCRIP and DHX9, which scored in the FL5.12 CRISPR screen, where shown to ensure stabilization of the *MYC* mRNA in association with IGF2BP[80]. These regulatory connections are unlikely to play a role here, however, as they were mediated through the untranslated regions of the *MYC* transcript, which are absent in our MycER^{TM} constructs used in our screens[363] (Figure 15A, B): we surmise that the

synthetic lethal interactions unraveled in our work must depend on other regulatory targets of these RBPs.

Examples of such alternative mechanisms are already available. HNRNPC, in particular, was identified, in addition to SRRT, as CBC interactor and modulator of various RNA maturation complexes, including those for 3' end processing, RNA transport and nuclear exosomal degradation[484]. Moreover, as YTHDF2, HNRNPC is also a regulator of m6A RNA modification[485]: while HNRNPC promote pre-mRNA splicing of methylated RNAs, YTHDF2 is an important m6A reader, involved in degradation of m6A-modified transcripts by recruiting the CCR4–NOT deadenylase complex[486].

Finally, we also identified the RNA-m6A-reader YTHDF2, which was recently involved in the regulation of MYC mRNA stability in glioblastoma stem cells, where it also constituted a targetable dependency[487] – although in this case YTHDF2 acted on *MYC* coding sequences, it remains to be addressed whether this might also apply to the recombinant mRNAs encoded by our MycER^{TM} constructs.

4.3 The NMD pathway as a liability in MYC-overexpressing cells

For the remainder of my thesis, we decided to focus on two of the validated hits, *Xrn1* and *Upf1*, depletion of which showed a strong effect in OHT-treated cells compared to their normal counterparts, as observed with all of the employed sgRNA constructs. Furthermore, as developed in the Introduction, both UPF1 and XRN1 belong to the cytoplasmic mRNA surveillance and quality-control system. We chose to follow up on these genes firstly with a series of experiments to assess any variation in proliferation and viability upon their knockout: deletion of *Xrn1* and *Upf1* induced apoptosis and impaired proliferation in MYC-overexpressing FL5.12 cells (Figure 28B). Furthermore, we performed proliferative competition assays in mouse-derived Eμ-myc/Cas9 lymphoma cells, in which the depletion of both hits impaired cell fitness (Figure 29B), confirming the effects observed in FL5.12 cells.

The DNA damage marker **γ**H2AX has been used in previous studies as a marker of MYC-induced genotoxic stress[488]: somewhat counter-intuitively, compared to the sgRosa control, XRN1- and UPF1-depleted FL5.12 cells showed lower levels of

γH2AX upon OHT treatment (Figure 28C). The DNA damage response (DDR) is known to be activated to repair DNA and avoid aberrant cell division and, in case of massive damage, to induce cell death. However, when associated with MYC overexpression, the DDR can generate two opposite and paradoxical effects: apoptosis as a tumor suppressive response, regulated by ATM/CHK2, or reduction of MYC-induced replication stress as tumor promoting response, modulated by the ATR/CHK1 branch[489]. The observed lower protein level of activated H2AX could indicate that depleted cells failed to activate the DDR, thus suggesting that XRN1 and UPF1 – and perhaps NMD – might indirectly have a role in the correct activation of DDR in response to replicative stress, for which their loss could eventually lead to the cell death that we observe in our experiments. Considering the plethora of factors involved in this scenario, such as also ARF, P53 and TIP60[490–493], deeper molecular investigations are required to better define the origin of cell death upon depletion of XRN1 or UPF1 in MYC-overexpressing cells.

Hypothesizing that the dependency of MYC-overexpressing cells on XRN1 and UPF1 might be ascribable to their common involvement in NMD, we decided to investigate this pathway and confirm its selective requirement in MYC overexpressing cells: toward this aim, we performed once again proliferative competition assays upon depletion of other critical NMD factors, such as SMG1, SMG6, SMG5 and SMG7 (see Introduction). These factors, which were not present in our screening libraries, are involved in critical steps of the NMD cascade (Figure 24): the kinase SMG1, which belongs to the phosphatidylinositol 3-kinase-related kinase (PIKK) family, phosphorylates UPF1 as a necessary step for the beginning of the targeted mRNA decay; the endoribonuclease SMG6 mediates the cleavage of the faulty RNA to subsequently allow its degradation; SMG5 and SMG7 form a heterodimer which recruits the decapping and deadenylase complexes for the 5'->3' and 3'->5' mRNA degradation, respectively. Interestingly, depletion of all these genes was detrimental in MYC-overexpressing cells compared to normal conditions, with a variable toxic effect also in untreated cells. Hence, loss of these NMD components reproduced the effect of *Xrn1* or *Upf1* deletion, further

strengthening the relevance of the NMD pathway in MYC-overexpressing cells (Figure 30). In particular, while loss of SMG7 displayed little effect in untreated cells, OHT-treated cells were strongly counter-selected. These results made us consider this factor worthy of further investigation, alongside UPF1 and XRN1.

NMD is a complex and not fully characterized pathway, composed of different upstream branches, which trigger a cascade of events that converge in mRNA decay. Each branch is primed by specific factors or specific features of the transcripts, although a number of NMD factors are common to all branches such as UPF1 that in particular covers a central role. The stronger effect that we observed upon SMG7 depletion compared to that of UPF1 loss might suggest that target specificity of SMG7 could provide a better therapeutic window in MYC-activated cells while the more critical requirement of UPF1 already in normal conditions could preclude the possibility to observe a different outcome between MYC-overexpressing and normal cells. In line with this consideration, we failed to obtained a full knockout of UPF1, by either infecting cells with different sgRNAs followed by selection (Figure 28), or generating stable knock-out clones (Figure 33A, B). Moreover, considering the central role of UPF1 in several decay pathways, it wouldn't be hazardous to postulate that UPF1 knockout is too detrimental in normal cells; indeed, knockout of this factor has been reported to slow-down proliferation in a cell type specific manner[494,495], although it has been demonstrated to be essential only during embryonic development[395]. To add a further layer of complexity, SMG7's role in the NMD pathways has been proposed as necessary for a step to enable SMG6 endonucleolytic cleavage of the target mRNA[399]. Furthermore, the contribution of each NMD factor may differ according to cell type, developmental stage and cellular context[410].

4.4 Future plans and perspectives

As future plans, we will test additional NMD factors to better characterize which components of the NMD pathway are mainly required in MYC-overexpressing cells. For this purpose, we planned to target UPF2, UPF3A/B (which may have a redundant or antagonistic roles), DCP2, PNRC2, DHX34 and finally CNOT8, the

catalytic component of the CCR4-NOT complex, which is also involved in NMD (see Introduction): these factors will be tested either singularly or pairwise, based on selected sgRNA combinations (for example between UPF proteins).

With the aim to further assess the requirement of the NMD pathway in MYC-overexpressing cells, we planned to test cell viability upon treatment with NMDI14, an NMD inhibitor that blocks the binding between UPF1 and SMG7[496]. However, this drug turned out to be insoluble in our hands, and showed no NMD-inhibitory effect in a recent study[497]. Other UPF1 inhibitors are not available at this time; as an alternative we plan to use an inhibitor of the human kinase SMG1 (hSMG1i)[498,499]. Most noteworthy here, hSMG1i efficiently suppressed UPF1 phosphorylation with little apparent effect on phospho-p70S6K and phospho-AKT, two substrates of the other PIKKs mTOR and PI3K, respectively.

In order to extend our observations, we plan to validate the synthetic-lethality of XRN1, UPF1 and SMG7 by siRNA-mediated knock-down coupled with conditional with MYC activation in a series of human cell lines, including osteosarcoma (U2OS) and glioblastoma (T98G) cell lines (the latter expressing low levels of endogenous MYC[114]), and hTERT-immortalized retinal RPE1 cells. We engineered these cell lines for MycER^{TM} expression and successfully evaluated its activity upon OHT treatment. Interestingly, we could notice that MYC activation increased UPF1 protein levels, as already observed in FL5.12 cells (Figure 28C), although further investigations are required to ensure consistency of these data and to discriminate mRNA/protein stabilization from transcriptional upregulation. In such case, validated results would corroborate the major requirement of UPF1 in MYC-overexpressing cells. While waiting for available siRNAs targeting *SMG7*, we obtained preliminary data upon transfection of hTERT RPE1^{Mycer} cells with two different siRNAs targeting *XRN1* and *UPF1*. My current preliminary data (not shown here) indicate that these siRNAs effectively suppress their targets, lead to the up-regulation of select NMD-regulated mRNAs, and may preferentially increase cell death upon OHT treatment of silenced cells. Altogether, these preliminary data appear to confirm the vulnerability of MYC-overexpressing human cells upon depletion of particular

NMD, although completion and further analysis are required to confirm the observed phenotype.

Our results so far pointed to the NMD pathway as a critical dependency, and thus a potential target for therapeutical intervention in MYC-driven tumors, warranting a focused characterization of this pathway in the final part of this project. At the mechanistic level, a key priority lies in the identification of the mRNAs that show NMD-dependent control upon MYC activation, by mapping their abundance both in the bulk- and translated mRNA pools. Toward this end, by engineering stable clonal lines knocked out for *Xnr1*, *Upf1 or Smg7*, we will use these cells to establish RNA-seq and Ribo-seq profiles following MycER^{TM} activation.

The necessity of having stable knockout populations originated by the encountered difficulties in establishing a suitable model for concomitant expression of Cas9, sgRNAs and high level of MYC (Figure 31). In the clonal population that we employed for the execution of the screen, technical validations and competition assays of the NMD factors, we observed a higher level of cell death upon OHT treatment also in control samples, owing to the high level of constitutive expression of either Cas9, which off-target effects could have activated the DDR program (Figure 31C), or MycER^{TM}, known to induce apoptosis when hyperactivated (see Introduction). Another system employing a doxycycline-inducible Cas9 expression was tested but failed to maintain a stable Cas9 expression upon doxycycline treatment owing to the selection of Cas9-silenced cells (data not shown).

To solve this issue, we decided to proceed with a transient expression of both sgRNA and Cas9 elements and generate *Xrn1*, *Upf1* and *Smg7* knock-out clones. Apart from UPF1 KO clones which are now being generated, XRN1- and SMG7-depleted clonal populations present proliferation impediment and apoptosis increase upon MYC hyperactivation with respect to WT cells. As said above, these clones will be critical to achieve molecular insight into the requirement for a correct NMD activity in MYC-overexpressing cells. Deep profiling of bulk and translating mRNA species will clarify whether NMD functions are essential for a specific set of targets or a general mechanism of mRNA surveillance and quality control upon

MYC hyperactivation. For example, NMD negatively modulate the expression of key effectors of the unfolded protein response and integrated stress response, such as ATF4[400,500,501]. The increased protein synthesis and robust proliferative programs in MYC-overexpressing cells require an adequate activation and regulation of intrinsic cellular stress response[502]. In absence of NMD, prolongated expression of such stress-related factors might result critical and lead to opposite consequences such as apoptosis.

Previous works has involved the NMD pathway in the suppression of anti-tumoral immunity, in particular by preventing the accumulation of aberrant transcripts which could produce neoantigens, particularly when the splicing machine is impaired[503–505]. Treatment with 5-azacytidine (an hypomethylating agent clinically approved against myelodysplastic syndrome) in a model of colorectal cancer *in vivo* showed to inhibit NMD and increase the presentation of immunogenic neoepitopes supporting the clinical potential of NMD inhibition in anti-cancer immunotherapy strategies[506]. Furthermore, a recent study aimed to uncover the mechanisms behind the potent anti-tumor activity of spliceosome-targeted therapies across many cancers, such as MYC-driven tumors, demonstrated that this therapy induces widespread cytoplasmic accumulation of mis-spliced mRNAs with retained introns, many of which form double-stranded RNA (dsRNA) structures: dsRNA-binding proteins recognize these endogenous dsRNAs and trigger antiviral signaling and extrinsic apoptosis via adaptive immune activation improving tumor-free survival[335]. On note, NMD can also be activated upon recognition of viral RNA within the cell, which can present atypical features for their compact genome structures, thus contributing to cell-intrinsic antiviral response[507]. In line with these observations, we hypothesized that splicing and mRNA decay of aberrant/mispliced transcripts are two redundant process which prevent toxic effects that could lead to cell death, such as viral mimicry, neoantigen production or uncontrolled synthesis of stress-related factors, such as ATF4.

Despite indications that the NMD pathway is preferentially required in MYC-overexpressing cells, our results might also be explained by a number of alternative

mechanisms, owing to the involvement of the same factors in other pathways. For example, several NMD regulators (UPF1, UPF2, SMG1, SMG5, SMG6 and SMG7) were link to telomere integrity[508]. UPF1 was shown to bind newly transcribed mRNAs and to guide their nuclear export in *Drosophila*[406], and to have a role in cell cycle regulation, DNA replication and S phase progression, in a NMD-independent fashion[494,509]. SMG1 was shown to phosphorylate p53 and improve its activation in response of genotoxic stress, and also plays a role genome stability[398,510,511], In yeast, XRN1 shuttles between the cytoplasm and the nucleus, associates preferentially with transcription start-sites and promotes transcription initiation and elongation, mRNA translation and decay of a specific group of transcripts encoding membrane proteins[512,513].

A series of additional observations linked UPF1 and XRN1 to nucleo-cytoplasmic communication, although the specific mechanisms are not yet fully understood. Diverse studies, reviewed by Hartenian and Glaunsinger[514], reported the existence of a crosstalk between Pol II transcription and mRNA decay, which are differentially modulated during homeostasis or upon perturbation: in particular, decreased abundance of specific mRNAs can be buffered by increased transcription of the respective genes; reciprocally, stabilization of mRNAs can result in decreased transcription[513,516–522]. Some of these studies[516,521] and others[513,522] suggested both direct and indirect roles of XRN1 in transcriptional regulation. On the other hand, UPF1 may play a role in nonsense-induced transcriptional compensation (NITC)[523] or "genetic compensation", a response to the degradation of transcripts with premature termination codons that leads to the upregulation of homologous genes with similar sequence[524,525].

While these considerations may suggest that UPF1 SMG7 and XRN1 might be necessary in MYC-overexpressing cells owing to their participation in alternative, NMD-independent processes, the fact that all the different NMD factor that we depleted showed a synthetic lethal interaction with MYC (albeit to variable degrees) allows us to hypothesize that NMD impairment is likely to be the leading cause of cell death in those conditions. Testing additional NMD factors in competitive

proliferation assays and evaluation of possible involvement of other pathways might help to confirm or reject our hypothesis. Likewise, the proposed RNA profiles shall be instrumental in pinning down the mechanistic basis for the phenotypes reported here, and shall provide important cues for their potential therapeutic exploitation.

4.5 Conclusion

In summary, the negative impact on proliferation upon *Upf1*, *Smg7* and *Xrn1* knockout in MYC-overexpressing cells might conceivably be explained by a number of possible mechanisms, including impaired degradation of mutated transcripts (that may result in a lethal cellular effect), loss of genetic compensatory responses that buffer the abundance in mRNA levels, or loss of an XRN1-mediated transcriptional feedback. Altogether, we hypothesize that one or more of the aforementioned compensatory responses might be particularly critical in MYC-overexpressing cells. To investigate this aspect, we will firstly proceed with gene expression profiling in FL5.12 cells upon MycER^{TM} activation in the absence of either *Upf1*, *Smg7* or *Xrn1*, and will characterize differentially expressed genes in a time-course experiment in order to assess their rate of mRNA synthesis, processing and degradation, as in previous studies[58,129,526]. Successively, we will perform ribosome profiling in the same cells, in order to identify those mRNAs that are preferentially translated in *Upf1*-, *Smg7*- and *Xrn1*- depleted cells with or without MycER^{TM} activation, and could thus represent critical transcripts that need to be specifically degraded in MYC-overexpressing cells. Finally, we surmise that, by identifying new liabilities of MYC-overexpressing cells and characterizing them at the molecular and functional levels, our work has the potential to provide better understanding of MYC's role at the post-transcriptional level, a still under-investigated layer of regulation. More importantly, our work will pave the way for the development of new therapeutic opportunities toward MYC-dependent tumors.

5. Supplementary Tables

Use the following link to access the supplementary files:

https://ieo-my.sharepoint.com/:f:/g/personal/ieo4423_ieo_it/Evxd8igidNpDimnlSk65haYBfnezRqnzmyhQBqP3PkNZBg

Table S1. Library design and composition.
The RBP-coding genes targeted in our sgRNA and shRNA libraries were selected based on the following criteria: first, we listed genes reported to be either up-regulated[373,380] or amplified[373] in different human cancers; second, we added genes that had emerged as synthetic lethal interactors with over-expressed MYC in a series of published screens[224,263,265], but had not been validated. Positive controls comprise essential genes, including *Dnmt1*, *Mcm6*, *Myc*, *Pcna*, *Plk1*, *Pola1*, *Psma1*, *Psmb1*, *Rpa1*, *Rpa3*, *Rpl15*, *Rrm1* and *Top2a* (J. Zuber personal communication), as well as validated synthetic lethal interactors, including Brd4[414], Bud31[175], Cdk2[299], Cdk9[224], *Cecr2*[263], *Csnk1e*[263], *Pes1*[263], *Prmt5*[154], *Sae2*[265] and *Sf3bp1*[175]. The *Myc* gene itself was also included as a control. Negative controls correspond to genes whose depletion does not affect cell fitness (J. Zuber personal communication). The columns in the first table (**sgRNA library**) are as follows. **Gene**: human gene ID for each of the targeted genes; **Group:** indicates whether the entry is an experimental target or a control (positive or negative); **Dang**, **Sebestyen** and **Synthetic lethal**: "yes" indicates that the gene was selected either from the corresponding publications[373,380], or from one of the previous synthetic lethal screens[224,263,265]; **Mouse GS** and **Mouse GeneID**: identity of the targeted mouse genes, given as Gene Symbol and GeneID (NCBI Entrez Gene), respectively; **sgRNA#**: internal reference numbers (1-6) of the different sgRNAs used for each gene; **sgRNA:** sequence of the sgRNA; **strand**: the positive or negative sign corresponds to the targeted DNA strand. The same definitions apply to the second table with the **shRNA library**.

Table S2. Gene beta scores in the three screens.
Beta scores were calculated with the MAGeCK tool for each gene targeted in the library, in each sample, at the beginning (Post Selection: PS) and at the end of the screen in the two experimental conditions (WT-MYC and HIGH-MYC). As baseline, we used the pooled sgRNA library for the CRISPR screen in 3T9 cells, and the Post Infection (PI) sample for each of the two screens in FL5.12 cells (see text, sections 2.7, 3.4 and 3.5). The genes indicated in red are those candidates that passed each of the three filtering criteria (as highlighted in the corresponding column), including: (i.) a negative beta score in the HIGH-MYC condition; (ii.) a difference between HIGH-MYC and WT-MYC below -0.1 (indicated as $\Delta 1$); (iii.) a difference between WT-MYC and PS below 0.05 (indicated as $\Delta 2$). Genes are ranked based on $\Delta 1$.

Table S3. Intersection of hits with putative synthetic lethal genes.
The first four columns show the lists of synthetic lethal candidates with over-expressed MYC from previous screens[224,263,265] (1) and of the hits that emerged from our 3T9 CRISPR (2), FL5.12 CRISPR (3) and FL5.12 shRNA screens (4). The last four columns show the common hits between the different lists, as indicated.

6. References

1. Duesberg, P. H. & Vogt, P. K. Avian acute leukemia viruses MC29 and MH2 share specific RNA sequences: evidence for a second class of transforming genes. *Proc Natl Acad Sci U S A* **76**, 1633–1637 (1979).
2. Sheiness, D. & Bishop, J. M. DNA and RNA from uninfected vertebrate cells contain nucleotide sequences related to the putative transforming gene of avian myelocytomatosis virus. *J Virol* **31**, 514–521 (1979).
3. Dalla-Favera, R. *et al.* Human c-myc onc gene is located on the region of chromosome 8 that is translocated in Burkitt lymphoma cells. *Proc Natl Acad Sci U S A* **79**, 7824–7827 (1982).
4. Taub, R. *et al.* Translocation of the c-myc gene into the immunoglobulin heavy chain locus in human Burkitt lymphoma and murine plasmacytoma cells. *Proceedings of the National Academy of Sciences* **79**, 7837–7841 (1982).
5. Nesbit, C. E., Tersak, J. M. & Prochownik, E. V. MYC oncogenes and human neoplastic disease. *Oncogene* **18**, 3004–3016 (1999).
6. Dang, C. V. MYC on the path to cancer. *Cell* **149**, 22–35 (2012).
7. Kalkat, M. *et al.* MYC Deregulation in Primary Human Cancers. *Genes* **8**, 151 (2017).
8. Schwab, M. *et al.* Amplified DNA with limited homology to myc cellular oncogene is shared by human neuroblastoma cell lines and a neuroblastoma tumour. *Nature* **305**, 245–248 (1983).
9. Kohl, N. E. *et al.* Transposition and amplification of oncogene-related sequences in human neuroblastomas. *Cell* **35**, 359–367 (1983).
10. Nau, M. M. *et al.* L-myc, a new myc-related gene amplified and expressed in human small cell lung cancer. *Nature* **318**, 69–73 (1985).
11. Rickman, D. S., Schulte, J. H. & Eilers, M. The Expanding World of N-MYC–Driven Tumors. *Cancer Discov* **8**, 150–163 (2018).
12. Zimmerman, K. A. *et al.* Differential expression of myc family genes during murine development. *Nature* **319**, 780–783 (1986).
13. Oster, S. K., Ho, C. S. W., Soucie, E. L. & Penn, L. Z. The myc Oncogene: omplex. in *Advances in Cancer Research* vol. 84 81–154 (Elsevier, 2002).
14. Meyer, N. & Penn, L. Z. Reflecting on 25 years with MYC. *Nat. Rev. Cancer* **8**, 976–990 (2008).
15. Kress, T. R., Sabò, A. & Amati, B. MYC: connecting selective transcriptional control to global RNA production. *Nat Rev Cancer* **15**, 593–607 (2015).
16. Beaulieu, M.-E., Castillo, F. & Soucek, L. Structural and Biophysical Insights into the Function of the Intrinsically Disordered Myc Oncoprotein. *Cells* **9**, 1038 (2020).
17. Kato, G. J., Barrett, J., Villa-Garcia, M. & Dang, C. V. An amino-terminal c-myc domain required for neoplastic transformation activates transcription. *Mol Cell Biol* **10**, 5914–5920 (1990).
18. Cowling, V. H. & Cole, M. D. Mechanism of transcriptional activation by the Myc oncoproteins. *Seminars in Cancer Biology* **16**, 242–252 (2006).
19. Blackwell, T. K., Kretzner, L., Blackwood, E. M., Eisenman, R. N. & Weintraub, H. Sequence-Specific DNA Binding by the c-Myc Protein. *Science* **250**, 1149–1151 (1990).
20. Blackwood, E. M. & Eisenman, R. N. Max: A Helix-Loop-Helix Zipper Protein That Forms a Sequence-Specific DNA-Binding Complex with Myc. *Science* **251**, 1211–1217 (1991).
21. Amati, B. *et al.* Transcriptional activation by the human c-Myc oncoprotein in yeast requires interaction with Max. *Nature* **359**, 423–426 (1992).
22. Kretzner, L., Blackwood, E. M. & Eisenman, R. N. Myc and Max proteins possess distinct transcriptional activities. *Nature* **359**, 426–429 (1992).
23. Amati, B. *et al.* Oncogenic activity of the c-Myc protein requires dimerization with Max. *Cell* **72**, 233–245 (1993).
24. Amati, B., Littlewood, T. D., Evan, G. I. & Land, H. The c-Myc protein induces cell cycle progression and apoptosis through dimerization with Max. *EMBO J* **12**, 5083–5087 (1993).
25. Conacci-Sorrell, M., McFerrin, L. & Eisenman, R. N. An Overview of MYC and Its Interactome. *Cold Spring Harbor Perspectives in Medicine* **4**, a014357–a014357 (2014).
26. Dingar, D. *et al.* MYC dephosphorylation by the PP1/PNUTS phosphatase complex regulates chromatin binding and protein stability. *Nat Commun* **9**, 3502 (2018).
27. Wei, Y. *et al. The PNUTS-PAD domain recruits MYC to the PNUTS:PP1 phosphatase complex via the oncogenic MYC-MB0 region*. http://biorxiv.org/lookup/doi/10.1101/2021.12.02.470928 (2021) doi:10.1101/2021.12.02.470928.
28. Kalkat, M. *et al.* MYC Protein Interactome Profiling Reveals Functionally Distinct Regions that Cooperate to Drive Tumorigenesis. *Molecular Cell* **72**, 836-848.e7 (2018).
29. Hann, S. R. & Eisenman, R. N. Proteins encoded by the human c-myc oncogene: differential expression in neoplastic cells. *Mol. Cell. Biol.* **4**, 2486–2497 (1984).
30. Farrell, A. S. & Sears, R. C. MYC Degradation. *Cold Spring Harbor Perspectives in Medicine* **4**, a014365–a014365 (2014).
31. Helander, S. *et al.* Pre-Anchoring of Pin1 to Unphosphorylated c-Myc in a Fuzzy Complex Regulates c-Myc Activity. *Structure* **23**, 2267–2279 (2015).
32. Cohn, G. M., Liefwalker, D. F., Langer, E. M. & Sears, R. C. PIN1 Provides Dynamic Control of MYC in Response to Extrinsic Signals. *Front. Cell Dev. Biol.* **8**, 224 (2020).
33. Richards, M. W. *et al.* Structural basis of N-Myc binding by Aurora-A and its destabilization by kinase inhibitors. *Proc Natl Acad Sci USA* **113**, 13726–13731 (2016).
34. Bahram, F., von der Lehr, N., Cetinkaya, C. & Larsson, L.-G. c-Myc hot spot mutations in lymphomas result in inefficient ubiquitination and decreased proteasome-mediated turnover. *Blood* **95**, 2104–2110 (2000).
35. Pineda-Lucena, A. *et al.* A Structure-based Model of the c-Myc/Bin1 Protein Interaction Shows Alternative Splicing of Bin1 and c-Myc Phosphorylation are Key Binding Determinants. *Journal of Molecular Biology* **351**, 182–194 (2005).
36. Wei, Y. *et al.* Multiple direct interactions of TBP with the MYC oncoprotein. *Nat Struct Mol Biol* **26**, 1035–1043 (2019).

37. Price, D. H. P-TEFb, a Cyclin-Dependent Kinase Controlling Elongation by RNA Polymerase II. *Mol Cell Biol* **20**, 2629–2634 (2000).
38. Rahl, P. B. & Young, R. A. MYC and Transcription Elongation. *Cold Spring Harbor Perspectives in Medicine* **4**, a020990–a020990 (2014).
39. McMahon, S. B., Van Buskirk, H. A., Dugan, K. A., Copeland, T. D. & Cole, M. D. The Novel ATM-Related Protein TRRAP Is an Essential Cofactor for the c-Myc and E2F Oncoproteins. *Cell* **94**, 363–374 (1998).
40. Frank, S. R. *et al.* MYC recruits the TIP60 histone acetyltransferase complex to chromatin. *EMBO Rep* **4**, 575–580 (2003).
41. Doyon, Y., Selleck, W., Lane, W. S., Tan, S. & Côté, J. Structural and Functional Conservation of the NuA4 Histone Acetyltransferase Complex from Yeast to Humans. *Mol Cell Biol* **24**, 1884–1896 (2004).
42. Adhikary, S. & Eilers, M. Transcriptional regulation and transformation by Myc proteins. *Nat Rev Mol Cell Biol* **6**, 635–645 (2005).
43. Knoepfler, P. S. *et al.* Myc influences global chromatin structure. *EMBO J* **25**, 2723–2734 (2006).
44. McMahon, S. B., Wood, M. A. & Cole, M. D. The Essential Cofactor TRRAP Recruits the Histone Acetyltransferase hGCN5 to c-Myc. *Mol Cell Biol* **20**, 556–562 (2000).
45. Dang, C. V. & Lee, W. M. Identification of the human c-myc protein nuclear translocation signal. *Mol Cell Biol* **8**, 4048–4054 (1988).
46. Herbst, A. *et al.* A conserved element in Myc that negatively regulates its proapoptotic activity. *EMBO Rep* **6**, 177–183 (2005).
47. Kurland, J. F. & Tansey, W. P. Myc-Mediated Transcriptional Repression by Recruitment of Histone Deacetylase. *Cancer Res* **68**, 3624–3629 (2008).
48. Thomas, L. R. *et al.* Interaction with WDR5 Promotes Target Gene Recognition and Tumorigenesis by MYC. *Molecular Cell* **58**, 440–452 (2015).
49. Thomas, L. R. *et al.* Interaction of the oncoprotein transcription factor MYC with its chromatin cofactor WDR5 is essential for tumor maintenance. *Proc Natl Acad Sci USA* **116**, 25260–25268 (2019).
50. Thomas, L. R. *et al.* Interaction of MYC with host cell factor-1 is mediated by the evolutionarily conserved Myc box IV motif. *Oncogene* **35**, 3613–3618 (2016).
51. Boija, A. *et al.* Transcription Factors Activate Genes through the Phase-Separation Capacity of Their Activation Domains. *Cell* **175**, 1842-1855.e16 (2018).
52. Chong, S. *et al. Tuning levels of low-complexity domain interactions to modulate endogenous oncogenic transcription*. http://biorxiv.org/lookup/doi/10.1101/2021.08.16.456551 (2021) doi:10.1101/2021.08.16.456551.
53. Trojanowski, J., Frank, L., Rademacher, A., Grigaitis, P. & Rippe, K. *Transcription activation is enhanced by multivalent interactions independent of phase separation*. http://biorxiv.org/lookup/doi/10.1101/2021.01.27.428421 (2021) doi:10.1101/2021.01.27.428421.
54. Lambert, S. A. *et al.* The Human Transcription Factors. *Cell* **172**, 650–665 (2018).
55. Lüscher, B. & Larsson, L.-G. The basic region/helix–loop–helix/leucine zipper domain of Myc proto-oncoproteins: Function and regulation. *Oncogene* **18**, 2955–2966 (1999).
56. Nair, S. K. & Burley, S. K. X-Ray Structures of Myc-Max and Mad-Max Recognizing DNA. *Cell* **112**, 193–205 (2003).
57. Blackwell, T. K. *et al.* Binding of myc proteins to canonical and noncanonical DNA sequences. *Mol Cell Biol* **13**, 5216–5224 (1993).
58. de Pretis, S. *et al.* Integrative analysis of RNA polymerase II and transcriptional dynamics upon MYC activation. *Genome Res.* **27**, 1658–1664 (2017).
59. Pellanda, P. *et al.* Integrated requirement of non-specific and sequence-specific DNA binding in Myc-driven transcription. *EMBO J* **40**, (2021).
60. Staller, P. *et al.* Repression of p15INK4b expression by Myc through association with Miz-1. *Nat Cell Biol* **3**, 392–399 (2001).
61. Wiese, K. E. *et al.* The Role of MIZ-1 in MYC-Dependent Tumorigenesis. *Cold Spring Harbor Perspectives in Medicine* **3**, a014290–a014290 (2013).
62. Zhang, L. *et al.* Myc-Miz-1 signaling promotes self-renewal of leukemia stem cells by repressing Cebp**α** and Cebp**δ**. *Blood* blood.2019001863 (2020) doi:10.1182/blood.2019001863.
63. Diolaiti, D., McFerrin, L., Carroll, P. A. & Eisenman, R. N. Functional interactions among members of the MAX and MLX transcriptional network during oncogenesis. *Biochimica et Biophysica Acta (BBA) - Gene Regulatory Mechanisms* **1849**, 484–500 (2015).
64. Carroll, P. A., Freie, B. W., Mathsyaraja, H. & Eisenman, R. N. The MYC transcription factor network: balancing metabolism, proliferation and oncogenesis. *Front Med* **12**, 412–425 (2018).
65. Nguyen, H. V. *et al.* Development and Survival of MYC-driven Lymphomas Requires MYC-Antagonist MNT to Curb MYC-induced Apoptosis. *Blood* blood.2019003014 (2020) doi:10.1182/blood.2019003014.
66. Winkles, J. A. Serum- and Polypeptide Growth Factor-Inducible Gene Expression in Mouse Fibroblasts. in *Progress in Nucleic Acid Research and Molecular Biology* vol. 58 41–78 (Elsevier, 1997).
67. Kelly, K., Cochran, B. H., Stiles, C. D. & Leder, P. Cell-specific regulation of the c-myc gene by lymphocyte mitogens and platelet-derived growth factor. *Cell* **35**, 603–610 (1983).
68. Palomero, T. *et al.* NOTCH1 directly regulates c-MYC and activates a feed-forward-loop transcriptional network promoting leukemic cell growth. *Proceedings of the National Academy of Sciences* **103**, 18261–18266 (2006).
69. He, T.-C. *et al.* Identification of c- *MYC* as a Target of the APC Pathway. *Science* **281**, 1509–1512 (1998).
70. Sicklick, J. K. *et al.* Dysregulation of the Hedgehog pathway in human hepatocarcinogenesis. *Carcinogenesis* **27**, 748–757 (2006).
71. Murn, J. *et al.* A Myc-regulated transcriptional network controls B-cell fate in response to BCR triggering. *BMC Genomics* **10**, 323 (2009).
72. Luo, W., Weisel, F. & Shlomchik, M. J. B Cell Receptor and CD40 Signaling Are Rewired for Synergistic Induction of the c-Myc Transcription Factor in Germinal Center B Cells. *Immunity* **48**, 313-326.e5 (2018).
73. Kiuchi, N. *et al.* STAT3 is required for the gp130-mediated full activation of the c-myc gene. *J Exp Med* **189**, 63–73 (1999).
74. Frederick, J. P., Liberati, N. T., Waddell, D. S., Shi, Y. & Wang, X.-F. Transforming growth factor beta-mediated transcriptional repression of c-myc is

dependent on direct binding of Smad3 to a novel repressive Smad binding element. *Mol Cell Biol* **24**, 2546–2559 (2004).
75. Penn, L. J., Brooks, M. W., Laufer, E. M. & Land, H. Negative autoregulation of c-myc transcription. *EMBO J* **9**, 1113–1121 (1990).
76. Culjkovic, B., Topisirovic, I., Skrabanek, L., Ruiz-Gutierrez, M. & Borden, K. L. B. eIF4E is a central node of an RNA regulon that governs cellular proliferation. *Journal of Cell Biology* **175**, 415–426 (2006).
77. Dani, C. *et al.* Extreme instability of myc mRNA in normal and transformed human cells. *Proceedings of the National Academy of Sciences* **81**, 7046–7050 (1984).
78. Liao, B., Hu, Y. & Brewer, G. Competitive binding of AUF1 and TIAR to MYC mRNA controls its translation. *Nat Struct Mol Biol* **14**, 511–518 (2007).
79. Keene, J. D. RNA regulons: coordination of post-transcriptional events. *Nat Rev Genet* **8**, 533–543 (2007).
80. Weidensdorfer, D. *et al.* Control of c-myc mRNA stability by IGF2BP1-associated cytoplasmic RNPs. *RNA* **15**, 104–115 (2009).
81. Zhang, K. *et al.* AGO2 Mediates *MYC* mRNA Stability in Hepatocellular Carcinoma. *Mol Cancer Res* **18**, 612–622 (2020).
82. van Kouwenhove, M., Kedde, M. & Agami, R. MicroRNA regulation by RNA-binding proteins and its implications for cancer. *Nat Rev Cancer* **11**, 644–656 (2011).
83. Li, X. *et al.* Decreased c-Myc mRNA Stability via the MicroRNA 141-3p/AUF1 Axis Is Crucial for p63**α** Inhibition of Cyclin D1 Gene Transcription and Bladder Cancer Cell Tumorigenicity. *Mol Cell Biol* **38**, (2018).
84. Csibi, A. *et al.* The mTORC1/S6K1 Pathway Regulates Glutamine Metabolism through the eIF4B-Dependent Control of c-Myc Translation. *Current Biology* **24**, 2274–2280 (2014).
85. Kozak, M. Circumstances and mechanisms of inhibition of translation by secondary structure in eucaryotic mRNAs. *Mol. Cell. Biol.* **9**, 5134–5142 (1989).
86. Nanbru, C. *et al.* Alternative Translation of the Proto-oncogene c-mycby an Internal Ribosome Entry Site. *Journal of Biological Chemistry* **272**, 32061–32066 (1997).
87. Cobbold, L. C. *et al.* Identification of Internal Ribosome Entry Segment (IRES)- *trans* -Acting Factors for the Myc Family of IRESs. *Mol Cell Biol* **28**, 40–49 (2008).
88. Mazan-Mamczarz, K., Lal, A., Martindale, J. L., Kawai, T. & Gorospe, M. Translational repression by RNA-binding protein TIAR. *Mol Cell Biol* **26**, 2716–2727 (2006).
89. Deshaies, R. J. SCF and Cullin/RING H2-Based Ubiquitin Ligases. *Annu. Rev. Cell Dev. Biol.* **15**, 435–467 (1999).
90. Sears, R. C. The life cycle of C-myc: from synthesis to degradation. *Cell Cycle* **3**, 1133–1137 (2004).
91. Bachireddy, P., Bendapudi, P. K. & Felsher, D. W. Getting at MYC through RAS. *Clin Cancer Res* **11**, 4278–4281 (2005).
92. Farrell, A. S. *et al.* Pin1 Regulates the Dynamics of c-Myc DNA Binding To Facilitate Target Gene Regulation and Oncogenesis. *Mol Cell Biol* **33**, 2930–2949 (2013).
93. Su, Y. *et al.* Post-translational modification localizes MYC to the nuclear pore basket to regulate a subset of target genes involved in cellular responses to environmental signals. *Genes Dev.* **32**, 1398–1419 (2018).
94. Gregory, M. A., Qi, Y. & Hann, S. R. Phosphorylation by glycogen synthase kinase-3 controls c-myc proteolysis and subnuclear localization. *J Biol Chem* **278**, 51606–51612 (2003).
95. Welcker, M. *et al.* The Fbw7 tumor suppressor regulates glycogen synthase kinase 3 phosphorylation-dependent c-Myc protein degradation. *PNAS* **101**, 9085–9090 (2004).
96. Yeh, E. *et al.* A signalling pathway controlling c-Myc degradation that impacts oncogenic transformation of human cells. *Nat Cell Biol* **6**, 308–318 (2004).
97. Arnold, H. K. & Sears, R. C. Protein phosphatase 2A regulatory subunit B56alpha associates with c-myc and negatively regulates c-myc accumulation. *Mol Cell Biol* **26**, 2832–2844 (2006).
98. Sears, R. *et al.* Multiple Ras-dependent phosphorylation pathways regulate Myc protein stability. *Genes Dev.* **14**, 2501–2514 (2000).
99. Nijman, S. M. B. *et al.* A Genomic and Functional Inventory of Deubiquitinating Enzymes. *Cell* **123**, 773–786 (2005).
100. Popov, N. *et al.* The ubiquitin-specific protease USP28 is required for MYC stability. *Nat Cell Biol* **9**, 765–774 (2007).
101. Popov, N., Herold, S., Llamazares, M., Schülein, C. & Eilers, M. Fbw7 and Usp28 Regulate Myc Protein Stability in Response to DNA Damage. *Cell Cycle* **6**, 2327–2331 (2007).
102. Popov, N., Schülein, C., Jaenicke, L. A. & Eilers, M. Ubiquitylation of the amino terminus of Myc by SCF**β**-TrCP antagonizes SCFFbw7-mediated turnover. *Nat Cell Biol* **12**, 973–981 (2010).
103. Kim, S. Y., Herbst, A., Tworkowski, K. A., Salghetti, S. E. & Tansey, W. P. Skp2 Regulates Myc Protein Stability and Activity. *Molecular Cell* **11**, 1177–1188 (2003).
104. von der Lehr, N. *et al.* The F-Box Protein Skp2 Participates in c-Myc Proteosomal Degradation and Acts as a Cofactor for c-Myc-Regulated Transcription. *Molecular Cell* **11**, 1189–1200 (2003).
105. Vervoorts, J. *et al.* Stimulation of c-MYC transcriptional activity and acetylation by recruitment of the cofactor CBP. *EMBO Rep* **4**, 484–490 (2003).
106. Faiola, F. *et al.* Dual regulation of c-Myc by p300 via acetylation-dependent control of Myc protein turnover and coactivation of Myc-induced transcription. *Mol Cell Biol* **25**, 10220–10234 (2005).
107. Vervoorts, J., Lüscher-Firzlaff, J. & Lüscher, B. The Ins and Outs of MYC Regulation by Posttranslational Mechanisms. *Journal of Biological Chemistry* **281**, 34725–34729 (2006).
108. Sabò, A., Doni, M. & Amati, B. SUMOylation of Myc-Family Proteins. *PLoS ONE* **9**, e91072 (2014).
109. González-Prieto, R., Cuijpers, S. A., Kumar, R., Hendriks, I. A. & Vertegaal, A. C. c-Myc is targeted to the proteasome for degradation in a SUMOylation-dependent manner, regulated by PIAS1, SENP7 and RNF4. *Cell Cycle* **14**, 1859–1872 (2015).
110. Kalkat, M. *et al.* Identification of c-MYC SUMOylation by Mass Spectrometry. *PLoS ONE* **9**, e115337 (2014).
111. Rabellino, A. *et al.* PIAS1 Promotes Lymphomagenesis through MYC Upregulation. *Cell Reports* **15**, 2266–2278 (2016).
112. Small, G. W., Chou, T.-Y., Dang, C. V. & Orlowski, R. Z. Evidence for involvement of calpain in c-Myc

proteolysis in vivo. *Archives of Biochemistry and Biophysics* **400**, 151–161 (2002).
113. Conacci-Sorrell, M., Ngouenet, C. & Eisenman, R. N. Myc-Nick: A Cytoplasmic Cleavage Product of Myc that Promotes **α**-Tubulin Acetylation and Cell Differentiation. *Cell* **142**, 480–493 (2010).
114. Fernandez, P. C. *et al.* Genomic targets of the human c-Myc protein. *Genes Dev.* **17**, 1115–1129 (2003).
115. Mao, D. Y. L. *et al.* Analysis of Myc Bound Loci Identified by CpG Island Arrays Shows that Max Is Essential for Myc-Dependent Repression. *Current Biology* **13**, 882–886 (2003).
116. Li, Z. *et al.* A global transcriptional regulatory role for c-Myc in Burkitt's lymphoma cells. *PNAS* **100**, 8164–8169 (2003).
117. Cawley, S. *et al.* Unbiased Mapping of Transcription Factor Binding Sites along Human Chromosomes 21 and 22 Points to Widespread Regulation of Noncoding RNAs. *Cell* **116**, 499–509 (2004).
118. Kim, J., Chu, J., Shen, X., Wang, J. & Orkin, S. H. An Extended Transcriptional Network for Pluripotency of Embryonic Stem Cells. *Cell* **132**, 1049–1061 (2008).
119. Zeller, K. I. *et al.* Global mapping of c-Myc binding sites and target gene networks in human B cells. *Proceedings of the National Academy of Sciences* **103**, 17834–17839 (2006).
120. Lin, C. Y. *et al.* Transcriptional Amplification in Tumor Cells with Elevated c-Myc. *Cell* **151**, 56–67 (2012).
121. Sabò, A. *et al.* Selective transcriptional regulation by Myc in cellular growth control and lymphomagenesis. *Nature* **511**, 488–492 (2014).
122. Guccione, E. *et al.* Myc-binding-site recognition in the human genome is determined by chromatin context. *Nat Cell Biol* **8**, 764–770 (2006).
123. Soufi, A., Donahue, G. & Zaret, K. S. Facilitators and Impediments of the Pluripotency Reprogramming Factors' Initial Engagement with the Genome. *Cell* **151**, 994–1004 (2012).
124. Nie, Z. *et al.* c-Myc Is a Universal Amplifier of Expressed Genes in Lymphocytes and Embryonic Stem Cells. *Cell* **151**, 68–79 (2012).
125. Walz, S. *et al.* Activation and repression by oncogenic MYC shape tumour-specific gene expression profiles. *Nature* **511**, 483–487 (2014).
126. Perna, D. *et al.* Genome-wide mapping of Myc binding and gene regulation in serum-stimulated fibroblasts. *Oncogene* **31**, 1695–1709 (2012).
127. Kress, T. R. *et al.* Identification of MYC-Dependent Transcriptional Programs in Oncogene-Addicted Liver Tumors. *Cancer Research* **76**, 3463–3472 (2016).
128. Tesi, A. *et al.* An early Myc-dependent transcriptional program orchestrates cell growth during B-cell activation. *EMBO Rep* **20**, (2019).
129. Muhar, M. *et al.* SLAM-seq defines direct gene-regulatory functions of the BRD4-MYC axis. *Science* **360**, 800–805 (2018).
130. Sabò, A. & Amati, B. BRD4 and MYC—clarifying regulatory specificity. *Science* **360**, 713–714 (2018).
131. Amati, B. Myc and the cell cycle. *Front Biosci* **3**, d250-268 (1998).
132. Bretones, G., Delgado, M. D. & León, J. Myc and cell cycle control. *Biochimica et Biophysica Acta (BBA) - Gene Regulatory Mechanisms* **1849**, 506–516 (2015).
133. Takayama, M., Taira, T., Iguchi-Ariga, S. M. M. & Ariga, H. CDC6 interacts with c-Myc to inhibit E-box-dependent transcription by abrogating c-Myc/Max complex. *FEBS Letters* **477**, 43–48 (2000).
134. Dominguez-Sola, D. *et al.* Non-transcriptional control of DNA replication by c-Myc. *Nature* **448**, 445–451 (2007).
135. Dominguez-Sola, D. & Gautier, J. MYC and the Control of DNA Replication. *Cold Spring Harbor Perspectives in Medicine* **4**, a014423–a014423 (2014).
136. Stine, Z. E., Walton, Z. E., Altman, B. J., Hsieh, A. L. & Dang, C. V. MYC, Metabolism, and Cancer. *Cancer Discovery* **5**, 1024–1039 (2015).
137. Dejure, F. R. & Eilers, M. MYC and tumor metabolism: chicken and egg. *EMBO J* **36**, 3409–3420 (2017).
138. Iritani, B. M. & Eisenman, R. N. c-Myc enhances protein synthesis and cell size during B lymphocyte development. *Proceedings of the National Academy of Sciences* **96**, 13180–13185 (1999).
139. Schuhmacher, M. *et al.* Control of cell growth by c-Myc in the absence of cell division. *Current Biology* **9**, 1255–1258 (1999).
140. Gallant, P. Myc Function in Drosophila. *Cold Spring Harbor Perspectives in Medicine* **3**, a014324–a014324 (2013).
141. Rosenwald, I. B., Rhoads, D. B., Callanan, L. D., Isselbacher, K. J. & Schmidt, E. V. Increased expression of eukaryotic translation initiation factors eIF-4E and eIF-2 alpha in response to growth induction by c-myc. *Proceedings of the National Academy of Sciences* **90**, 6175–6178 (1993).
142. Oskarsson, T. & Trumpp, A. The Myc trilogy: lord of RNA polymerases. *Nat Cell Biol* **7**, 215–217 (2005).
143. Gomez-Roman, N. *et al.* Activation by c-Myc of transcription by RNA polymerases I, II and III. *Biochemical Society Symposia* **73**, 141–154 (2006).
144. Ji, H. *et al.* Cell-Type Independent MYC Target Genes Reveal a Primordial Signature Involved in Biomass Accumulation. *PLoS ONE* **6**, e26057 (2011).
145. Campbell, K. J. & White, R. J. MYC Regulation of Cell Growth through Control of Transcription by RNA Polymerases I and III. *Cold Spring Harbor Perspectives in Medicine* **4**, a018408–a018408 (2014).
146. Schlosser, I. A role for c-Myc in the regulation of ribosomal RNA processing. *Nucleic Acids Research* **31**, 6148–6156 (2003).
147. Chou, C. *et al.* c-Myc-induced transcription factor AP4 is required for host protection mediated by CD8+ T cells. *Nat Immunol* **15**, 884–893 (2014).
148. Fujii, M. *et al.* SNIP1 Is a Candidate Modifier of the Transcriptional Activity of c-Myc on E Box-Dependent Target Genes. *Molecular Cell* **24**, 771–783 (2006).
149. Bracken, C. P. *et al.* Regulation of Cyclin D1 RNA Stability by SNIP1. *Cancer Res* **68**, 7621–7628 (2008).
150. Rounbehler, R. J. *et al.* Tristetraprolin Impairs Myc-Induced Lymphoma and Abolishes the Malignant State. *Cell* **150**, 563–574 (2012).
151. Mukherjee, N. *et al.* Global target mRNA specification and regulation by the RNA-binding protein ZFP36. *Genome Biol* **15**, R12 (2014).
152. Das, S., Anczuków, O., Akerman, M. & Krainer, A. R. Oncogenic Splicing Factor SRSF1 Is a Critical Transcriptional Target of MYC. *Cell Reports* **1**, 110–117 (2012).
153. David, C. J., Chen, M., Assanah, M., Canoll, P. & Manley, J. L. HnRNP proteins controlled by c-Myc deregulate pyruvate kinase mRNA splicing in cancer. *Nature* **463**, 364–368 (2010).
154. Koh, C. M. *et al.* MYC regulates the core pre-mRNA splicing machinery as an essential step in lymphomagenesis. *Nature* **523**, 96–100 (2015).

155. Hirsch, C. L. *et al.* Myc and SAGA rewire an alternative splicing network during early somatic cell reprogramming. *Genes Dev.* **29**, 803–816 (2015).
156. Askew, D. S., Ashmun, R. A., Simmons, B. C. & Cleveland, J. L. Constitutive c-myc expression in an IL-3-dependent myeloid cell line suppresses cell cycle arrest and accelerates apoptosis. *Oncogene* **6**, 1915–1922 (1991).
157. Fanidi, A., Harrington, E. A. & Evan, G. I. Cooperative interaction between c-myc and bcl-2 proto-oncogenes. *Nature* **359**, 554–556 (1992).
158. Bissonnette, R. P., Echeverri, F., Mahboubi, A. & Green, D. R. Apoptotic cell death induced by c-myc is inhibited by bcl-2. *Nature* **359**, 552–554 (1992).
159. Harrington, E. A., Bennett, M. R., Fanidi, A. & Evan, G. I. c-Myc-induced apoptosis in fibroblasts is inhibited by specific cytokines. *EMBO J* **13**, 3286–3295 (1994).
160. Soucie, E. L. *et al.* Myc Potentiates Apoptosis by Stimulating Bax Activity at the Mitochondria. *Mol Cell Biol* **21**, 4725–4736 (2001).
161. de Alborán, I. M., Baena, E. & Martinez-A, C. c-Myc-deficient B lymphocytes are resistant to spontaneous and induced cell death. *Cell Death Differ* **11**, 61–68 (2004).
162. Meyer, N., Kim, S. S. & Penn, L. Z. The Oscar-worthy role of Myc in apoptosis. *Seminars in Cancer Biology* **16**, 275–287 (2006).
163. McMahon, S. B. MYC and the Control of Apoptosis. *Cold Spring Harbor Perspectives in Medicine* **4**, a014407–a014407 (2014).
164. Strasser, A., Harris, A. W., Bath, M. L. & Cory, S. Novel primitive lymphoid tumours induced in transgenic mice by cooperation between myc and bcl-2. *Nature* **348**, 331–333 (1990).
165. Zindy, F. *et al.* Myc signaling via the ARF tumor suppressor regulates p53-dependent apoptosis and immortalization. *Genes Dev.* **12**, 2424–2433 (1998).
166. Hermeking, H. & Eick, D. Mediation of c-Myc-Induced Apoptosis by p53. *Science* **265**, 2091–2093 (1994).
167. Wagner, A. J., Kokontis, J. M. & Hay, N. Myc-mediated apoptosis requires wild-type p53 in a manner independent of cell cycle arrest and the ability of p53 to induce p21waf1/cip1. *Genes Dev.* **8**, 2817–2830 (1994).
168. Schmitt, C. A., McCurrach, M. E., de Stanchina, E., Wallace-Brodeur, R. R. & Lowe, S. W. INK4a/ARF mutations accelerate lymphomagenesis and promote chemoresistance by disabling p53. *Genes & Development* **13**, 2670–2677 (1999).
169. Eischen, C. M., Woo, D., Roussel, M. F. & Cleveland, J. L. Apoptosis Triggered by Myc-Induced Suppression of Bcl-X $_L$ or Bcl-2 Is Bypassed during Lymphomagenesis. *Mol Cell Biol* **21**, 5063–5070 (2001).
170. Alt, J. R. Mdm2 haplo-insufficiency profoundly inhibits Myc-induced lymphomagenesis. *The EMBO Journal* **22**, 1442–1450 (2003).
171. Egle, A., Harris, A. W., Bouillet, P. & Cory, S. Bim is a suppressor of Myc-induced mouse B cell leukemia. *Proceedings of the National Academy of Sciences* **101**, 6164–6169 (2004).
172. Qi, Y. *et al.* p19ARF directly and differentially controls the functions of c-Myc independently of p53. *Nature* **431**, 712–717 (2004).
173. Finch, A. *et al.* Bcl-xL gain of function and p19ARF loss of function cooperate oncogenically with Myc in vivo by distinct mechanisms. *Cancer Cell* **10**, 113–120 (2006).
174. Dansen, T. B., Whitfield, J., Rostker, F., Brown-Swigart, L. & Evan, G. I. Specific Requirement for Bax, Not Bak, in Myc-induced Apoptosis and Tumor Suppression in Vivo. *Journal of Biological Chemistry* **281**, 10890–10895 (2006).
175. Hsu, T. Y.-T. *et al.* The spliceosome is a therapeutic vulnerability in MYC-driven cancer. *Nature* **525**, 384–388 (2015).
176. Koh, C. M., Sabò, A. & Guccione, E. Targeting MYC in cancer therapy: RNA processing offers new opportunities. *BioEssays* **38**, 266–275 (2016).
177. Hanahan, D. & Weinberg, R. A. Hallmarks of Cancer: The Next Generation. *Cell* **144**, 646–674 (2011).
178. Casey, S. C., Baylot, V. & Felsher, D. W. The MYC oncogene is a global regulator of the immune response. *Blood* **131**, 2007–2015 (2018).
179. Schaub, F. X. *et al.* Pan-cancer Alterations of the MYC Oncogene and Its Proximal Network across the Cancer Genome Atlas. *Cell Systems* **6**, 282-300.e2 (2018).
180. Gabay, M., Li, Y. & Felsher, D. W. MYC Activation Is a Hallmark of Cancer Initiation and Maintenance. *Cold Spring Harbor Perspectives in Medicine* **4**, a014241–a014241 (2014).
181. Adams, J. M. *et al.* The c-myc oncogene driven by immunoglobulin enhancers induces lymphoid malignancy in transgenic mice. *Nature* **318**, 533–538 (1985).
182. Felsher, D. W. & Bishop, J. M. Reversible Tumorigenesis by MYC in Hematopoietic Lineages. *Molecular Cell* **4**, 199–207 (1999).
183. Beer, S. *et al.* Developmental Context Determines Latency of MYC-Induced Tumorigenesis. *PLoS Biol* **2**, e332 (2004).
184. Vaux, D. L., Cory, S. & Adams, J. M. Bcl-2 gene promotes haemopoietic cell survival and cooperates with c-myc to immortalize pre-B cells. *Nature* **335**, 440–442 (1988).
185. Teitz, T. *et al.* Caspase 8 is deleted or silenced preferentially in childhood neuroblastomas with amplification of MYCN. *Nat Med* **6**, 529–535 (2000).
186. DeoCampo, N. D., Wilson, M. R. & Trosko, J. E. Cooperation of bcl-2 and myc in the neoplastic transformation of normal rat liver epithelial cells is related to the down-regulation of gap junction-mediated intercellular communication. *Carcinogenesis* **21**, 1501–1506 (2000).
187. Welm, A. L., Kim, S., Welm, B. E. & Bishop, J. M. MET and MYC cooperate in mammary tumorigenesis. *Proceedings of the National Academy of Sciences* **102**, 4324–4329 (2005).
188. Clegg, N. J. *et al.* MYC Cooperates with AKT in Prostate Tumorigenesis and Alters Sensitivity to mTOR Inhibitors. *PLoS ONE* **6**, e17449 (2011).
189. Bailey, S. T. *et al.* MYC activation cooperates with Vhl and Ink4a/Arf loss to induce clear cell renal cell carcinoma. *Nat Commun* **8**, 15770 (2017).
190. García-Gutiérrez, L., Delgado, M. D. & León, J. MYC Oncogene Contributions to Release of Cell Cycle Brakes. *Genes* **10**, 244 (2019).
191. Malumbres, M. & Barbacid, M. RAS oncogenes: the first 30 years. *Nat Rev Cancer* **3**, 459–465 (2003).
192. Beroukhim, R. *et al.* The landscape of somatic copy-number alteration across human cancers. *Nature* **463**, 899–905 (2010).

193. Ciriello, G. *et al.* Emerging landscape of oncogenic signatures across human cancers. *Nat Genet* **45**, 1127–1133 (2013).
194. Boxer, L. M. & Dang, C. V. Translocations involving c-myc and c-myc function. *Oncogene* **20**, 5595–5610 (2001).
195. Pasqualucci, L. & Dalla-Favera, R. Genetics of diffuse large B-cell lymphoma. *Blood* **131**, 2307–2319 (2018).
196. Bisso, A., Sabò, A. & Amati, B. MYC in Germinal Center-derived lymphomas: Mechanisms and therapeutic opportunities. *Immunol Rev* **288**, 178–197 (2019).
197. Sansom, O. J. *et al.* Myc deletion rescues Apc deficiency in the small intestine. *Nature* **446**, 676–679 (2007).
198. Weng, A. P. *et al.* c-Myc is an important direct target of Notch1 in T-cell acute lymphoblastic leukemia/lymphoma. *Genes Dev* **20**, 2096–2109 (2006).
199. Tuupanen, S. *et al.* The common colorectal cancer predisposition SNP rs6983267 at chromosome 8q24 confers potential to enhanced Wnt signaling. *Nat Genet* **41**, 885–890 (2009).
200. Sur, I. K. *et al.* Mice Lacking a *Myc* Enhancer That Includes Human SNP rs6983267 Are Resistant to Intestinal Tumors. *Science* **338**, 1360–1363 (2012).
201. Wasserman, N. F., Aneas, I. & Nobrega, M. A. An 8q24 gene desert variant associated with prostate cancer risk confers differential in vivo activity to a *MYC* enhancer. *Genome Res.* **20**, 1191–1197 (2010).
202. Farrell, A. S. *et al.* MYC regulates ductal-neuroendocrine lineage plasticity in pancreatic ductal adenocarcinoma associated with poor outcome and chemoresistance. *Nat Commun* **8**, 1728 (2017).
203. Kauko, O. *et al.* PP2A inhibition is a druggable MEK inhibitor resistance mechanism in KRAS-mutant lung cancer cells. *Sci Transl Med* **10**, eaaq1093 (2018).
204. Cheng, C.-W. & Tse, E. PIN1 in Cell Cycle Control and Cancer. *Front Pharmacol* **9**, 1367 (2018).
205. Wang, X. *et al.* Phosphorylation Regulates c-Myc's Oncogenic Activity in the Mammary Gland. *Cancer Res* **71**, 925–936 (2011).
206. King, B. *et al.* The ubiquitin ligase FBXW7 modulates leukemia-initiating cell activity by regulating MYC stability. *Cell* **153**, 1552–1566 (2013).
207. Yeh, C.-H., Bellon, M. & Nicot, C. FBXW7: a critical tumor suppressor of human cancers. *Mol Cancer* **17**, 115 (2018).
208. Dhanasekaran, R. *et al.* The MYC oncogene — the grand orchestrator of cancer growth and immune evasion. *Nat Rev Clin Oncol* (2021) doi:10.1038/s41571-021-00549-2.
209. Weinstein, I. B. Addiction to Oncogenes--the Achilles Heal of Cancer. *Science* **297**, 63–64 (2002).
210. Jain, M. *et al.* Sustained Loss of a Neoplastic Phenotype by Brief Inactivation of *MYC*. *Science* **297**, 102–104 (2002).
211. Wu, C.-H. *et al.* Cellular senescence is an important mechanism of tumor regression upon c-Myc inactivation. *Proc Natl Acad Sci U S A* **104**, 13028–13033 (2007).
212. Shachaf, C. M. *et al.* MYC inactivation uncovers pluripotent differentiation and tumour dormancy in hepatocellular cancer. *Nature* **431**, 1112–1117 (2004).
213. Tran, P. T. *et al.* Combined Inactivation of MYC and K-Ras Oncogenes Reverses Tumorigenesis in Lung Adenocarcinomas and Lymphomas. *PLoS ONE* **3**, e2125 (2008).
214. Shroff, E. H. *et al.* MYC oncogene overexpression drives renal cell carcinoma in a mouse model through glutamine metabolism. *Proc Natl Acad Sci U S A* **112**, 6539–6544 (2015).
215. Soucek, L. *et al.* Inhibition of Myc family proteins eradicates KRas-driven lung cancer in mice. *Genes Dev.* **27**, 504–513 (2013).
216. Whitfield, J. R., Beaulieu, M.-E. & Soucek, L. Strategies to Inhibit Myc and Their Clinical Applicability. *Front. Cell Dev. Biol.* **5**, (2017).
217. Mertz, J. A. *et al.* Targeting MYC dependence in cancer by inhibiting BET bromodomains. *Proceedings of the National Academy of Sciences* **108**, 16669–16674 (2011).
218. Delmore, J. E. *et al.* BET Bromodomain Inhibition as a Therapeutic Strategy to Target c-Myc. *Cell* **146**, 904–917 (2011).
219. Devaiah, B. N. *et al.* MYC protein stability is negatively regulated by BRD4. *Proc Natl Acad Sci USA* **117**, 13457–13467 (2020).
220. Puissant, A. *et al.* Targeting MYCN in Neuroblastoma by BET Bromodomain Inhibition. *Cancer Discovery* **3**, 308–323 (2013).
221. Filippakopoulos, P. & Knapp, S. Targeting bromodomains: epigenetic readers of lysine acetylation. *Nat Rev Drug Discov* **13**, 337–356 (2014).
222. Fowler, T. *et al.* Regulation of MYC Expression and Differential JQ1 Sensitivity in Cancer Cells. *PLoS ONE* **9**, e87003 (2014).
223. Rahl, P. B. *et al.* c-Myc Regulates Transcriptional Pause Release. *Cell* **141**, 432–445 (2010).
224. Huang, C.-H. *et al.* CDK9-mediated transcription elongation is required for MYC addiction in hepatocellular carcinoma. *Genes Dev.* **28**, 1800–1814 (2014).
225. Gregory, G. P. *et al.* CDK9 inhibition by dinaciclib potently suppresses Mcl-1 to induce durable apoptotic responses in aggressive MYC-driven B-cell lymphoma in vivo. *Leukemia* **29**, 1437–1441 (2015).
226. Hashiguchi, T. *et al.* Cyclin-Dependent Kinase-9 Is a Therapeutic Target in MYC-Expressing Diffuse Large B-Cell Lymphoma. *Mol Cancer Ther* **18**, 1520–1532 (2019).
227. Chipumuro, E. *et al.* CDK7 Inhibition Suppresses Super-Enhancer-Linked Oncogenic Transcription in MYCN-Driven Cancer. *Cell* **159**, 1126–1139 (2014).
228. Christensen, C. L. *et al.* Targeting Transcriptional Addictions in Small Cell Lung Cancer with a Covalent CDK7 Inhibitor. *Cancer Cell* **26**, 909–922 (2014).
229. Wang, C. *et al.* A CRISPR screen identifies CDK7 as a therapeutic target in hepatocellular carcinoma. *Cell Res* **28**, 690–692 (2018).
230. Zeng, M. *et al.* Targeting MYC dependency in ovarian cancer through inhibition of CDK7 and CDK12/13. *eLife* **7**, e39030 (2018).
231. Brown, R. V., Danford, F. L., Gokhale, V., Hurley, L. H. & Brooks, T. A. Demonstration that drug-targeted down-regulation of MYC in non-Hodgkins lymphoma is directly mediated through the promoter G-quadruplex. *J Biol Chem* **286**, 41018–41027 (2011).
232. Chen, B.-J., Wu, Y.-L., Tanaka, Y. & Zhang, W. Small Molecules Targeting c-Myc Oncogene: Promising Anti-Cancer Therapeutics. *Int. J. Biol. Sci.* **10**, 1084–1096 (2014).

233. Pourdehnad, M. *et al.* Myc and mTOR converge on a common node in protein synthesis control that confers synthetic lethality in Myc-driven cancers. *Proc Natl Acad Sci U S A* **110**, 11988–11993 (2013).
234. Wiegering, A. *et al.* Targeting Translation Initiation Bypasses Signaling Crosstalk Mechanisms That Maintain High MYC Levels in Colorectal Cancer. *Cancer Discov* **5**, 768–781 (2015).
235. Tolcher, A. W. *et al.* Safety and activity of DCR-MYC, a first-in-class Dicer-substrate small interfering RNA (DsiRNA) targeting MYC, in a phase I study in patients with advanced solid tumors. *JCO* **33**, 11006–11006 (2015).
236. Zhu, Q., Feng, C., Liao, W., Zhang, Y. & Tang, S. Target delivery of MYCN siRNA by folate-nanoliposomes delivery system in a metastatic neuroblastoma model. *Cancer Cell Int* **13**, 65 (2013).
237. Dhanasekaran, R. *et al.* MYC ASO Impedes Tumorigenesis and Elicits Oncogene Addiction in Autochthonous Transgenic Mouse Models of HCC and RCC. *Molecular Therapy - Nucleic Acids* **21**, 850–859 (2020).
238. Balaji, K. C. *et al.* Antiproliferative effects of c-myc antisense oligonucleotide in prostate cancer cells: a novel therapy in prostate cancer. *Urology* **50**, 1007–1015 (1997).
239. Iversen, P. L., Arora, V., Acker, A. J., Mason, D. H. & Devi, G. R. Efficacy of antisense morpholino oligomer targeted to c-myc in prostate cancer xenograft murine model and a Phase I safety study in humans. *Clin Cancer Res* **9**, 2510–2519 (2003).
240. Sekhon, H. S., London, C. A., Sekhon, M., Iversen, P. L. & Devi, G. R. c-MYC antisense phosphosphorodiamidate morpholino oligomer inhibits lung metastasis in a murine tumor model. *Lung Cancer* **60**, 347–354 (2008).
241. Liu, L. *et al.* Competition between RNA-binding proteins CELF1 and HuR modulates MYC translation and intestinal epithelium renewal. *Mol Biol Cell* **26**, 1797–1810 (2015).
242. Gustafson, W. C. *et al.* Drugging MYCN through an allosteric transition in Aurora kinase A. *Cancer Cell* **26**, 414–427 (2014).
243. Xiao, D. *et al.* Polo-like Kinase-1 Regulates Myc Stabilization and Activates a Feedforward Circuit Promoting Tumor Cell Survival. *Mol Cell* **64**, 493–506 (2016).
244. Winter, G. E. *et al.* Phthalimide conjugation as a strategy for in vivo target protein degradation. *Science* **348**, 1376–1381 (2015).
245. Berg, T. Small-molecule modulators of c-Myc/Max and Max/Max interactions. *Curr Top Microbiol Immunol* **348**, 139–149 (2011).
246. Fletcher, S. & Prochownik, E. V. Small-molecule inhibitors of the Myc oncoprotein. *Biochimica et Biophysica Acta (BBA) - Gene Regulatory Mechanisms* **1849**, 525–543 (2015).
247. Jung, K.-Y. *et al.* Perturbation of the c-Myc-Max protein-protein interaction via synthetic **α**-helix mimetics. *J Med Chem* **58**, 3002–3024 (2015).
248. Whitfield, J. R. & Soucek, L. The long journey to bring a Myc inhibitor to the clinic. *J Cell Biol* **220**, e202103090 (2021).
249. Soucek, L. *et al.* Design and properties of a Myc derivative that efficiently homodimerizes. *Oncogene* **17**, 2463–2472 (1998).
250. Jung, L. A. *et al.* OmoMYC blunts promoter invasion by oncogenic MYC to inhibit gene expression characteristic of MYC-dependent tumors. *Oncogene* **36**, 1911–1924 (2017).
251. Savino, M. *et al.* The action mechanism of the Myc inhibitor termed Omomyc may give clues on how to target Myc for cancer therapy. *PLoS One* **6**, e22284 (2011).
252. Soucek, L. *et al.* Omomyc, a potential Myc dominant negative, enhances Myc-induced apoptosis. *Cancer Res* **62**, 3507–3510 (2002).
253. Soucek, L. *et al.* Modelling Myc inhibition as a cancer therapy. *Nature* **455**, 679–683 (2008).
254. Dobzhansky, T. Genetics of natural populations; recombination and variability in populations of Drosophila pseudoobscura. *Genetics* **31**, 269–290 (1946).
255. Farmer, H. *et al.* Targeting the DNA repair defect in BRCA mutant cells as a therapeutic strategy. *Nature* **434**, 917–921 (2005).
256. Bryant, H. E. *et al.* Specific killing of BRCA2-deficient tumours with inhibitors of poly(ADP-ribose) polymerase. *Nature* **434**, 913–917 (2005).
257. Yap, T. A., Sandhu, S. K., Carden, C. P. & de Bono, J. S. Poly(ADP-Ribose) polymerase (PARP) inhibitors: Exploiting a synthetic lethal strategy in the clinic. *CA: A Cancer Journal for Clinicians* **61**, 31–49 (2011).
258. Wang, Y. *et al.* Synthetic lethal targeting of MYC by activation of the DR5 death receptor pathway. *Cancer Cell* **5**, 501–512 (2004).
259. Weidle, U. H., Maisel, D. & Eick, D. Synthetic lethality-based targets for discovery of new cancer therapeutics. *Cancer Genomics Proteomics* **8**, 159–171 (2011).
260. Lord, C. J., Tutt, A. N. J. & Ashworth, A. Synthetic lethality and cancer therapy: lessons learned from the development of PARP inhibitors. *Annu. Rev. Med.* **66**, 455–470 (2015).
261. Lee, H. Y. *et al.* c-MYC Drives Breast Cancer Metastasis to the Brain, but Promotes Synthetic Lethality with TRAIL. *Mol Cancer Res* **17**, 544–554 (2019).
262. Cermelli, S., Jang, I. S., Bernard, B. & Grandori, C. Synthetic Lethal Screens as a Means to Understand and Treat MYC-Driven Cancers. *Cold Spring Harbor Perspectives in Medicine* **4**, a014209–a014209 (2014).
263. Toyoshima, M. *et al.* Functional genomics identifies therapeutic targets for MYC-driven cancer. *Proc. Natl. Acad. Sci. U.S.A.* **109**, 9545–9550 (2012).
264. Biederstädt, A. *et al.* SUMO pathway inhibition targets an aggressive pancreatic cancer subtype. *Gut* (2020) doi:10.1136/gutjnl-2018-317856.
265. Kessler, J. D. *et al.* A SUMOylation-dependent transcriptional subprogram is required for Myc-driven tumorigenesis. *Science* **335**, 348–353 (2012).
266. Hoellein, A. *et al.* Myc-induced SUMOylation is a therapeutic vulnerability for B-cell lymphoma. *Blood* **124**, 2081–2090 (2014).
267. Zhou, Z. *et al.* Identification of synthetic lethality of PRKDC in MYC-dependent human cancers by pooled shRNA screening. *BMC Cancer* **14**, 944 (2014).
268. Cossa, G. *et al.* Localized Inhibition of Protein Phosphatase 1 by NUAK1 Promotes Spliceosome Activity and Reveals a MYC-Sensitive Feedback Control of Transcription. *Molecular Cell* **77**, 1322-1339.e11 (2020).
269. Liu, L. *et al.* Deregulated MYC expression induces dependence upon AMPK-related kinase 5. *Nature* **483**, 608–612 (2012).

270. Rottmann, S., Wang, Y., Nasoff, M., Deveraux, Q. L. & Quon, K. C. A TRAIL receptor-dependent synthetic lethal relationship between MYC activation and GSK3 /FBW7 loss of function. *Proceedings of the National Academy of Sciences* **102**, 15195–15200 (2005).
271. Horiuchi, D. *et al.* PIM1 kinase inhibition as a targeted therapy against triple-negative breast tumors with elevated MYC expression. *Nat. Med.* **22**, 1321–1329 (2016).
272. Zhang, X., Song, M., Kundu, J. K., Lee, M.-H. & Liu, Z.-Z. PIM Kinase as an Executional Target in Cancer. *J Cancer Prev* **23**, 109–116 (2018).
273. Chen, L. *et al.* CRISPR-Cas9 screen reveals a MYCN-amplified neuroblastoma dependency on EZH2. *J Clin Invest* **128**, 446–462 (2018).
274. D'Andrea, A. *et al.* The mitochondrial translation machinery as a therapeutic target in Myc-driven lymphomas. *Oncotarget* **7**, 72415–72430 (2016).
275. Ravà, M. *et al.* Therapeutic synergy between tigecycline and venetoclax in a preclinical model of *MYC* / *BCL2* double-hit B cell lymphoma. *Sci. Transl. Med.* **10**, eaan8723 (2018).
276. Andrews, P. D., Knatko, E., Moore, W. J. & Swedlow, J. R. Mitotic mechanics: the auroras come into view. *Curr. Opin. Cell Biol.* **15**, 672–683 (2003).
277. den Hollander, J. *et al.* Aurora kinases A and B are up-regulated by Myc and are essential for maintenance of the malignant state. *Blood* **116**, 1498–1505 (2010).
278. Yang, D. *et al.* Therapeutic potential of a synthetic lethal interaction between the MYC proto-oncogene and inhibition of aurora-B kinase. *Proc. Natl. Acad. Sci. U.S.A.* **107**, 13836–13841 (2010).
279. Brockmann, M. *et al.* Small molecule inhibitors of aurora-a induce proteasomal degradation of N-myc in childhood neuroblastoma. *Cancer Cell* **24**, 75–89 (2013).
280. Hook, K. E. *et al.* An Integrated Genomic Approach to Identify Predictive Biomarkers of Response to the Aurora Kinase Inhibitor PF-03814735. *Molecular Cancer Therapeutics* **11**, 710–719 (2012).
281. Diaz, R. J. *et al.* Mechanism of action and therapeutic efficacy of Aurora kinase B inhibition in MYC overexpressing medulloblastoma. *Oncotarget* **6**, 3359–3374 (2015).
282. Dauch, D. *et al.* A MYC-aurora kinase A protein complex represents an actionable drug target in p53-altered liver cancer. *Nat. Med.* **22**, 744–753 (2016).
283. Mahadevan, D. *et al.* Aurora A inhibitor (MLN8237) plus vincristine plus rituximab is synthetic lethal and a potential curative therapy in aggressive B-cell non-Hodgkin lymphoma. *Clin. Cancer Res.* **18**, 2210–2219 (2012).
284. Friedberg, J. W. *et al.* Phase II study of alisertib, a selective Aurora A kinase inhibitor, in relapsed and refractory aggressive B- and T-cell non-Hodgkin lymphomas. *J. Clin. Oncol.* **32**, 44–50 (2014).
285. Borisa, A. C. & Bhatt, H. G. A comprehensive review on Aurora kinase: Small molecule inhibitors and clinical trial studies. *Eur J Med Chem* **140**, 1–19 (2017).
286. Kelly, K. R. *et al.* Phase I Study of the Investigational Aurora A Kinase Inhibitor Alisertib plus Rituximab or Rituximab/Vincristine in Relapsed/Refractory Aggressive B-cell Lymphoma. *Clin. Cancer Res.* **24**, 6150–6159 (2018).
287. Beltran, H. *et al.* A Phase II Trial of the Aurora Kinase A Inhibitor Alisertib for Patients with Castration-resistant and Neuroendocrine Prostate Cancer: Efficacy and Biomarkers. *Clin. Cancer Res.* **25**, 43–51 (2019).
288. Rohban, S. & Campaner, S. Myc induced replicative stress response: How to cope with it and exploit it. *Biochim. Biophys. Acta* **1849**, 517–524 (2015).
289. Murga, M. *et al.* Exploiting oncogene-induced replicative stress for the selective killing of Myc-driven tumors. *Nat. Struct. Mol. Biol.* **18**, 1331–1335 (2011).
290. Höglund, A. *et al.* Therapeutic implications for the induced levels of Chk1 in Myc-expressing cancer cells. *Clin. Cancer Res.* **17**, 7067–7079 (2011).
291. Ferrao, P. T., Bukczynska, E. P., Johnstone, R. W. & McArthur, G. A. Efficacy of CHK inhibitors as single agents in MYC-driven lymphoma cells. *Oncogene* **31**, 1661–1672 (2012).
292. Walton, M. I. *et al.* CCT244747 is a novel potent and selective CHK1 inhibitor with oral efficacy alone and in combination with genotoxic anticancer drugs. *Clin. Cancer Res.* **18**, 5650–5661 (2012).
293. Höglund, A., Strömvall, K., Li, Y., Forshell, L. P. & Nilsson, J. A. Chk2 deficiency in Myc overexpressing lymphoma cells elicits a synergistic lethal response in combination with PARP inhibition. *Cell Cycle* **10**, 3598–3607 (2011).
294. Roeschert, I. *et al.* Combined inhibition of Aurora-A and ATR kinase results in regression of MYCN-amplified neuroblastoma. *Nat Cancer* **2**, 312–326 (2021).
295. Goga, A., Yang, D., Tward, A. D., Morgan, D. O. & Bishop, J. M. Inhibition of CDK1 as a potential therapy for tumors over-expressing MYC. *Nat. Med.* **13**, 820–827 (2007).
296. Horiuchi, D. *et al.* MYC pathway activation in triple-negative breast cancer is synthetic lethal with CDK inhibition. *J. Exp. Med.* **209**, 679–696 (2012).
297. Ortega, S. *et al.* Cyclin-dependent kinase 2 is essential for meiosis but not for mitotic cell division in mice. *Nat. Genet.* **35**, 25–31 (2003).
298. Hydbring, P. & Larsson, L.-G. Cdk2: a key regulator of the senescence control function of Myc. *Aging (Albany NY)* **2**, 244–250 (2010).
299. Campaner, S. *et al.* Cdk2 suppresses cellular senescence induced by the c-myc oncogene. *Nat. Cell Biol.* **12**, 54–59; sup pp 1-14 (2010).
300. Vijayaraghavan, S., Moulder, S., Keyomarsi, K. & Layman, R. M. Inhibiting CDK in Cancer Therapy: Current Evidence and Future Directions. *Targ Oncol* **13**, 21–38 (2018).
301. MacCallum, D. E. *et al.* Seliciclib (CYC202, R-Roscovitine) Induces Cell Death in Multiple Myeloma Cells by Inhibition of RNA Polymerase II–Dependent Transcription and Down-regulation of Mcl-1. *Cancer Res* **65**, 5399–5407 (2005).
302. Diepstraten, S. T. *et al.* The manipulation of apoptosis for cancer therapy using BH3-mimetic drugs. *Nat Rev Cancer* **22**, 45–64 (2022).
303. Morschhauser, F. *et al.* A phase 2 study of venetoclax plus R-CHOP as first-line treatment for patients with diffuse large B-cell lymphoma. *Blood* **137**, 600–609 (2021).
304. Cummin, T. E. C. *et al.* BET inhibitors synergize with venetoclax to induce apoptosis in MYC-driven lymphomas with high BCL-2 expression. *Blood Advances* **4**, 3316–3328 (2020).
305. Grabow, S. *et al.* Critical B-lymphoid cell intrinsic role of endogenous MCL-1 in c-MYC-induced

lymphomagenesis. *Cell Death Dis* **7**, e2132–e2132 (2016).
306. Lourenco, C. *et al.* MYC protein interactors in gene transcription and cancer. *Nat Rev Cancer* **21**, 579–591 (2021).
307. Sun, Y. *et al.* WDR5 Supports an N-Myc Transcriptional Complex That Drives a Protumorigenic Gene Expression Signature in Neuroblastoma. *Cancer Research* **75**, 5143–5154 (2015).
308. Tian, J. *et al.* Discovery and Structure-Based Optimization of Potent and Selective WD Repeat Domain 5 (WDR5) Inhibitors Containing a Dihydroisoquinolinone Bicyclic Core. *J. Med. Chem.* **63**, 656–675 (2020).
309. Yang, Z. *et al.* Hijacking a key chromatin modulator creates epigenetic vulnerability for MYC-driven cancer. *Journal of Clinical Investigation* **128**, 3605–3618 (2018).
310. Shah, K. K. *et al.* Specific inhibition of DPY30 activity by ASH2L-derived peptides suppresses blood cancer cell growth. *Experimental Cell Research* **382**, 111485 (2019).
311. Garcia-Carpizo, V. *et al.* CREBBP/EP300 bromodomains are critical to sustain the GATA1/MYC regulatory axis in proliferation. *Epigenetics & Chromatin* **11**, 30 (2018).
312. Crawford, T. D. *et al.* Discovery of a Potent and Selective in Vivo Probe (GNE-272) for the Bromodomains of CBP/EP300. *J. Med. Chem.* **59**, 10549–10563 (2016).
313. Mustachio, L. M., Roszik, J., Farria, A. T., Guerra, K. & Dent, S. Y. Repression of GCN5 expression or activity attenuates c-MYC expression in non-small cell lung cancer. *Am J Cancer Res* **9**, 1830–1845 (2019).
314. Farria, A. T., Mustachio, L. M., Akdemir, Z. H. C. & Dent, S. Y. R. GCN5 HAT inhibition reduces human Burkitt lymphoma cell survival through reduction of MYC target gene expression and impeding BCR signaling pathways. *Oncotarget* **10**, 5847–5858 (2019).
315. Kretzner, L. *et al.* Combining histone deacetylase inhibitor vorinostat with aurora kinase inhibitors enhances lymphoma cell killing with repression of c-Myc, hTERT, and microRNA levels. *Cancer Res* **71**, 3912–3920 (2011).
316. Pei, Y. *et al.* HDAC and PI3K Antagonists Cooperate to Inhibit Growth of MYC-Driven Medulloblastoma. *Cancer Cell* **29**, 311–323 (2016).
317. Lernoux, M. *et al.* Novel HDAC inhibitor MAKV-8 and imatinib synergistically kill chronic myeloid leukemia cells via inhibition of BCR-ABL/MYC-signaling: effect on imatinib resistance and stem cells. *Clin Epigenet* **12**, 69 (2020).
318. Topper, M. J. *et al.* Epigenetic Therapy Ties MYC Depletion to Reversing Immune Evasion and Treating Lung Cancer. *Cell* **171**, 1284-1300.e21 (2017).
319. Dang, C. V. A Time for MYC: Metabolism and Therapy. *Cold Spring Harb Symp Quant Biol* **81**, 79–83 (2016).
320. Wolpaw, A. J. & Dang, C. V. MYC-induced metabolic stress and tumorigenesis. *Biochimica et Biophysica Acta (BBA) - Reviews on Cancer* **1870**, 43–50 (2018).
321. Shen, Y.-A. *et al.* Inhibition of the MYC-regulated glutaminase metabolic axis is an effective synthetic lethal approach for treating chemoresistant cancers. *Cancer Res* canres.3971.2019 (2020) doi:10.1158/0008-5472.CAN-19-3971.
322. Hu, S. *et al.* 13C-pyruvate imaging reveals alterations in glycolysis that precede c-Myc-induced tumor formation and regression. *Cell Metab* **14**, 131–142 (2011).
323. He, T.-L. *et al.* The c-Myc-LDHA axis positively regulates aerobic glycolysis and promotes tumor progression in pancreatic cancer. *Med Oncol* **32**, 187 (2015).
324. Oran, A. R. *et al.* Multi-focal control of mitochondrial gene expression by oncogenic MYC provides potential therapeutic targets in cancer. *Oncotarget* **7**, 72395–72414 (2016).
325. Donati, G. *et al.* Targeting mitochondrial respiration and the BCL2 family in high-grade MYC-associated B-cell lymphoma. *Molecular Oncology* 1878–0261.13115 (2021) doi:10.1002/1878-0261.13115.
326. Lim, J.-H. *et al.* PRMT5 is essential for the eIF4E-mediated 5′-cap dependent translation. *Biochem Biophys Res Commun* **452**, 1016–1021 (2014).
327. Hubert, C. G. *et al.* Genome-wide RNAi screens in human brain tumor isolates reveal a novel viability requirement for PHF5A. *Genes Dev.* **27**, 1032–1045 (2013).
328. Zhang, S. *et al.* MYCN controls an alternative RNA splicing program in high-risk metastatic neuroblastoma. *Cancer Lett* **371**, 214–224 (2016).
329. Iwai, K. *et al.* Anti-tumor efficacy of a novel CLK inhibitor via targeting RNA splicing and MYC-dependent vulnerability. *EMBO Mol Med* **10**, e8289 (2018).
330. Obeng, E. A. *et al.* Physiologic Expression of Sf3b1(K700E) Causes Impaired Erythropoiesis, Aberrant Splicing, and Sensitivity to Therapeutic Spliceosome Modulation. *Cancer Cell* **30**, 404–417 (2016).
331. Lee, S. C.-W. & Abdel-Wahab, O. Therapeutic targeting of splicing in cancer. *Nat Med* **22**, 976–986 (2016).
332. Shirai, C. L. *et al.* Mutant U2AF1-expressing cells are sensitive to pharmacological modulation of the spliceosome. *Nat Commun* **8**, 14060 (2017).
333. Seiler, M. *et al.* H3B-8800, an orally available small-molecule splicing modulator, induces lethality in spliceosome-mutant cancers. *Nat Med* **24**, 497–504 (2018).
334. Dvinge, H. & Bradley, R. K. Widespread intron retention diversifies most cancer transcriptomes. *Genome Med* **7**, 45 (2015).
335. Bowling, E. A. *et al.* Spliceosome-targeted therapies trigger an antiviral immune response in triple-negative breast cancer. *Cell* **184**, 384-403.e21 (2021).
336. van Riggelen, J., Yetil, A. & Felsher, D. W. MYC as a regulator of ribosome biogenesis and protein synthesis. *Nat Rev Cancer* **10**, 301–309 (2010).
337. Bywater, M. J. *et al.* Inhibition of RNA polymerase I as a therapeutic strategy to promote cancer-specific activation of p53. *Cancer Cell* **22**, 51–65 (2012).
338. Poortinga, G., Quinn, L. M. & Hannan, R. D. Targeting RNA polymerase I to treat MYC-driven cancer. *Oncogene* **34**, 403–412 (2015).
339. Negi, S. S. & Brown, P. rRNA synthesis inhibitor, CX-5461, activates ATM/ATR pathway in acute lymphoblastic leukemia, arrests cells in G2 phase and induces apoptosis. *Oncotarget* **6**, 18094–18104 (2015).
340. Barna, M. *et al.* Suppression of Myc oncogenic activity by ribosomal protein haploinsufficiency. *Nature* **456**, 971–975 (2008).
341. Miluzio, A. *et al.* Impairment of cytoplasmic eIF6 activity restricts lymphomagenesis and tumor

progression without affecting normal growth. *Cancer Cell* **19**, 765–775 (2011).
342. Ruggero, D. *et al.* The translation factor eIF-4E promotes tumor formation and cooperates with c-Myc in lymphomagenesis. *Nat Med* **10**, 484–486 (2004).
343. Guertin, D. A. & Sabatini, D. M. Defining the role of mTOR in cancer. *Cancer Cell* **12**, 9–22 (2007).
344. Ruggero, D. The Role of Myc-Induced Protein Synthesis in Cancer. *Cancer Res* **69**, 8839–8843 (2009).
345. Sander, S. *et al.* Synergy between PI3K Signaling and MYC in Burkitt Lymphomagenesis. *Cancer Cell* **22**, 167–179 (2012).
346. Lin, C.-J. *et al.* Targeting synthetic lethal interactions between Myc and the eIF4F complex impedes tumorigenesis. *Cell Rep* **1**, 325–333 (2012).
347. Shortt, J. *et al.* Combined inhibition of PI3K-related DNA damage response kinases and mTORC1 induces apoptosis in MYC-driven B-cell lymphomas. *Blood* **121**, 2964–2974 (2013).
348. Wall, M. *et al.* The mTORC1 Inhibitor Everolimus Prevents and Treats Eμ- *Myc* Lymphoma by Restoring Oncogene-Induced Senescence. *Cancer Discovery* **3**, 82–95 (2013).
349. Thng, D. K. H., Toh, T. B. & Chow, E. K.-H. Capitalizing on Synthetic Lethality of MYC to Treat Cancer in the Digital Age. *Trends in Pharmacological Sciences* **42**, 166–182 (2021).
350. Lai, I. *et al.* Lipid nanoparticles that deliver IL-12 messenger RNA suppress tumorigenesis in MYC oncogene-driven hepatocellular carcinoma. *J Immunother Cancer* **6**, 125 (2018).
351. Swaminathan, S. *et al.* MYC functions as a switch for natural killer cell-mediated immune surveillance of lymphoid malignancies. *Nat Commun* **11**, 2860 (2020).
352. Casey, S. C. *et al.* MYC regulates the antitumor immune response through CD47 and PD-L1. *Science* **352**, 227–231 (2016).
353. Han, H. *et al.* Small-Molecule MYC Inhibitors Suppress Tumor Growth and Enhance Immunotherapy. *Cancer Cell* **36**, 483-497.e15 (2019).
354. Pan, Y. *et al.* Synergistic inhibition of pancreatic cancer with anti-PD-L1 and c-Myc inhibitor JQ1. *OncoImmunology* **8**, e1581529 (2019).
355. Cory, S. Activation of cellular oncogenes in hemopoietic cells by chromosome translocation. *Adv Cancer Res* **47**, 189–234 (1986).
356. Corcoran, L. M., Cory, S. & Adams, J. M. Transposition of the immunoglobulin heavy chain enhancer to the myc oncogene in a murine plasmacytoma. *Cell* **40**, 71–79 (1985).
357. Langdon, W. Y., Harris, A. W., Cory, S. & Adams, J. M. The c-myc oncogene perturbs B lymphocyte development in Eμ-myc transgenic mice. *Cell* **47**, 11–18 (1986).
358. Alexander, W. S., Schrader, J. W. & Adams, J. M. Expression of the c-myc oncogene under control of an immunoglobulin enhancer in E mu-myc transgenic mice. *Mol Cell Biol* **7**, 1436–1444 (1987).
359. Mattioni, T., Louvion, J.-F. & Picard, D. Chapter 16 Regulation of Protein Activities by Fusion to Steroid Binding Domains. in *Methods in Cell Biology* vol. 43 335–352 (Elsevier, 1994).
360. Eilers, M., Picard, D., Yamamoto, K. R. & Bishop, J. M. Chimaeras of Myc oncoprotein and steroid receptors cause hormone-dependent transformation of cells. *Nature* **340**, 66–68 (1989).
361. Eilers, M., Schirm, S. & Bishop, J. M. The MYC protein activates transcription of the alpha-prothymosin gene. *EMBO J* **10**, 133–141 (1991).
362. Whitfield, J., Littlewood, T., Evan, G. I. & Soucek, L. The Estrogen Receptor Fusion System in Mouse Models: A Reversible Switch. *Cold Spring Harb Protoc* **2015**, pdb.top069815 (2015).
363. Littlewood, T. D., Hancock, D. C., Danielian, P. S., Parker, M. G. & Evan, G. I. A modified oestrogen receptor ligand-binding domain as an improved switch for the regulation of heterologous proteins. *Nucleic Acids Research* **23**, 1686–1690 (1995).
364. Gerstberger, S., Hafner, M. & Tuschl, T. A census of human RNA-binding proteins. *Nat Rev Genet* **15**, 829–845 (2014).
365. Neelamraju, Y., Gonzalez-Perez, A., Bhat-Nakshatri, P., Nakshatri, H. & Janga, S. C. Mutational landscape of RNA-binding proteins in human cancers. *RNA Biology* **15**, 115–129 (2018).
366. Wang, Z.-L. *et al.* Comprehensive Genomic Characterization of RNA-Binding Proteins across Human Cancers. *Cell Reports* **22**, 286–298 (2018).
367. Kelaini, S., Chan, C., Cornelius, V. A. & Margariti, A. RNA-Binding Proteins Hold Key Roles in Function, Dysfunction, and Disease. *Biology* **10**, 366 (2021).
368. Müller-McNicoll, M. & Neugebauer, K. M. How cells get the message: dynamic assembly and function of mRNA-protein complexes. *Nat Rev Genet* **14**, 275–287 (2013).
369. Mitchell, S. F. & Parker, R. Principles and properties of eukaryotic mRNPs. *Mol Cell* **54**, 547–558 (2014).
370. Corley, M., Burns, M. C. & Yeo, G. W. How RNA-Binding Proteins Interact with RNA: Molecules and Mechanisms. *Molecular Cell* **78**, 9–29 (2020).
371. Castello, A. *et al.* Comprehensive Identification of RNA-Binding Domains in Human Cells. *Molecular Cell* **63**, 696–710 (2016).
372. Mittal, N., Roy, N., Babu, M. M. & Janga, S. C. Dissecting the expression dynamics of RNA-binding proteins in posttranscriptional regulatory networks. *Proc Natl Acad Sci U S A* **106**, 20300–20305 (2009).
373. Sebestyén, E. *et al.* Large-scale analysis of genome and transcriptome alterations in multiple tumors unveils novel cancer-relevant splicing networks. *Genome Res.* **26**, 732–744 (2016).
374. Montanaro, L., Treré, D. & Derenzini, M. Nucleolus, ribosomes, and cancer. *Am J Pathol* **173**, 301–310 (2008).
375. Qin, H. *et al.* RNA-binding proteins in tumor progression. *J Hematol Oncol* **13**, 90 (2020).
376. Avdulov, S. *et al.* Activation of translation complex eIF4F is essential for the genesis and maintenance of the malignant phenotype in human mammary epithelial cells. *Cancer Cell* **5**, 553–563 (2004).
377. Graff, J. R. *et al.* Therapeutic suppression of translation initiation factor eIF4E expression reduces tumor growth without toxicity. *J Clin Invest* **117**, 2638–2648 (2007).
378. Foulkes, W. D., Priest, J. R. & Duchaine, T. F. DICER1: mutations, microRNAs and mechanisms. *Nat Rev Cancer* **14**, 662–672 (2014).
379. Karni, R. *et al.* The gene encoding the splicing factor SF2/ASF is a proto-oncogene. *Nat Struct Mol Biol* **14**, 185–193 (2007).
380. Dang, H. *et al.* Oncogenic Activation of the RNA Binding Protein NELFE and MYC Signaling in

Hepatocellular Carcinoma. *Cancer Cell* **32**, 101-114.e8 (2017).
381. Mohibi, S., Chen, X. & Zhang, J. Cancer the'RBP'eutics-RNA-binding proteins as therapeutic targets for cancer. *Pharmacol Ther* **203**, 107390 (2019).
382. Kang, D., Lee, Y. & Lee, J.-S. RNA-Binding Proteins in Cancer: Functional and Therapeutic Perspectives. *Cancers* **12**, 2699 (2020).
383. Schoenberg, D. R. & Maquat, L. E. Regulation of cytoplasmic mRNA decay. *Nat Rev Genet* **13**, 246–259 (2012).
384. Garneau, N. L., Wilusz, J. & Wilusz, C. J. The highways and byways of mRNA decay. *Nat Rev Mol Cell Biol* **8**, 113–126 (2007).
385. Braun, K. A. & Young, E. T. Coupling mRNA Synthesis and Decay. *Mol Cell Biol* **34**, 4078–4087 (2014).
386. Luo, Y., Na, Z. & Slavoff, S. A. P-Bodies: Composition, Properties, and Functions. *Biochemistry* **57**, 2424–2431 (2018).
387. Graille, M. & Séraphin, B. Surveillance pathways rescuing eukaryotic ribosomes lost in translation. *Nat Rev Mol Cell Biol* **13**, 727–735 (2012).
388. Doma, M. K. & Parker, R. Endonucleolytic cleavage of eukaryotic mRNAs with stalls in translation elongation. *Nature* **440**, 561–564 (2006).
389. Lykke-Andersen, S. & Jensen, T. H. Nonsense-mediated mRNA decay: an intricate machinery that shapes transcriptomes. *Nat Rev Mol Cell Biol* **16**, 665–677 (2015).
390. Karousis, E. D., Nasif, S. & Mühlemann, O. Nonsense-mediated mRNA decay: novel mechanistic insights and biological impact: Nonsense-mediated mRNA decay. *WIREs RNA* **7**, 661–682 (2016).
391. Kurosaki, T., Popp, M. W. & Maquat, L. E. Quality and quantity control of gene expression by nonsense-mediated mRNA decay. *Nat Rev Mol Cell Biol* **20**, 406–420 (2019).
392. Conti, E. & Izaurralde, E. Nonsense-mediated mRNA decay: molecular insights and mechanistic variations across species. *Curr Opin Cell Biol* **17**, 316–325 (2005).
393. Pulak, R. & Anderson, P. mRNA surveillance by the Caenorhabditis elegans smg genes. *Genes Dev.* **7**, 1885–1897 (1993).
394. He, F., Brown, A. H. & Jacobson, A. Upf1p, Nmd2p, and Upf3p are interacting components of the yeast nonsense-mediated mRNA decay pathway. *Mol Cell Biol* **17**, 1580–1594 (1997).
395. Medghalchi, S. M. Rent1, a trans-effector of nonsense-mediated mRNA decay, is essential for mammalian embryonic viability. *Human Molecular Genetics* **10**, 99–105 (2001).
396. Weischenfeldt, J. *et al.* NMD is essential for hematopoietic stem and progenitor cells and for eliminating by-products of programmed DNA rearrangements. *Genes Dev.* **22**, 1381–1396 (2008).
397. Wittkopp, N. *et al.* Nonsense-mediated mRNA decay effectors are essential for zebrafish embryonic development and survival. *Mol Cell Biol* **29**, 3517–3528 (2009).
398. Han, X. *et al.* Nonsense-mediated mRNA decay: a 'nonsense' pathway makes sense in stem cell biology. *Nucleic Acids Research* **46**, 1038–1051 (2018).
399. Boehm, V. *et al.* SMG5-SMG7 authorize nonsense-mediated mRNA decay by enabling SMG6 endonucleolytic activity. *Nat Commun* **12**, 3965 (2021).
400. Gardner, L. B. Hypoxic inhibition of nonsense-mediated RNA decay regulates gene expression and the integrated stress response. *Mol Cell Biol* **28**, 3729–3741 (2008).
401. Harding, H. P. *et al.* Regulated Translation Initiation Controls Stress-Induced Gene Expression in Mammalian Cells. *Molecular Cell* **6**, 1099–1108 (2000).
402. Lewis, B. P., Green, R. E. & Brenner, S. E. Evidence for the widespread coupling of alternative splicing and nonsense-mediated mRNA decay in humans. *Proc Natl Acad Sci U S A* **100**, 189–192 (2003).
403. Yi, Z., Sanjeev, M. & Singh, G. The Branched Nature of the Nonsense-Mediated mRNA Decay Pathway. *Trends in Genetics* S0168952520302109 (2020) doi:10.1016/j.tig.2020.08.010.
404. Rufener, S. C. & Mühlemann, O. eIF4E-bound mRNPs are substrates for nonsense-mediated mRNA decay in mammalian cells. *Nat Struct Mol Biol* **20**, 710–717 (2013).
405. Kim, Y. K. & Maquat, L. E. UPFront and center in RNA decay: UPF1 in nonsense-mediated mRNA decay and beyond. *RNA* **25**, 407–422 (2019).
406. Singh, A. K. *et al.* The RNA helicase UPF1 associates with mRNAs co-transcriptionally and is required for the release of mRNAs from gene loci. *eLife* **8**, e41444 (2019).
407. Hwang, J., Sato, H., Tang, Y., Matsuda, D. & Maquat, L. E. UPF1 Association with the Cap-Binding Protein, CBP80, Promotes Nonsense-Mediated mRNA Decay at Two Distinct Steps. *Molecular Cell* **39**, 396–409 (2010).
408. Maquat, L. E. & Serin, G. Nonsense-mediated mRNA decay: insights into mechanism from the cellular abundance of human Upf1, Upf2, Upf3, and Upf3X proteins. *Cold Spring Harb Symp Quant Biol* **66**, 313–320 (2001).
409. Feng, Q., Jagannathan, S. & Bradley, R. K. The RNA Surveillance Factor UPF1 Represses Myogenesis via Its E3 Ubiquitin Ligase Activity. *Molecular Cell* **67**, 239-251.e6 (2017).
410. Lavysh, D. & Neu-Yilik, G. UPF1-Mediated RNA Decay—Danse Macabre in a Cloud. *Biomolecules* **10**, 999 (2020).
411. Fellmann, C. *et al.* An Optimized microRNA Backbone for Effective Single-Copy RNAi. *Cell Reports* **5**, 1704–1713 (2013).
412. Michlits, G. *et al.* Multilayered VBC score predicts sgRNAs that efficiently generate loss-of-function alleles. *Nat Methods* **17**, 708–716 (2020).
413. Kessler, J. D. *et al.* A SUMOylation-Dependent Transcriptional Subprogram Is Required for Myc-Driven Tumorigenesis. *Science* **335**, 348–353 (2012).
414. Zuber, J. *et al.* RNAi screen identifies Brd4 as a therapeutic target in acute myeloid leukaemia. *Nature* **478**, 524–528 (2011).
415. Ge, S. X., Jung, D. & Yao, R. ShinyGO: a graphical gene-set enrichment tool for animals and plants. *Bioinformatics* **36**, 2628–2629 (2020).
416. Sabò, A. *et al.* Selective transcriptional regulation by Myc in cellular growth control and lymphomagenesis. *Nature* **511**, 488–492 (2014).
417. Bojes, H. K., Feng, X., Kehrer, J. P. & Cohen, G. M. Apoptosis in hematopoietic cells (FL5.12) caused by interleukin-3 withdrawal: relationship to caspase activity and the loss of glutathione. *Cell Death Differ* **6**, 61–70 (1999).
418. Chu, V. T. *et al.* Efficient generation of Rosa26 knock-in mice using CRISPR/Cas9 in C57BL/6 zygotes. *BMC Biotechnol* **16**, 4 (2016).

419. D'Andrea, A. *et al.* The mitochondrial translation machinery as a therapeutic target in Myc-driven lymphomas. *Oncotarget* **7**, 72415–72430 (2016).
420. Zuber, J. *et al.* Toolkit for evaluating genes required for proliferation and survival using tetracycline-regulated RNAi. *Nat Biotechnol* **29**, 79–83 (2011).
421. R Core Team (2021). R: A language and environment for statistical computing. R Foundation for Statistical Computing, Vienna, Austria. URL https://www.R-project.org/.
422. Li, W. *et al.* MAGeCK enables robust identification of essential genes from genome-scale CRISPR/Cas9 knockout screens. *Genome Biol* **15**, 554 (2014).
423. Li, W. *et al.* Quality control, modeling, and visualization of CRISPR screens with MAGeCK-VISPR. *Genome Biol* **16**, 281 (2015).
424. Wang, B. *et al.* Integrative analysis of pooled CRISPR genetic screens using MAGeCKFlute. *Nat Protoc* **14**, 756–780 (2019).
425. Hart, T. *et al.* High-Resolution CRISPR Screens Reveal Fitness Genes and Genotype-Specific Cancer Liabilities. *Cell* **163**, 1515–1526 (2015).
426. Wang, T. *et al.* Identification and characterization of essential genes in the human genome. *Science* **350**, 1096–1101 (2015).
427. Aguirre, A. J. *et al.* Genomic Copy Number Dictates a Gene-Independent Cell Response to CRISPR/Cas9 Targeting. *Cancer Discov* **6**, 914–929 (2016).
428. Tzelepis, K. *et al.* A CRISPR Dropout Screen Identifies Genetic Vulnerabilities and Therapeutic Targets in Acute Myeloid Leukemia. *Cell Reports* **17**, 1193–1205 (2016).
429. Steinhart, Z. *et al.* Genome-wide CRISPR screens reveal a Wnt–FZD5 signaling circuit as a druggable vulnerability of RNF43-mutant pancreatic tumors. *Nat Med* **23**, 60–68 (2017).
430. Wang, T. *et al.* Gene Essentiality Profiling Reveals Gene Networks and Synthetic Lethal Interactions with Oncogenic Ras. *Cell* **168**, 890-903.e15 (2017).
431. Morgens, D. W. *et al.* Genome-scale measurement of off-target activity using Cas9 toxicity in high-throughput screens. *Nat Commun* **8**, 15178 (2017).
432. Blomen, V. A. *et al.* Gene essentiality and synthetic lethality in haploid human cells. *Science* **350**, 1092–1096 (2015).
433. Oliveros, J.C. (2007-2015) Venny. An interactive tool for comparing lists with Venn's diagrams. https://bioinfogp.cnb.csic.es/tools/venny/index.html.
434. Madeira, F. *et al.* The EMBL-EBI search and sequence analysis tools APIs in 2019. *Nucleic Acids Research* **47**, W636–W641 (2019).
435. Mohr, S. E., Smith, J. A., Shamu, C. E., Neumüller, R. A. & Perrimon, N. RNAi screening comes of age: improved techniques and complementary approaches. *Nat Rev Mol Cell Biol* **15**, 591–600 (2014).
436. Shalem, O., Sanjana, N. E. & Zhang, F. High-throughput functional genomics using CRISPR–Cas9. *Nat Rev Genet* **16**, 299–311 (2015).
437. Evan, G. I. *et al.* Induction of apoptosis in fibroblasts by c-myc protein. *Cell* **69**, 119–128 (1992).
438. Abedon, S. T. Multiplicity of Infection ☆. in *Reference Module in Life Sciences* B9780128096338067000 (Elsevier, 2017). doi:10.1016/B978-0-12-809633-8.06748-0.
439. Robinson, M. D., McCarthy, D. J. & Smyth, G. K. edgeR: a Bioconductor package for differential expression analysis of digital gene expression data. *Bioinformatics* **26**, 139–140 (2010).
440. Kim, S., Li, Q., Dang, C. V. & Lee, L. A. Induction of ribosomal genes and hepatocyte hypertrophy by adenovirus-mediated expression of c-Myc in vivo. *Proceedings of the National Academy of Sciences* **97**, 11198–11202 (2000).
441. Dai, M.-S., Sears, R. & Lu, H. Feedback Regulation of c-Myc by Ribosomal Protein L11. *Cell Cycle* **6**, 2735–2741 (2007).
442. Qu, H., Liu, H., Jin, Y., Cui, Z. & Han, G. HUWE1 upregulation has tumor suppressive effect in human prostate cancer cell lines through c-Myc. *Biomedicine & Pharmacotherapy* **106**, 309–315 (2018).
443. Crawford, L. J. *et al.* The E3 ligase HUWE1 inhibition as a therapeutic strategy to target MYC in multiple myeloma. *Oncogene* **39**, 5001–5014 (2020).
444. Bonazzoli, E. *et al.* Derangements in HUWE1/c-MYC pathway confer sensitivity to the BET bromodomain inhibitor GS-626510 in uterine cervical carcinoma. *Gynecologic Oncology* **158**, 769–775 (2020).
445. Evers, B. *et al.* CRISPR knockout screening outperforms shRNA and CRISPRi in identifying essential genes. *Nat Biotechnol* **34**, 631–633 (2016).
446. Schuster, A. *et al.* RNAi/CRISPR Screens: from a Pool to a Valid Hit. *Trends in Biotechnology* **37**, 38–55 (2019).
447. Campaner, S. & Amati, B. Two sides of the Myc-induced DNA damage response: from tumor suppression to tumor maintenance. *Cell Div* **7**, 6 (2012).
448. Jinek, M. *et al.* A Programmable Dual-RNA–Guided DNA Endonuclease in Adaptive Bacterial Immunity. *Science* **337**, 816–821 (2012).
449. Cong, L. *et al.* Multiplex Genome Engineering Using CRISPR/Cas Systems. *Science* **339**, 819–823 (2013).
450. Chen, H., Liu, H. & Qing, G. Targeting oncogenic Myc as a strategy for cancer treatment. *Sig Transduct Target Ther* **3**, 5 (2018).
451. Donati, G. *et al.* Targeting mitochondrial respiration and the BCL2 family in high-grade MYC-associated B-cell lymphoma. *Mol Oncol* 1878–0261.13115 (2021) doi:10.1002/1878-0261.13115.
452. Hentze, M. W., Castello, A., Schwarzl, T. & Preiss, T. A brave new world of RNA-binding proteins. *Nat Rev Mol Cell Biol* **19**, 327–341 (2018).
453. Gandin, V. *et al.* Eukaryotic initiation factor 6 is rate-limiting in translation, growth and transformation. *Nature* **455**, 684–688 (2008).
454. Wang, J. *et al.* FDA-approved drug screen identifies proteasome as a synthetic lethal target in MYC-driven neuroblastoma. *Oncogene* **38**, 6737–6751 (2019).
455. Zhang, J. *et al.* A high-content screen identifies the vulnerability of MYC-overexpressing cells to dimethylfasudil. *PLoS ONE* **16**, e0248355 (2021).
456. Hinterndorfer, M. & Zuber, J. Functional-genetic approaches to understanding drug response and resistance. *Current Opinion in Genetics & Development* **54**, 41–47 (2019).
457. Wang, B. *et al.* Integrative analysis of pooled CRISPR genetic screens using MAGeCKFlute. *Nat Protoc* **14**, 756–780 (2019).
458. Park, S. *et al.* Differential Functions of Splicing Factors in Mammary Transformation and Breast Cancer Metastasis. *Cell Reports* **29**, 2672-2688.e7 (2019).
459. Alawi, F. & Lee, M. N. DKC1 is a direct and conserved transcriptional target of c-MYC. *Biochemical and*

Biophysical Research Communications **362**, 893–898 (2007).
460. Rauch, J. *et al.* c-Myc Regulates RNA Splicing of the A-Raf Kinase and Its Activation of the ERK Pathway. *Cancer Res* **71**, 4664–4674 (2011).
461. Liu, X. *et al.* YTHDF1 Facilitates the Progression of Hepatocellular Carcinoma by Promoting FZD5 mRNA Translation in an m6A-Dependent Manner. *Molecular Therapy - Nucleic Acids* **22**, 750–765 (2020).
462. O'Donnell, K. A. *et al.* Activation of Transferrin Receptor 1 by c-Myc Enhances Cellular Proliferation and Tumorigenesis. *Mol Cell Biol* **26**, 2373–2386 (2006).
463. Chang, Y.-F., Imam, J. S. & Wilkinson, M. F. The Nonsense-Mediated Decay RNA Surveillance Pathway. *Annu. Rev. Biochem.* **76**, 51–74 (2007).
464. Hug, N., Longman, D. & Cáceres, J. F. Mechanism and regulation of the nonsense-mediated decay pathway. *Nucleic Acids Res* **44**, 1483–1495 (2016).
465. Jones, C. I., Zabolotskaya, M. V. & Newbury, S. F. The 5′ → 3′ exoribonuclease XRN1/Pacman and its functions in cellular processes and development: The 5′ → 3′ exoribonuclease XRN1/Pacman and its functions. *WIREs RNA* **3**, 455–468 (2012).
466. Łabno, A., Tomecki, R. & Dziembowski, A. Cytoplasmic RNA decay pathways - Enzymes and mechanisms. *Biochimica et Biophysica Acta (BBA) - Molecular Cell Research* **1863**, 3125–3147 (2016).
467. Giacometti, S. *et al.* Mutually Exclusive CBC-Containing Complexes Contribute to RNA Fate. *Cell Reports* **18**, 2635–2650 (2017).
468. Gebhardt, A. *et al.* mRNA export through an additional cap-binding complex consisting of NCBP1 and NCBP3. *Nat Commun* **6**, 8192 (2015).
469. Tominaga, K., Johmura, Y., Nishizuka, M. & Imagawa, M. Fad24, a mammalian homolog of Noc3p, is a positive regulator in adipocyte differentiation. *Journal of Cell Science* **117**, 6217–6226 (2004).
470. Cheung, M.-H. *et al.* Human NOC3 is essential for DNA replication licensing in human cells. *Cell Cycle* **18**, 605–620 (2019).
471. Johmura, Y., Suzuki, M., Osada, S., Nishizuka, M. & Imagawa, M. FAD24, a regulator of adipogenesis and DNA replication, inhibits H-RAS-mediated transformation by repressing NF-κB activity. *Biochemical and Biophysical Research Communications* **369**, 464–470 (2008).
472. Milkereit, P. *et al.* A Noc Complex Specifically Involved in the Formation and Nuclear Export of Ribosomal 40 S Subunits. *Journal of Biological Chemistry* **278**, 4072–4081 (2003).
473. Zhang, Y., Yu, Z., Fu, X. & Liang, C. Noc3p, a bHLH Protein, Plays an Integral Role in the Initiation of DNA Replication in Budding Yeast. *Cell* **109**, 849–860 (2002).
474. Lee, B. J. *et al.* Rules for Nuclear Localization Sequence Recognition by Karyopherinβ2. *Cell* **126**, 543–558 (2006).
475. Mboukou, A. *et al.* Transportin-1: A Nuclear Import Receptor with Moonlighting Functions. *Front. Mol. Biosci.* **8**, 638149 (2021).
476. Hofweber, M. *et al.* Phase Separation of FUS Is Suppressed by Its Nuclear Import Receptor and Arginine Methylation. *Cell* **173**, 706-719.e13 (2018).
477. Austenaa, L. M. I. *et al.* A first exon termination checkpoint preferentially suppresses extragenic transcription. *Nat Struct Mol Biol* **28**, 337–346 (2021).
478. Wang, E. *et al.* Targeting an RNA-Binding Protein Network in Acute Myeloid Leukemia. *Cancer Cell* **35**, 369-384.e7 (2019).
479. Lai, J. C. *et al.* The DEAH-box helicase RHAU is an essential gene and critical for mouse hematopoiesis. *Blood* **119**, 4291–4300 (2012).
480. Shen, L. & Pelletier, J. General and Target-Specific DExD/H RNA Helicases in Eukaryotic Translation Initiation. *IJMS* **21**, 4402 (2020).
481. Briata, P. *et al.* Diverse roles of the nucleic acid-binding protein KHSRP in cell differentiation and disease. *WIREs RNA* **7**, 227–240 (2016).
482. Kim, H. H. *et al.* HuR recruits let-7/RISC to repress c-Myc expression. *Genes Dev* **23**, 1743–1748 (2009).
483. Kim, J. H. *et al.* Heterogeneous Nuclear Ribonucleoprotein C Modulates Translation of c- *myc* mRNA in a Cell Cycle Phase-Dependent Manner. *Mol Cell Biol* **23**, 708–720 (2003).
484. Müller-McNicoll, M. & Neugebauer, K. M. Good cap/bad cap: how the cap-binding complex determines RNA fate. *Nat Struct Mol Biol* **21**, 9–12 (2014).
485. He, L. *et al.* Functions of N6-methyladenosine and its role in cancer. *Mol Cancer* **18**, 176 (2019).
486. Du, H. *et al.* YTHDF2 destabilizes m6A-containing RNA through direct recruitment of the CCR4–NOT deadenylase complex. *Nat Commun* **7**, 12626 (2016).
487. Dixit, D. *et al.* The RNA m6A Reader YTHDF2 Maintains Oncogene Expression and Is a Targetable Dependency in Glioblastoma Stem Cells. *Cancer Discov* **11**, 480–499 (2021).
488. Kumari, A., Folk, W. & Sakamuro, D. The Dual Roles of MYC in Genomic Instability and Cancer Chemoresistance. *Genes* **8**, 158 (2017).
489. Campaner, S. & Amati, B. Two sides of the Myc-induced DNA damage response: from tumor suppression to tumor maintenance. *Cell Div* **7**, 6 (2012).
490. Bartkova, J. *et al.* DNA damage response as a candidate anti-cancer barrier in early human tumorigenesis. *Nature* **434**, 864–870 (2005).
491. Gorgoulis, V. G. *et al.* Activation of the DNA damage checkpoint and genomic instability in human precancerous lesions. *Nature* **434**, 907–913 (2005).
492. Sharpless, N. E. INK4a/ARF: A multifunctional tumor suppressor locus. *Mutation Research/Fundamental and Molecular Mechanisms of Mutagenesis* **576**, 22–38 (2005).
493. Gorrini, C. *et al.* Tip60 is a haplo-insufficient tumour suppressor required for an oncogene-induced DNA damage response. *Nature* **448**, 1063–1067 (2007).
494. Azzalin, C. M. & Lingner, J. The Human RNA Surveillance Factor UPF1 Is Required for S Phase Progression and Genome Stability. *Current Biology* **16**, 433–439 (2006).
495. Ngo, G. H. P., Grimstead, J. W. & Baird, D. M. UPF1 promotes the formation of R loops to stimulate DNA double-strand break repair. *Nat Commun* **12**, 3849 (2021).
496. Martin, L. *et al.* Identification and Characterization of Small Molecules That Inhibit Nonsense-Mediated RNA Decay and Suppress Nonsense p53 Mutations. *Cancer Res* **74**, 3104–3113 (2014).
497. Baudu, T. *et al.* The NMD Pathway Regulates GABARAPL1 mRNA during the EMT. *Biomedicines* **9**, 1302 (2021).
498. Laselva, O. *et al.* Functional rescue of c.3846G>A (W1282X) in patient-derived nasal cultures achieved by

inhibition of nonsense mediated decay and protein modulators with complementary mechanisms of action. *Journal of Cystic Fibrosis* **19**, 717–727 (2020).
499. McHugh, D. R., Cotton, C. U. & Hodges, C. A. Synergy between Readthrough and Nonsense Mediated Decay Inhibition in a Murine Model of Cystic Fibrosis Nonsense Mutations. *IJMS* **22**, 344 (2020).
500. Wang, D. *et al.* Inhibition of Nonsense-Mediated RNA Decay by the Tumor Microenvironment Promotes Tumorigenesis. *Mol Cell Biol* **31**, 3670–3680 (2011).
501. Karam, R. *et al.* The unfolded protein response is shaped by the NMD pathway. *EMBO Rep* **16**, 599–609 (2015).
502. Tameire, F. *et al.* ATF4 couples MYC-dependent translational activity to bioenergetic demands during tumour progression. *Nat Cell Biol* **21**, 889–899 (2019).
503. Pastor, F., Kolonias, D., Giangrande, P. H. & Gilboa, E. Induction of tumour immunity by targeted inhibition of nonsense-mediated mRNA decay. *Nature* **465**, 227–230 (2010).
504. Oka, M. *et al.* Aberrant splicing isoforms detected by full-length transcriptome sequencing as transcripts of potential neoantigens in non-small cell lung cancer. *Genome Biol* **22**, 9 (2021).
505. Leeksma, A. C. *et al.* The Effect of SF3B1 Mutation on the DNA Damage Response and Nonsense-Mediated mRNA Decay in Cancer. *Front. Oncol.* **10**, 609409 (2021).
506. Becker, J. P. *et al.* NMD inhibition by 5-azacytidine augments presentation of immunogenic frameshift-derived neoepitopes. *iScience* **24**, 102389 (2021).
507. Rigby, R. E. & Rehwinkel, J. RNA degradation in antiviral immunity and autoimmunity. *Trends in Immunology* **36**, 179–188 (2015).
508. Chawla, R. & Azzalin, C. M. The telomeric transcriptome and SMG proteins at the crossroads. *Cytogenet Genome Res* **122**, 194–201 (2008).
509. Azzalin, C. M. & Lingner, J. The Double Life of UPF1 in RNA and DNA Stability Pathways. *Cell Cycle* **5**, 1496–1498 (2006).
510. Brumbaugh, K. M. *et al.* The mRNA Surveillance Protein hSMG-1 Functions in Genotoxic Stress Response Pathways in Mammalian Cells. *Molecular Cell* **14**, 585–598 (2004).
511. Gehen, S. C., Staversky, R. J., Bambara, R. A., Keng, P. C. & O'Reilly, M. A. hSMG-1 and ATM sequentially and independently regulate the G1 checkpoint during oxidative stress. *Oncogene* **27**, 4065–4074 (2008).
512. Haimovich, G. *et al.* Gene Expression Is Circular: Factors for mRNA Degradation Also Foster mRNA Synthesis. *Cell* **153**, 1000–1011 (2013).
513. Blasco-Moreno, B. *et al.* The exonuclease Xrn1 activates transcription and translation of mRNAs encoding membrane proteins. *Nat Commun* **10**, 1298 (2019).
514. Hartenian, E. & Glaunsinger, B. A. Feedback to the central dogma: cytoplasmic mRNA decay and transcription are interdependent processes. *Critical Reviews in Biochemistry and Molecular Biology* **54**, 385–398 (2019).
515. Haimovich, G., Choder, M., Singer, R. H. & Trcek, T. The fate of the messenger is pre-determined: A new model for regulation of gene expression. *Biochimica et Biophysica Acta (BBA) - Gene Regulatory Mechanisms* **1829**, 643–653 (2013).
516. Sun, M. *et al.* Global Analysis of Eukaryotic mRNA Degradation Reveals Xrn1-Dependent Buffering of Transcript Levels. *Molecular Cell* **52**, 52–62 (2013).
517. Sun, M. *et al.* Comparative dynamic transcriptome analysis (cDTA) reveals mutual feedback between mRNA synthesis and degradation. *Genome Research* **22**, 1350–1359 (2012).
518. Rossi, A. *et al.* Genetic compensation induced by deleterious mutations but not gene knockdowns. *Nature* **524**, 230–233 (2015).
519. Singh, P., James, R. S., Mee, C. J. & Morozov, I. Y. mRNA levels are buffered upon knockdown of RNA decay and translation factors via adjustment of transcription rates in human HepG2 cells. *RNA Biology* **16**, 1147–1155 (2019).
520. Dori-Bachash, M., Shalem, O., Manor, Y. S., Pilpel, Y. & Tirosh, I. Widespread promoter-mediated coordination of transcription and mRNA degradation. *Genome Biol* **13**, R114 (2012).
521. Begley, V. *et al.* The mRNA degradation factor Xrn1 regulates transcription elongation in parallel to Ccr4. *Nucleic Acids Research* **47**, 9524–9541 (2019).
522. Fischer, J. *et al.* The yeast exoribonuclease Xrn1 and associated factors modulate RNA polymerase II processivity in 5′ and 3′ gene regions. *J. Biol. Chem.* **295**, 11435–11454 (2020).
523. Wilkinson, M. F. Genetic paradox explained by nonsense. *Nature* **568**, 179–180 (2019).
524. El-Brolosy, M. A. *et al.* Genetic compensation triggered by mutant mRNA degradation. *Nature* **568**, 193–197 (2019).
525. Ma, Z. *et al.* PTC-bearing mRNA elicits a genetic compensation response via Upf3a and COMPASS components. *Nature* **568**, 259–263 (2019).
526. Furlan, M. *et al.* Genome-wide dynamics of RNA synthesis, processing, and degradation without RNA metabolic labeling. *Genome Res.* **30**, 1492–1507 (2020).